

RECEIVED MAY 07 1985

EGG-TMI-6685  
April 1985

PRELIMINARY REPORT: EXAMINATION OF H8 AND B8 LEADSCREWS FROM  
THREE MILE ISLAND UNIT 2 (TMI-2)

Krishna Vinjamuri  
Douglas W. Akers  
Richard R. Hobbins

DO NOT MICROFILM  
COVER

Idaho National Engineering Laboratory  
Operated by the U.S. Department of Energy

Informal Report



Prepared for the  
U.S. DEPARTMENT OF ENERGY  
Under DOE Contract No. DE-AC07-76ID01570



REPRODUCTION OF THIS DOCUMENT IS U.S.

COVER

#### DISCLAIMER

This book was prepared as an account of work sponsored by an agency of the United States Government. Neither the United States Government nor any agency thereof, nor any of their employees, makes any warranty, express or implied, or assumes any legal liability or responsibility for the accuracy, completeness, or usefulness of any information, apparatus, product or process disclosed, or represents that its use would not infringe privately owned rights. References herein to any specific commercial product, process, or service by trade name, trademark, manufacturer, or otherwise, does not necessarily constitute or imply its endorsement, recommendation, or favoring by the United States Government or any agency thereof. The views and opinions of authors expressed herein do not necessarily state or reflect those of the United States Government or any agency thereof.

## **DISCLAIMER**

**This report was prepared as an account of work sponsored by an agency of the United States Government. Neither the United States Government nor any agency Thereof, nor any of their employees, makes any warranty, express or implied, or assumes any legal liability or responsibility for the accuracy, completeness, or usefulness of any information, apparatus, product, or process disclosed, or represents that its use would not infringe privately owned rights. Reference herein to any specific commercial product, process, or service by trade name, trademark, manufacturer, or otherwise does not necessarily constitute or imply its endorsement, recommendation, or favoring by the United States Government or any agency thereof. The views and opinions of authors expressed herein do not necessarily state or reflect those of the United States Government or any agency thereof.**

## **DISCLAIMER**

**Portions of this document may be illegible in electronic image products. Images are produced from the best available original document.**

MASTER

EGG-TMI--6685

DE85 010919

**DISCLAIMER**

This report was prepared as an account of work sponsored by an agency of the United States Government. Neither the United States Government nor any agency thereof, nor any of their employees, makes any warranty, express or implied, or assumes any legal liability or responsibility for the accuracy, completeness, or usefulness of any information, apparatus, product, or process disclosed, or represents that its use would not infringe privately owned rights. Reference herein to any specific commercial product, process, or service by trade name, trademark, manufacturer, or otherwise does not necessarily constitute or imply its endorsement, recommendation, or favoring by the United States Government or any agency thereof. The views and opinions of authors expressed herein do not necessarily state or reflect those of the United States Government or any agency thereof.

PRELIMINARY REPORT: EXAMINATION OF H8 AND B8 LEADSCREWS  
FROM THREE MILE ISLAND UNIT 2 (TMI-2)

Krishna Vinjamuri  
Douglas W. Akers  
Richard R. Hobbins

Published April 1985

EG&G Idaho, Inc.  
Idaho Falls, ID 83415

Prepared for the  
U.S. Department of Energy  
Idaho Operations Office  
Under DOE Contract No. DE-AC07-76ID01570

DISTRIBUTION OF THIS DOCUMENT IS UNLIMITED.

*Jones*

## ABSTRACT

Two control rod drive leadscrews from the TMI-2 reactor, H8 and B8, were examined by EG&G Idaho, Inc., at the Idaho National Engineering Laboratory (INEL). Visual examinations, preliminary temperature estimates, and chemical and radiological analyses were conducted on samples removed from the leadscrews. The objectives of the H8 and B8 leadscrew examinations are: (a) to estimate the maximum temperature experienced along the length of the leadscrew in the plenum assembly region; and (b) to determine the extent and nature of the core component material and radionuclide deposition on plenum assembly surfaces. Hardness measurements and microstructure analysis suggest that significant temperature differences existed between the portions of the leadscrews closest to the bottom and top of the plenum assembly. Preliminary analysis indicates that the temperatures ranged from 700 to 1255 K (800 to 1800°F) for H8 and 755 to 1116 K (900 to 1550°F) for B8. The uncertainty in the temperature estimates is about  $\pm 28$  to 56 K ( $\pm 50$  to 100°F); however, detailed analyses will be performed to confirm or revise these temperatures. Chemical analyses indicate that  $UO_2$  and zirconium were deposited to a greater extent on surfaces closer to the core. Radiological analyses suggest that a number of the H8 radionuclides are insoluble in strong acid solutions. In contrast, more of the B8 radionuclides are soluble in strong acidic solutions. Also, an axial gradient in surface radionuclide concentrations was observed, with the highest concentration near the top of the plenum assembly. The data indicate changes in chemical composition and gradients in the surface radionuclide concentrations in the plenum assembly. The fractions of total core inventory of radionuclides retained on the plenum assembly surfaces are small (<2%).

The preliminary H8 and B8 leadscrew examination task demonstrated the feasibility of the analytical techniques to determine temperatures and radionuclide and core material plateout along the length of the leadscrews. The leadscrew examination task should be expanded and additional leadscrews examined to characterize the axial and radial temperature, radionuclide, and core material plateout profiles for the entire plenum assembly region.

## SUMMARY

Examinations are being performed to acquire data on the extent and nature of the damage to the Three Mile Island Unit 2 (TMI-2) core. One of the TMI-2 core examination tasks is the analysis of the control rod drive leadscrews, which were removed from the reactor head as part of the July 1982 closed-circuit television inspection of the damaged core. One leadscrew was removed from each of three different core positions: H8, from the center of the core; E9, from approximately midradius; and B8, from near the outer edge (see Figure S-1).

Leadscrew sections from B8 and H8 [except for 0.76 m (30-in.)] were shipped to and examined at the Idaho National Engineering Laboratory (INEL). Three short sections of the H8 leadscrew from near the top of the plenum assembly were examined by Pacific Northwest Laboratory (PNL), Babcock & Wilcox (B&W), and GPU Nuclear. Leadscrew E9 was also shipped to the INEL, but it has not been examined at this time. The objectives of the H8 and B8 examinations at INEL are: (a) to estimate the temperatures experienced along the length of the leadscrew in the plenum assembly region; and (b) to determine the extent and nature of the core component and radionuclide deposition on the leadscrew surfaces.

This report presents and discusses the following: (a) leadscrew acquisition, sample types, and analytical techniques used to analyze the various types of samples; (b) results from the visual examination; (c) preliminary leadscrew surface temperature estimates; (d) chemical and radiological analyses; (e) comparisons of temperature estimates and the chemical and radiological behavior in the plenum assembly region; and (f) the principal observations and recommendations made on the basis of this study. This portion of the report presents a brief summary of each section contained in the report.

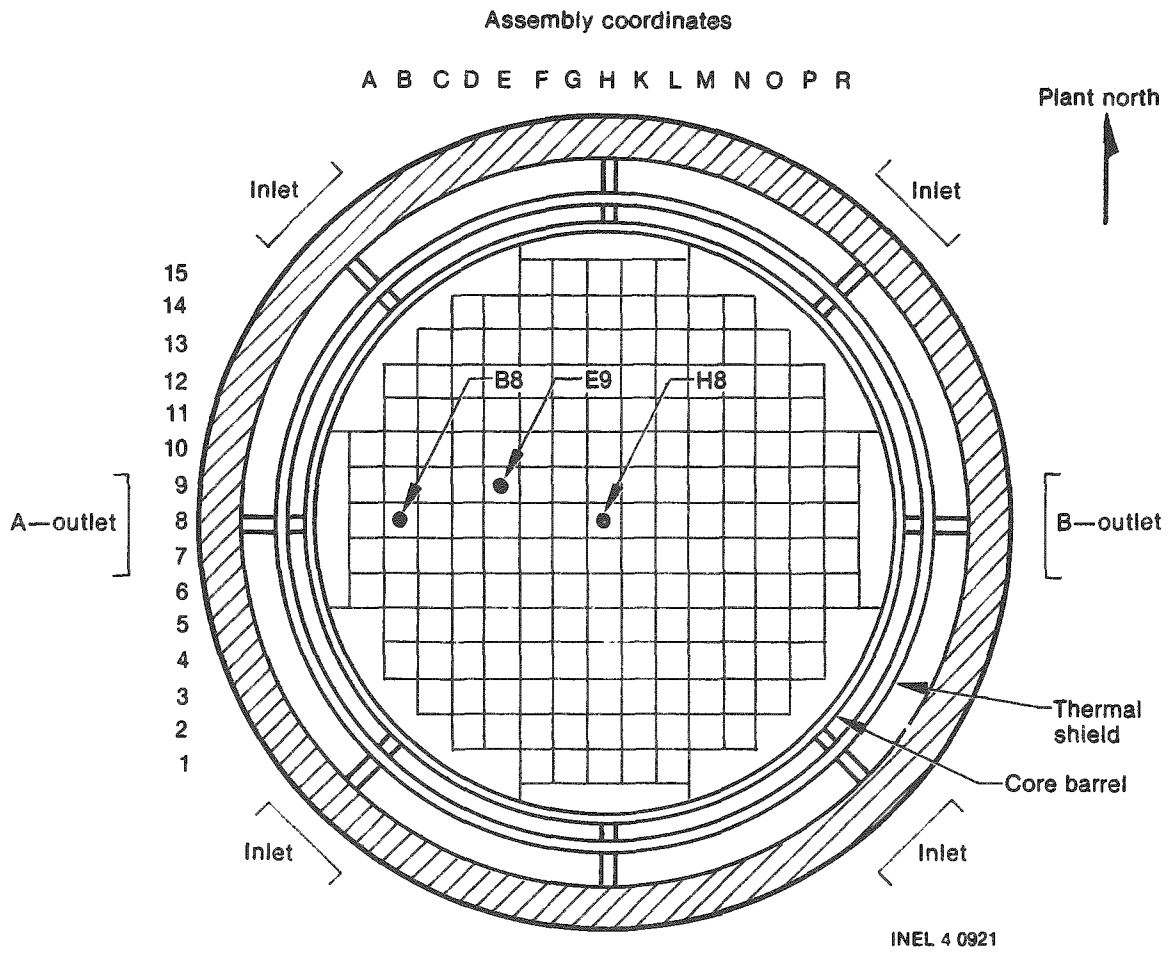


Figure S-1. H8, B8, and E9 leadscrew locations in the TMI-2 core.



## Leadscrew Acquisition, Sample Types, and Analytical Techniques

Each leadscrew is approximately 7.3 m (24 ft) long. During removal from the reactor vessel, GPU Nuclear cut the leadscrews into sections and gamma-scanned the sections. Each section was bagged in polyethylene sleeving, inserted into a premarked 10-cm (4-in.) dia polyvinyl chloride (PVC) tube, and put into a shipping container. Three sections from just above the middle of the H8 leadscrew, each 23 to 30 cm (9 to 12 in.) long, were examined by PNL, B&W, and GPU Nuclear. Leadscrews B8, E9 and the remainder of H8 were shipped to EG&G Idaho.

At the INEL hot cells, the leadscrews were unpackaged and visually examined. Various types of samples were acquired for subsequent examination. Figure S-2 is a general flow diagram showing the types of samples removed and the analytical techniques used on each type of sample. Briefly, the sample types include:

1. Brushoff debris--the loosely adhering material obtained by brushing the outer surface of the leadscrew sections with a nylon bristle brush.
2. Metallurgical samples--these samples were used for structural examination after they were decontaminated using different types of leaching solutions.
3. Decontamination solutions--obtained while decontaminating the metallurgical samples. These solutions contain the tightly adhering material which could not be brushed from the samples, requiring a strong acid solution to remove it from the surface of the leadscrews.
4. Surface samples--lightly brushed samples with the surface layer left basically intact.

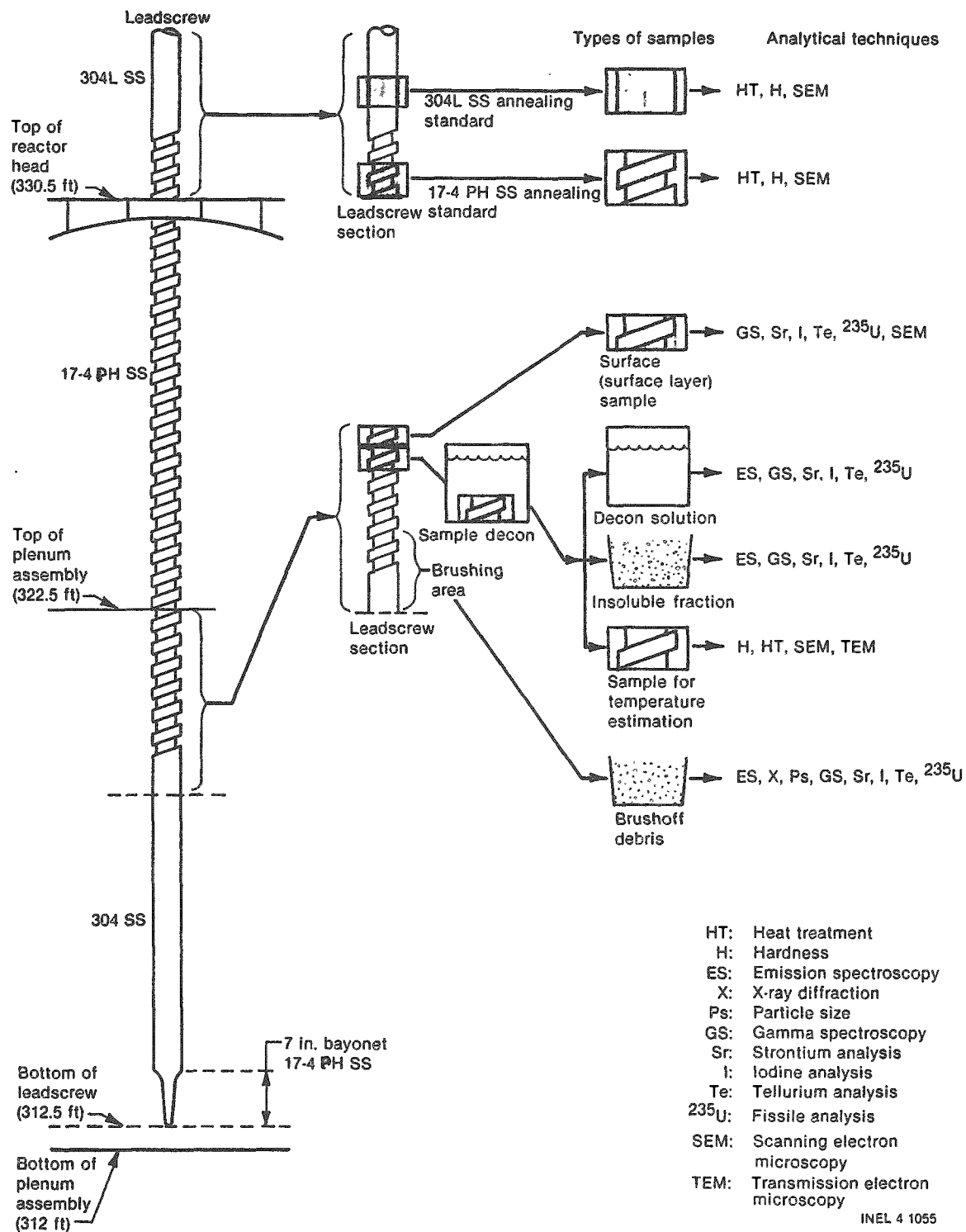


Figure S-2. A typical flow diagram depicting sample types and analytical techniques.

5. Annealing Standards--304L and 17-4 PH stainless steel (SS) standards for an annealing study conducted to estimate the temperatures experienced in the plenum assembly region of the leadscrew.

Many examination techniques were used to analyze the samples. They include: (a) visual examination, using a hot cell periscope; (b) temperature estimates, using metallography, scanning electron microscopy (SEM), annealing study of 304L and 17-4 PH SS standards, and transmission electron microscopy (TEM); (c) chemical analyses, using emission spectroscopy (ES), scanning electron microscopy together with energy dispersive spectroscopy (SEM/EDS), and X-ray diffraction; and (d) radiological analyses, using gamma ray spectroscopy (GS), neutron activation and delayed neutron counting for fissile material assay, chemical separation and beta emitter analyses for  $^{90}\text{Sr}$ , and neutron activation analysis for  $^{129}\text{I}$ . Inductively coupled plasma (ICP) spectroscopy was used for elemental tellurium analysis.

#### Visual Examination

Cursory visual examinations of the H8 and B8 leadscrews were performed at the INEL Hot Cells as part of the sample acquisition process. In general, the leadscrew sections appeared to be intact with no visible signs of damage (melting, cracking, warping, etc.). The leadscrew sections were coated with a very fine powdery material, which varied in color, texture, and relative amount along the length of the leadscrews. Some of the loosely adhering debris was attached to the polyethylene material used to wrap the sections for shipment from TMI-2. The amount of debris deposited on the surfaces gradually increased from almost nothing at the leadscrew bottom to a heavy coating near the top of the plenum assembly. At that location, there was a distinct, stepped decrease. Only one section from the upper half of the H8 leadscrew (adjacent to the reactor vessel head) was inspected. There was almost no debris observed on that section; in fact, it was clean and shiny.

The debris on the lower sections, near the leadscrew bottom, was black in color and contained metal shavings generated during sectioning of the

leadscrews. Flakes of silvery colored material were also observed, both in the brushoff debris and on the surface of the leadscrews. Analyses by ES and EDS identified silver, cadmium, indium, and other metals. In contrast, the loose material deposited on the surfaces of the upper leadscrew sections and the collected brushoff debris were gray in color. In general, corrosion of the leadscrew from the bottom to the top of the plenum assembly was indicated by variations in color. All features, such as the bayonet coupling, threads, and transition from 304 SS to the 17-4 PH threaded portion, are well defined.

#### Preliminary Temperature Estimates

Samples removed from the H8 and B8 leadscrews were analyzed by metallographic, SEM, and TEM examination techniques. The microstructure and Rockwell-C hardness were measured to estimate temperatures. These examinations suggest that the H8 and B8 samples close to the top of the plenum assembly experienced temperatures of about 700 and 755 K (800 and 900°F), respectively.

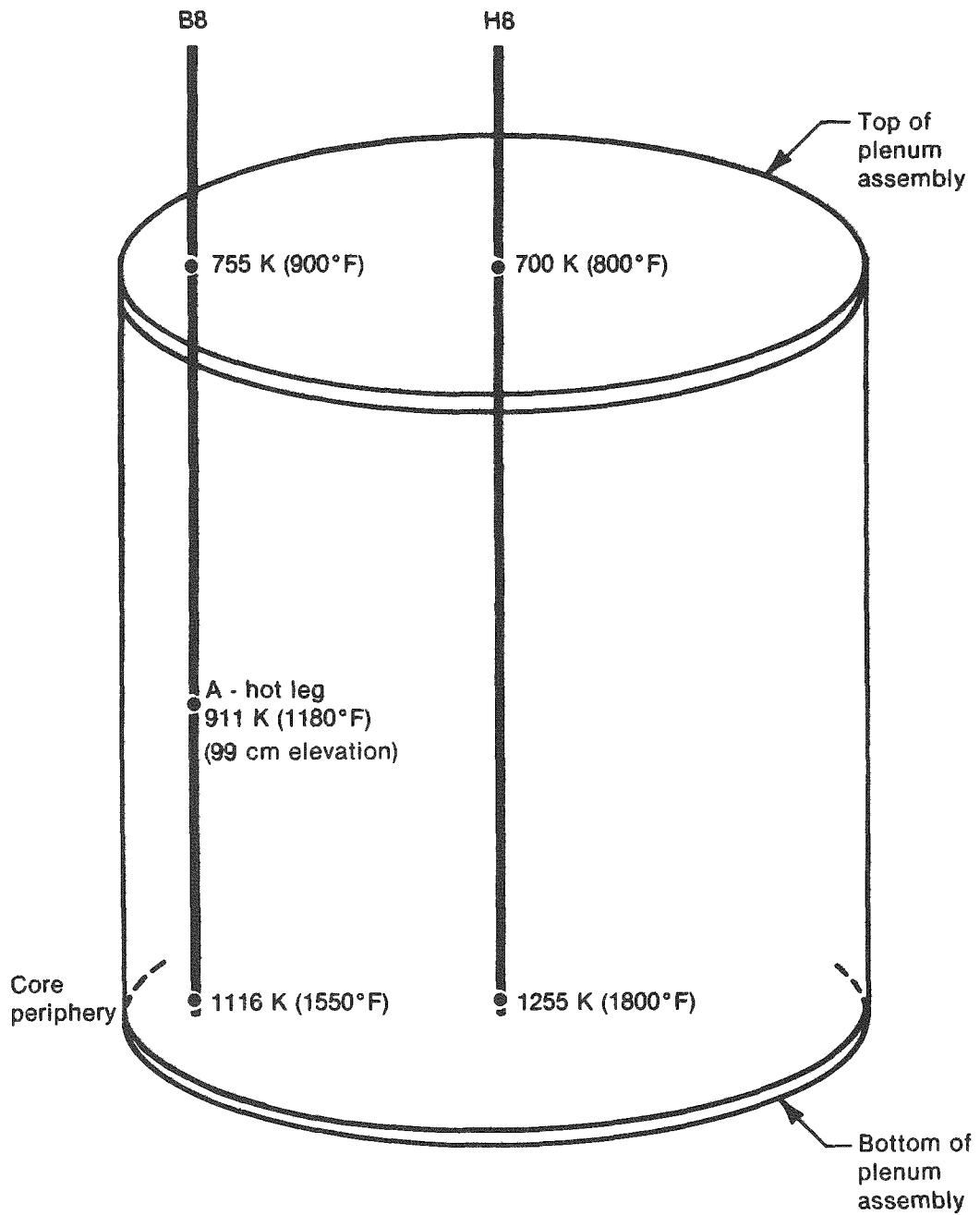
The temperatures experienced by the H8 and B8 samples near the bottom of the plenum assembly have been estimated by comparing the microstructure and hardness to a set of annealed standards which had been heat-treated at different times (60 to 240 min) and temperatures [977 to 1477 K (1300 to 2200°F)]. Additionally, heat treatment of H8 and B8 samples from near the bottom of the plenum assembly to the H900 condition (heated at 900°F for one hour and air-quenched) increased the hardness, suggesting the probable temperature range experienced by these samples. The estimated temperatures of the H8 and B8 samples near the bottom of the plenum assembly are 1255 and 1116 K (1800 and 1550°F), respectively. TEM examination of copper precipitates supports the estimated temperatures. In addition, a sample from near the bottom of the plenum assembly at the H8 position and a sample from B8 at the A-hot leg axial location have been examined, and the estimated temperatures are 1189 and 911 K (1670 and 1180°F), respectively.

The estimated temperatures of the H8 and B8 leadscrews are shown in Figure S-3. The uncertainty in the temperature estimates is about  $\pm 28$  to 56 K ( $\pm 50$  to 100°F); however, detailed analyses are being performed to confirm these temperatures.

### Chemical Analyses

The chemical analyses (ES, SEM/EDS and X-ray diffraction) were performed to determine the extent and nature of the material deposited on the leadscrew surfaces, i.e., chemical compounds and elements. Figure S-4 shows the elements identified in the brushoff debris near the bottom and top of the plenum assembly. The principal elements of interest are uranium, zirconium, silver, and boron. The uranium concentration indicates a definite axial gradient (a decrease of a factor of 10) from the bottom to the top of the plenum assembly. Also, there is a radial gradient (a decrease of a factor of 4.5) in the uranium content from the H8 to the B8 positions at the bottom of the plenum assembly. The behavior of zirconium is similar to uranium, as both axial and radial gradients are present. The silver is uniformly distributed in the brushoff debris at three axial locations on H8 and B8, with an undetectable amount at the top of the plenum assembly at the H8 location. The element boron remained relatively uniform over the length of both leadscrews.

ES analyses were performed on both soluble and insoluble fractions of the decontamination solutions. These fractions were obtained by filtering the decontamination solutions (40 wt%  $\text{HNO}_3$  + 0.12 M HF) with a 0.45  $\mu\text{m}$  vacuum filter system. In contrast to the brushoff debris, very little uranium was measured in either the liquid or solid fractions of the decontamination solutions. The only uranium measured was found near the top of the plenum assembly at the B8 location, with 4 wt% in the solid fraction and 0.2 wt% in solution. The zirconium concentrations were also low ( $\leq 4$  wt%) at all measured locations. The highest silver concentration (14.5 wt%) in the decontamination solutions was found at the top of the plenum assembly at the B8 location. From these data, the plenum assembly surface deposition of silver is estimated to be 1% of the total silver content in the control rods. Very little ( $< 0.2$  wt%) was measured at other locations. The boron concentrations were significantly higher in



INEL 4 0961

Figure S-3. A comparison of estimated surface temperatures on H8 and B8 leadscrews.

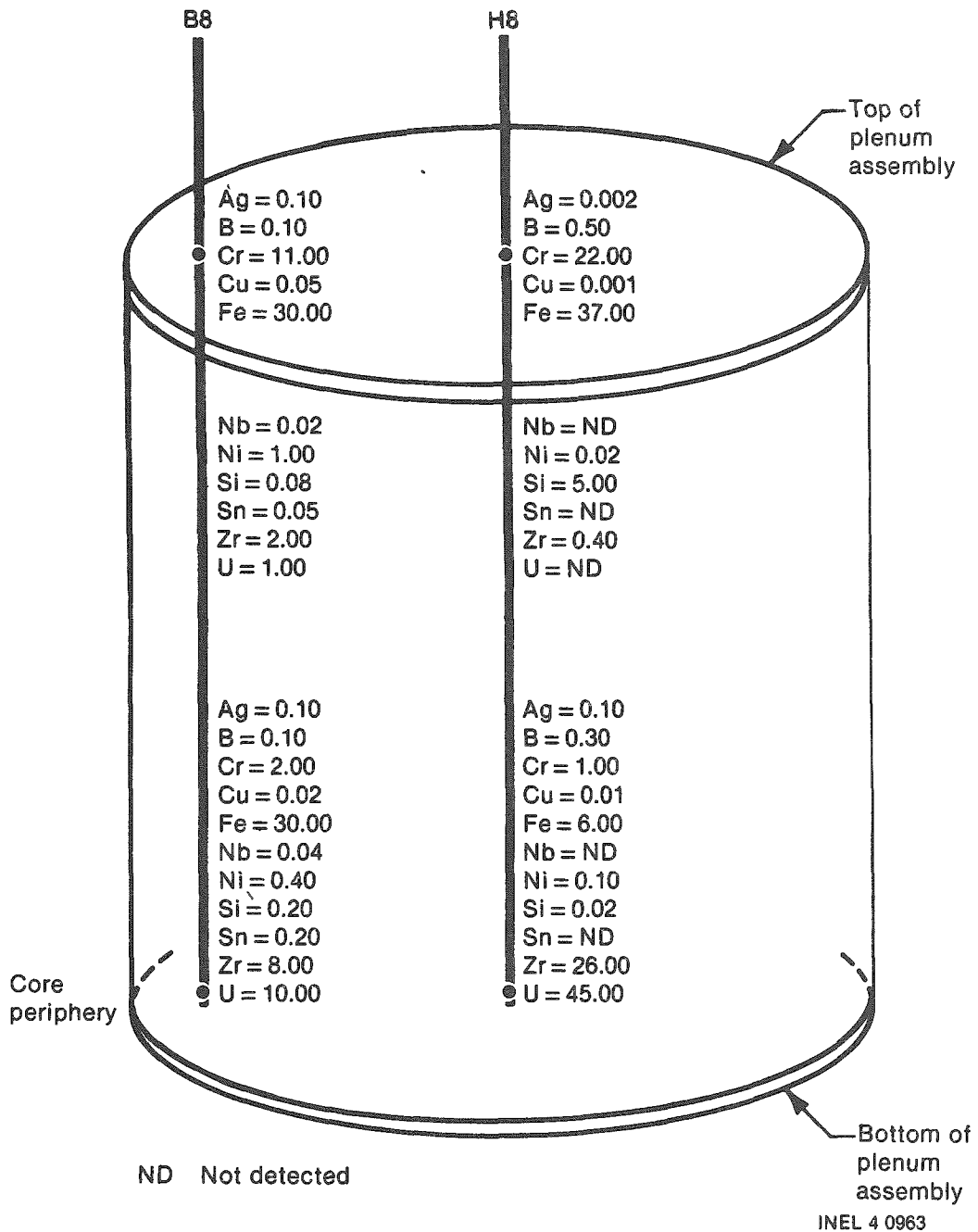


Figure S-4. The concentrations of elements identified in brushoff debris at the H8 and B8 locations (wt%).

the decontamination solution than in the brushoff debris. About 62 to 89% of the boron deposited is soluble in strong acid solution (40 wt%  $\text{HNO}_3$  + 0.12 M HF).

The data from the brushoff debris and the soluble and insoluble fractions of the decontamination solutions provide a number of indications:

1. There is a gradient in uranium deposition from the bottom to the top of the plenum assembly, with higher concentrations at the bottom.
2. Uranium and zirconium are principally present in the brushoff debris, with significantly lower fractions present in the tightly adherent material (decontamination solution).
3. Silver appears to be uniformly distributed in the brushoff debris.
4. Boron is principally present in the decontamination solutions, rather than the brushoff debris.
5. At the top of the plenum assembly, the principal components of the brushoff debris are constituents of stainless steel (iron, chromium, nickel).

SEM/EDS analyses were performed on portions of the lightly brushed H8 and B8 surface samples. The top and bottom thread surfaces were examined on samples taken from near the top of the plenum assembly, and smooth surfaces were examined on samples taken from near the bottom of the leadscrew. On the samples near the top of the plenum assembly, the elements of interest that were identified are silver, barium, cadmium, cesium, indium, tellurium, zirconium, and uranium, whereas on the samples near the bottom of the plenum assembly only barium, cadmium, and zirconium were identified. On the threaded samples, zirconium and uranium were found deposited only on the bottom threaded surfaces, whereas cesium was found only on upward facing surfaces. The remainder of the identified elements were found on both surfaces.



X-ray diffraction analysis of the solid material, brushoff debris, and insoluble decontamination solution fractions indicates only the presence of magnetite ( $\text{Fe}_3\text{O}_4$ ), with the exception of the brushoff debris sample from the bottom of the H8 leadscrew. In this sample,  $\text{UO}_2$  was identified.

### Radiological Analyses

Radiological analyses were performed on the H8 and B8 leadscrews to determine fission product and activation product surface concentrations. Also, analyses were performed to obtain information about the deposition behavior and chemical structure of individual fission products. The radiological analysis methods used have been previously identified, and the samples analyzed were obtained from locations near the bottom and top of the plenum assembly. The radiological measurements are reported in terms of radionuclide concentration ( $\mu\text{Ci/g}$ ), which may be extrapolated to surface radionuclide concentrations in terms of  $\mu\text{Ci/cm}^2$ . The radionuclide concentration data provide information on the intrinsic radiological characteristics of the material measured. The data are evaluated and comparisons are made based on both radionuclide concentration ( $\mu\text{Ci/g}$ ) and surface deposited concentration ( $\mu\text{Ci/cm}^2$ ). The data are evaluated in the following order: (a) brushoff debris; (b) decontamination solutions; and (c) surface samples. The radionuclide concentration and surface concentration data were also compared in that order.

Figure S-5 shows the comparison of the principal radionuclide concentrations in the brushoff debris and the decontamination solutions (both soluble and insoluble fractions). A comparison of principal radionuclide concentrations in the brushoff debris indicates large axial gradients. However, the radial brushoff debris radionuclide concentration gradients at the bottom and the top of the plenum assembly are relatively small. These data generally indicate gradients in the composition of the brushoff debris that are dependent on core location.

The concentrations of radionuclides measured in the B8 brushoff debris show a gradient from the bottom to the top of the plenum assembly for

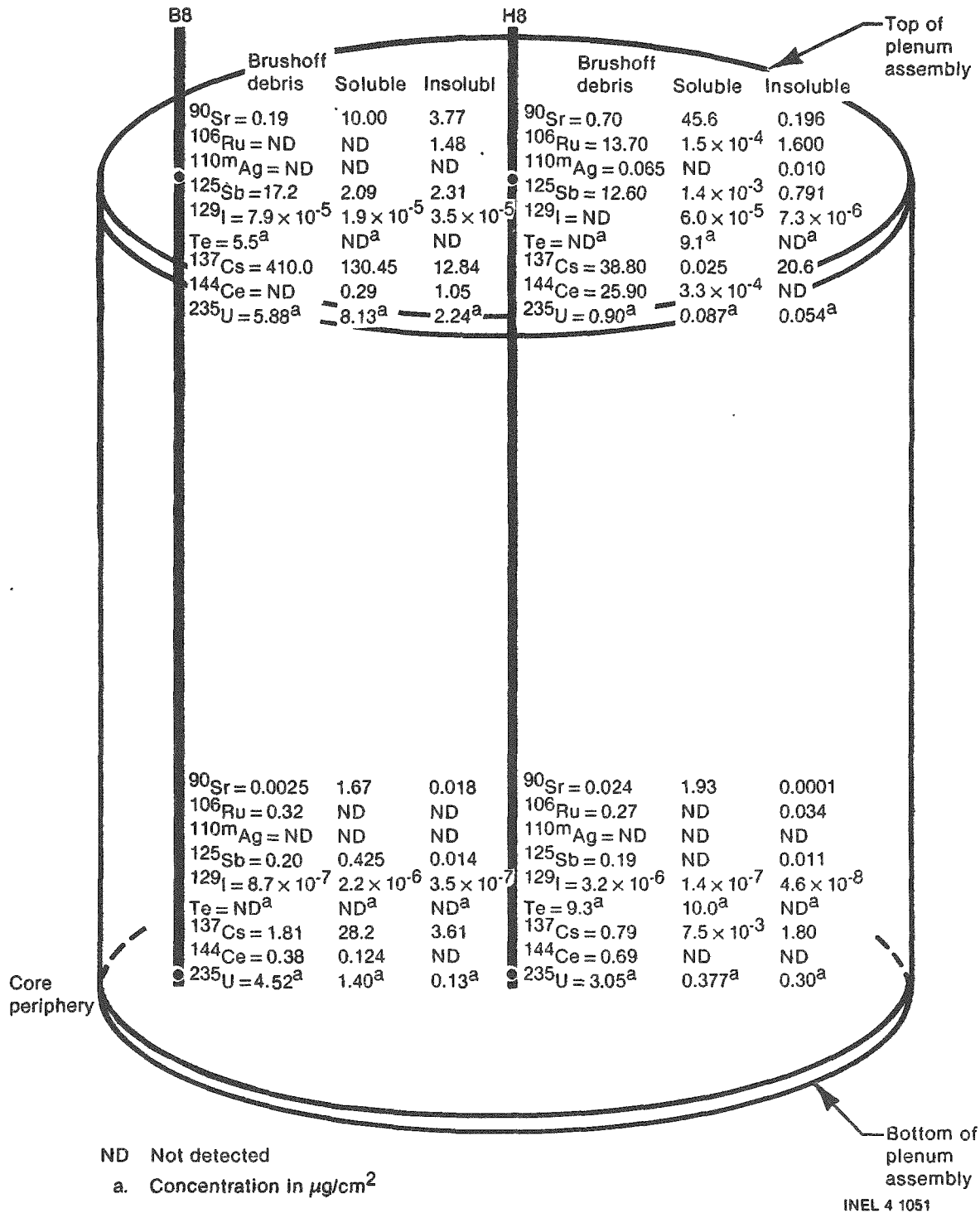


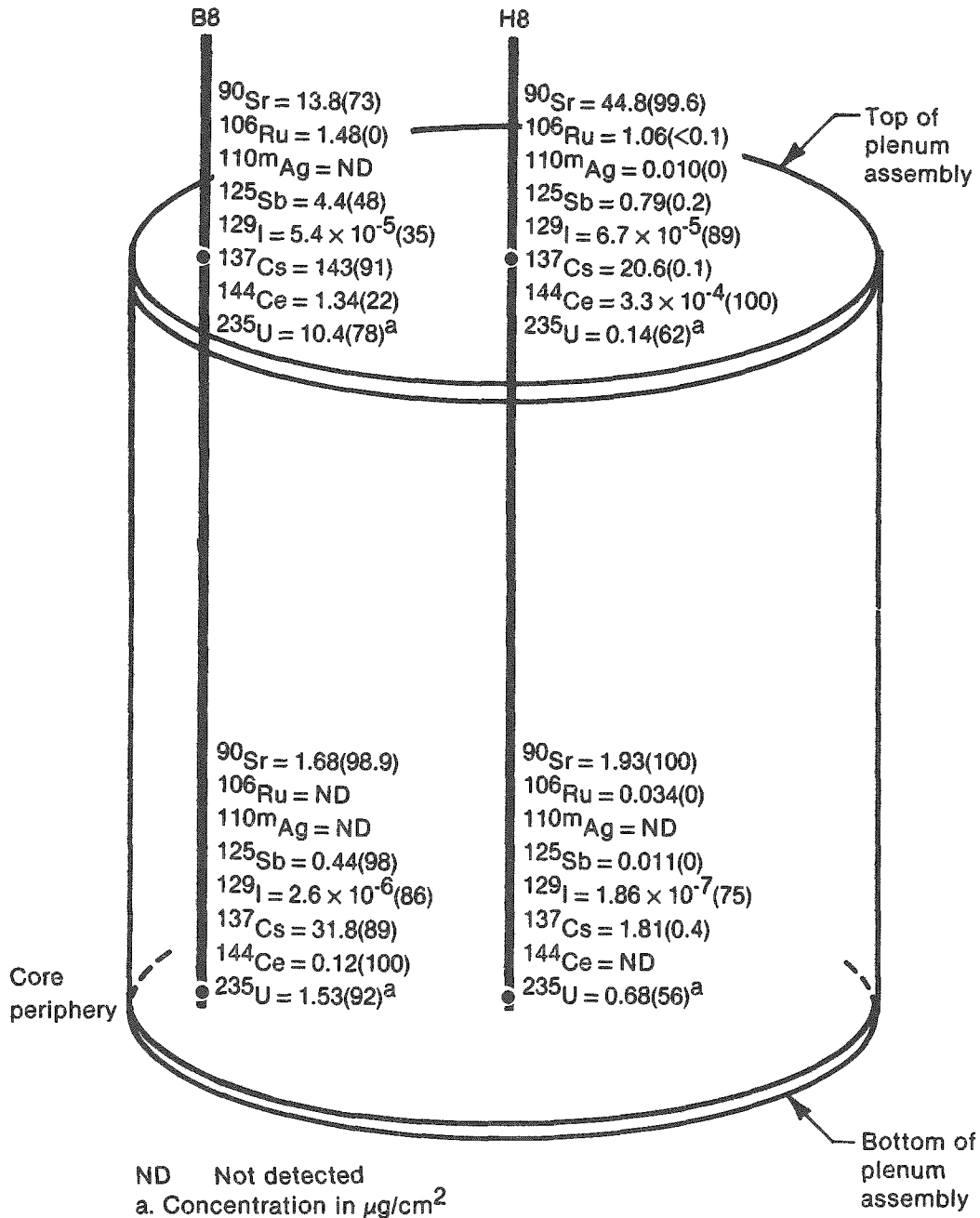
Figure S-5. Surface radionuclide concentrations in brushoff debris, soluble and insoluble concentrations ( $\mu\text{Ci}/\text{cm}^2$ ).

$^{125}\text{Sb}$ ,  $^{134}\text{Cs}$ , and  $^{137}\text{Cs}$ . Some radionuclides ( $^{106}\text{Ru}$ ,  $^{144}\text{Ce}$ ,  $^{154}\text{Eu}$ , and  $^{155}\text{Eu}$ ) were measured at the bottom but not at the top of the plenum assembly. The  $^{90}\text{Sr}$ ,  $^{129}\text{I}$ , and  $^{235}\text{U}$  concentrations also indicate an axial gradient, with higher  $^{90}\text{Sr}$ , and  $^{129}\text{I}$  concentrations measured at the top of the plenum assembly.

To provide further information on the radiological and physical characteristics of the leadscrew brushoff debris, a particle size distribution analysis was performed on portions of brushoff debris samples from the bottom and top of the plenum assembly at the H8 position. The particle size analysis was performed using a wet particle sizing method in which a vacuum was applied to the bottom of a series of particle sizing sieves and the sample was washed through the sieves using a Freon wash. The data indicate an axial gradient in the particle size distributions, with a predominance of the smaller sizes (45 to 60  $\mu\text{m}$ ) at the top of the plenum assembly. Also, significant quantities of the radionuclide concentrations (16 to 34% at the bottom and 4 to 10% at top of the plenum assembly) are associated with the smallest particle size ( $\leq 0.45 \mu\text{m}$ ), suggesting that the transport mechanism for the surface deposits may have been aerosols or hydrosols. These data address the current condition of the leadscrew surfaces only; changes in the reactor coolant system during the previous five years may have affected surface deposition.

In Figure S-5, the decontamination solution concentration data are also shown. Axial gradients are present for the majority of the soluble and insoluble radionuclides. The largest axial gradient is for  $^{129}\text{I}$ , which is significantly higher at the top of the plenum assembly. At the H8 and B8 locations, the factors are 159 and 100, respectively. Also, significant radial concentration gradients were observed.

The combined decontamination solution radionuclide concentration data and the percentage of soluble and insoluble radionuclides are shown in Figure S-6. A gradient in solubility is present for all radionuclides except strontium, which is highly soluble at all locations (top and bottom of the plenum assembly at the H8 and B8 positions). The radionuclides



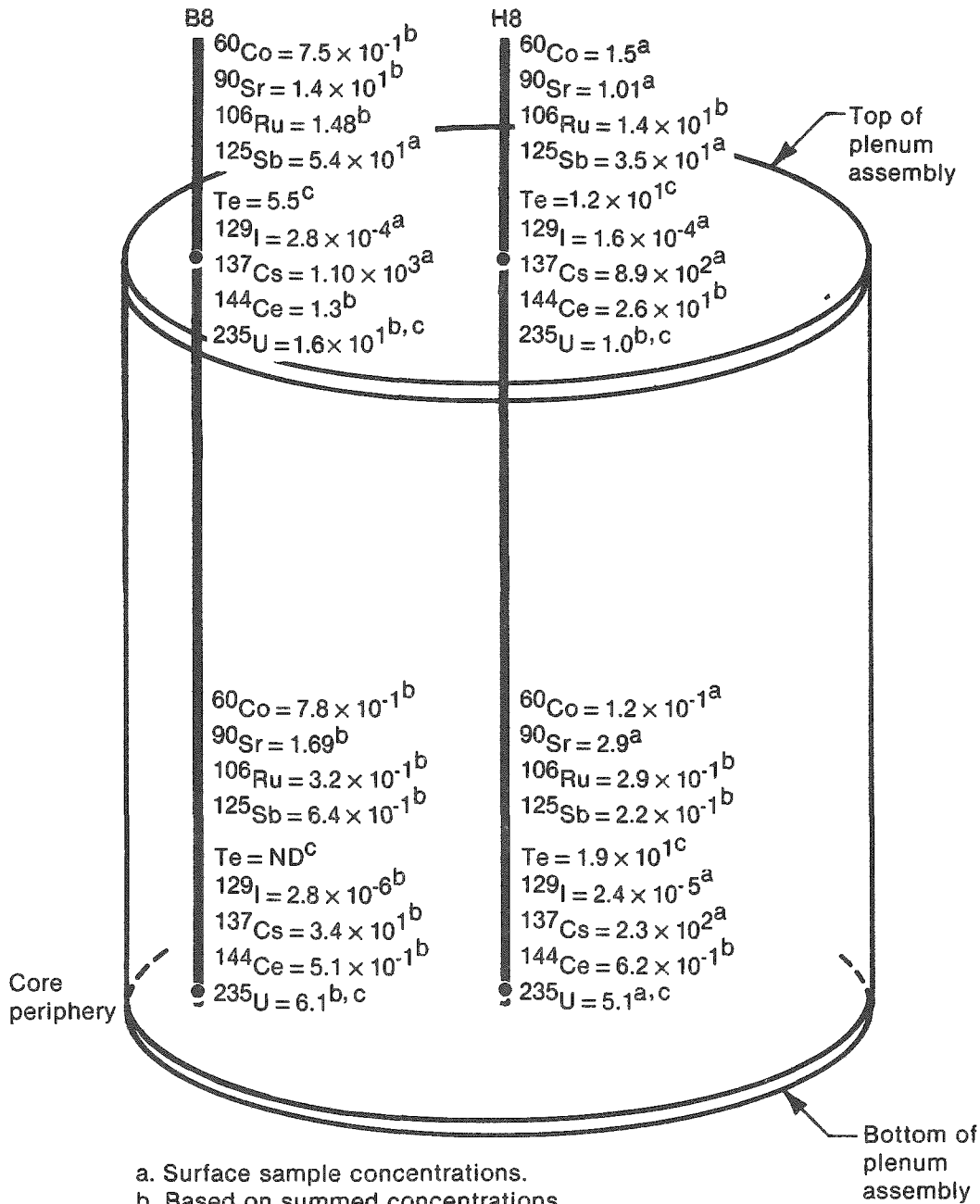
INEL 4 1010

Figure S-6. Total decontamination solution surface radionuclide concentrations in  $\mu\text{Ci}/\text{cm}^2$  (soluble fractions in percent).

deposited at the H8 position have the lowest solubility (<1% for  $^{106}\text{Ru}$ ,  $^{110\text{m}}\text{Ag}$ ,  $^{125}\text{Sb}$  and  $^{137}\text{Cs}$ ), whereas the solubility fractions at the B8 locations are 48 and 89% for  $^{125}\text{Sb}$  and  $^{137}\text{Cs}$ , respectively.

Figure S-7 shows the total surface radionuclide concentrations at all locations, based on either the summed (sum of concentrations in brushoff debris and the decontamination solution) or surface sample concentrations. As indicated, there are significant variations in the surface deposition. Figure S-8 shows the calculated fraction of core fission product inventory (in percent) retained on the plenum assembly surfaces for the individual radionuclides. These data are also based on the highest radionuclide concentrations; i.e., either the concentrations obtained by summing the concentrations in the brushoff debris decontamination solutions and insoluble fractions or those obtained from the lightly brushed surface samples. Significant axial and radial gradients exist in the fission product retention on the plenum assembly surfaces. The axial gradient at the H8 location ranges from a factor of about 2 for  $^{110\text{m}}\text{Ag}$  to a factor of 175 for  $^{125}\text{Sb}$ , with most radionuclides having gradients with factors from 16 to 55. The axial gradients at the B8 location range from factors of about 4 for  $^{144}\text{Ce}$  and  $^{235}\text{U}$  to a factor of 93 for  $^{125}\text{Sb}$ . The radial gradient at the bottom of the plenum assembly is maximum for  $^{144}\text{Ce}$ , which is a factor of 92 higher at the B8 location. The radial gradients for  $^{90}\text{Sr}$ ,  $^{106}\text{Ru}$ , and  $^{125}\text{Sb}$  are within a factor of 3. The  $^{129}\text{I}$  and  $^{137}\text{Cs}$  have radial gradients with factors of about 8 and 7, respectively. The data also indicate that the largest amounts (core fractions in percent) of radionuclides were retained near the top of the plenum assembly. The axial gradients may have resulted from higher temperatures, resuspension, or washout experienced by leadscrew surfaces near the bottom of the plenum assembly. As shown in Figure S-8, the fractions of the core inventory of the radionuclide retained on the plenum assembly surfaces are small (<2%). The estimated uncertainty is a factor of 2.

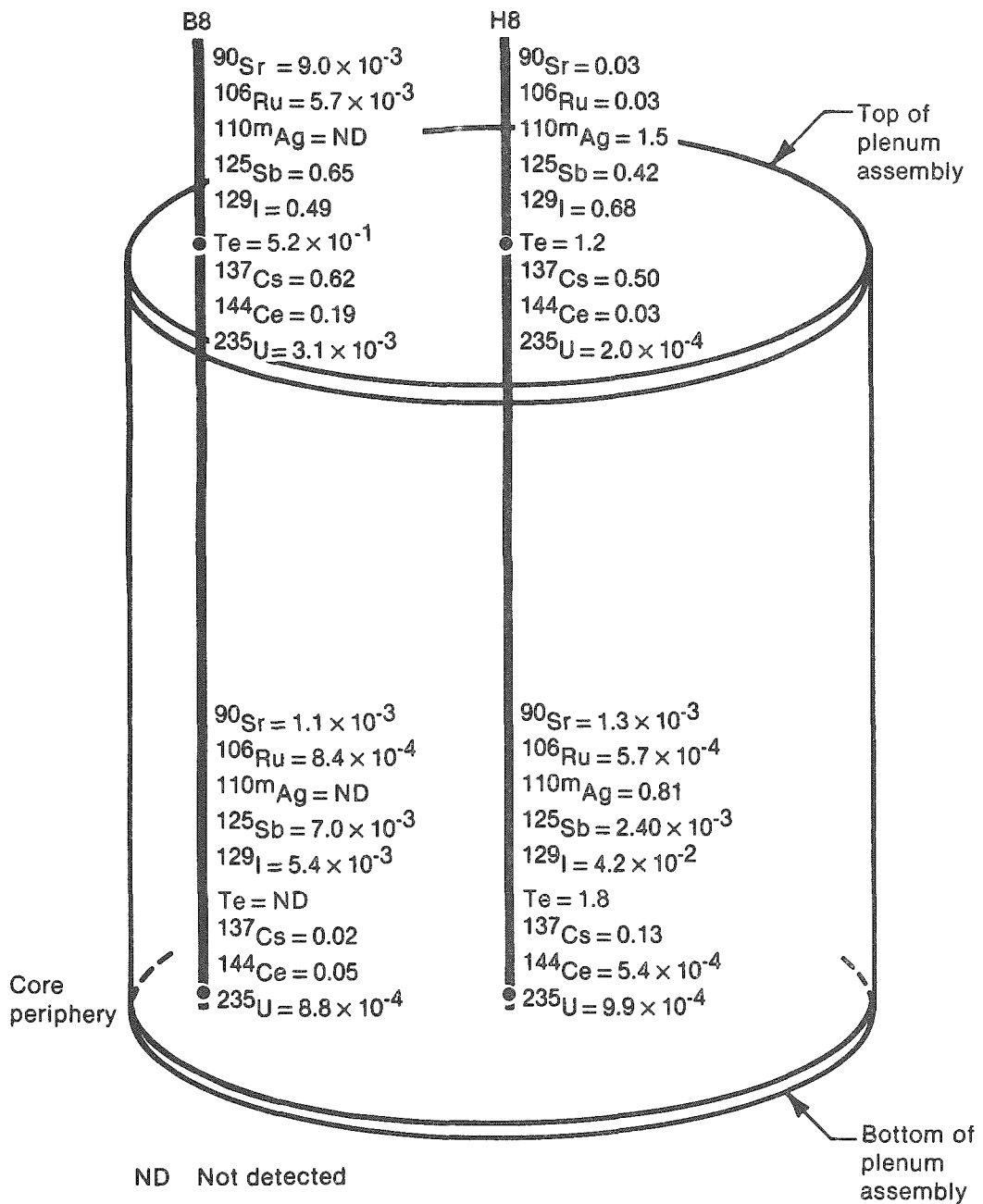
The ratios of fission product to fissile material ( $^{235}\text{U}$ ) were calculated for the H8 and B8 brushoff debris. The fraction of each fission product carried with  $^{235}\text{U}$  was calculated from the following equation.



- a. Surface sample concentrations.  
 b. Based on summed concentrations.  
 c. Concentration in  $\mu\text{g}/\text{cm}^2$ .  
 ND Not detected

INEL 4 1011

Figure S-7. Total surface radionuclide concentrations in  $\mu\text{Ci}/\text{cm}^2$  (based on highest surface or summed sample concentrations).



INEL 4 0969

Figure S-8. A comparison of retained radionuclides on the plenum assembly surfaces (core fraction in percent).

$$\text{Fission products carried with fuel (\%)} = \frac{\text{measured fission product to } ^{235}\text{U ratio}}{\text{calculated fission product to } ^{235}\text{U ratio}} \times 100$$

The data indicate that the measured ratios are much greater than the ORIGEN2 code-calculated ratios for the amount of  $^{235}\text{U}$  present in the core. The discrepancy ( $\sim 10^2$  to  $10^3$ ) was much greater at the top of the plenum assembly than at the bottom. The calculated and measured fission-product-to-fissile-material ratios for the decontamination solutions indicate behavior similar to the brushoff debris.

The  $^{137}\text{Cs}$ -to- $^{129}\text{I}$  radionuclide concentration ratios are consistent within a factor of 2 near the H8 and B8 locations respectively, indicating similar transport mechanisms for both radionuclides. Thermodynamic calculations were made, using calculated steam temperatures and measured pressures. Those calculations suggest that the concentration of cesium iodide was 50 to 75% at the time of the accident.

#### Principal Observations

Principal observations based on the analyses performed are:

1. The lower portions of the H8 and B8 leadscrews near the bottom of the plenum assembly have probably experienced temperatures of 1255 and 1116 K (1800 and 1550°F), respectively. The upper portions of H8 and B8 near the top of the plenum assembly experienced temperatures of 700 and 755 K (800 and 900°F), respectively. The uncertainty in the temperature estimates is about  $\pm 28$  to 56 K ( $\pm 50$  to 100°F).
2. Axial temperature differences of 555 K (1000°F) and 361 K (650°F) exist near the core center (H8 position) and core periphery (B8 position) of the plenum assembly. A radial temperature difference of 139 K (250°F) exists near the bottom of the plenum assembly. A small radial temperature difference of 56 K (100°F) exists at the top of the plenum assembly.



3. The temperature estimates are preliminary, and additional analyses will be performed to confirm or revise these temperatures.
4. Significantly higher concentrations (wt%) of uranium and zirconium were found deposited near the bottom than were found near the top of the plenum assembly.
5. Very little silver (1%) is deposited on the plenum assembly surfaces from control rod material.
6. From 62 to 89% of the boron deposited on the surface was soluble in strong acidic solution (40-wt%  $\text{HNO}_3$  + 0.12-M HF).
7. The radionuclide concentration of the H8 brushoff debris ( $\mu\text{Ci/g}$ ) was relatively uniform along the axial length of the leadscrew. A gradient was observed on the B8 leadscrew, with the highest radionuclide concentrations near the top of the plenum assembly. The radionuclides  $^{144}\text{Ce}$ ,  $^{154}\text{Eu}$ , and  $^{155}\text{Eu}$  were not measurable near the top of the plenum assembly at the B8 position. Also, a gradient in  $^{235}\text{U}$  concentration ( $\mu\text{g/g}$ ) was observed at both the H8 and B8 positions, with it being highest near the bottom of the plenum assembly.
8. Most of the tightly adherent surface deposition layer on H8 containing  $^{125}\text{Sb}$  and  $^{137}\text{Cs}$  is insoluble in strong acidic solutions. In contrast, the B8 layer containing these radionuclides is significantly more soluble in strong acidic solutions, indicating a radial gradient in the chemical behavior of fission products.
9. In general, highest surface radionuclide concentrations ( $\mu\text{Ci/cm}^2$ ) were found in the region near the top of the plenum assembly, which was also the lowest in temperature [700 to 755 K (800 to 900°F)].

10. Significant fractions ( $\leq 50\%$ ) of the radionuclide content of the brushoff debris at the bottom and top of the plenum assembly (H8 position) are associated with particle sizes  $\leq 60 \mu\text{m}$ , indicating that many radionuclides may have been transported as aerosols or hydrosols. (Sixteen to 34% of the particle sizes are  $\leq 0.45 \mu\text{m}$ .)
11. The fractions of total core inventory of  $^{90}\text{Sr}$ ,  $^{106}\text{Ru}$ ,  $^{110\text{m}}\text{Ag}$ ,  $^{125}\text{Sb}$ ,  $^{129}\text{I}$ ,  $^{137}\text{Cs}$ ,  $^{144}\text{Ce}$ , and  $^{235}\text{U}$  retained on the plenum assembly surfaces are small ( $< 2\%$ ), based on the extrapolation of the leadscrew analyses data to the plenum assembly.
12. Small radial gradients in radionuclide concentrations are present between the H8 and B8 positions, with the highest at the top of the plenum assembly.
13. The measured ratios of fission product concentration to fissile material content are much higher than would be expected from ORIGEN2 calculation. This difference is much greater ( $\sim 10^2 - 10^3$ ) at the top of the plenum assembly than at the bottom and may be related to the volatility of the individual radionuclides.
14. Similar  $^{137}\text{Cs}$ -to- $^{129}\text{I}$  ratios at different axial leadscrew locations suggest that the transport mechanism for both radionuclides is similar.

#### Recommendations

A technical review committee (M. L. Picklesimer, metallurgical consultant, PIC Products; H. W. Garvin, metallurgical consultant, ARMCO Research Center (ARMCO); and G. O. Hayner, Supervisor, Failure Analysis, B&W) has reviewed the temperature estimates section of the report and recommended that the following work be done on both 17-4 PH SS and 304 SS

in order to complete the present examination in an orderly and acceptable fashion. The essential elements for completion of the basic temperature study of 17-4 PH SS and 304 SS standards are as follows:

1. Incorporate the results of the low-temperature study of leadscrew 17-4 PH samples into Figure 14 of this report. (These data were obtained after issuing the draft report.)
2. Complete the test matrix listed in Appendix A (Figure A-1); make hardness, optical, and SEM comparisons of the control samples from the test matrix with the unknowns from the leadscrews, based on an H900 and quenched heat-treated condition for the control samples. The H900 heat-treated condition will provide a larger range of hardness values for comparison with the unknowns and a more reliable interpretation of their history.
3. Perform scanning transmission electron microscopy (STEM) work, including selected area X-ray diffraction and elemental analyses as appropriate. This work should be performed on at least the following test matrix specimens: A<sub>11</sub>, A<sub>31</sub>, A<sub>41</sub> (1300°F); A<sub>17</sub>, A<sub>27</sub>, A<sub>37</sub> (1800°F); A<sub>24</sub>, A<sub>25</sub>, A<sub>26</sub> (60 min. isochronal). Based on the results obtained from the samples indicated above, STEM work on additional specimens from the completed test matrix may be required. The objective of this work is to more fully characterize key samples in the test matrix in the following areas: substructure, selected area X-ray diffraction, and selected area elemental analyses. These data will be used to more fully understand and characterize phase, microstructural, and hardness changes observed in the specimens.
4. An X-ray diffraction study should be performed on the unknown samples and all controls from the completed Appendix A test matrix specimens in the as-received and as-quenched conditions, respectively. The objective of this study is to qualitatively determine the reaction products and approximate reaction kinetics

(from the crystal structures) present in the controls and unknowns. These data would provide support for comparison with hardness and microstructural data to further verify temperatures attained by the leadscrew unknowns.

5. Based on the additional work to be performed and described previously, establish revised estimates of peak temperatures for the unknowns.
6. Complete the 1°F/min cooling rate study. Determine the microstructures and hardness values in the H900 condition. If a lamellar structure is not seen in this work, a reheat study should be performed. A 1°F/min specimen which was not reheated to either the H900 or H1100 condition should be subdivided into seven separate specimens. These seven specimens should be reheated, one each to 1300, 1350, 1400, 1450, 1500, 1550, and 1600°F, respectively, and held for one hour at each temperature. The microstructures from these specimens should be compared to that of B8-2. If a lamellar structure is produced which is comparable to the B8-2 unknown, then a hardness comparison should be made in the H900 condition. The lamellar spacing of this specimen should be determined and compared to the B8-2 specimen. The reasons for this study are to determine the B8-2 unknown temperature from lamellar spacing measurements and to determine if the previous temperature prediction may be low.
7. Perform a microstructural examination of a longitudinal section of the leadscrew specimens. This will indicate if differences exist between the transverse and longitudinal structures.
8. Repeat the hardness measurements performed on the H8-2 sample in the H900 condition. If these measurements are close to Rc47, then repeat the hardness test using the H8-3 specimen in the H900 condition.

9. Determine the bulk chemistry of H8-15 and B8-7 by suitable techniques. These data will further assist the interpretation of the microstructures, since the microstructure and hardness of the alloy are sensitive to the exact balance of the elemental composition.
10. Perform a microprobe line scan analysis of at least one specimen showing a lamellar microstructure to determine any compositional differences between the plates composing the structure.
11. A strong effort should be made to obtain higher and more uniform contrast for the photomicrographs used in the final report. It is suggested that Polaroid P/N film be used to produce slightly underexposed negatives which will allow much more control and variation in printing.

The following recommendations apply to 304 SS samples:

1. Archive 304 SS material (if available) should be used for all control specimens for comparison with the lower extension piece specimens of the leadscrews. The 304L upper extension piece material should not be used for control samples, since it has a much lower carbon content. If archive material is not available, then 1-1/2 to 2-in. OD commercial 304 SS rod with hardness in the range of 80-95 Rb (88-92 Rb preferred) should be used for the control specimens. The interpretation of the microstructures to allow an estimate of peak temperatures will depend to a very large extent on the presence or absence of carbides and their type, size, and concentration.
2. Determine the bulk chemistry of the upper and low extension pieces by suitable techniques. This will provide assurances that the materials are actually 304 SS.

3. Repeat the work already performed with the 304 SS material as noted above (to replace that done with the 304L SS). This should include, as a minimum, the comparison of control and leadscrew specimens with regard to hardness and microstructure for the temperature range of interest.

The authors recommend that additional leadscrews be examined in order to characterize the axial and radial profile for temperatures and radionuclide and core material plateout in the entire plenum assembly. The H8 and B8 leadscrew examination task demonstrated the feasibility of the analytical techniques; however, the data obtained are too limited to adequately characterize the plenum assembly as a whole. Additional data from several strategic leadscrew locations within the plenum assembly region are needed for an adequate characterization.

Garry Thomas, of the Electric Power Research Institute (EPRI), suggests several reasons why characterization of the plenum assembly is critical and why the leadscrews can provide the data needed to accomplish the characterization. They include the following:

1. The plenum assembly acts as a major buffer for the reactor primary system by moderating the temperature of the core exit gases. It alters the thermodynamic and thermochemical states of fission products leaving the core. Therefore, its real effect should be characterized.
2. The strategic placement of leadscrews allows for a three-dimensional sampling of the entire (~70 ton) plenum assembly.
3. The leadscrews are the most accessible components in the plenum assembly.
4. Visual examination and temperature estimates of the leadscrews indicate no signs of extensive damage to the plenum assembly at

these locations, in contrast to modeling predictions. The temperature characterization of several leadscrews across the plenum assembly will spatially define core boundary temperatures to benchmark core degradation codes.

5. Characterization of the plenum assembly as a whole will help understand the convection recirculation between the degraded core and the plenum assembly. If recirculation occurs to the magnitude indicated by models, then (a) the plenum assembly has a major impact on the development of core damage and fission product movement, and (b) it should be traceable at TMI-2 via temperature mapping of the plenum assembly.
6. The closed-circuit television examinations of the core void region indicates asymmetric damage to the core and the underside of the plenum assembly.

## ACKNOWLEDGMENTS

The authors wish to thank the large number of individuals who contributed to the completion of this analysis effort. They include the hot cell and hot shop personnel, for cutting, brushing and visual examination; and D. V. Miley and G. E. Korth, for their contributions to the metallographic and SEM examinations. Other SEM and TEM work was performed by D. A. Pavlica, Westinghouse Idaho Nuclear Co. (WINCO), and L. H. Schoenlein. Contributors to the chemical and radiological analysis effort were T. R. Lyon (WINCO), for the ES and X-ray diffraction analysis, the Physical and Biological Sciences Division Radiological Measurements Laboratory staff for GS analysis; R. P. Schuman and C. P. Willis, for the development of the radiochemical methods; and R. W. Kanady, for health physics support. The authors thank M. D. Gorman, of ARMCO Research Center, for his advise to heat-treat 17-4 PH SS samples at the H900 condition. Thanks also go to Dr. M. L. Picklesimer, H. W. Garvin, and G. O. Hayner for their review and recommendations made for additional analyses to be performed on 17-4 PH and 304 SS standards. The authors acknowledge C. S. Caldwell, V. F. Baston, V. R. Fricke, J. C. Devine, Jr., R. D. Schmicker, and D. E. Owen for their review and comments. The authors sincerely thank Nancy L. Bergeman for typing the manuscript and J. O. Carlson for reviewing the report. Finally, the authors acknowledge the editor of this report, Nadine Wade, for her prompt and professional handling of the document.



## CONTENTS

ABSTRACT .....	ii
SUMMARY .....	iii
ACKNOWLEDGMENTS .....	xxviii
ACRONYMS AND CHEMICAL COMPOUNDS .....	xxxix
INTRODUCTION .....	1
LEADSCREW ACQUISITION, SAMPLE TYPES, AND ANALYTICAL TECHNIQUES .....	9
Leadscrew Acquisition .....	9
Design Description .....	9
Leadscrew Shipment .....	9
Sample Types .....	11
Analytical Techniques .....	18
Visual/Photography .....	18
Preliminary Temperature Estimates .....	18
Chemical Analyses .....	18
Radiological Analyses .....	20
RESULTS AND DISCUSSION .....	23
Visual Examination .....	23
H8 Leadscrew .....	23
B8 Leadscrew .....	27
Preliminary Temperature Estimates .....	27
H8 Leadscrew .....	30
H8 Surface Layers .....	44
B8 Leadscrew .....	51
B8 Surface Layers .....	61
Chemical Analyses .....	68
H8 Leadscrew Chemical Analyses .....	68
Brushoff Debris .....	68
Decontamination Solutions .....	71
Comparison of Brushoff Debris and Decontamination Solutions .....	74
Surface Samples .....	79

B8 Leadscrew Chemical Analyses .....	90
Brushoff Debris .....	90
Decontamination Solutions .....	94
Surface Samples .....	101
Radiological Analyses .....	105
H8 Leadscrew Radiological Analyses .....	110
Brushoff Debris Analysis .....	110
Decontamination Solutions .....	115
Summed Brushoff Debris and Decontamination Solution Surface Concentrations .....	122
Surface Sample Analysis Results .....	125
Core Inventory Deposition Fractions .....	130
B8 Leadscrew Radiological Analyses .....	134
Brushoff Debris .....	134
Decontamination Solutions .....	137
Summed Brushoff Debris and Decontamination Solution Surface Concentrations .....	142
Surface Samples .....	147
COMPARISON OF TEMPERATURES, ELEMENTAL BEHAVIOR, AND RADIONUCLIDE BEHAVIOR IN THE PLENUM REGION .....	151
Temperature Comparisons .....	151
Surface Layer Thickness Analysis .....	154
Chemical Analyses .....	157
Comparison of Radionuclide Analysis Results .....	161
PRINCIPAL OBSERVATIONS AND RECOMMENDATIONS .....	177
Observations .....	177
Recommendations .....	179
REFERENCES .....	184
APPENDIX A--ANNEALING STUDY OF 17-4 PH AND 304L SS STANDARDS .....	A-1

## FIGURES

S-1.	H8, B8, and E9 leadscrew locations in the TMI-2 core .....	iv
S-2.	A typical flow diagram depicting sample types and analytical techniques .....	vi
S-3.	A comparison of estimated surface temperatures on H8 and B8 leadscrews .....	x
S-4.	The concentrations of elements identified in brushoff debris at the H8 and B8 locations (wt%) .....	xi
S-5.	Surface radionuclide concentrations in brushoff debris, soluble and insoluble concentrations ( $\mu\text{Ci}/\text{cm}^2$ ) .....	xiv
S-6.	Total decontamination solution surface radionuclide concentrations in $\mu\text{Ci}/\text{cm}^2$ (soluble fractions in percent) .....	xvi
S-7.	Total surface radionuclide concentrations in $\mu\text{Ci}/\text{cm}^2$ (based on highest surface or summed sample concentrations) ....	xviii
S-8.	A comparison of retained radionuclides on the plenum assembly surfaces (core fraction in percent) .....	xix
1.	H8, B8, and E9 leadscrew locations in the TMI-2 core .....	2
2.	The sectioning and sampling diagram for the H8 leadscrew .....	4
3.	The sectioning and sampling diagram for the B8 leadscrew .....	5
4.	Surface deposition layer ( $<1 \mu\text{m}$ thick) on the TMI-2 leadscrew .....	7
5.	The hypothesized region of glassy adherent film formation on the plenum assembly surfaces including the leadscrews .....	8
6.	A schematic of a control rod drive leadscrew .....	10
7.	Photographs of the lower end of Section H8-9 .....	24
8.	Photographs of Section H8-7 .....	25
9.	Photograph of H8-2 section showing transition from 17-4 PH threaded portion to 304L SS extension piece (close to the top of the reactor head) .....	26
10.	Photographs of section B8-3 (close to the bottom of the plenum assembly) .....	28
11.	Photographs of section B8-1 (close to the top of the plenum assembly) .....	29

12.	Optical micrographs of H8 Samples 2 and 15 .....	33
13.	SEM micrographs of H8 Samples 2 and 15 .....	34
14.	Leadscrew hardness versus temperature for H8 and B8 Samples and standards heat-treated for 13 h .....	36
15.	SEM micrographs of H8 Sample 15 and a 17-4 PH SS commercial standard heat-treated for 13 h .....	37
16.	TEM micrographs of H8 Samples 11 and 15 and a standard at the H1100 condition .....	39
17.	SEM micrographs of heat-treated standards of H900, H950, and H1100 grain structure .....	41
18.	TEM micrographs of H8 Samples 2 and 4 .....	43
19.	SEM micrograph of Sample 7a (304 SS) microstructure .....	45
20.	SEM micrograph of standard A <sub>27</sub> from H8-2 section annealed at 1255K (1800°F) for 1 hour and air-quenched .....	45
21.	Macrographs of H8 surface Samples 3, 13, and 16 .....	47
22.	Micrographs of H8 Sample 3 showing surface layers .....	49
23.	Micrographs of H8 Sample 13 showing surface layers .....	52
24.	Micrographs of H8 Sample 16 showing surface layers .....	54
25.	Optical micrographs of grain structure in B8 Samples 2 and 7 .....	56
26.	SEM micrographs of grain structure in B8 Samples 2 and 7 .....	57
27.	Hardness versus isothermal holding temperature .....	59
28.	Macrographs of B8 surface Samples 3 and 8 .....	63
29.	Micrographs of B8 Sample 3 showing surface layers .....	64
30.	Micrographs of B8 Sample 8 showing surface layers .....	66
31.	SEM photographs of the smooth surface on H8 Sample 3 (close to the bottom of the plenum assembly) .....	81
32.	SEM photographs of the top threaded surface of H8 Sample 16 (close to top of the plenum assembly) .....	82
33.	SEM photographs of the bottom threaded surface of H8 Sample 16 (close to the top of the plenum assembly) .....	83

34.	EDS spectrum of the nodule shown in Figure 33(c) .....	86
35.	SEM micrograph of the smooth surface of H8 Sample 3 .....	88
36.	SEM micrographs of the top threaded surface from H8 Sample 16 .....	89
37.	SEM photographs of the smooth surface on B8 Sample 3 (close to the bottom of the plenum assembly) .....	102
38.	SEM photographs of the top threaded surface of B8 Sample 8 (close to the top of the plenum assembly) .....	103
39.	SEM photographs of the bottom threaded surface of B8 Sample 8 (close to the top of the plenum assembly) .....	104
40.	SEM micrograph of B8 Sample 3 surface layer on smooth surface .....	107
41.	SEM micrographs of B8 Sample 8 surface layers on (a) the thread top surface, (b) the thread face, and (c) the thread bottom surface .....	108
42.	Surface temperatures on H8 and B8 leadscrews .....	152
43.	Axial temperature profiles of the H8 and B8 leadscrews .....	155
44.	The thickness of the surface layers on the H8 and B8 leadscrews .....	156
45.	The concentrations of elements identified in the brushoff debris at the H8 and B8 leadscrew locations (wt%) .....	158
46.	The concentrations of soluble elements identified in the decontamination solutions (wt%) .....	159
47.	The concentrations of insoluble elements identified in the decontamination solutions (wt%) .....	160
48.	The total concentrations removed by decontamination ( $\mu\text{g}/\text{cm}^2$ ) .....	162
49.	The surface radionuclide concentrations in the brushoff debris ( $\mu\text{Ci}/\text{cm}^2$ ) .....	163
50.	The soluble radionuclide concentrations in the decontamination solutions ( $\mu\text{Ci}/\text{cm}^2$ ) .....	165
51.	The insoluble surface radionuclide concentrations in the decontamination solutions ( $\mu\text{Ci}/\text{cm}^2$ ) .....	166
52.	Total decontamination solution surface radionuclide concentrations in $\mu\text{Ci}/\text{cm}^2$ (soluble fraction in %) .....	167

53.	The total surface radionuclide concentrations based on highest surface or summed surface concentrations ( $\mu\text{Ci}/\text{cm}^2$ ) .....	169
54.	The comparison of retained radionuclides on plenum assembly surfaces (core fraction in %) .....	171
A-1.	The time-temperature matrix for 17-4 PH SS annealing study ....	A-4
A-2.	Optical micrographs of 17-4 PH SS Standards A <sub>11</sub> , A <sub>15</sub> , A <sub>16</sub> and A <sub>17</sub> .....	A-7
A-3.	Optical micrographs of 17-4 PH SS Standards A <sub>21</sub> , A <sub>22</sub> , A <sub>23</sub> , and A <sub>24</sub> .....	A-8
A-4.	Optical micrographs of 17-4 PH Standards A <sub>25</sub> , A <sub>26</sub> , A <sub>27</sub> and A <sub>28</sub> .....	A-9
A-5.	Optical micrograph of 17-4 PH SS Standards A <sub>29</sub> .....	A-10
A-6.	Optical micrographs of 17-4 PH SS Standards A <sub>31</sub> , A <sub>35</sub> , A <sub>36</sub> , and A <sub>37</sub> .....	A-11
A-7.	Optical micrographs of 17-4 PH SS Standards A <sub>41</sub> , A <sub>45</sub> , A <sub>46</sub> and A <sub>47</sub> .....	A-12
A-8.	SEM micrographs of 17-4 PH SS Standards A <sub>11</sub> , A <sub>15</sub> , A <sub>16</sub> , and A <sub>17</sub> .....	A-13
A-9.	SEM micrographs of 17-4 PH SS Standards A <sub>21</sub> , A <sub>22</sub> , A <sub>23</sub> and A <sub>24</sub> .....	A-14
A-10.	SEM micrographs of 17-4 PH SS Standards A <sub>25</sub> , A <sub>26</sub> , A <sub>27</sub> and A <sub>28</sub> .....	A-15
A-11.	SEM micrographs of 17-4 PH SS Standard A <sub>29</sub> .....	A-16
A-12.	SEM micrographs of 17-4 PH SS Standards A <sub>31</sub> , A <sub>35</sub> , A <sub>36</sub> and A <sub>37</sub> .....	A-17
A-13.	SEM micrographs of 17-4 PH SS Standards A <sub>41</sub> , A <sub>45</sub> , A <sub>46</sub> and A <sub>47</sub> .....	A-18
A-14.	A comparison of H8 Sample 2 and B8 Sample 2 with annealed Standards A <sub>27</sub> and A <sub>24</sub> .....	A-19
A-15.	Rockwell-B hardness versus temperature of 304L SS standards .....	A-22
A-16.	Optical micrographs of annealed 304L SS standards B <sub>11</sub> , B <sub>12</sub> and B <sub>13</sub> , and B8-A Hot Leg Sample 5 .....	A-23
A-17.	Optical micrographs of annealed Standards B <sub>14</sub> , B <sub>15</sub> , B <sub>16</sub> and B <sub>17</sub> .....	A-24

A-18.	SEM micrographs of annealed 304L SS Standards B <sub>11</sub> , B <sub>12</sub> , and B <sub>13</sub> , and B8-A Hot Leg Sample 5 .....	A-25
A-19.	SEM micrographs of annealed 304L SS Standards B <sub>14</sub> , B <sub>15</sub> , B <sub>16</sub> , and B <sub>17</sub> .....	A-26

TABLES

1.	Scheme for examination of H8 and B8 leadscrews .....	12
2.	H8 and B8 leadscrew cutting identification, component length, and component location .....	14
3.	Hardness of H8 and B8 leadscrew samples and commercial and annealed standards .....	31
4.	Surface layer thicknesses on H8 surface samples .....	46
5.	Surface layer thicknesses on B8 surface samples .....	62
6.	Core material composition .....	69
7.	Emission spectroscopic analysis of the brushoff debris from the H8 leadscrew (wt%) .....	70
8.	Emission spectroscopic analysis of the soluble portions of the decontamination solutions from the H8 leadscrew samples ( $\mu\text{g/mL}$ and total weight removed in mg) .....	72
9.	Emission spectroscopic analysis of the insoluble materials from the H8 leadscrew decontamination solutions (wt% and total weight removed in mg) .....	73
10.	Total elemental content removed by decontamination of H8 samples ( $\text{mg removed/cm}^2$ ) .....	75
11.	Element content from H8 leadscrew samples as determined from emission spectroscopy (atom ppm) .....	76
12.	H8 boron content (atom ppm) .....	78
13.	Qualitative elemental identification of H8 and B8 leadscrew surface samples .....	85
14.	Elemental composition of H8 leadscrew surface layers on Samples 3 and 16 (wt%) .....	87
15.	Elemental analysis of H8 and B8 leadscrew surface samples (wt%) .....	91
16.	Emission spectroscopic analysis of the brushoff debris from the B8 leadscrew (wt%) .....	92

17.	Emission spectroscopic analysis of the soluble portions of the B8 leadscrew decontamination solutions ( $\mu\text{g/mL}$ and total weight removed in mg) .....	95
18.	Emission spectroscopic analysis of insoluble materials from the B8 leadscrew decontamination solutions (wt% and total weight removed in mg) .....	96
19.	Percentages of total elemental content removed from B8 Sample 7 (%) .....	98
20.	Total elemental content removed by decontamination of B8 Samples 2 and 7 ( $\text{mg removed/cm}^2$ ) .....	99
21.	Element content from B8 leadscrew samples as determined from emission spectroscopy (atom ppm) .....	100
22.	Elemental composition of B8 leadscrew surface layers on Samples 3 and 8 (wt%) .....	106
23.	Radionuclide content of the H8 brushoff debris ( $\mu\text{Ci/mg}$ ) .....	111
24.	Radionuclide concentrations by particle size on H8-9 and H8-7 brushoff debris (% of total radionuclide content/gram of sample) .....	113
25.	H8 brushoff debris $^{90}\text{Sr}$ , $^{129}\text{I}$ (beta emitters), tellurium, and $^{235}\text{U}$ concentrations .....	114
26.	Gamma spectral analysis of the H8 decontamination solutions .....	116
27.	Comparison of total radionuclide concentrations in the H8 decontamination solids (insolubles in % of Sample 15 .....	121
28.	H8 leadscrew sample decontamination data for $^{90}\text{Sr}$ , $^{129}\text{I}$ (beta emitters), tellurium, and $^{235}\text{U}$ .....	123
29.	Surface radionuclide concentrations of leadscrew H8 brushoff debris ( $\mu\text{Ci/cm}^2$ ) .....	124
30.	H8 surface radionuclide concentrations from insoluble radionuclides ( $\mu\text{Ci/cm}^2$ ) .....	126
31.	H8 surface radionuclide concentrations from soluble radionuclides ( $\mu\text{Ci/cm}^2$ ) .....	127
32.	H8 brushoff debris contributions to total surface radionuclide concentrations (%) .....	128
33.	Total H8 surface radionuclide concentrations and radionuclide core inventory ( $\mu\text{Ci/cm}^2$ ) .....	129
34.	H8 leadscrew surface sample radionuclide content ( $\mu\text{Ci/cm}^2$ ) .....	131



35.	Surface radionuclide concentrations of H8 Sample 18 near the top of the reactor head ( $\mu\text{Ci}/\text{cm}^2$ ) .....	132
36.	Radionuclide deposition fractions (%) on plenum assembly surfaces from the H8 data .....	133
37.	Radionuclide deposition fractions (%) on the plenum assembly surfaces from the H8 surface samples .....	135
38.	Radionuclide content of the B8 brushoff debris ( $\mu\text{Ci}/\text{mg}$ ) .....	136
39.	B8 brushoff debris $^{90}\text{Sr}$ , $^{129}\text{I}$ , (beta emitters), tellurium, and $^{235}\text{U}$ concentrations ( $\mu\text{Ci}/\text{g}$ ) .....	138
40.	B8 leadscrew decontamination solution radionuclide concentrations .....	139
41.	B8 leadscrew sample decontamination data for $^{90}\text{Sr}$ , $^{129}\text{I}$ (beta emitters), tellurium, and $^{235}\text{U}$ .....	140
42.	B8 Sample 7 decontamination solution removal efficiencies .....	141
43.	Surface radionuclide concentrations of the B8 brushoff debris ( $\mu\text{Ci}/\text{cm}^2$ ) .....	143
44.	Surface radionuclide concentrations of B8 samples from decontamination solutions (soluble and insoluble fractions) ( $\mu\text{Ci}/\text{cm}^2$ ) .....	144
45.	Total radionuclide concentrations on the B8 leadscrew ( $\mu\text{Ci}/\text{cm}^2$ ) .....	145
46.	B8 brushoff debris contribution to total surface radionuclide concentration (%) .....	146
47.	Surface radionuclide concentrations based on B8 surface samples ( $\mu\text{Ci}/\text{cm}^2$ ) .....	148
48.	Radionuclide deposition fractions (%) on the plenum assembly surfaces from the B8 data .....	149
49.	Radionuclide deposition fractions on the plenum assembly surfaces from the B8 surface samples (%) .....	150
50.	Estimated temperatures on H8 and B8 leadscrews .....	153
51.	Fission-product-to- $^{235}\text{U}$ ratios for H8 and B8 brushoff debris .....	173
52.	Fission-product-to- $^{235}\text{U}$ ratios for H8 and B8 decontamination solutions .....	174

53.	Comparison of $^{137}\text{Cs}$ to $^{129}\text{I}$ atom ratios .....	176
A-1.	Rockwell-C hardness measurements from as-received and annealed 17-4 PH SS standards .....	A-5
A-2.	Rockwell-B hardness measurements from annealed 304L SS standards and samples .....	A-21

## ACRONYMS AND CHEMICAL COMPOUNDS

Å	angstrom
AD	tightly adherent deposition layer
Ag-In-Cd	silver-indium-cadmium control material
B <sub>4</sub> C-Al <sub>2</sub> O <sub>3</sub>	poison material from the Burnable Poison Rod Assemblies
B&W	Babcock and Wilcox Co.
B8	core grid position B8--also refers to leadscrew B8
Ba(OH) <sub>2</sub>	barium hydroxide
B <sub>2</sub> O <sub>3</sub>	boron oxide
BaO	barium oxide
CsI	cesium iodide
CsOH	cesium hydroxide
Ci	curies
DOE	Department of Energy
EDS	energy dispersive spectroscopy
ES	emission spectroscopy
F	degree fahrenheit (temperature)
Fe <sub>3</sub> O <sub>4</sub>	magnetite
GEND	General Public Utilities Nuclear Corp., Electric Power Research Institute, Nuclear Regulatory Commission, and Department of Energy
GS	gamma spectroscopy
H <sub>2</sub> C <sub>2</sub> O <sub>4</sub>	oxalic acid
H8	core grid position H8 (center)--also refers to leadscrew H8

HF	hydrofluoric acid
HNO <sub>3</sub>	nitric acid
ICP	inductively coupled plasma spectroscopy
INEL	Idaho National Engineering Laboratory
K	degree kelvin (temperature)
KMnO <sub>4</sub>	potassium permanganate
KeV	one thousand electron volts (unit)
LAD	loosely adherent deposition layer
<u>M</u>	molar
MWd/t	megawatt days per metric ton
μ	micro or 10 <sup>-6</sup>
μCi	microcuries
μCi/cm <sup>2</sup>	microcuries per square centimeter
μCi/g	microcuries per gram
μg	microgram
μg/mL	micrograms per milliliter
μm	micrometer
mg	milligram
mL	milliliters
NAA	neutron activation analysis
(NH <sub>4</sub> ) <sub>2</sub> HC <sub>6</sub> H <sub>5</sub> O <sub>7</sub>	dibasic ammonium citrate
NRC	Nuclear Regulatory Commission
NaOH	sodium hydroxide
ORIGEN2	Oak Ridge isotope generation and depletion code
PNL	Pacific Northwest Laboratory
ppm	parts per million
PVC	polyvinyl chloride

Rb	Rockwell-B (hardness)
Rc	Rockwell-C (hardness)
SEM	scanning electron microscopy
SEM/EDS	scanning electron microscopy with energy dispersive spectroscopy
STEM	scanning transmission electron microscopy
TEM	transmission electron microscopy
TMI-2	Three Mile Island Unit 2
TTT	time-temperature-transformation diagram
UO <sub>2</sub>	uranium dioxide (fuel pellets material)
WINCO	Westinghouse Idaho Nuclear Co.
wt%	weight percent
ZrO <sub>2</sub>	zirconium dioxide
304 SS	304 stainless steel
304L SS	low carbon 304 stainless steel
17-4 PH	17-4 precipitation hardened stainless steel
410 SS	410 stainless steel



PRELIMINARY REPORT: EXAMINATION of H8 AND B8 LEADSCREWS FROM  
THREE MILE ISLAND UNIT 2 (TMI-2)

INTRODUCTION

On March 28, 1979, the Three Mile Island Unit 2 (TMI-2) pressurized water reactor underwent an accident that resulted in severe damage to the reactor core. As a consequence of the TMI-2 accident, numerous aspects of light-water-reactor safety have been questioned; and the U.S. Nuclear Regulatory Commission (NRC) has embarked on a thorough review of reactor safety issues, particularly the causes and effects of core damage accidents. The nuclear community generally acknowledges the importance of examining TMI-2 in order to understand the nature of the core damage and fission product release from the fuel, and transport and deposition of fission products within the primary coolant system and containment. About one year after the TMI-2 accident, four organizations with interests in both plant recovery and accident data acquisition formally agreed to cooperate in these areas. These organizations [General Public Utilities Nuclear Corp. (GPU Nuclear), Electric Power Research Institute (EPRI), the NRC, and the Department of Energy (DOE)], collectively referred to as the GEND Group, are actively involved in reactor recovery and accident research. At present, DOE is providing a portion of the funds for reactor recovery (in those areas where accident recovery knowledge will be of generic benefit to the U.S. light-water-reactor industry), as well as the preponderance of funds for severe accident technical data acquisition (such as the examination of the damaged core).

A TMI-2 Core Examination Plan<sup>1</sup> has been prepared, which describes what technical/scientific data should be acquired during the TMI-2 core examination and how these data will be used to address specific reactor safety issues.<sup>2,3</sup> One of the TMI-2 Core Examination Plan tasks is the inspection of the control rod drive leadscrews which were removed from the reactor head as part of the July 1982 closed-circuit television inspection of the damaged core.<sup>4</sup> Leadscrews were removed from positions H8 (at the center of the core), B8 (near the outer edge), and E9 (approximately midradius), as shown in Figure 1. The objectives of the H8 and B8

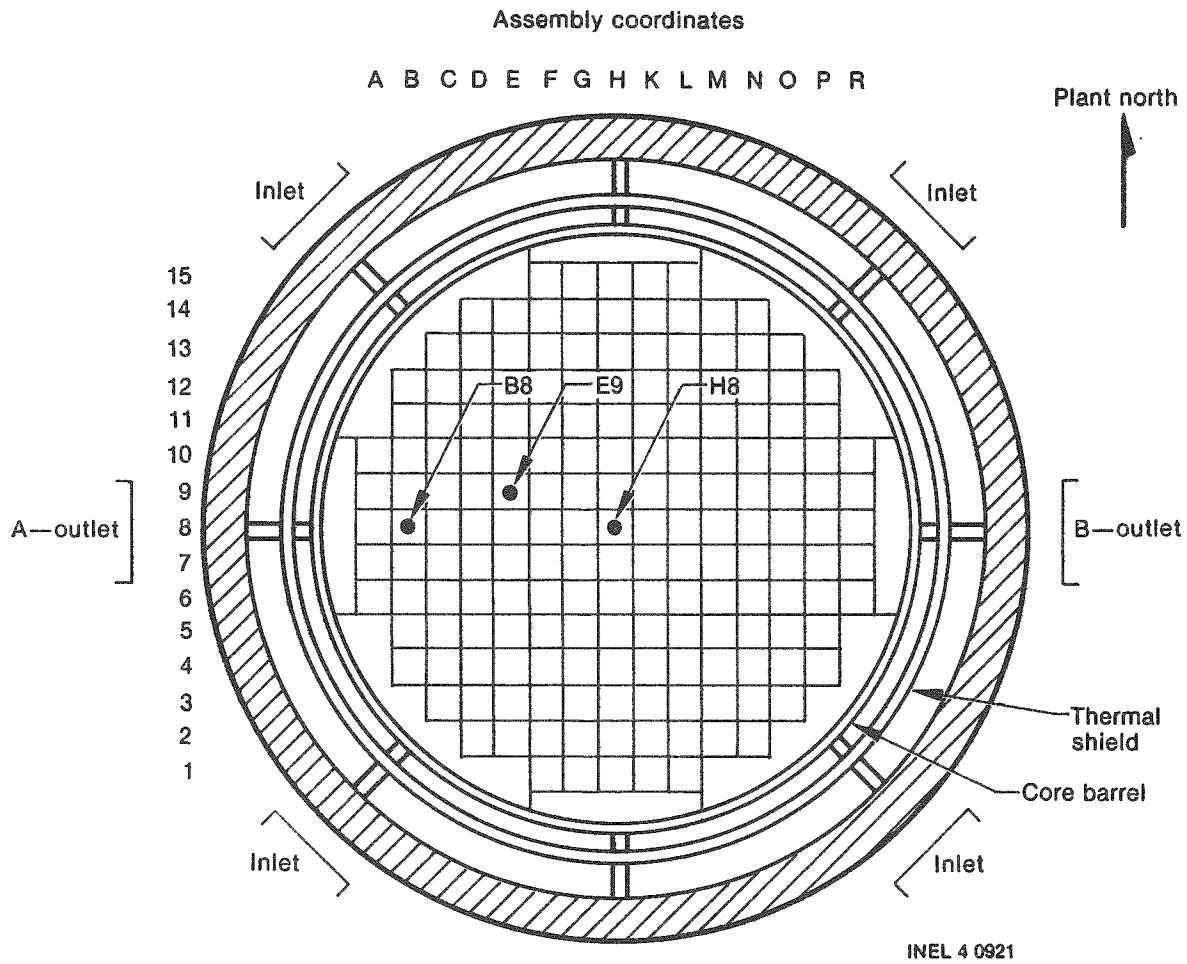


Figure 1. H8, B8, and E9 leadscrew locations in the TMI-2 core.



leadscrew examinations at the INEL are: (a) to estimate the maximum temperature experienced along the length of the leadscrew in the plenum assembly region; and (b) to determine the extent and nature of the core component material and radionuclide deposition. The examination is designed to provide data to help estimate structural temperatures in the plenum assembly and to determine the chemical and radioisotopic characteristics of the materials deposited in the plenum assembly region. The results contribute to an improved understanding of core boundary temperature conditions and fission-product release, transport, and deposition during the accident, which is necessary to define the degraded core accident progression and fission-product source terms in such accidents. The data on fission-product plateout in the plenum assembly are also useful in assessing fission-product behavior codes, such as TRAP-MELT,<sup>5</sup> and will be helpful in evaluating proposed methods to decontaminate the TMI-2 assembly components.

At TMI-2, the leadscrews were cut into several sections; Figures 2 and 3 show the H8 and B8 leadscrew sections, respectively. One 0.23-m (9-in.) section, H8-4, and several decontamination samples were examined by PNL; a 0.23-m (9-in.) section, H8-5, was analyzed by B&W; and a 0.30-m (12-in.) section, H8-6, was examined by GPU Nuclear. The remaining portions of the H8 leadscrew and the sections from B8 were examined at the INEL. Examination of E9 has not been planned at this time.

The initial analyses performed by PNL<sup>6</sup> on the 0.23-m (9-in.) H8 leadscrew section concentrated on the detection of pyrophoric material. The reported data by PNL indicate that pyrophoricity is of minimum concern. Results<sup>7</sup> from the B&W examination indicate that radionuclide contamination on section H8-5 was contained in two distinct outer and inner surface layers. Approximately 85% of the <sup>90</sup>Sr activity was in the outer loosely adherent deposition layer (LAD) and 15% in the inner tightly adherent deposition layer (AD). About 10% of the <sup>134</sup>Cs and <sup>137</sup>Cs activity was in the outer LAD and 90% in the AD. Chemical leaching of the GPU Nuclear segment<sup>8,9,10</sup> indicated that the radioactive cesium was tightly bound to the surface, and an aggressive acid solution (HNO<sub>3</sub>-HF) was required for removal of the cesium activity. Hofstetter et al.,<sup>8</sup>

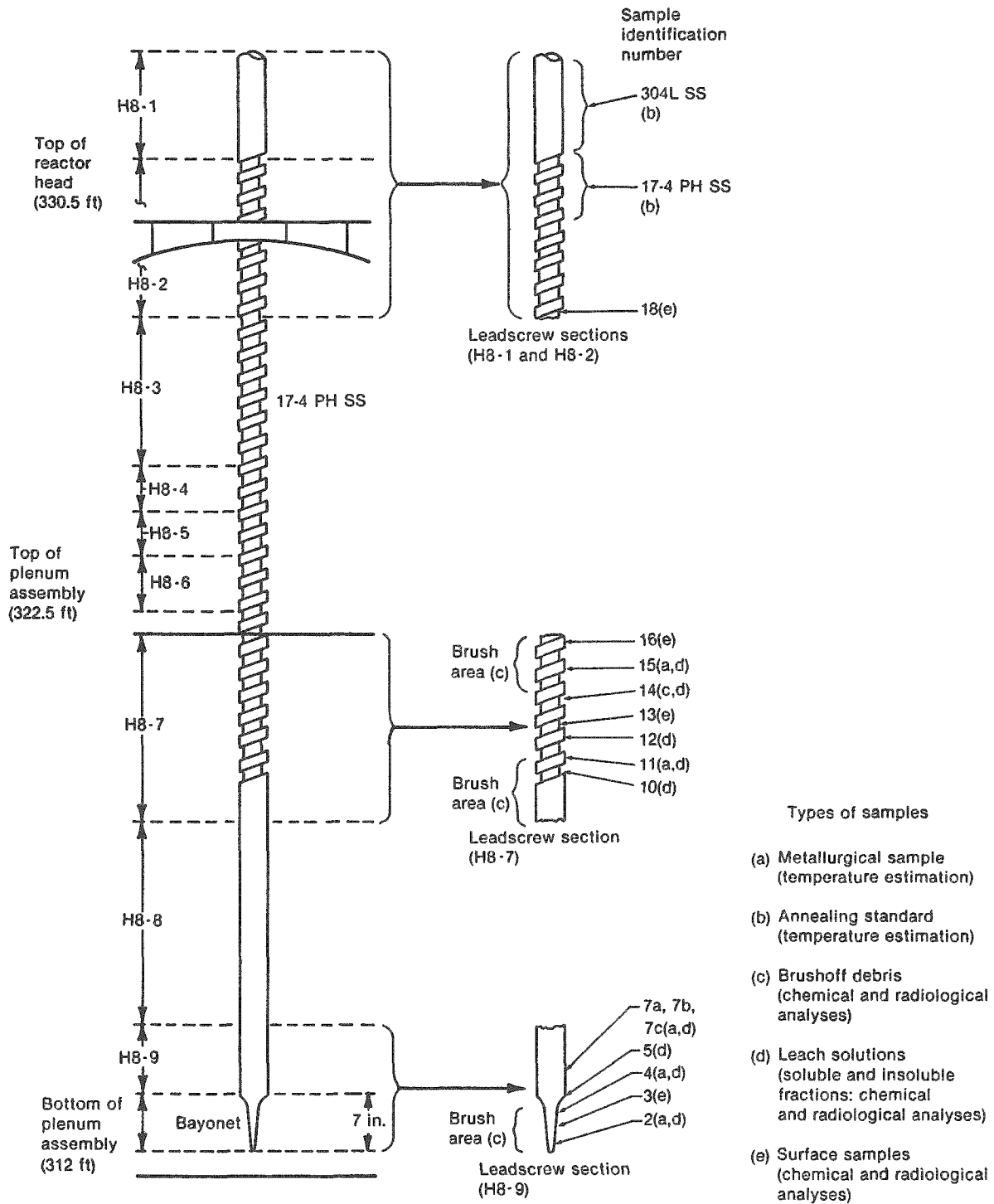


Figure 2. The sectioning and sampling diagram for the H8 leadscrew.

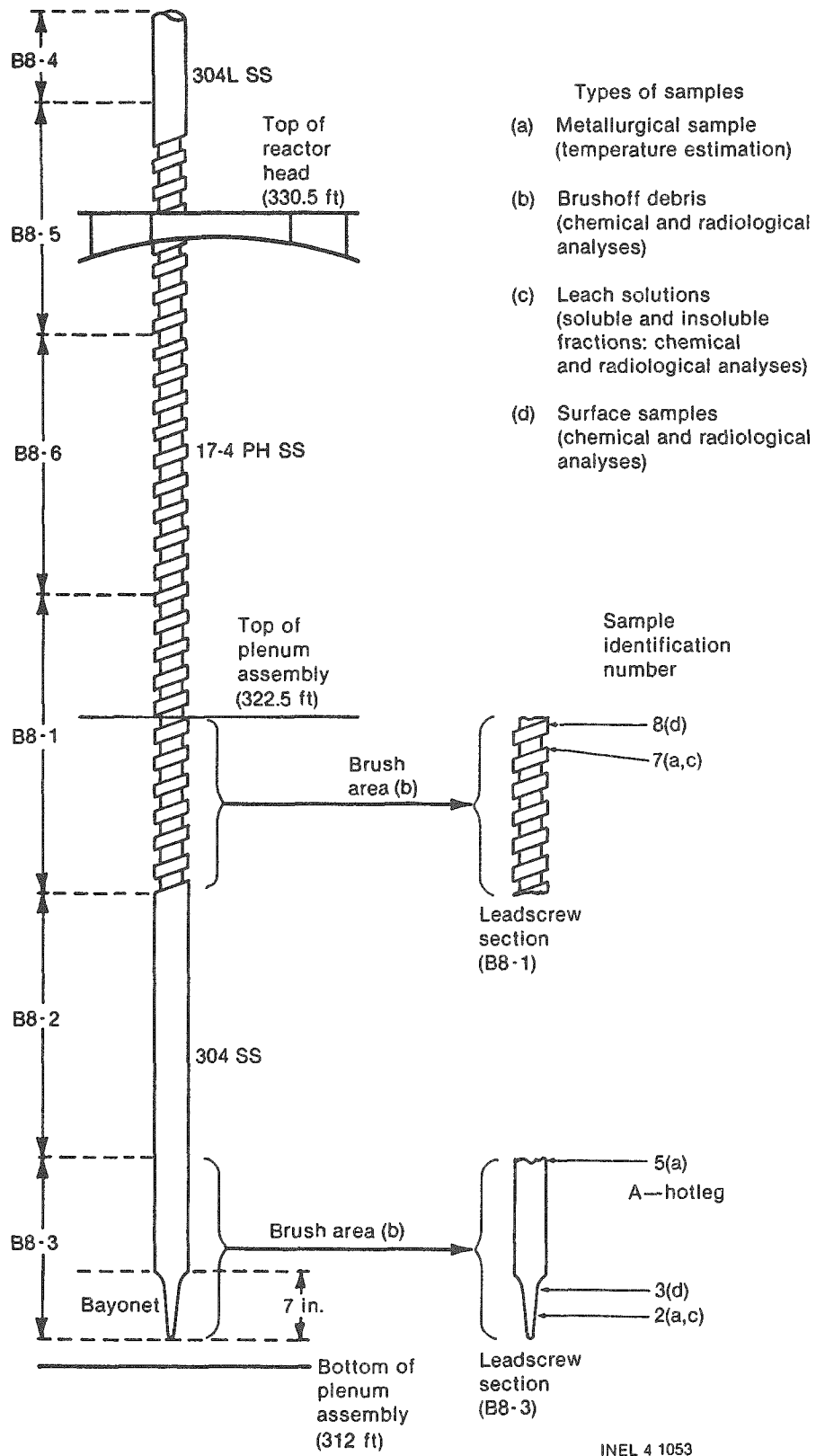
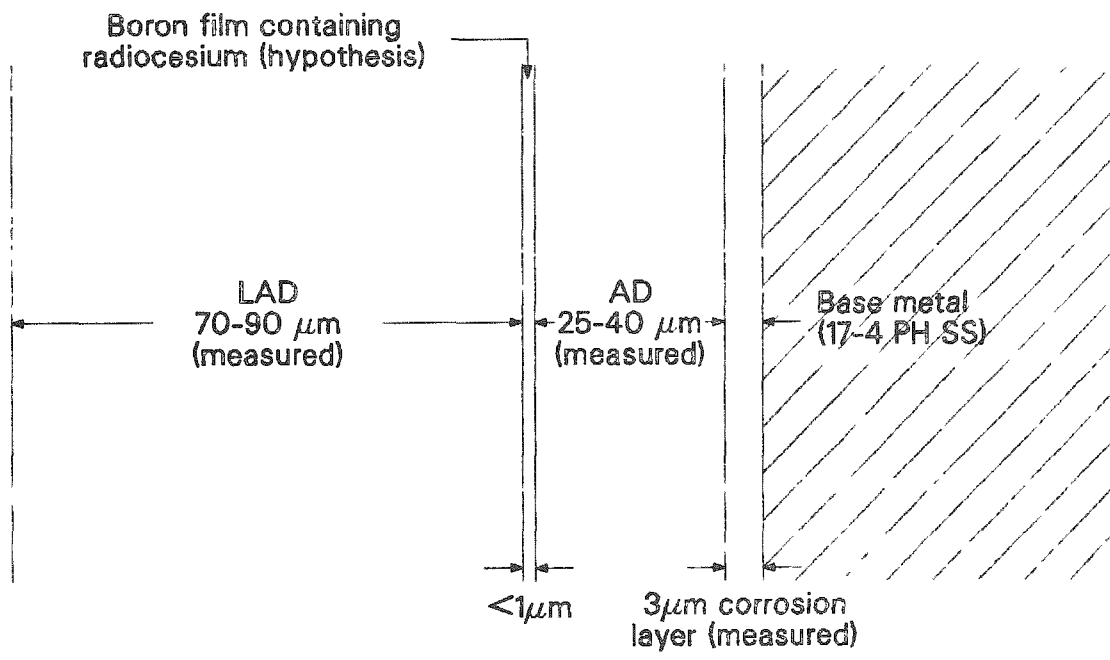


Figure 3. The sectioning and sampling diagram for the B8 leadscrew.

have hypothesized that radiocesium is chemically bound within a boron film less than 1  $\mu\text{m}$  thick between the AD and LAD layers, as shown in Figure 4. Chemical vapor deposition of a thin boron film may have occurred during the high-temperature transient, which entrained the available cesium vapor and particulates into a thin, glassy deposit on AD which is enriched in chromium relative to the 17-4 PH base metal. A source of boron (boric acid) existed during the accident. Boric acid decomposes at 573 K (572°F) and may exist as anhydrous boron oxide ( $\text{B}_2\text{O}_3$ ), which may react with fission product vapors (iodine, cesium, tellurium, etc.). Both cesium hydroxide ( $\text{CsOH}$ ) and cesium iodide ( $\text{CsI}$ ) react with  $\text{B}_2\text{O}_3$  to give cesium borate.<sup>11</sup> R. P. Wichner and R. D. Spence<sup>11</sup> indicate that cesium released from the fuel will be tied up as a borate that may serve as an aerosol source.

Buchanan<sup>12</sup> has also hypothesized that a glassy, tightly adherent film was formed on the upper plenum surfaces (including leadscrews) in the region shown in Figure 5. The shaded area of the plenum assembly may not have been subjected to the tightly adherent film. This hypothesis suggests that the components in the shaded area may be easily decontaminated with conventional techniques. Examination of leadscrews located in and out of the shaded area may provide an assessment of this hypothesis.

The results of the H8 and B8 leadscrew examinations and analyses are presented in this report in the following order: (a) a brief discussion of leadscrew acquisition, the types of samples, and analytical techniques used; (b) results and a discussion of the visual examination, temperature estimates, and chemical and radiological analyses; (c) a comparison of the temperatures, elemental behavior, and radionuclide behavior in the plenum assembly region; and (d) observations and recommendations resulting from the study. Details of the annealing studies performed at INEL on 17-4 PH and 304L SS standards from the H8-2 leadscrew section are presented in Appendix A.



ALA84063-1A

Figure 4. Surface deposition layer (<1  $\mu\text{m}$  thick) on the TMI-2 leadscrews.

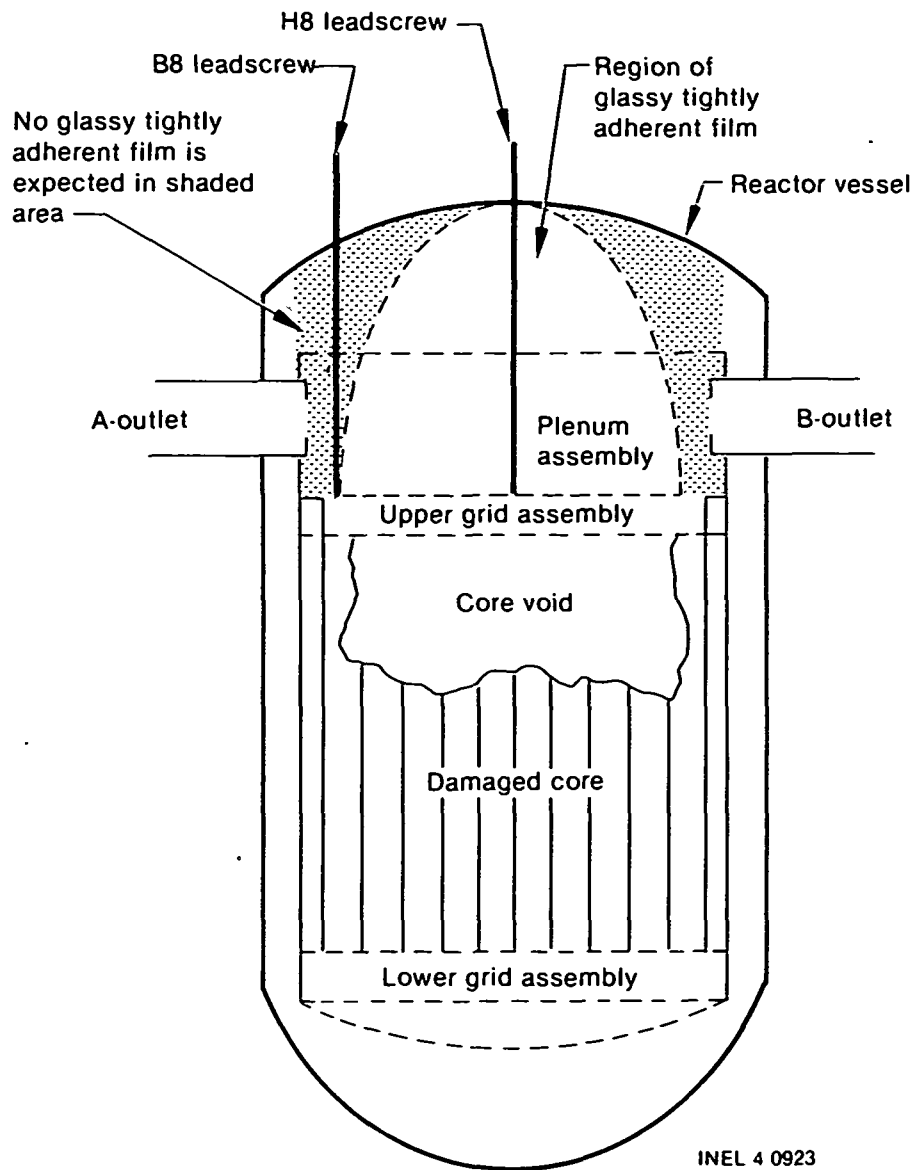


Figure 5. The hypothesized region of glassy adherent film formation on the plenum assembly surfaces including the lead screws.

## LEADSCREW ACQUISITION, SAMPLE TYPES, AND ANALYTICAL TECHNIQUES

This section discusses how the leadscrews were removed from TMI-2 and shipped to the INEL, how the various types of examination samples were acquired, and what types of analytical techniques were used to examine the leadscrews.

### Leadscrew Acquisition

#### Design Description

Leadscrews are part of the control rod drive system used to raise and lower the control rods in the reactor core region. A schematic of a leadscrew is shown in Figure 6. It is comprised of four major components; a male coupling, Type 17-4 PH SS, 18 cm (7 in.) long; a lower extension, 304 SS, 193 cm (76 in.) long; a threaded section, 17-4 PH SS, 384 cm (151 in.) long; and an upper extension, 304L SS, 137 cm (54 in.) long. All leadscrews were fully inserted during the high-temperature transient.

#### Leadscrew Shipment

Three leadscrews from core positions H8 (center), B8 (periphery of core at A-Hot Leg), and E9 (midradius) were removed as part of the July 1982 closed-circuit television inspection of the damaged core. Following their removal, GPU Nuclear cut the leadscrews into short, manageable lengths (sections) approximately 120 cm (4 ft) long. Each section was gamma-scanned to determine the general distribution of gamma-emitting radionuclides. Three short [23-30 cm (9-12 in.)] sections from just above the midregion of leadscrew H8 were examined by PNL, B&W, and GPU Nuclear. All sections from leadscrews B8, E9, and the remainder from H8 were individually bagged in polyethylene sleeving and inserted into premarked, 10-cm (4-in.) dia, polyvinyl chloride (PVC) tubes. The tubes were sealed and placed inside shielded 110-gal drums (three per drum) and shipped to the INEL.

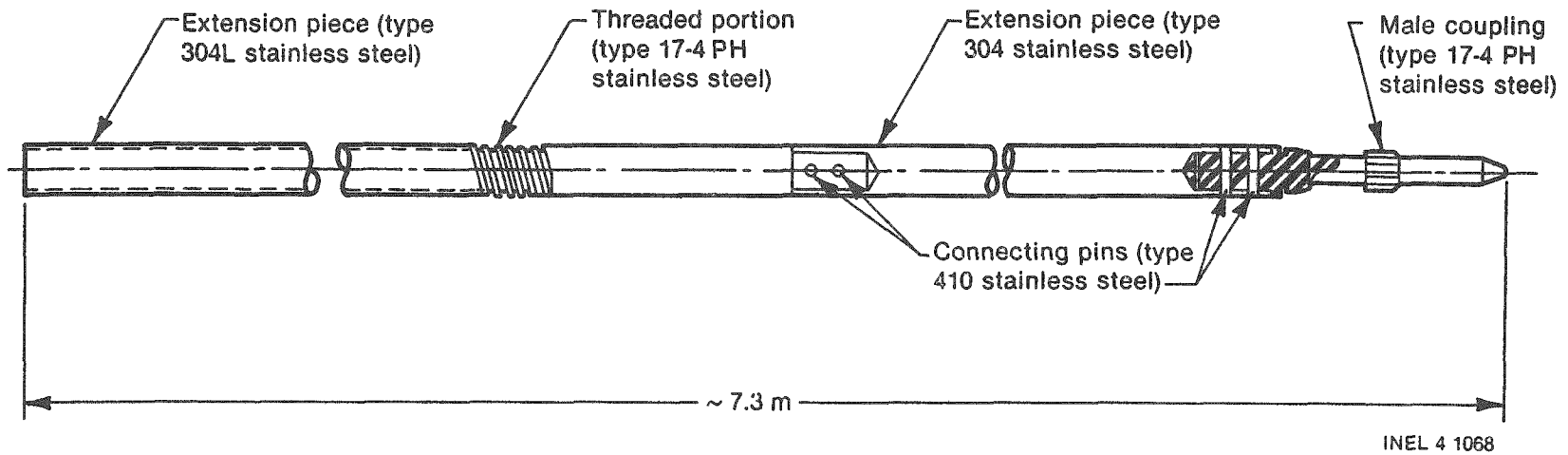


Figure 6. A schematic of a control rod drive leadscrew.



## Sample Types

At the INEL hot cells, selected sections from the H8 and B8 leadscrews were unpackaged and visually examined. Various types of samples were acquired for follow-up examination. Figures 2 and 3 and Table 1 show the types of samples and summarize the analytical techniques used during examination. Samples were removed from H8 sections H8-9, H8-8, H8-7, H8-2, and H8-1 and from B8 sections B8-3 and B8-1. Table 2 lists the sample designations, lengths, and locations (distance from bottom of leadscrew).

The types of samples and methods of obtaining them are summarized below:

1. Brushoff Debris--A layer of fine, loosely adherent debris was attached to the outer surface of the leadscrews. The loosely adherent debris layer is consistent with the loosely adherent surface deposits (LAD) defined by GPU/B&W.<sup>8</sup> Some of the debris had been rubbed off or jarred loose from the leadscrews during packaging, shipping, and unpackaging the leadscrew sections. This dislodged debris was collected from the polyethylene wrapping and included as part of the brushoff debris samples.

In addition, designated areas on some of the leadscrew sections were brushed using a stiff-bristled nylon brush. Little debris was present on the lower sections of the H8 and B8 leadscrews; in order to obtain an adequate amount of debris for examination, the sections required rigorous brushing to remove most of the available material. Significantly more loose debris was present on the higher sections located near the top of the plenum assembly; therefore, the brushing process for these sections was not as rigorous as for the lower sections. The collected debris were sent to the Test Reactor Area (TRA) physics laboratory for chemical and radiological examination.

The brushoff debris samples retained the same number as the leadscrew sections and/or samples they were removed from. The samples used were: H8-9, H8-8, H8-7, H8 Sample 3, H8 Sample 14,

TABLE 1. SCHEME FOR EXAMINATION OF H8 AND B8 LEADSCREWS

Task	Types of Examination Samples/Standards	
	H8	B8
I Temperature estimates	<u>Decontaminated Metallurgical Samples</u>	
1. Metallography	2, 4, 7a (304 SS), 11, 15	2, 5, 7
2. SEM	2, 4, 7a (304 SS), 11, 15	2, 5, 7
3. TEM	2, 4, 11, 15	2, 7
II Temperature estimates	<u>Annealing Standards<sup>a</sup></u>	
1. Metallography	H8-17, H8-19, H8-20, H8-21, H8-22	--
2. SEM	H8-17, H8-19, H8-20, H8-21, H8-22	--
3. TEM	H8-19, H8-20	--
III Chemical and radiological analysis	<u>Brushoff Debris From Sections and Samples<sup>a</sup></u>	
1. Emission spectroscopy	H8-7, H8-8, H8-9, 14, 15	B8-1, B8-3
2. X-ray diffraction	H8-7, H8-8, H8-9	B8-1, B8-3
3. Gamma spectroscopy	H8-7, H8-8, H8-9, 14, 15	B8-1, B8-3
4. Neutron activation and delayed neutron counting for fissile material analysis	H8-7, H8-9	B8-1, B8-3
5. Strontium analysis	3, H8-7, H8-9	B8-1, B8-3
6. Tellurium analysis	H8-7, H8-9	B8-1, B8-3
7. Iodine-129 analysis	H8-7, H8-9	B8-1, B8-3
IV Chemical and radiological analyses	<u>Leach Solutions</u>	
1. Emission spectroscopy	2, 7a (304 SS), 7b (410 SS), 7c (304 SS and 17-4 PH), 11, 14, 15	2, 7
2. X-ray diffraction	2, 7a (304 SS), 7b (410 SS), 7c (304 SS and 17-4 PH), 11, 14.1, 14.2, 15	--
3. Gamma spectroscopy	2, 4, 5, 7a, 7b, 7c, 10, 11, 12, 14, 15	2, 7
4. Neutron activation and delayed neutron counting for fissile material analysis	2, 15	2, 7
5. Strontium analysis	2, 15, 7	2, 7

TABLE 1. (continued)

Task	Types of Examination Samples/Standards	
	H8	B8
IV Chemical and radiological analyses (continued)	Leach Solutions	
6. Tellurium analysis	2, 15	2, 7
7. Iodine-129 analysis	2, 15	2, 7
V Chemical and radiological analysis	Surface Sample	
1. SEM	3, 13, 16	3, 8
2. Emission spectroscopy	3, 13, 16	3, 8
3. X-ray diffraction	3, 13, 16	3, 8
4. Gamma spectroscopy	3, 13, 16, 18,	3, 8
5. I, Te, Sr, <sup>235</sup> U	3, 13, 16	3, 8

a. H8-7, H8-8, H8-9, H8-17, H8-19, H8-20, H8-21, H8-22, B8-1, and B8-3 are sections from which standards or samples were removed for examination.

TABLE 2. H8 AND B8 LEADSCREW CUTTING IDENTIFICATION, COMPONENT LENGTH, AND COMPONENT LOCATION

Section Number <sup>a</sup>	Component Identification Number	Material	Component Length		Distance From Bottom of Leadscrew	
			cm	(in.)	cm	(in.) <sup>b</sup>
H8-9, 81.28 cm long (32 in.)	1 <sup>c</sup>	17-4 pH	2.54	(1.0)	0.00 - 2.54	(0.00 - 1.00)
	2	17-4 pH	1.91	(0.75)	2.54 - 4.45	(1.0 - 1.75)
	3	17-4 pH	0.635	(0.25)	4.450 - 5.085	(1.75 - 2.00)
	3A	17-4 PH	8.255	(3.25)	5.085 - 13.340	(2.00 - 5.25)
	4	17-4 pH	1.91	(0.75)	13.34 - 15.24	(5.25 - 6.00)
	5 <sup>c</sup>	17-4 pH	1.91	(0.75)	15.24 - 17.15	(6.00 - 6.75)
	6 <sup>c</sup>	-- <sup>d</sup>	3.81	(1.5)	17.15 - 20.96	(6.75 - 8.25)
	7a	304 SS	3.81	(1.5)	20.96 - 22.86	(8.25 - 9.00)
	7b	410 SS	3.81	(1.5)	20.96 - 22.86	(8.25 - 9.00)
	7c	304 SS and 17-4 pH	3.81	(1.5)	20.96 - 22.86	(8.25 - 9.00)
	8 <sup>c</sup>	-- <sup>c</sup>	2.54	(1.0)	22.86 - 25.40	(9.00 - 10.0)
	DECON 1	304 SS	27.94	(11.0)	25.40 - 53.34	(10.0 - 21.0)
	DECON 2	304 SS	27.94	(11.0)	53.34 - 81.28	(21.0 - 32.0)
	H8-8, 121.92 cm long (48 in.)	DECON 3	304 SS	30.48	(12.0)	81.28 - 111.76
DECON 4		304 SS	30.48	(12.0)	111.76 - 142.24	(44.0 - 56.0)
DECON 5		304 SS	30.48	(12.0)	142.24 - 172.72	(56.0 - 68.0)
DECON 6		304 SS	30.48	(12.0)	172.72 - 203.20	(68.0 - 80.0)
H8-7, 114.3 cm long (45 in.)	9 <sup>c</sup>	-- <sup>d</sup>	5.08	(2.0)	203.20 - 208.28	(80.0 - 82.0)
	10	-- <sup>d</sup>	2.54	(1.0)	208.28 - 210.82	(82.0 - 83.0)
	DECON 7	17-4 pH	18.42	(7.25)	210.82 - 229.24	(83.0 - 90.25)
	11	17-4 pH	1.91	(0.75)	229.24 - 231.14	(90.25 - 91.0)
	12	17-4 pH	1.91	(0.75)	231.14 - 233.05	(91.0 - 91.75)
	13	17-4 pH	0.64	(0.25)	233.05 - 233.68	(91.75 - 92.0)
	DECON 8	17-4 pH	33.02	(13.0)	233.68 - 245.36	(92.0 - 105.0)
	14	17-4 pH	1.91	(0.75)	245.36 - 268.61	(105.0 - 105.75)
	DECON 9	17-4 pH	33.66	(13.25)	268.61 - 302.26	(105.75 - 119.0)
	15	17-4 pH	1.91	(0.75)	302.26 - 302.90	(119.0 - 119.25)
16	17-4 pH	0.64	(0.25)	302.90 - 304.80	(119.25 - 120.0)	
DECON 10	17-4 pH	12.70	(5.0)	304.80 - 317.50	(120.0 - 125.0)	

TABLE 2. (continued)

Section Number <sup>a</sup>	Component Identification Number	Material	Component Length		Distance From Bottom of Leadscrew	
			cm	(in.)	cm	(in.) <sup>b</sup>
H8-2, 128.27 cm long (50.5 in.)	18 <sup>C</sup>	17-4 pH	1.91	(0.75)	528.32 - 530.23	(208.0 - 208.75)
	17	17-4 pH	26.04	(10.25)	530.23 - 556.26	(208.75 - 219.0)
	19	17-4 pH	26.04	(10.25)	556.26 - 582.29	(219.0 - 229.25)
	20	17-4 pH	12.70	(5.0)	582.29 - 595.00	(229.25 - 234.25)
	22	17-4 pH	1.91	(0.75)	595.00 - 596.90	(234.25 - 235.0)
	21	304 SS	30.48	(12.0)	596.90 - 627.38	(235.0 - 247.0)
	23	304 SS	29.21	(11.5)	627.38 - 656.59	(247.0 - 258.5)
B8-3, 121.92 cm long (48 in.)	1 <sup>C</sup>	17-4 pH	2.54	(1.0)	0.00 - 2.54	(0.00 - 1.00)
	2	17-4 pH	1.91	(0.75)	2.54 - 4.45	(1.00 - 1.75)
	3	17-4 pH	0.635	(0.25)	4.450 - 5.085	(1.75 - 2.00)
	3A	17-4 PH	6.985	(2.75)	5.085 - 12.070	(2.00 - 4.75)
	4 <sup>C</sup>	17-4 pH	1.91	(0.75)	12.07 - 13.97	(4.75 - 5.50)
	5A	304 SS	83.19	(32.75)	13.97 - 97.16	(5.50 - 38.25)
	5 <sup>e</sup>	304 SS	1.90	(0.75)	38.25 - 99.06	(38.25 - 39.0)
5B	304 SS	22.86	(9.0)	99.06 - 121.92	(39.0 - 48.0)	
B8-1, 121.92 cm long (48 in.)	6 <sup>C</sup>	17-4 pH	58.42	(23.0)	243.84 - 302.26	(96.0 - 119.0)
	7	17-4 pH	1.91	(0.75)	302.26 - 304.17	(119.0 - 119.75)
	8	17-4 pH	0.64	(0.25)	304.17 - 304.80	(119.75 - 120.0)
	9 <sup>C</sup>	17-4 pH	60.96	(24.0)	304.80 - 365.76	(120.0 - 144.0)

a. The sample numbers referred throughout this report are the same as the section and/or component numbers. For example, component Number 2 from H8 Section 9 (H8-9) is H8 Sample 2.

b. The bottom of the leadscrews were 15.24 cm (6 in.) above the bottom of plenum assembly.

c. Archive sample.

d. Indicated components contain a combination of materials, i.e., 17-4 pH, 304, and 410 SS pins.

e. 304 SS sample near A-hot leg.

H8 Sample 15, B8-3, and B8-1. Two samples, H8-7 and H8-9, were particle sized by sieving the samples into a number of progressively smaller particle-sized groups. Each size fraction was independently analyzed.

2. Metallurgical Samples--Metallurgical samples were cut from designated axial locations along the leadscrews using a reciprocating hacksaw. These samples were approximately 2 cm (0.75 in.) thick and were removed from the "brushed" areas of the leadscrew sections. After cutting, the samples were decontaminated to remove the surface deposits and to reduce the radiation levels to zero. The samples were subsequently cross-sectioned into smaller sized pieces which were used to study the temperature history of the leadscrews. The samples used were: H8 numbers 2, 4, 7a, 11, and 15 and B8 numbers 2, 5, and 7.
3. Decontamination Solutions--After cutting, the pieces designated as "metallurgical samples" were decontaminated using acid solutions to remove the surface deposits. The resulting decontamination solutions contained visible amounts of solid (insoluble) materials. The solids were separated from the liquid by filtering the solutions through a 0.45- $\mu$ m vacuum filter system. The resulting solids are referred to as "insolubles" and the liquids as "solubles". These samples should not be compared to the adherent surfaces deposit (AD) layers as defined by GPU/B&W.<sup>8</sup>

All samples except B8 Sample 7 were decontaminated using a 40-wt%  $\text{HNO}_3$  + 0.12-M HF (nitric + hydrofluoric acid) solution at elevated temperatures, [ $\sim 363$  K (194°F)], for approximately one hour. B8 Sample 7 was decontaminated using a serial decontamination technique with progressively stronger agents. The solutions in order of use are:

- 10-wt% sodium hydroxide plus 3-wt% potassium permanganate ( $\text{NaOH} + \text{KMnO}_4$ )

- 25-g/L oxalic acid plus 50-g/L dibasic ammonium citrate  
( $\text{H}_2\text{C}_2\text{O}_4 + (\text{NH}_4)_2\text{HC}_6\text{H}_5\text{O}_7$ )
- 40-wt% nitric acid plus 0.12-M hydrofluoric acid ( $\text{HNO}_3 + \text{HF}$ )

These decontamination agents were used at the recommendation of GPU Nuclear for comparison purposes with data obtained from other examination sources. The decontamination temperature was approximately 363 K (194°F).

The samples used to obtain decontamination solutions for examination were: H8 Samples 2, 4, 5, 7a, 7b, 7c, 10, 11, 12, 14, and 15 and B8 Samples 2 and 7. H8 Sample 14 required two decontaminations to remove the surface deposit.

4. Surface Sample--The surface samples are 0.635 cm (0.25 in.) long samples cut from the "brushed" areas of designated leadscrew sections using a reciprocating hacksaw. The brushing process was minimal at the surface sample locations, leaving some of the loosely adherent debris intact. The surface samples used were H8 Samples 3, 13, 16, and 18 and B8 Samples 3 and 8. These samples may correspond somewhat to GPU/B&W's LAD + AD.
5. Annealing Standards--In order to estimate the temperature history of the metallurgical samples, a set of annealing standards was developed, using the same types of materials as the examination samples. The materials used for the annealing standards were: (a) commercial 17-4 PH SS Condition A, (b) commercial 304 SS, and (c) pieces removed from the upper end of the threaded, 17-4 PH, and smooth 304L SS portions of the H8 leadscrew. The upper end of the H8 leadscrew was used because it was representative of the samples being analyzed and because the region those standards were removed from was located far enough away from the high-temperature zone to be structurally unaffected by the TMI-2 accident.

Appendix A discusses the development of the annealing standards in detail.

### Analytical Techniques

Table 1 and Figures 2 and 3 outline the types of samples/standards and the analytical techniques used to examine each type. The following is a brief overview of the analytical techniques used.

#### Visual/Photography

The leadscrew sections were visually examined and photographed through the hot cell periscope.

#### Preliminary Temperature Estimates

Metallography and SEM were used to measure the hardness and microstructure of the material, both in the as-received condition and after heat-treatment of the samples. TEM was used to examine copper precipitates of the as-received samples. The decontaminated metallurgical samples and standards were mounted in bakelite for metallurgical and SEM examination. Hardness measurements (Rockwell-C and Rockwell-B) were performed at three locations per sample--the center, midradius and periphery. The samples were polished and etched using Vilella's reagent (5 mL HCl + 1 g Picric acid + 100 mL ethanol) for 17-4 PH. Electrolytic oxalic acid ( $H_2C_2O_4$ ) was used to etch the 304 SS materials. The samples and standards were examined by optical microscopy at 200 to 500X magnification.

SEM was used to examine the microstructure and carbide precipitates at 1000 to 10,000X magnifications. Thin slices from the samples were used for TEM examination. Dark-field electron micrographs were taken using reflections unique to copper. The micrographs were used to examine the shape and distribution of copper precipitates.

#### Chemical Analyses

The chemical analysis techniques used for examination were as follows:



- Emission Spectroscopy (ES)--The technique known as emission spectroscopy utilizes thermal excitation of a sample to elevate atomic electrons to excited states, which in turn deexcite by radiating photons in the visible region of the electromagnetic spectrum. Each element radiates light of a unique wavelength; therefore, the spectral lines resulting from thermal excitation of a sample can be separated by wavelength using a dispersive grating and recorded on a photographic plate. By analyzing the spectrum, the elements present in a sample can be determined. For quantitative analysis, the intensities of the spectral lines are related to the mass of the element in the sample. This relationship is determined by comparison of the unknown spectrum to those of known standards.
- Scanning Electron Microscope Equipped with Energy Dispersive Spectrometer (SEM/EDS)--SEM/EDS can be used to qualitatively identify chemical elements. The EDS system is capable of identifying elements with atomic number  $Z \geq 11$ . The EDS detector collects the entire X-ray spectrum in a multichannel analyzer divided into energy packets. By determining the channel numbers of peaks in the spectrum, appropriate atomic numbers can be assigned for the elements present in the electron-irradiated region. The basic X-ray analyzers are designed to perform all routine data acquisition, reduction, and display functions for accumulation and meaningful interpretation of X-ray spectra.
- Inductively Coupled Plasma (ICP) Emission Spectroscopy--ICP is an analysis technique that provides quantitative elemental analysis of solutions for a number of elements. The sample being analyzed is prepared in solution and sprayed into a plasma flame. The radiation from the flame enters a dispersing device to isolate portions of the spectrum. After calibration with solutions of known composition and concentration, the identity and quantity of the unknown element may be determined.

- X-Ray Diffraction--Compound identification is possible using X-ray diffraction. Each atom in a crystal has the power of scattering an X-ray beam being, in effect, diffracted from each allowed crystal plane. Every crystalline substance scatters the X-rays in its own unique diffraction pattern, producing a "fingerprint" of its atomic and molecular structure. The intensity of each reflection forms the basic information required in crystal structure analysis. One unique feature of X-ray diffraction is that components are identified as specific compounds.

### Radiological Analyses

Radiological analysis techniques used on the H8 and B8 leadscrew samples were as follows:

- Gamma Spectroscopy (GS)--The initial radiological analysis performed on each sample fraction was gamma spectroscopy. This technique is based on gamma ray emissions which produce a spectrum specific to individual radionuclide species. The spectra are analyzed by an automated computerized analysis program. This program identifies the nuclides associated with the gamma-ray peaks and determines their emission rates corrected for detector efficiency, random pulse summing, and decay during the count. The values are converted to disintegration rates by dividing them by the gamma-ray emission probability. The results are scrutinized to remove or correct erroneous results, make appropriate decay corrections, and, where appropriate, provide corrections for gamma-ray attenuation in the sample itself.

The liquid samples (the soluble fraction of the decontamination solutions) were analyzed in 60 mL bottles at calibrated distances with a computerized Ge(Li) gamma spectroscopy system. The solids removed from the decontamination solutions were generally in the form of powders or flakes of insoluble material. These samples were analyzed as point source geometries at distances ranging

up to 195 cm (77 in.) from the detector. The mass of each sample analyzed was  $\leq 100$  mg to keep the specific radionuclide concentration low and to minimize the effects of mass attenuation. For all samples, both liquid and solid, the effects of sample mass attenuation were evaluated and corrections were applied when necessary. The uncertainty of the gamma spectroscopy analysis method is  $<10\%$ , with the exception of those radionuclides whose concentrations were determined using low energy gamma rays,  $^{152}\text{Eu}$  and  $^{125}\text{Sb}$ . The uncertainty associated with these radionuclides is approximately 30%.

- $^{129}\text{I}$ ,  $^{90}\text{Sr}$ ,  $^{235}\text{U}$ , and Tellurium Analysis--The remaining required analyses (fissile material,  $^{90}\text{Sr}$ ,  $^{129}\text{I}$ , and tellurium) were all performed on liquid samples. The soluble fractions of the decontamination solutions were analyzed directly, whereas the solid materials (brushoff debris and insolubles in the decontamination solutions) required special dissolution prior to analysis. A number of dissolution methods were tried before an acid was found which was strong enough to fully dissolve the solids. The dissolution of the materials was complicated by the fact that two species of interest,  $^{129}\text{I}$  and fission product tellurium, are volatile in the presence of strong acids and heat. A potassium bisulfate fusion process was used in a closed system whereby all volatile species generated during the fusion process were transferred via an air stream and bubbled through a sodium hydroxide solution which retained the volatile species. A stable iodine carrier and  $^{131}\text{I}$  were added to the sample prior to dissolution to measure the amount of volatile  $^{129}\text{I}$  lost during analysis. The analytical methods used for these samples will be fully documented in an analytical procedures manual to be released.

The volatiles and nonvolatiles were chemically separated from the dissolution solutions. The volatile fraction was analyzed via neutron activation for  $^{129}\text{I}$ . After being activated, the

samples were analyzed via gamma spectroscopy to determine the parent radionuclide concentrations from the activation products.

The nonvolatile sample fractions were analyzed for  $^{90}\text{Sr}$ , fissile material ( $^{235}\text{U}$ ), and elemental tellurium. The  $^{90}\text{Sr}$  analysis was performed by chemically separating the strontium from the other radionuclides, followed by beta analysis performed in a gas-filled thin window counter having a known efficiency. The  $^{235}\text{U}$  fissile material content was determined by measuring the delayed neutrons emitted after a known aliquot of the sample was irradiated for one minute in the thermal neutron region of the Coupled Fast Reactivity Measurement Facility (CFRMF) reactor.

The tellurium analysis was performed by ICP analysis to determine the quantity of elemental tellurium present in all sample fractions. These analyses were performed semiquantitatively as scoping measurements to determine total tellurium content. Methods are being developed to quantitatively measure the amount of fission product tellurium.

There is a total uncertainty in the radiological analysis of 40 to 50%. The uncertainties associated with these analyses principally result from the sample dissolution, as the individual analytical technique uncertainties are <10%. The uncertainty associated with the dissolution is estimated at ~30%, due to the potential sample losses on glassware surfaces and the occasional presence of small amounts (<10% of the total sample) of insoluble material after the dissolution. It should be noted that these samples contained pieces of material from the leadscrew cutting operation, estimated at <20%, which would bias the absolute concentrations measured.

## RESULTS AND DISCUSSION

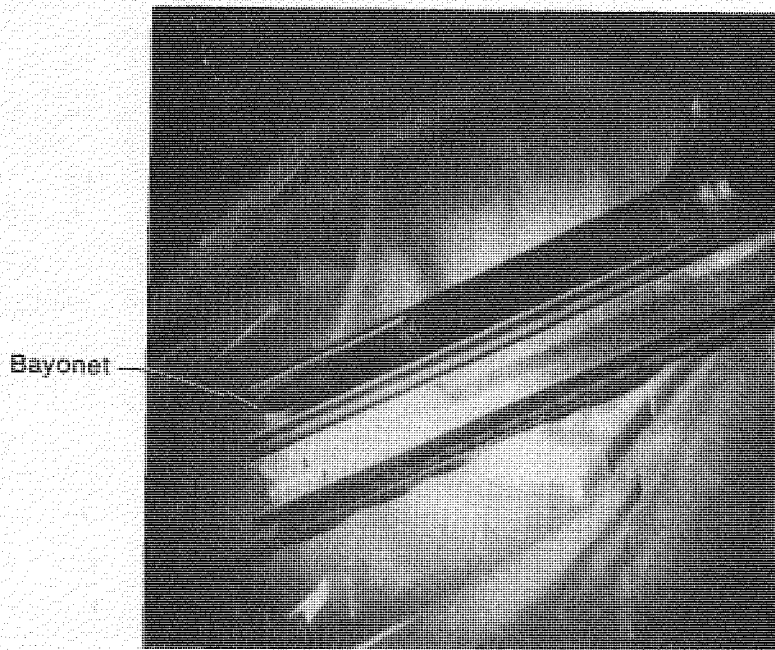
This section presents and discusses the results of the following examinations: (a) visual examination, (b) preliminary temperature estimates, (c) chemical analyses, and (d) radiological analyses. The types of samples or standards examined were: metallurgical samples for structure examination, brushoff debris, decontamination solutions, and samples for surface examination. Table 1 presents the scheme for the analyses performed on the H8 and B8 leadscrews. Sample designations, lengths, and locations (distance from bottom of leadscrew) are presented in Table 2.

### Visual Examination

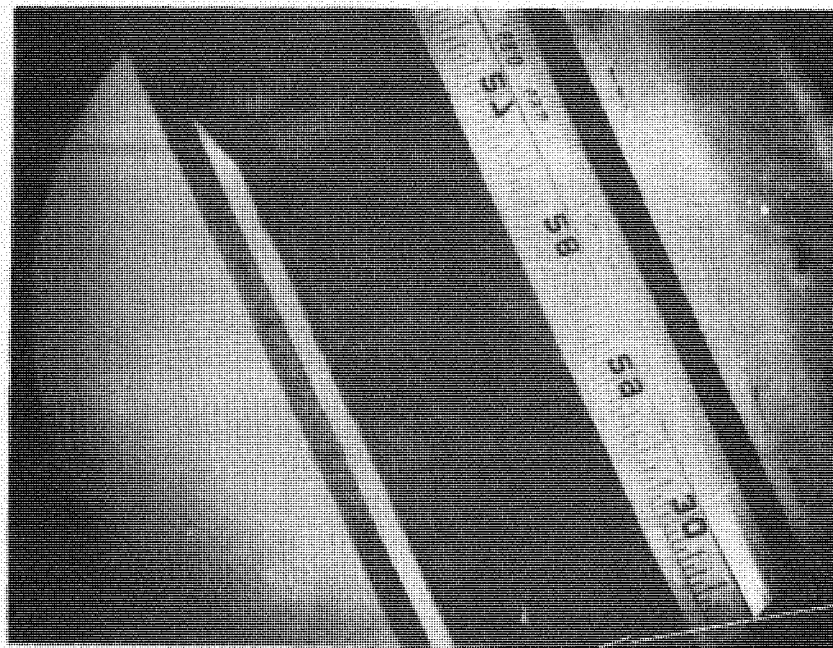
#### H8 Leadscrew

Visual examination of H8 leadscrew Sections H8-2, H8-7, H8-8, and H8-9 (as received from TMI-2) and the debris in the plastic bags which contained the sections was made through the hot cell periscope as the sections were unpackaged. cursory visual examination of the physical configuration of the leadscrew sections showed no evidence of melting, bending, or warpage. All features, such as the bayonet coupling, threads, and transition from 304 SS to the 17-4 PH threaded portion, were easily defined. Figures 7 through 9 are photographs taken of Sections H8-9, H8-7, and H8-2. Figures 7a and 7b show the lower end of Section H8-9, which contains the bayonet coupling. Samples 2 through 7 were cut from the lower end of Section H8-9. Figure 8 is a closeup of Section H8-7, near the top of the plenum assembly, in which general corrosion and surface deposition of material on threads can be seen. Samples 10 through 16 were cut from this section. Figure 8b shows the transition area from the 304 SS lower extension to the 17-4 PH threaded portion. Figure 9 is a closeup of Section H8-2 which was positioned at the top of the reactor vessel head. It shows the transition from the 17-4 PH threaded portion to the 304L SS upper extension.

Visually, Section H8-9 (the section closest to the core) and the debris collected from it were different from those of Sections H8-8 and



(a) TMI-2 H8-9 leadscrew section showing lower (bayonet) end



(b) Close-up of H8-9 leadscrew section, lower (bayonet) end spline area

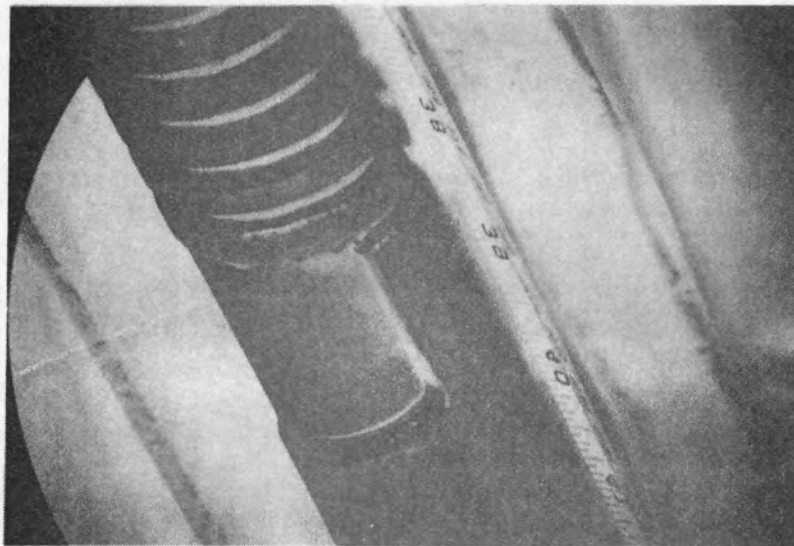
INEL 4 0924

Figure 7. Photographs of the lower end of Section H8-9.



Close to  
the top of  
plenum  
assembly

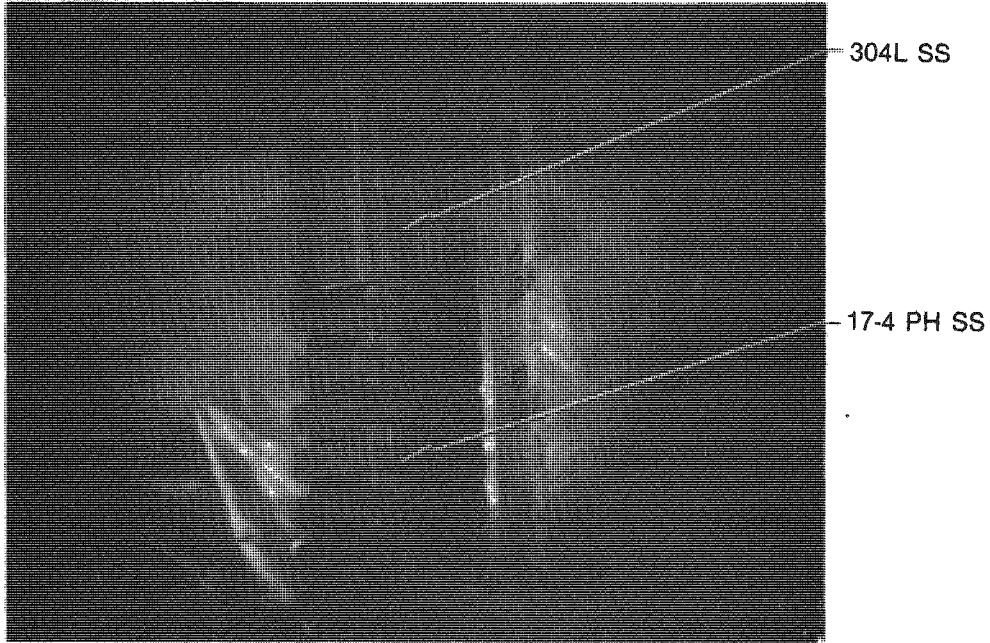
(a) Leadscrew section upper end



(b) Leadscrew section lower end

INEL 4 0925

Figure 8. Photographs of Section H8-7.



INEL 4 0926

Figure 9. Photograph of H8-2 section showing transition from 17-4 PH threaded portion to 304L SS extension piece (close to the top of the reactor head).



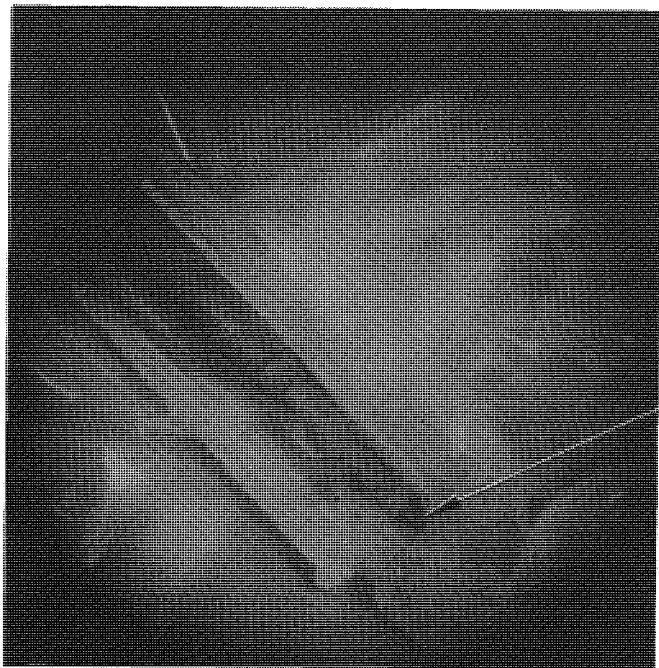
H8-7 (higher on the leadscrew) and the debris collected from these sections. The surface of Section H8-9 was coated with black debris. Several flakes of silver-colored material were observed both in the debris and on the surface of the leadscrew section near the bayonet. The loose material deposited on the surfaces of the higher leadscrew sections (H8-8 and H8-7) and the collected debris were gray in color, rather than black. The relative quantity of surface debris increased from almost none at the lower end of the leadscrew to a heavy coating near the top of the plenum assembly region, with a distinct (stepped) decrease just above the top of the plenum assembly. At the upper end of Section H8-2, there was no observable debris; that section was visually clean and shiny. The inner surface of the plastic bag used to ship the leadscrew sections was well coated with dark fine debris which could not be removed by brushing. There was a layer of debris on the leadscrew which was easily removed by brushing.

#### B8 Leadscrew

Figures 10 and 11 are photographs of Sections B8-3 and B8-1, respectively. Figure 10a shows the overall section; Figure 10b is a closeup of the lower (bayonet) end. Samples 2 and 3 were cut from this section. Figure 11 shows the lower and upper ends of Section B8-1 (near the top of the plenum assembly). Samples 7 and 8 were taken from this section. In general, the visual characteristics of debris deposition and corrosion are similar to H8 except that the lower (bayonet) end of B8 (Figure 10) is coated with white material that looks similar to solder spatter. Examination by EDS identified the elements barium, cadmium, chromium, copper, iron, nickel, and zirconium.

#### Preliminary Temperature Estimates

The peak local temperatures experienced by the H8 and B8 leadscrews were estimated by metallography, SEM, and TEM examinations of as-cut and subsequent heat-treated H8 and B8 samples and the 17-4 PH and 304L SS standards. The metallography examination methods included Rockwell hardness measurements and microstructure. SEM was used to examine the microstructure and intra- and intergranular carbide precipitates. Comparison of the Rockwell hardness, microstructure, and carbide



Bayonet

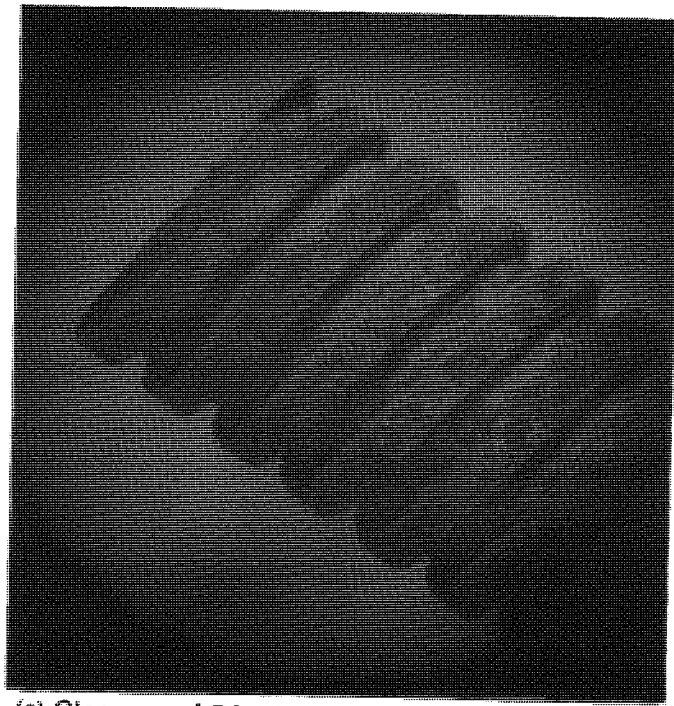
(a) B8-3 leadscrew section showing lower (bayonet) end



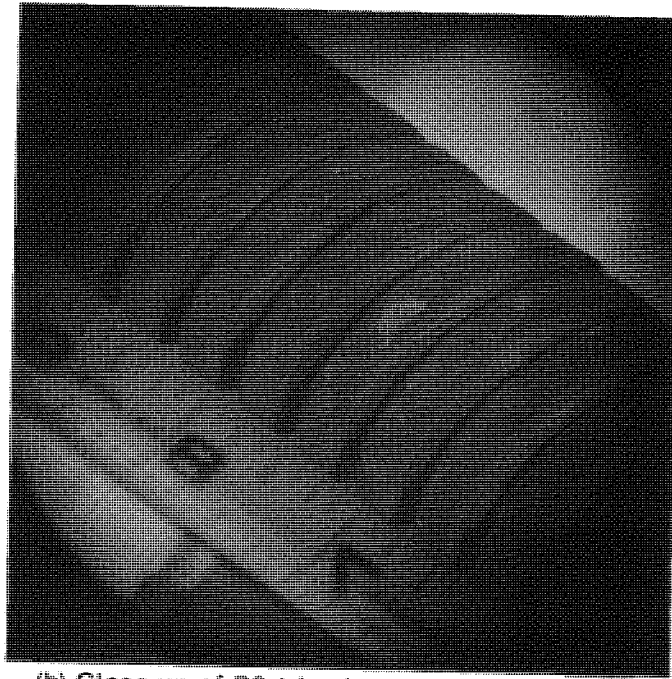
(b) Close-up of B8-3 leadscrew section, lower (bayonet) end

INEL 4 0927

Figure 10. Photographs of section B8-3 (close to the bottom of the plenum assembly).



(a) Close-up of B8-1 leadscrew section (upper end)



(b) Close-up of B8-1 leadscrew section (0.18 to 0.23 m above the lower end of the section)

INEL 4 0928

Figure 11. Photographs of section B8-1 (close to the top of the plenum assembly).

precipitation with the 17-4 PH and 304L SS annealing standards provided a quantitative estimate of peak local temperatures. Heat-treatment of the H8 and B8 samples to the H900 condition (heated at 900°F for one hour and air-quenched) was done to estimate the semiquantitative range of temperatures. The TEM examination of copper precipitates and grain sizes provided a qualitative confirmatory estimate of peak local temperatures. Details of these temperature estimates are discussed in the following sections for the H8 and B8 leadscrews.

### H8 Leadscrew

Following decontamination, five metallurgical samples (Numbers 2, 4, and 7 from Section H8-9 and 11 and 15 from H8-7) were polished; microstructures were examined by optical microscope and SEM, and Rockwell-C hardness measurements were taken. The optical and SEM micrographs of Samples 2 and 15 are shown in Figures 12 and 13. The Rockwell-C hardness values obtained from these samples are presented in Table 3, along with the hardness of five commercial 17-4 PH standards that were subsequently heat-treated at 900°F (H900), 950°F (H950), 1100°F (H1100), 1100°F to 900°F (H1100 to H900), and Condition A.<sup>a</sup> Sample 2 was heat-treated at the H900 condition after the initial hardness tests were made. The Rockwell-C hardness numbers of the 17-4 PH stainless steel leadscrew samples ranged from 34 to 41, and those of the five heat-treated commercial standards ranged from 36 to 44. Samples 2 and 4 are softer than Samples 11 and 15, indicating that these samples experienced higher temperatures.

During fabrication, the TMI-2 leadscrews were heat-treated to the H1100 condition,<sup>13</sup> which has an associated hardness in the neighborhood of 34. Table 3 shows that Samples 11 and 15 both have higher hardness numbers (39 and 41) than would be expected for material heat-treated at the H1100 condition. Conversations with persons from ARMCO at Middletown, Ohio, indicated that increased hardness can occur in H1100 heat-treated

---

a. Condition A: Solution annealed condition. Heated at 1900°F for 1/2 hour, air or oil quenched. Condition H1100: Condition A material heated at 1100°F for four hours and air cooled.

TABLE 3. HARDNESS OF H8 AND B8 LEADSCREW SAMPLES AND COMMERCIAL AND ANNEALED STANDARDS

<u>Sample/ Standard Number</u>	<u>Material</u>	<u>Distance from Bottom of the Plenum Assembly (cm)</u>	<u>Hardness<sup>a</sup></u>
<u>H8 Samples</u>			
2	17-4 PH SS <sup>b</sup>	18	34.0
2 at H900	17-4 PH SS <sup>c</sup>	18	47.0
4	17-4 PH SS <sup>b</sup>	30	35.0
7a	304 SS <sup>a</sup>	38	80.0
11	17-4 PH SS <sup>b</sup>	245	39.0
15	17-4 PH SS <sup>b</sup>	317	41.0
<u>Commercial 17-4 PH Standards</u>			
H900 <sup>d</sup>	17-4 PH SS	--	44.0
H950 <sup>d</sup>	17-4 PH SS	--	42.0
H1100 <sup>d</sup>	17-4 PH SS	--	36.0
H1100 <sup>e</sup>	17-4 PH SS	--	36.5
17-4 PH A <sup>f</sup>	17-4 PH SS	--	36.0
<u>B8 Samples</u>			
2	17-4 PH SS <sup>b</sup>	18	35.0
2 at H900	17-4 PH SS <sup>c</sup>	18	38.0
7	17-4 PH SS <sup>b</sup>	317	39.0
5 (A-hot leg)	304 SS	99	87.7
<u>Annealed Standards</u>			
A <sub>27</sub> <sup>g</sup>	17-4 PH SS	598-610	35.0
A <sub>24</sub> <sup>h</sup>	17-4 PH SS	572-598	35.4

a. Rockwell-B for Sample 7a and Rockwell-C for the remaining samples. Uncertainty =  $\pm 1$ .

b. The as-fabricated leadscrew was at H1100 condition (heated at 1100°F for four hours and air-cooled).

c. Sample 2 was heat-treated at the H900 condition by INEL after initial hardness measurements.

d. Commercial 17-4 PH Condition A standards were heat-treated at the H900, H950, and H1100 conditions, respectively. Condition A means the solution annealed condition: heated at 1900°F for 1/2 hour and air- or oil-quenched. Condition H950 or H1100: Condition A material heated at 950°F or 1100°F for 4 hours and air-quenched. Condition H900: Heated at 900°F for 1 hour and air-quenched.

TABLE 3. (continued)

---

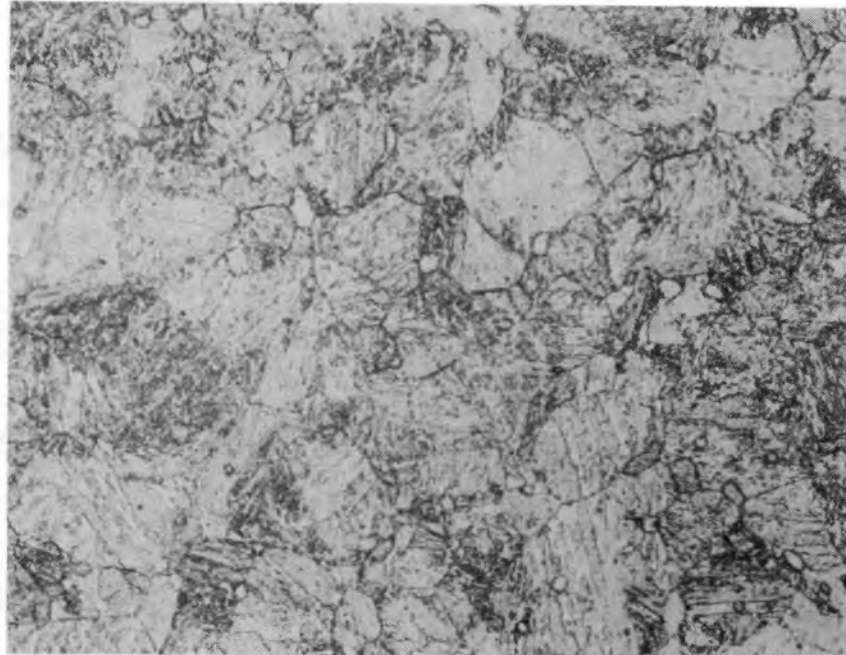
e. H1100 standard was heat-treated at the H900 condition. No significant change in hardness resulted compared with that at the H1100 condition.

f. 17-4 PH sample at annealed condition.

g. A standard from Section H8-20 was annealed at 1255 K (1800°F) for one hour and air-quenched.

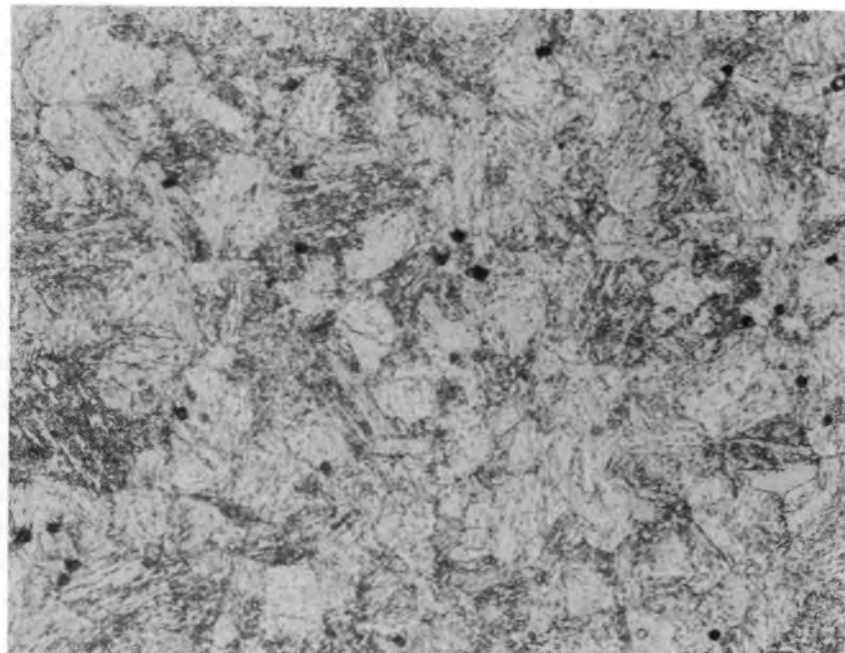
h. A standard from Section H8-19 was annealed at 1116 K (1550°F) for one hour and air-quenched.

---



(a) H8 sample 2

20  $\mu\text{m}$

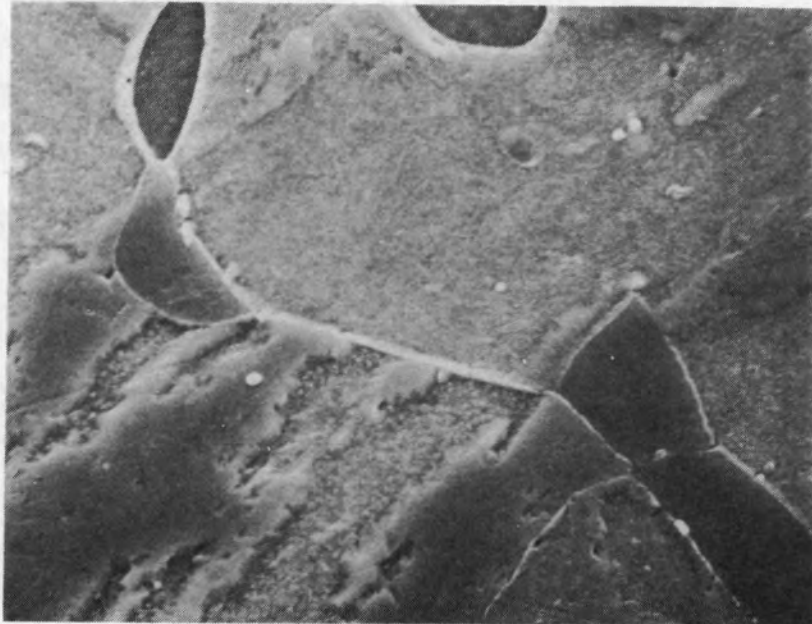


(b) H8 sample 15

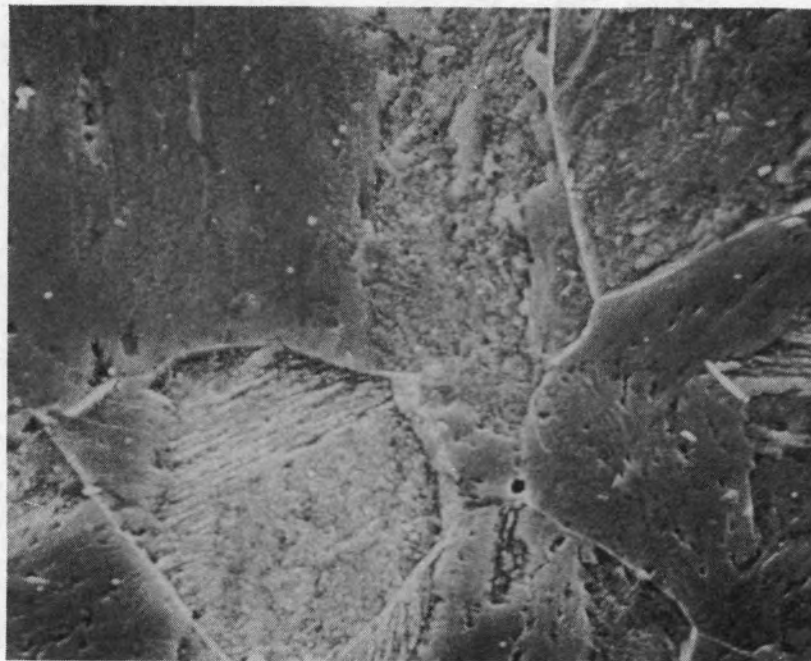
20  $\mu\text{m}$

INEL 4 0929

Figure 12. Optical micrographs of H8 Samples 2 and 15.



(a) H8 sample 2



(b) H8 sample 15

INEL 4 0930

Figure 13. SEM micrographs of H8 Samples 2 and 15.



material if the material is subjected to temperatures of approximately 700 K (800°F) for long periods of time.<sup>a</sup> It is unlikely that the increased hardness was caused by radiation damage, since radiation damage in metals occurs primarily from neutron bombardment. Because the TMI-2 fuel experienced a relatively low average burnup (3200 Mwd/t) and the leadscrews were away from the neutron field created by the core, radiation damage should have been minimal and, if present, should have been annealed during the high-temperature transient. Steam temperature measurements indicate that the hot-leg regions apparently contained a steam/gas mixture for about 13 h at about 700 K (800°F) during and after the transient.<sup>14</sup> Therefore, the high hardness of Samples 11 and 15 may be due to long exposures (up to 13 h) to temperatures of about 700 K (800°F).

In order to estimate the temperature of H8 Samples 11 and 15 (near the top of the plenum assembly), 17-4 PH commercial standards (condition H1100) were heat-treated at 700, 755, 783, and 866 K (800, 900, 950, and 1100°F) for 13 h and then air-quenched. Figure 14 compares the hardness values (39 and 41) of H8 Samples 11 and 15 with the hardness values (39 to 35) of the 13-h heat-treated standards. The hardness values for a Condition A standard and a standard heat-treated at the H1100 condition are also shown. The temperatures estimated from Figure 14 for Samples 11 and 15 are about 762 and 700 K (913 and 800°F), respectively. The uncertainty in temperature estimation was about  $\pm 28$  K (50°F).

SEM micrographs of the 13-h heat-treated 17-4 PH commercial standards are compared with the SEM micrographs of Sample 15 in Figure 15. The intragranular carbide precipitates in Sample 15 were comparable with the sample heat-treated for 13 h at 700 K (800°F).

The composition<sup>15</sup> of 17-4 PH stainless steel in weight percent is: carbon (0.07 maximum), chromium (15.5 to 17.5), nickel (3 to 5), copper (3.0 to 5.0) manganese (1 maximum), silicon (1 maximum), niobium + tantalum (0.15 to 0.45), phosphorus (0.04 maximum), sulphur (0.03 maximum) and

---

a. ARMCO is the developer and manufacturer of 17-4 PH material.

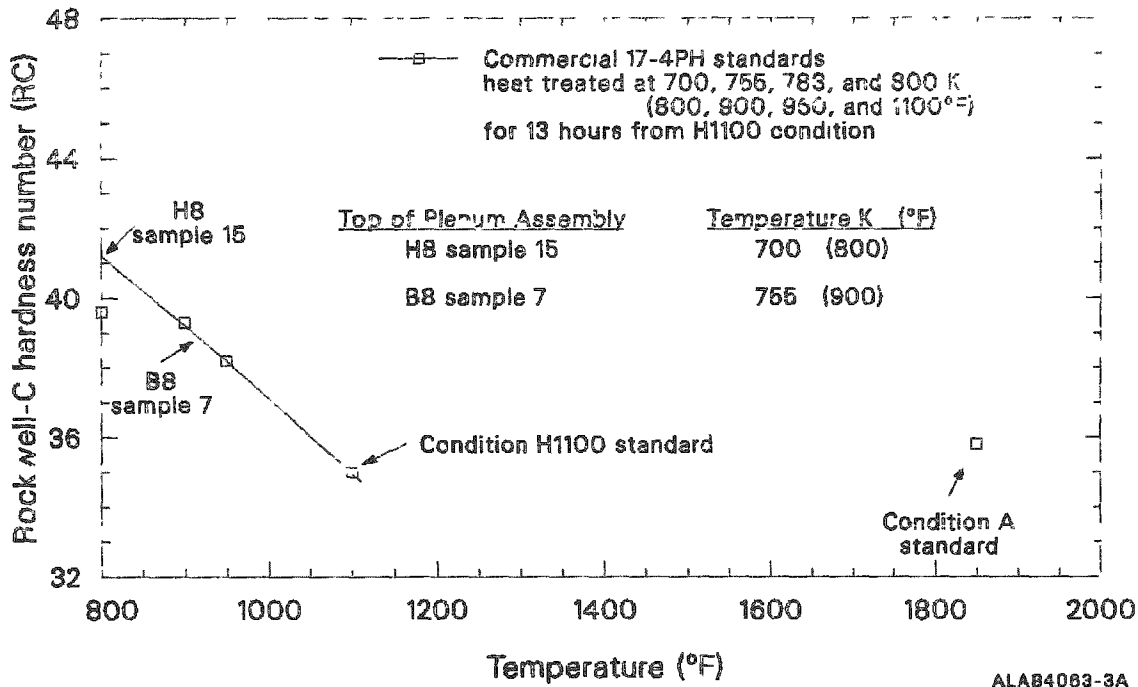
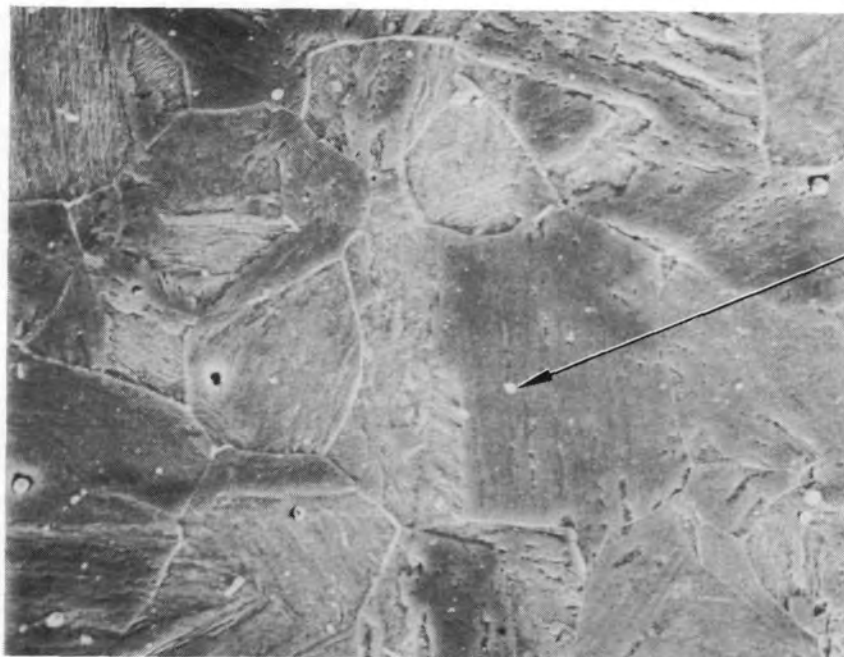


Figure 14. Leadscrew hardness versus temperature for H8 and B8 samples and standards heat-treated for 13 h.



(a) H8 sample 15

5  $\mu$ m

Intragranular  
carbide  
precipitates



(b) Standard heat-treated at 700 K (800°F) for 13 hours

5  $\mu$ m

INEL 4 0931

Intragranular  
carbide  
precipitates

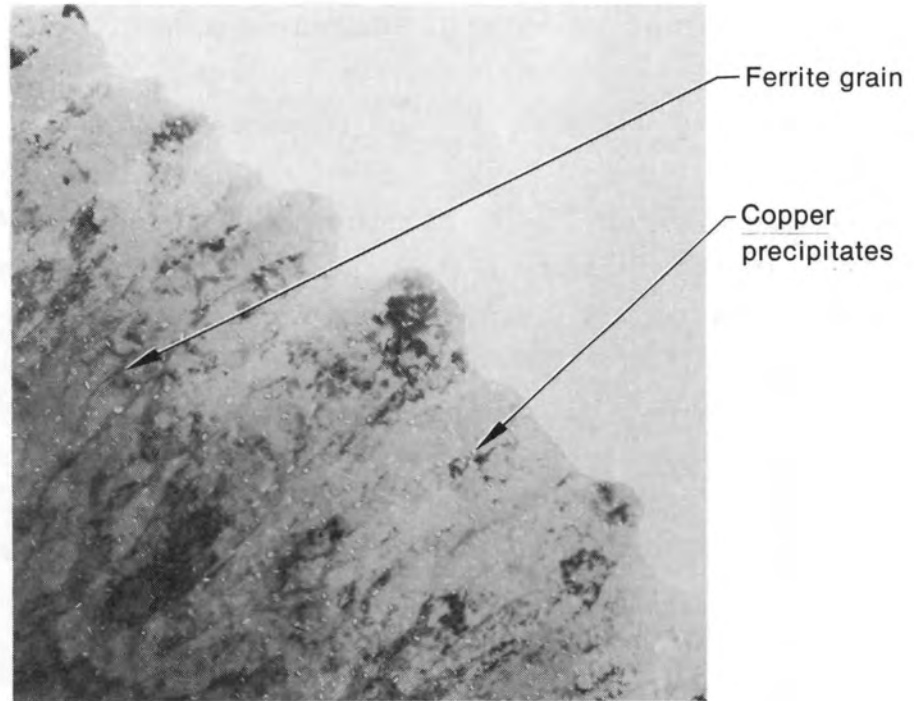
Figure 15. SEM micrographs of H8 Sample 15 and a 17-4 PH SS commercial standard heat-treated for 13 h.

iron (balance). The elements chromium and manganese are known to form carbides. The elements nickel, copper, and silicon form fine precipitates<sup>16</sup> that are the principal strengthening agents. Energy dispersive X-ray analysis revealed a high niobium concentration in many of the carbide precipitates in the H8 samples. The precipitates of nickel, copper, and silicon cannot be resolved by optical or SEM examination.

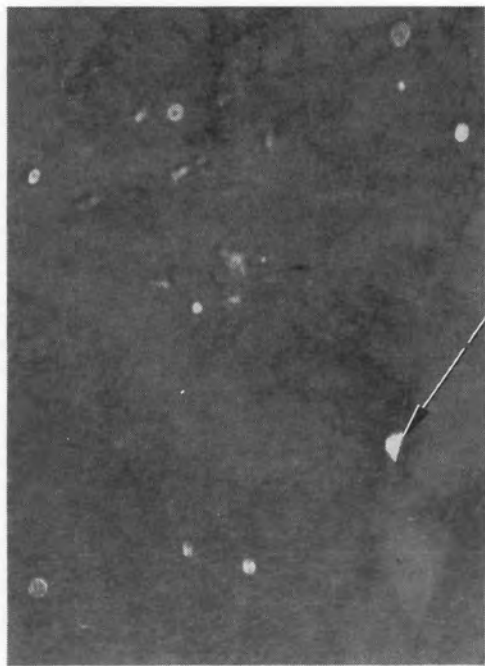
TEM examinations of Samples 11 and 15 and a H1100 condition standard were performed to determine the extent, size, and shape of copper precipitates. Figure 16 shows dark field TEM micrographs of those samples/standards using reflections unique to copper. Large-sized copper precipitates ( $\sim 600 \text{ \AA}$ ) are present in the ferrite grains of Samples 11 and 15. The H1100 condition standard exhibited a high density of copper precipitates in sizes ranging up to  $1000 \text{ \AA}$ . The size and distribution of copper precipitates in Samples 11 and 15 suggest that these samples probably did not experience significant heating above  $866 \text{ K}$  ( $1100^\circ\text{F}$ ).

This information, together with the intragranular carbide precipitates and hardness results discussed earlier, suggests that the leadscrew in the region of H8 Samples 11 and 15 (close to the top of the plenum assembly) probably experiences temperatures of about  $700$  and  $755 \text{ K}$  ( $800$  and  $900^\circ\text{F}$ ), respectively.

In order to estimate the temperature for H8 Sample 2 (near the bottom of the plenum assembly), heat treatments and analyses were performed. Hardness was measured on Samples 2 and 4 and found to be in the range expected for the fully annealed condition (34-36). Sample 2 was then heat-treated to the H900 condition. The hardness increased from 34 to 47, suggesting that the lower bayonet coupling was in a fully solution-annealed condition in the reactor vessel, rather than in an overaged or H1100 heat-treated condition. In an overaged and/or H1100 heat-treated condition, an increase in hardness is not expected; because alloying elements are not present in sufficient quantity to be precipitates (e.g., the H1100 sample heat-treated at H900 showed no significant increase in

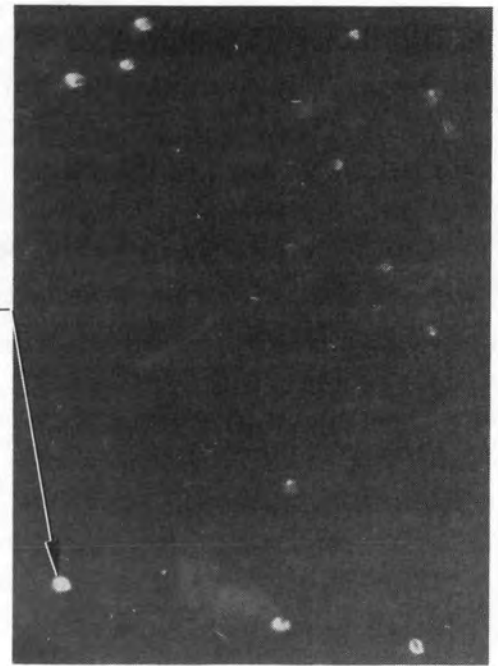


(a) 17-4 PH SS H1100 condition 1  $\mu$ m



(b) H8 sample 11 0.2  $\mu$ m

Copper precipitates



(c) H8 sample 15 0.2  $\mu$ m

INEL 4 0932

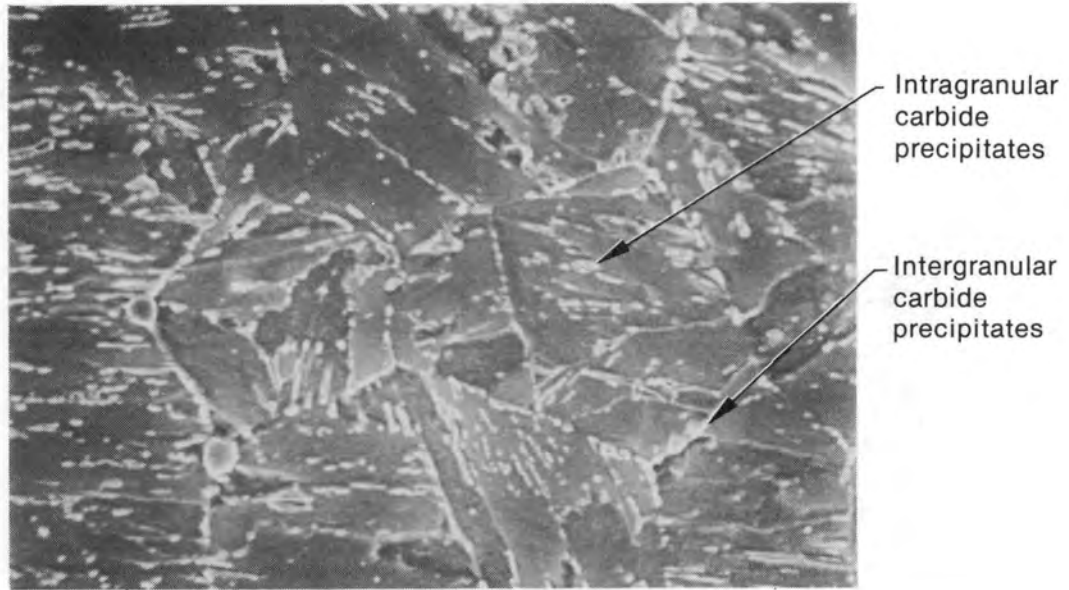
Figure 16. TEM micrographs of H8 Samples 11 and 15 and a standard at the H1100 condition.

hardness, as reported in Table 3). According to ARMCO, full solution annealing can occur within the temperature range of 1089 to 1477 K (1500 to 2200°F), depending on the duration of exposure.

SEM micrographs of 17-4 PH standards heat-treated to H900, H950, and H1100 are compared in Figure 17. In the H1100 heat-treated standard, carbide precipitates are found both within grains and on grain boundaries, whereas the carbide precipitates are seen only within the grains in the H950 and H900 standards. Also, the density of intragranular precipitates in the H1100 standard is higher than that of intragranular carbide precipitates in the H950 and H900 standards. In contrast, a low density of intragranular carbide precipitates is seen in Sample 2 (Figure 13a), suggesting that the carbide precipitates are in solution and this material was exposed to very high temperatures.

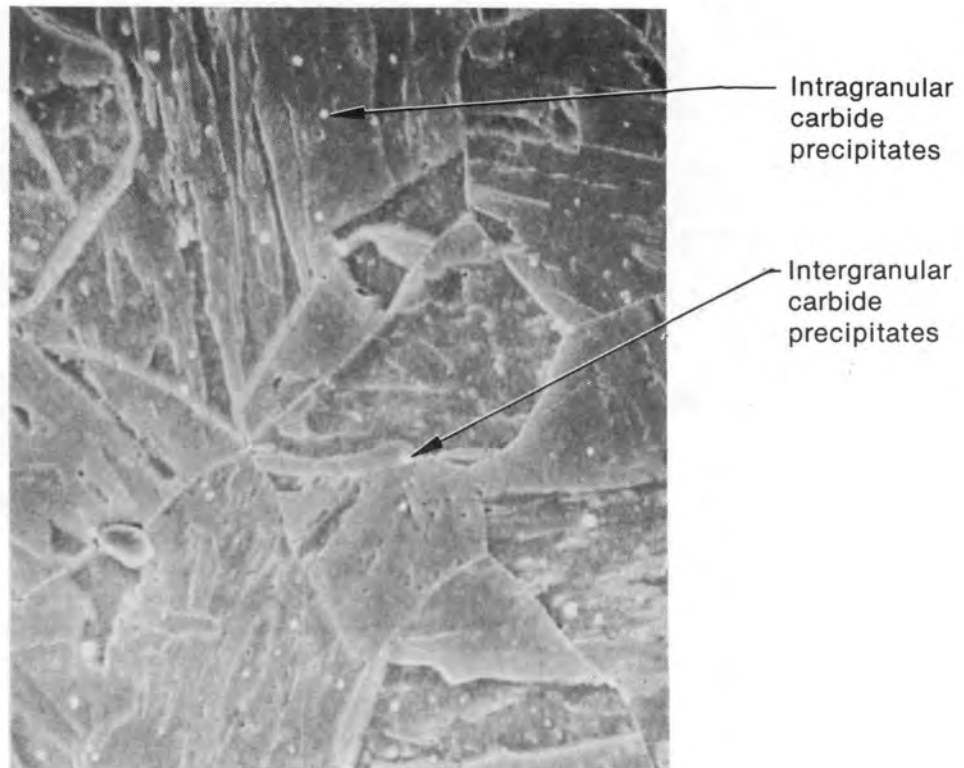
The microstructure shown in Figure 13a resembles a quenched martensite structure (quenched from the fully annealed condition). However, the measured lower hardness of 34 indicates a tempered martensite, because the hardness of a quenched martensite could be expected to be greater than the hardness characteristic of the fully annealed condition.

TEM examination of H8 Samples 2 and 4 (from Section H8-9) was performed to determine the extent, shape, and size of copper precipitates. The 17-4 PH material basically has a martensite structure and contains only a small amount of ferrite (alpha iron). Copper precipitates are present only in the ferrite and not in the martensite phase. Figure 18 shows the dark field TEM micrographs of Samples 2 and 4 formed using reflections unique to copper. Spherically shaped copper precipitates in the size range 200-400 Å, with a larger fraction being near 200 Å, are present in the ferrite grains in Samples 2 and 4. As discussed earlier, the H1100 condition sample exhibited a high density of precipitates in sizes ranging up to 1000 Å. The absence of large-sized precipitates in Samples 2 and 4 suggests that these specimens experienced temperatures in the solution-annealed condition [1089 to 1477 K (1500 to 2200°F)]. The small precipitates present in Samples 2 and 4 probably formed during cooldown from the elevated temperatures experienced during the high-temperature transient.



(a) Heat-treated at H1100 condition

2  $\mu$ m

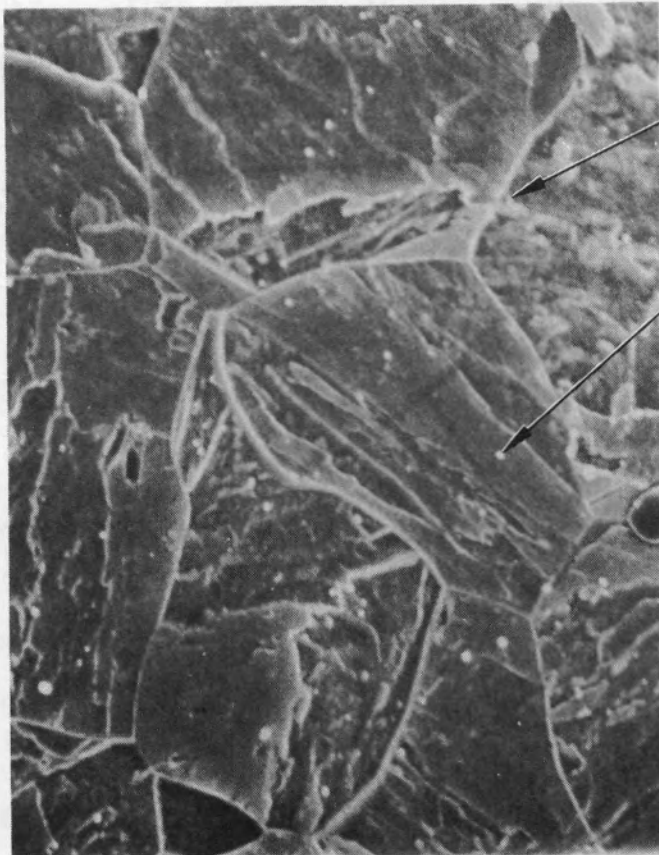


(b) Heat-treated at H950 condition

2  $\mu$ m

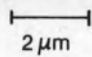
INEL 4 0933

Figure 17. SEM micrographs of heat-treated standards of H900, H950, and H1100 grain structure.



Intergranular  
carbide  
precipitates

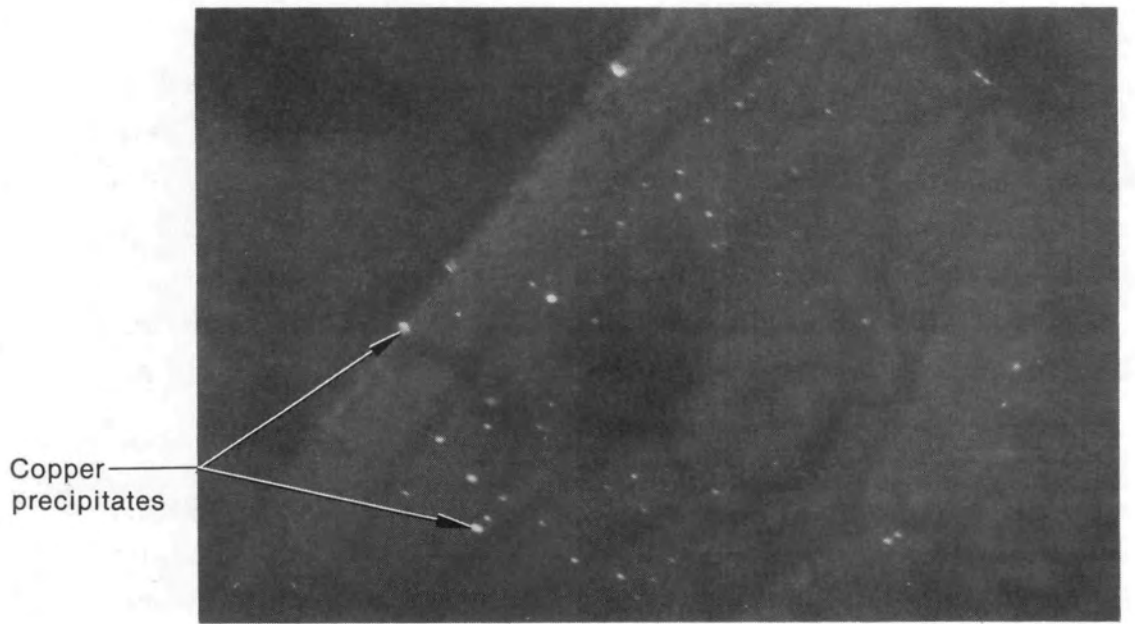
Intragranular  
carbide  
precipitates

(c) Heat-treated at H900 condition  2  $\mu\text{m}$

INEL 4 0934

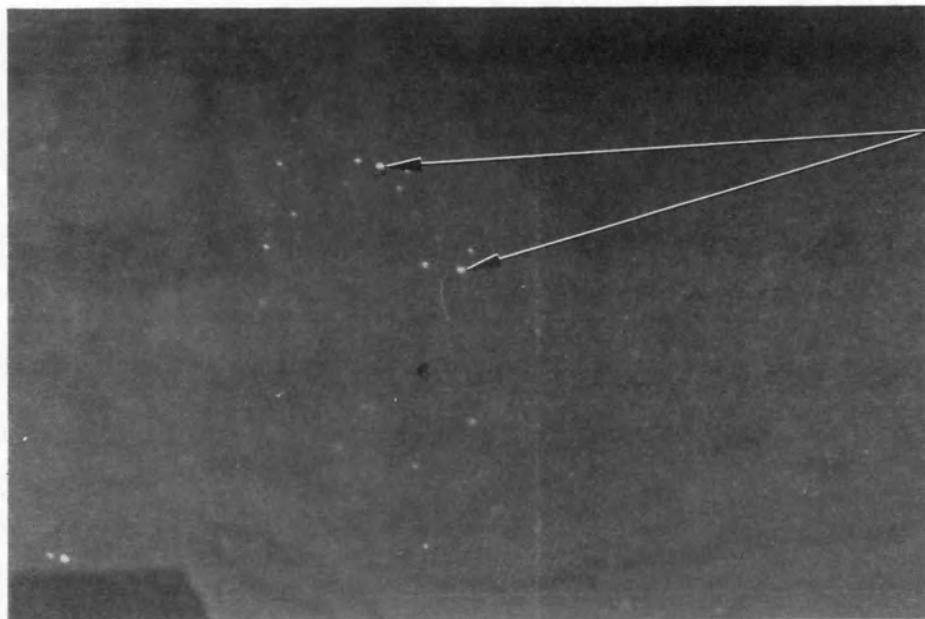
Figure 17. (continued)





(a) H8 sample 2

0.2  $\mu\text{m}$



(b) H8 sample 4

0.2  $\mu\text{m}$

INEL 4 0936

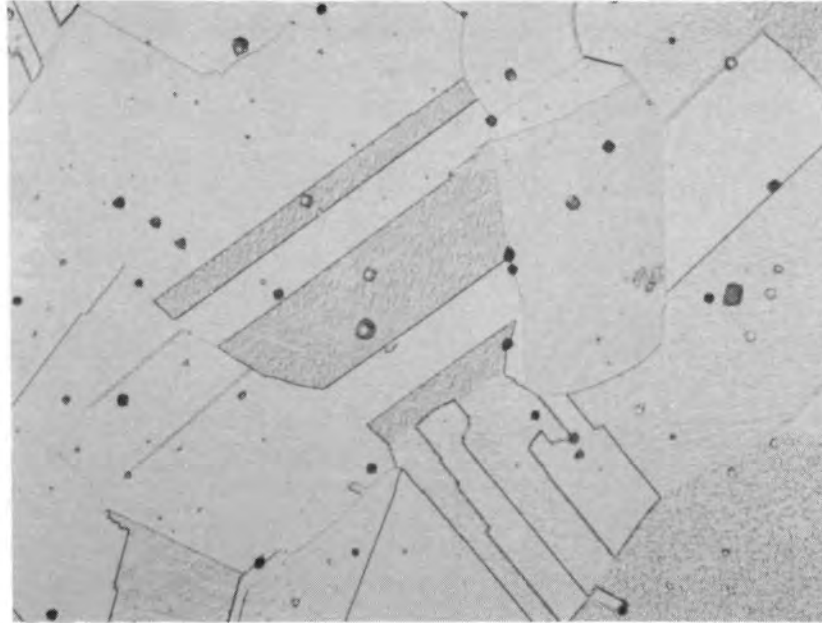
Figure 18. TEM micrographs of H8 Samples 2 and 4.

Sample 7a (304 SS) exhibits an equiaxed austenitic structure which is typical of annealed 304 SS, as shown in Figure 19. Chromium carbide precipitation occurs in this material at temperatures of 700 to 1089 K (800 to 1500°F), and it can occur within minutes at some temperatures in that range. Above 1089 K (1500°F), the precipitates will be in solution. The absence of these precipitates and a hardness typical of the annealed condition suggest that Sample 7a experienced temperatures above 1089 K (1500°F). The annealing study of 304L SS discussed in Appendix A indicates H8 Sample 7a experienced a temperature of about 1189 K (1670°F) based on hardness.

To narrow the temperature range, 17-4 PH standards from near the top of the H8 leadscrew (which is near the reactor vessel head) were annealed at different times and temperatures. Details of the annealing study are discussed in Appendix A. The microstructure (Figure 20) and hardness (35) of annealed Standard A<sub>27</sub>, annealed at 1255 K (1800°F) for one hour and air-quenched, is nearest in comparison with the microstructure (Figure 13a) and the hardness (34) of Sample 2. The data are presented in Table 3, along with the data for the H8 and B8 leadscrews. By comparison, the peak temperature experienced by Sample 2 was about 1255 K (1800°F).

### H8 Surface Sample Layers

H8 surface Samples 3, 13, and 16, located at elevations 4.45, 233, and 303 cm (1.75, 92, and 119 in.--see Table 2), were metallographically examined in the polished condition to determine the thickness and nature of the surface layer. The data are presented in Table 4, and macrographs of the metallurgical samples are shown in Figure 21. Figure 21a shows a quarter cross section of H8 Sample 3. Circumferential locations near A, B, and C were examined, and the micrographs are shown in Figure 22. The surface contained three distinct layers: an inner layer next to the 17-4 PH base metal (~28 μm thick), a middle layer (~1 μm thick), and an outer layer (~20 μm thick) next to the mounting epoxy. Figures 21b and 21c are 17-4 PH SS longitudinally threaded cross sections of Samples 13 and 16. Thread top, thread face, and thread bottom surfaces



20  $\mu\text{m}$

INEL 4 0935

Figure 19. SEM micrograph of Sample 7a (304 SS) microstructure.



2  $\mu\text{m}$

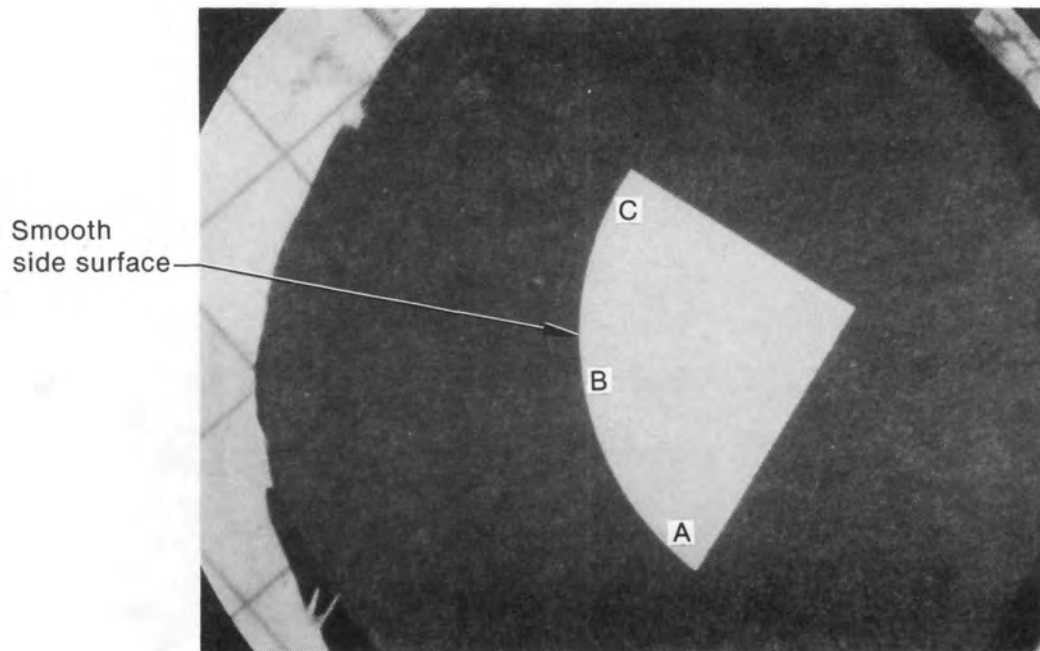
INEL 4 0937

Figure 20. SEM micrograph of standard A<sub>27</sub> from H8-2 section annealed at 1255K (1800°F) for 1 h and air-quenched.

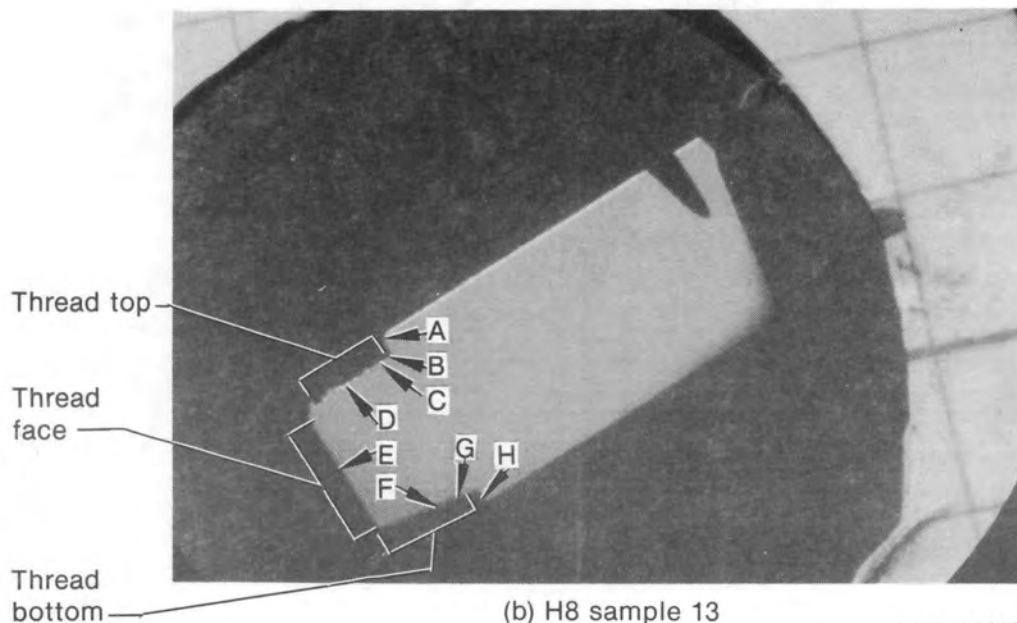
TABLE 4. SURFACE LAYER THICKNESSES ON H8 SURFACE SAMPLES

Leadscrew Sample	Distance from from Bottom of Leadscrew (cm)	Surface Characteristics	Examination Location	Surface Layer Thickness ( $\mu\text{m}$ )			Sum of Inner Middle and Outer Layers ( $\mu\text{m}$ )
				Inner	Middle	Outer	
3 (close to bottom of the plenum assembly)	4.45 - 13.34	Smooth side surface (17-4 pH SS)	A	28.0 <sup>a</sup>	0.0	20.0 <sup>b</sup>	48.0
			B	21.0 <sup>c</sup>	0.5 <sup>a</sup>	9.0 <sup>b</sup>	30.5
			C	25.0	1.0 <sup>a</sup>	6.0 <sup>b</sup>	32.0
13 (near the top of the plenum assembly)	233.05 - 233.68	Thread top surface (17-4 pH SS)	A	40.0 <sup>c</sup>	12.0 <sup>b</sup>	40.0 <sup>d</sup>	92.0
			B	48.0 <sup>c</sup>	0.0	20.0 <sup>d</sup>	68.0
			C	44.0 <sup>a</sup>	0.0	16.0 <sup>d</sup>	60.0
			D	12.0 <sup>a</sup>	0.0	58.0 <sup>d</sup>	70.0
		Thread face surface (17-4 pH SS)	E	28.0 <sup>b</sup>	28.0 <sup>c</sup>	10.0 <sup>c</sup>	66.0
			F	40.0 <sup>a,c</sup>	0.0	32.0 <sup>d</sup>	72.0
			G	30.0 <sup>c</sup>	10.0 <sup>b</sup>	38.0 <sup>d</sup>	78.0
			H	44.0 <sup>c</sup>	0.0	36.0 <sup>d</sup>	80.0
16 (close to the top of the plenum assembly)	302.90 - 304.80	Thread top surface (17-4 pH SS)	A	36.0 <sup>c</sup>	2.0 <sup>a</sup>	16.0 <sup>b</sup>	54.0
			B	14.0 <sup>c</sup>	0.0	30.0 <sup>d</sup>	44.0
			C	8.0 <sup>c</sup>	15.0 <sup>c,a</sup>	10.0 <sup>b</sup>	33.0
		Thread bottom surface (17-4 pH SS)	D	54.0 <sup>c</sup>	0.0	60.0 <sup>d</sup>	114.0
			E	40.0 <sup>c</sup>	0.0	40.0 <sup>d</sup>	80.0
			F	46.0 <sup>c</sup>	0.0	26.0 <sup>d</sup>	72.0

- a. Layer containing white spots.
- b. Dense layer. Visually, the layer appears to be dense.
- c. Porous layer. Visually, the layer appears to be porous.
- d. Detached loose layer.



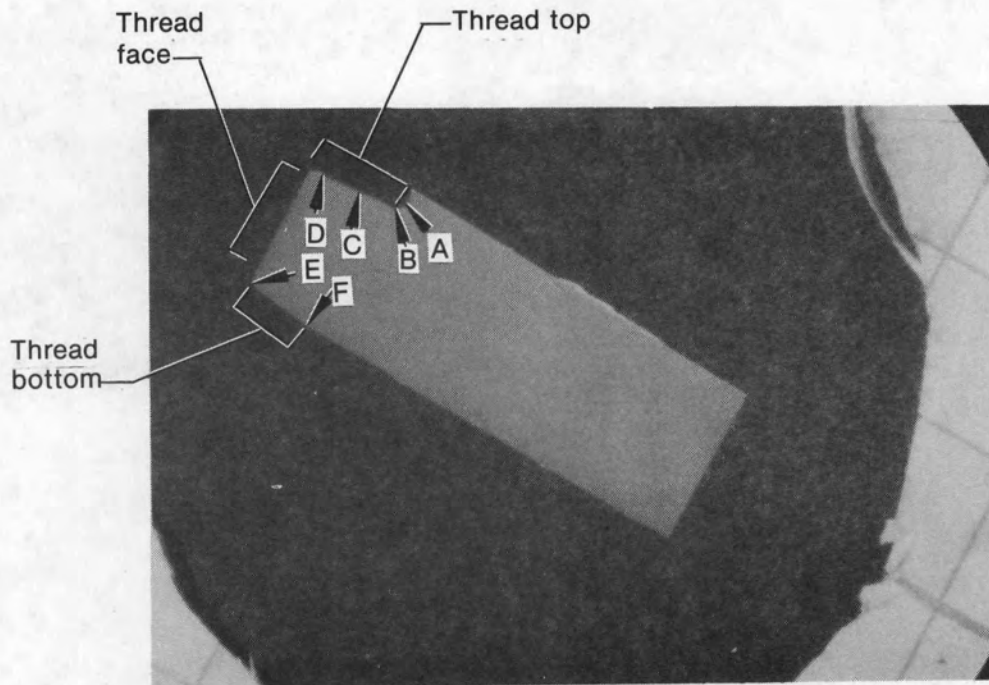
(a) H8 sample 3



(b) H8 sample 13

INEL 4 0938

Figure 21. Macrographs of H8 surface Samples 3, 13, and 16.



(c) H8 sample 16

INEL 4 0939

Figure 21. (continued)

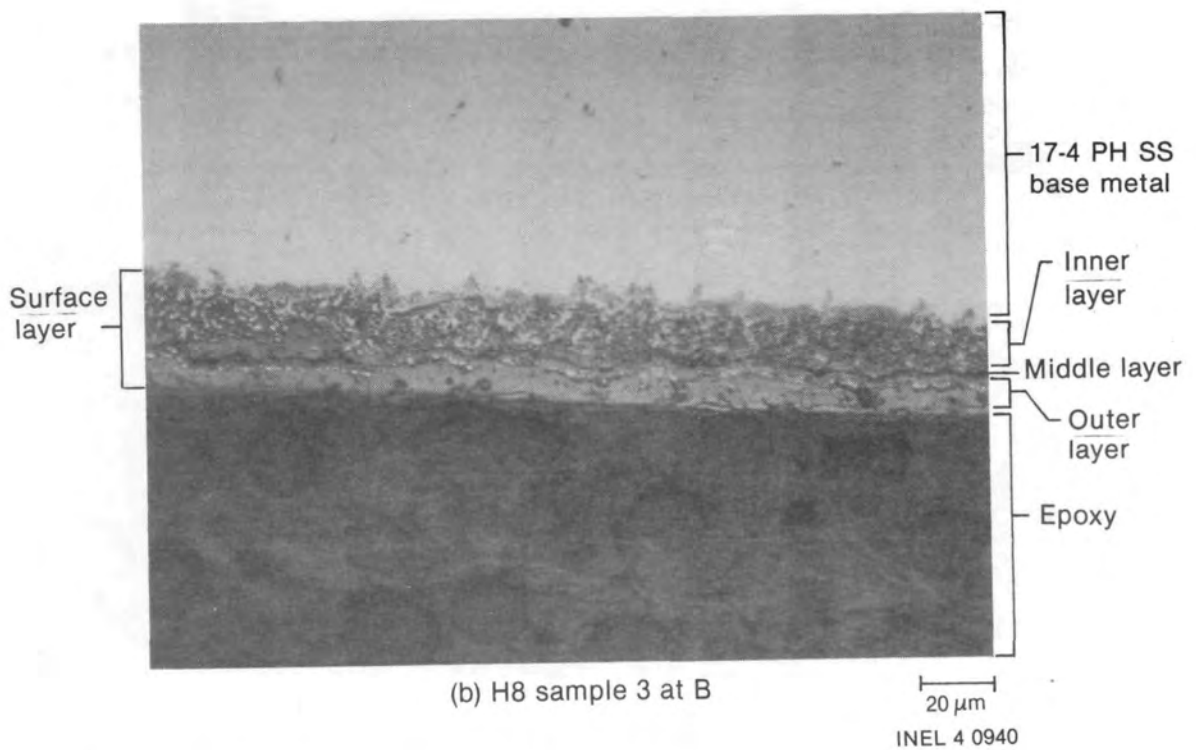
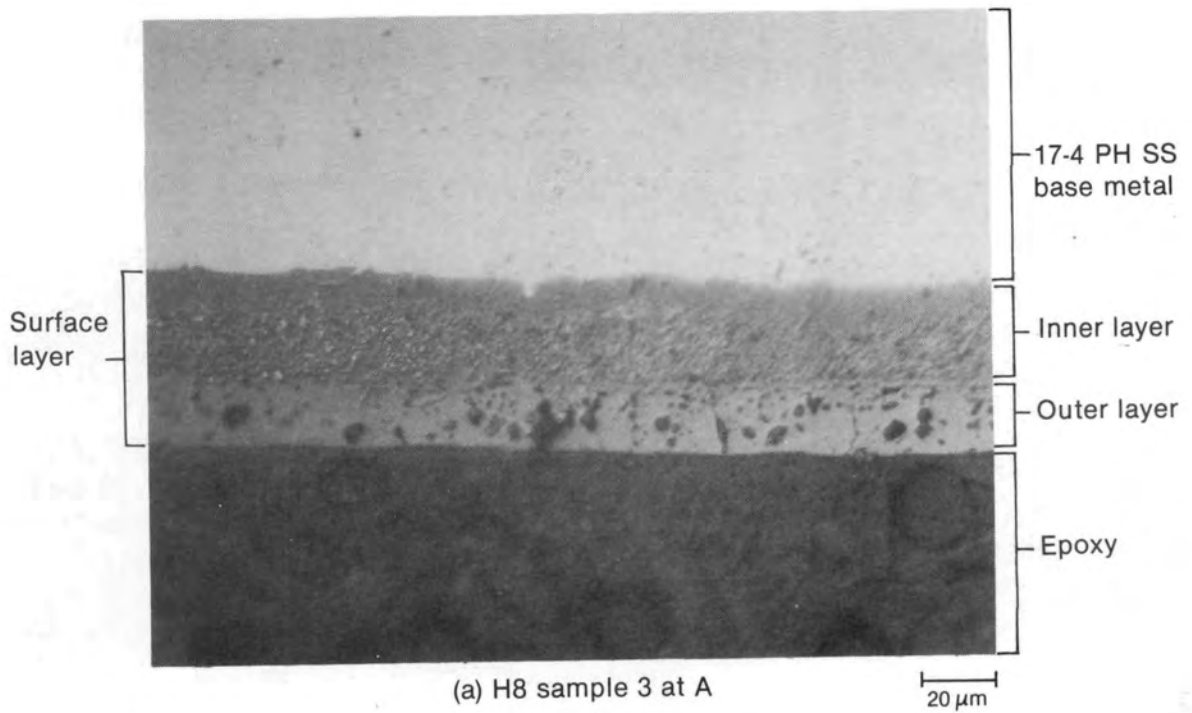


Figure 22. Micrographs of H8 Sample 3 showing surface layers.



(c) H8 sample 3 at C

20 μm  
INEL 4 0941

Figure 22. (continued)



were examined and shown in Figures 23 and 24. These two samples also contained inner, middle, and outer surface layers. Two observations are noted: (a) the combined thickness of all surface layers is greatest (114  $\mu\text{m}$ ) near the top of the plenum assembly, and (b) the thread top surface contained the thickest layer, followed by the thread bottom and then the thread face surfaces. Gravitational settling of fine debris on the thread top and vapor deposition on the thread bottom and thread face may account for the variations in deposition quantities within a thread.

Elemental composition of the surface layers on Samples 3 and 16 were measured by EDS, and the data are discussed in the following section.

### B8 Leadscrew

Two metallurgical samples (2 and 7 from Sections B8-3 and B8-1, respectively) were polished and measured for Rockwell-C hardness. These samples are 17-4 PH SS and were located at about 18 and 317 cm (7 and 125 in.) from the bottom of the plenum assembly (lower surface of the upper grid assembly). The morphology of the B8 grain structures is shown in Figures 25 and 26. The smaller hardness number of Sample 2 suggests that the region of the leadscrew closest to the bottom of plenum assembly experienced higher temperatures than near the top of the plenum assembly.

B8 Sample 7 has a higher hardness number (39) than would be expected for a material that was initially heat-treated at H1100 condition (34). Comparison of Sample 7 hardness (39) with that of standards heat-treated at 700, 755, 783, and 866 K (800, 900, 950, and 1100°F) for 13 h in Figure 14 suggests that the region of the B8 leadscrew close to the top of the plenum assembly experienced a temperature of about 755 K (900°F).

When B8 Sample 2 was heat-treated at the H900 condition, the hardness increased from 35 to 38. The relatively small increase in hardness suggests that it was in a partially solution-annealed condition rather than in an overaged or H1100 condition. These data suggest that B8 Sample 2 experienced a temperature close to the lower end of the solution-annealed

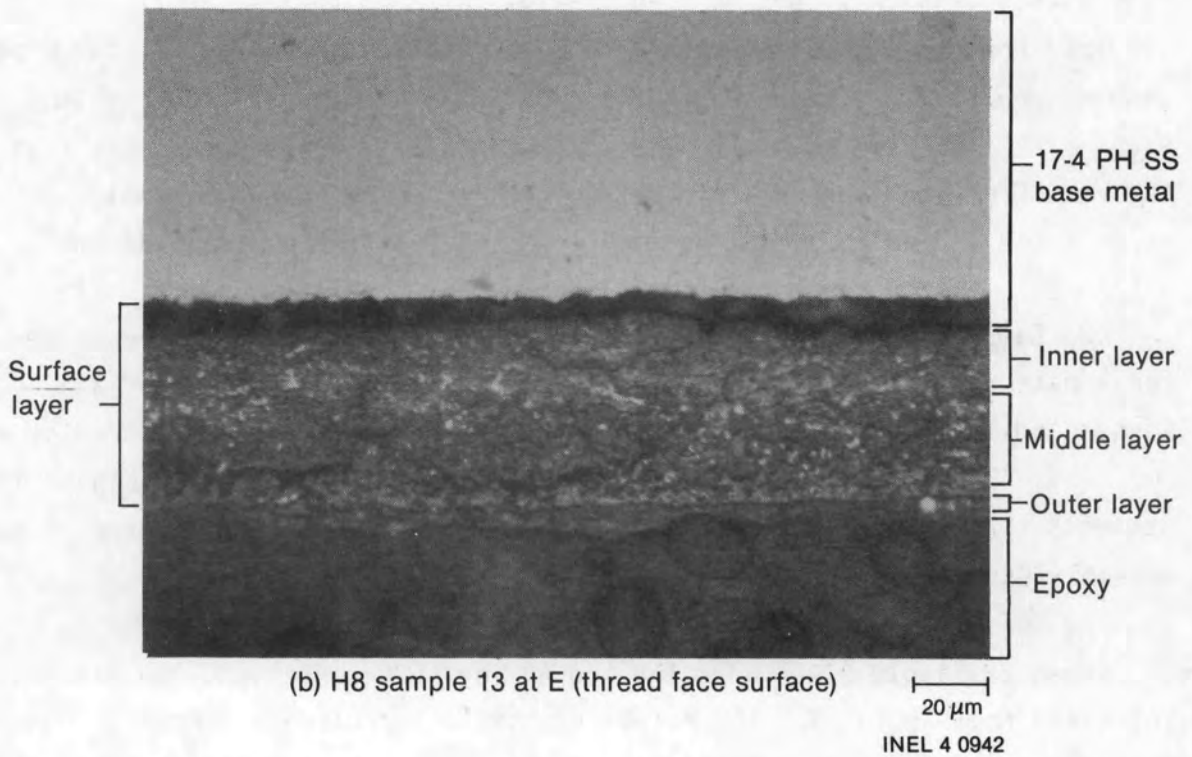
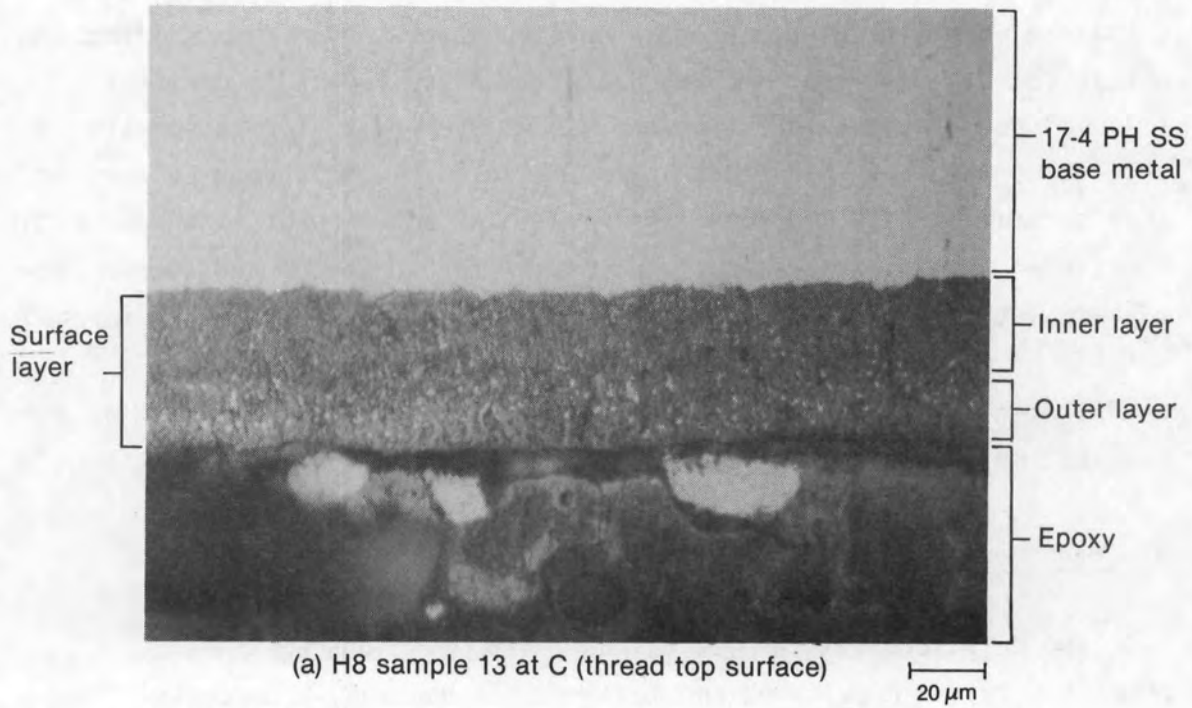
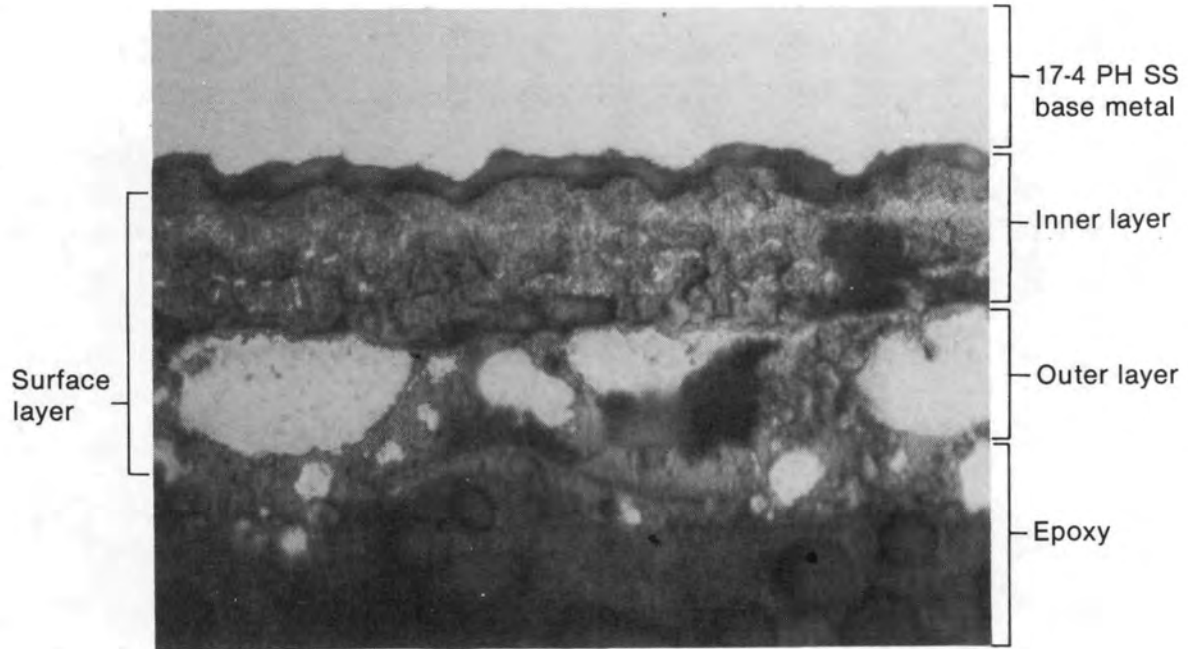


Figure 23. Micrographs of H8 Sample 13 showing surface layers.

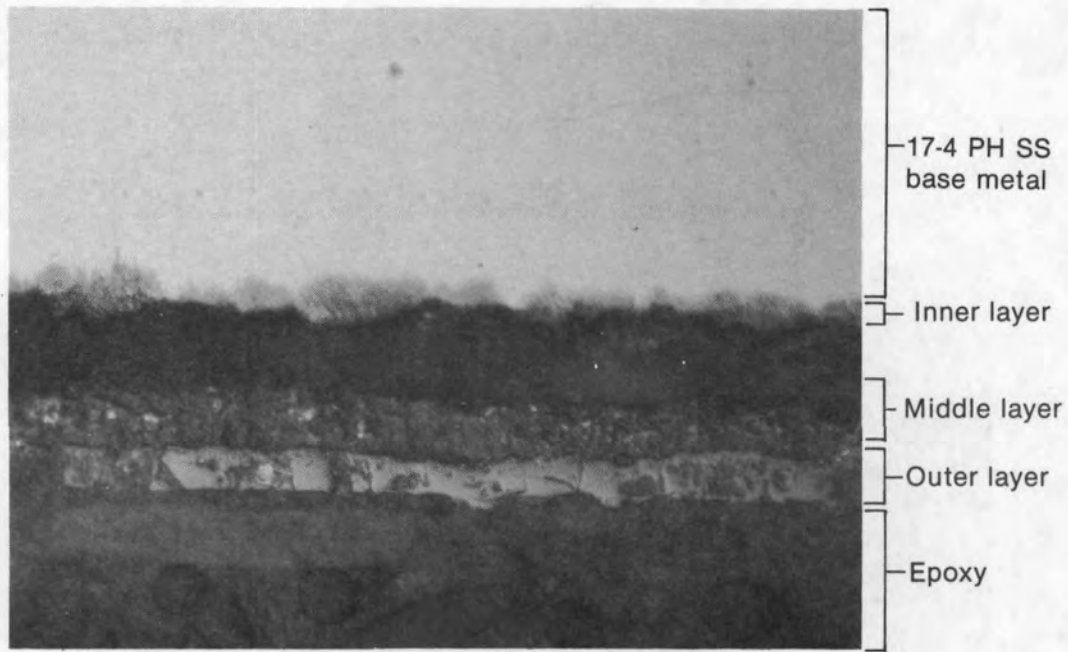


(c) H8 sample 13 at F (thread bottom surface)

20  $\mu\text{m}$

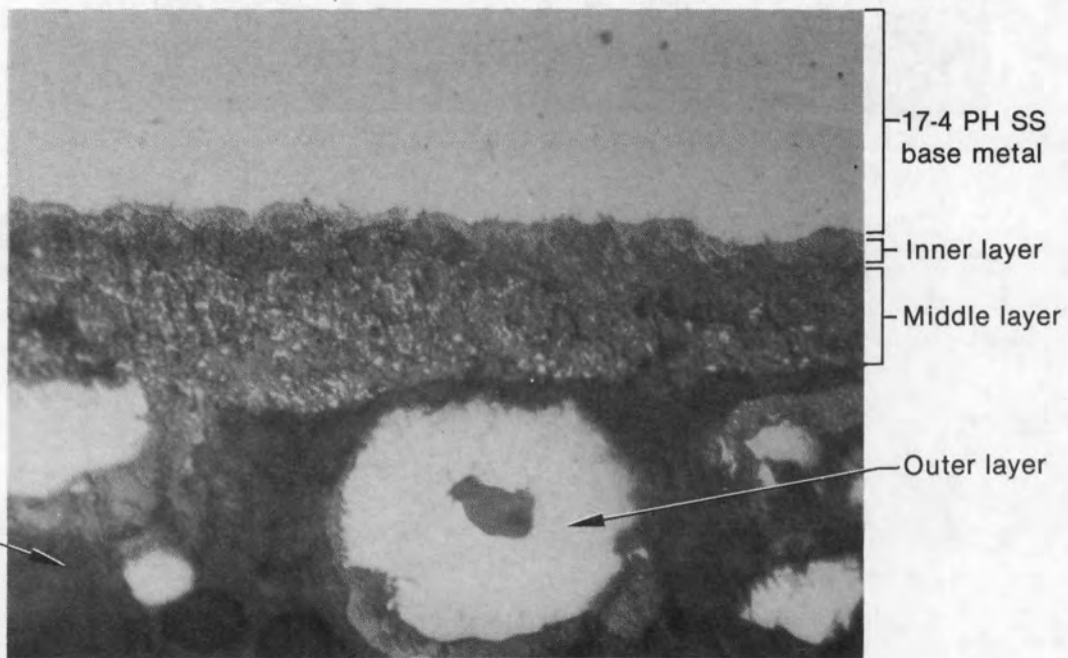
INEL 4 0943

Figure 23. (continued)



(a) H8 sample 16 at C (thread top surface)

20 μm



(b) H8 sample 16 at D (thread top surface)

20 μm

INEL 4 0944

Figure 24. Micrographs of H8 Sample 16 showing surface layers.

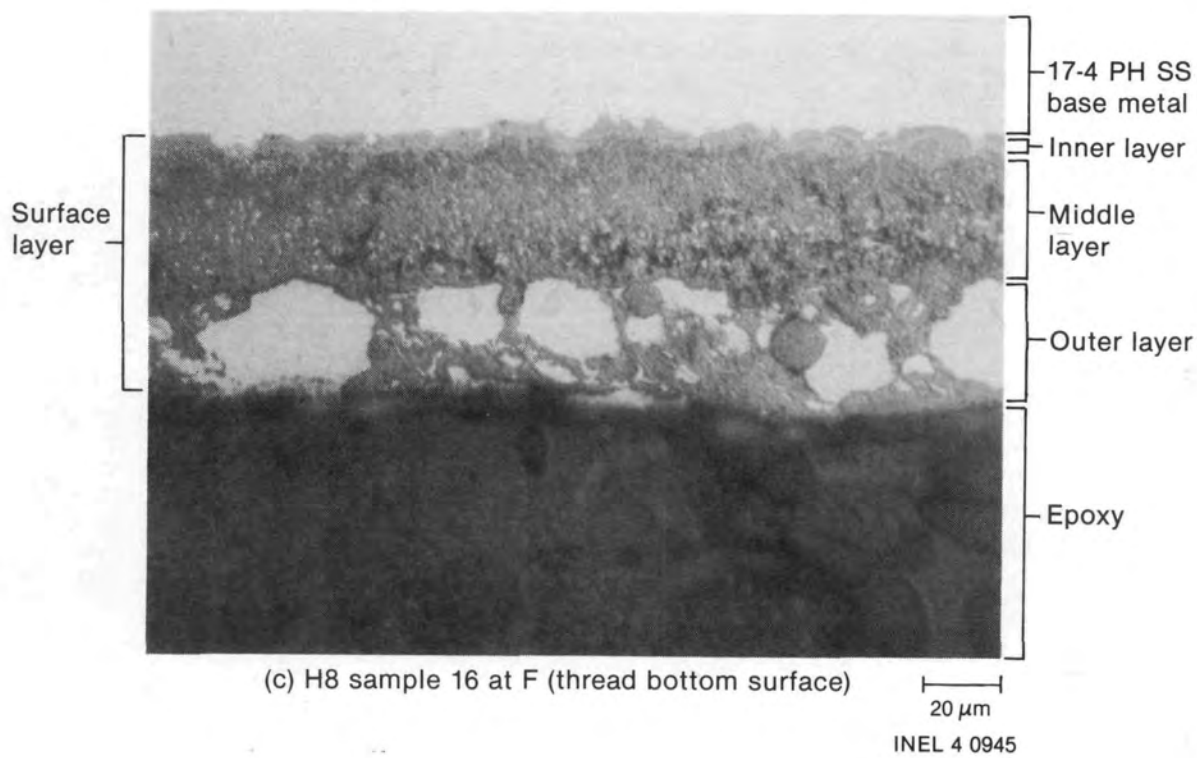
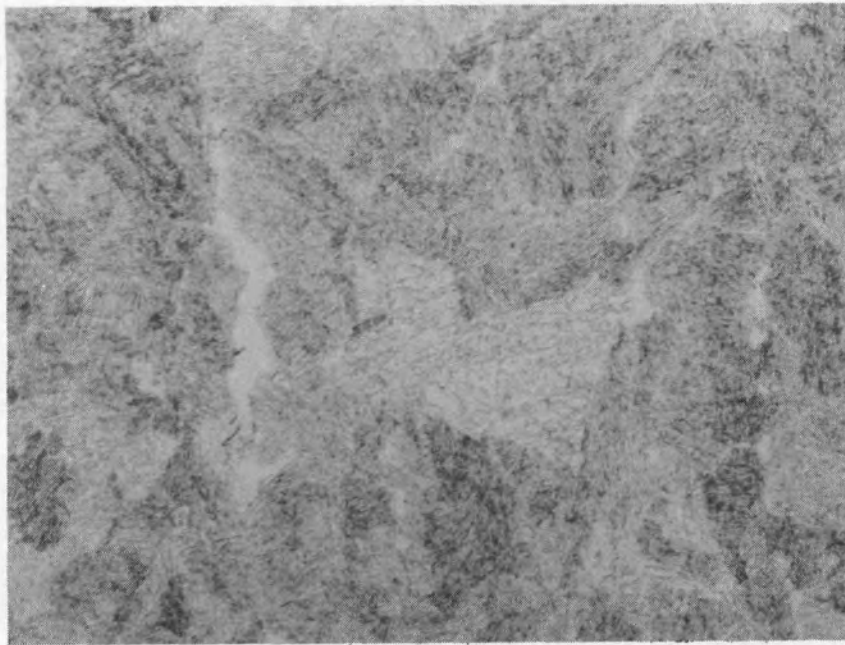
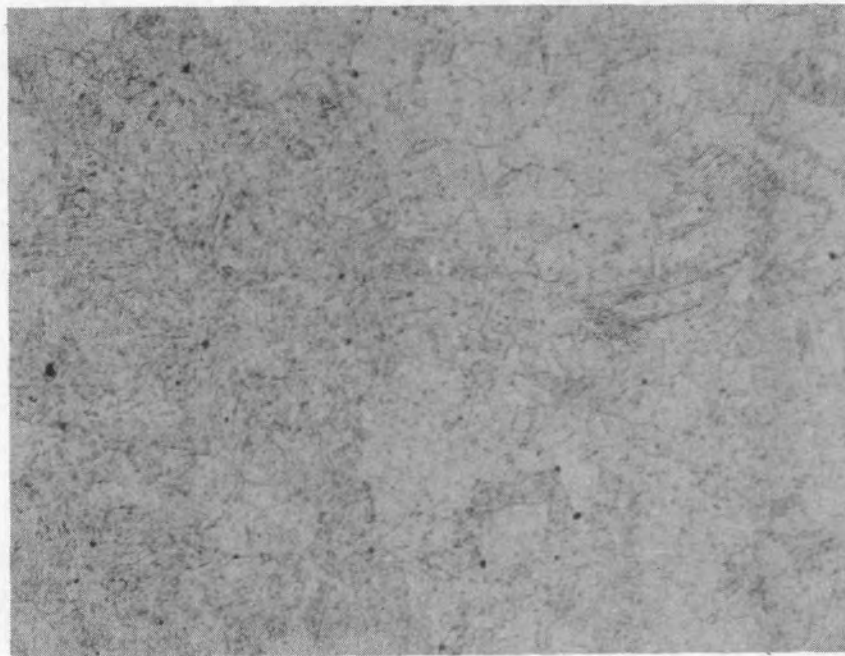


Figure 24. (continued)



(a) B8 sample 2

20  $\mu\text{m}$

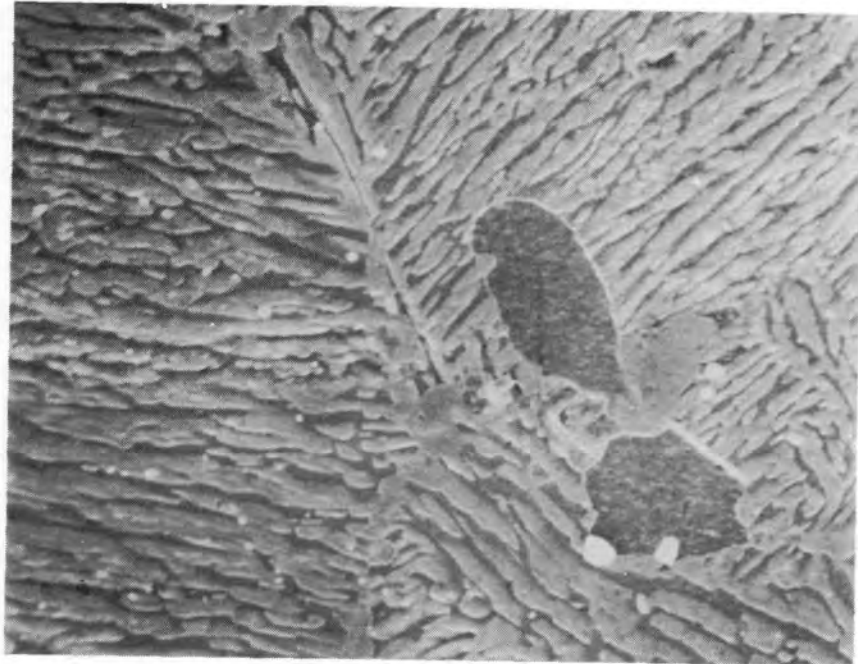


(b) B8 sample 7

20  $\mu\text{m}$

INEL 4 0946

Figure 25. Optical micrographs of grain structure in B8 Samples 2 and 7.



(a) B8 sample 2

2  $\mu$ m



(b) B8 sample 7

2  $\mu$ m

INEL 4 0947

Figure 26. SEM micrographs of grain structure in B8 Samples 2 and 7.

range [1089 to 1477 K (1500 to 2200°F)], depending on the duration of exposure and cooling rate. The microstructure of Sample 2 (Figure 26a) is lamellar.

Time-temperature-transformation (TTT) diagrams are graphical summaries of isothermal transformation data which are useful to examine microstructures and cooling rates. However, a TTT diagram does not exist for 17-4 PH, according to ARMCO. A recent study on 17-4 PH SS by ARMCO<sup>17</sup> concludes that the decomposition of austenite to ferrite does not occur in 17-4 PH SS during isothermal holds up to 30 h. The microstructures of all samples held isothermally at 700 to 1144 K (800 to 1600°F) during cooling from solution treatment were predominantly martensitic. Therefore, the TTT diagram does not show the nose observed for alloy steels up to the maximum times of 30 h tested.

Two isothermal holding times, 8 and 30 h, were tested by ARMCO on 17-4 PH SS. The Rockwell-C hardness of the isothermally held material in the as-quenched condition ranged from 29 to 39.5. After aging at H900, hardness increased in the range of 37 to 44.5. The condition A sample had a hardness of 43.5 after aging to H900. Hardness numbers versus isothermal holding temperatures are shown in Figure 27. One may infer that the prior isothermal holds up to 30 h, and subsequent heat treatment at H900 has no significant effect on hardness. From this figure, the temperature was obtained by comparing the hardness (38) of the aged B8 Sample 2 with aged samples at H900. The temperature for B8 Sample 2 ranged from 1089 to 1116 K (1500 to 1550°F), which is consistent with the estimated temperature of 1116 K (1550°F).

TEM examinations of B8 Samples 2 and 7 were performed. Sample 2 showed no copper precipitates, indicating it experienced a temperature in the solution-annealed range [1089 to 1477 K (1500 to 2200°F)]. Sample 7 showed large (2500 Å) copper precipitates, indicating it did not experience a temperature greater than 866 K (1100°F). This is consistent with the temperature estimated from hardness measurements.



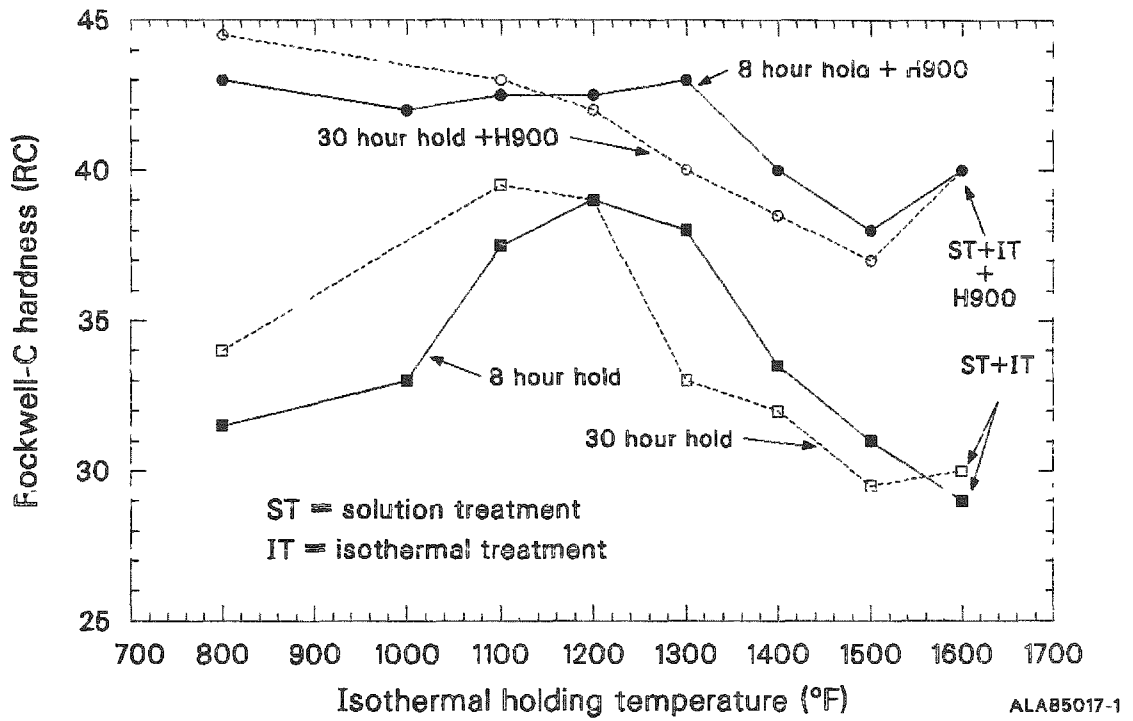


Figure 27. Hardness versus isothermal holding temperature.

The microstructure (lamellar), hardness (35.0), and lamellar spacing (0.24  $\mu\text{m}$ ) of B8 Sample 2 compares well with the microstructure (lamellar), hardness (35.4), and lamellar spacing (0.20  $\mu\text{m}$ ) of the annealed 17-4 PH standard [annealed at 1116 K (1550°F) for one hour and air-quenched]. Because of the difficulty experienced in measuring grain size, the grain size was not used to estimate the temperatures. As discussed earlier, heat-treatment of the B8 Sample 2 to the H900 condition resulted in a hardness number of about 38, which is lower than the hardness (47) measured for the H900 heat-treated H8 Sample 2. This lesser hardness suggests a partially solutionized condition for B8 Sample 2. A partially solutionized condition may be expected in the lower temperature range of the solutionized condition of 1089 to 1477 K (1500 to 2200°F). These observations suggest that B8 Sample 2 experienced a temperature of about 1116 K (1550°F). The uncertainty in the temperature estimate is about  $\pm 28$  to  $\pm 56$  K ( $\pm 50$  to  $\pm 100^\circ\text{F}$ ).

The temperature experienced by B8 Sample 3 (adjacent to B8 Sample 2) was estimated from the relative oxidation thicknesses measured at the H8 Sample 3 and the B8 Sample 3 locations. Assuming parabolic oxidation kinetics, the ratio of thicknesses is expressed in the following equation.

$$\left(\frac{x_2}{x_1}\right)^2 = e^{\frac{Q}{R} \left(\frac{T_2 - T_1}{T_1 T_2}\right)} \quad (1)$$

where

$x_2$  = Measured oxide thickness at H8 Sample 3 position =  
 $4.8 \times 10^{-3}$  cm

$x_1$  = Measured oxide thickness at B8 Sample 3 position =  
 $5.0 \times 10^{-4}$  cm

$Q$  = Activation energy for self-diffusion of iron in gamma iron =  
67.9 kcal/mol.

$T_2$  = Temperature at H8 Sample 3 position = 1255 K (assumed to be that of H8 Sample 2)

$T_1$  = Temperature at B8 Sample 3 position = unknown.

Substituting the above parameters in Eq. 1, the temperature  $T_1$  at the B8 Sample 3 location was 1080 K (1485°F). This temperature is consistent with the temperature estimated by the annealing study for B8 Sample 2, 1116 K (1550°F).

B8 Sample 5 (304 SS), adjacent to the A-hot leg axial location, was examined by SEM and optical metallography. A Rockwell-B hardness of 87.67 was measured. The annealing study of 304L SS standards discussed in Appendix A suggests that the B8 leadscrew near the A-hot leg axial location experienced a temperature of about 911 K (1180°F).

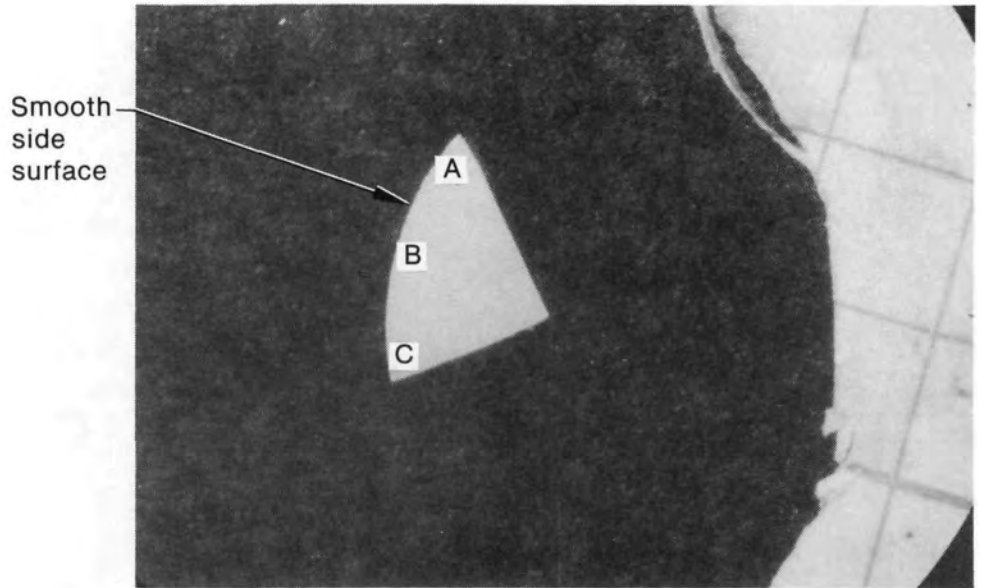
#### B8 Surface Layers

Two B8 surface Samples (3 and 8) were metallographically examined in the polished condition to determine the thickness of the surface layers. These thicknesses are presented in Table 5. Macrographs of these metallurgical samples are shown in Figure 28. Figure 28a shows a cross section of a smooth 17-4 PH SS surface on B8 Sample 3. Circumferential locations near A, B, and C were examined, and the micrographs are shown in Figure 29. Three thin layers were found: inner ( $\sim 4 \mu\text{m}$ ), middle ( $\sim 0.1 \mu\text{m}$ ), and outer ( $\sim 1.5 \mu\text{m}$ ). Figure 28b shows a longitudinal cross section of the thread portion of B8 Sample 8. Micrographs of the thread top and thread face are shown in Figure 30. Again, three layers were found: inner ( $\sim 8 \mu\text{m}$ ), middle ( $\sim 48 \mu\text{m}$ ), and outer ( $\sim 66 \mu\text{m}$ ). The surface layer thickness (66  $\mu\text{m}$ ) near the top of the plenum assembly is the largest found on the B8 leadscrew. The thread top and thread face of the threaded region contained the largest surface layers, indicating that both gravitational settling and vapor deposition may have occurred. Elemental composition of the surface layers on B8 Sample 3 and B8 Sample 8 were measured by EDS, and the data are discussed in the section on chemical analyses.

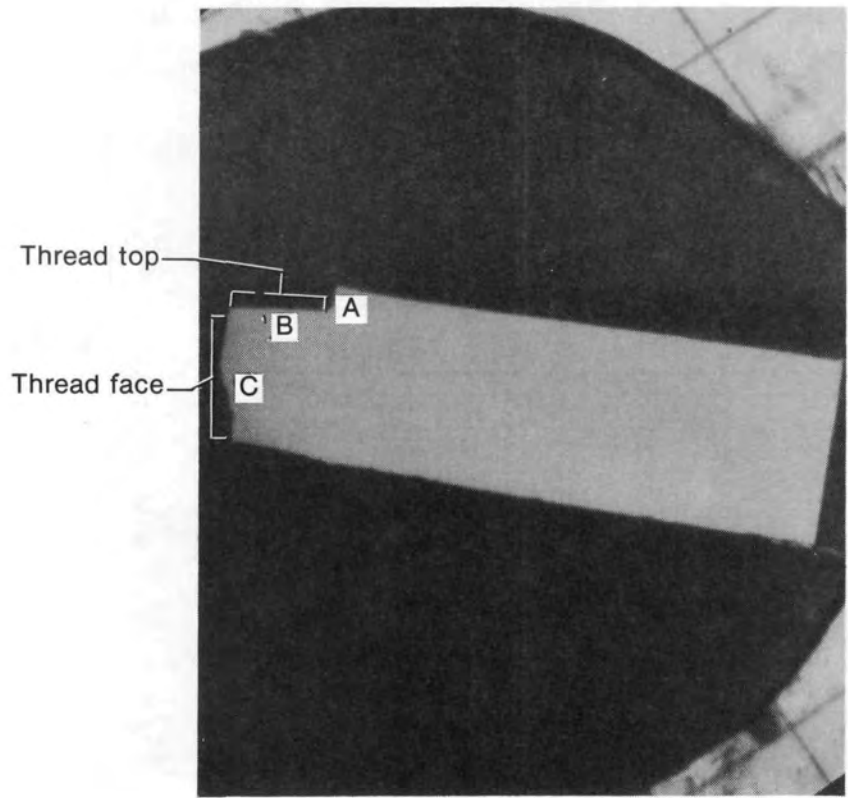
TABLE 5. SURFACE LAYER THICKNESSES ON B8 SURFACE SAMPLES

Leadscrew Sample	Distance from from Bottom of Leadscrew (cm)	Surface Characteristics	Examination Location	Surface Layer Thickness ( $\mu\text{m}$ )			Sum of Inner Middle and Outer Layers ( $\mu\text{m}$ )
				Inner	Middle	Outer	
3 (close to bottom of plenum assembly)	4.45 - 12.07	Smooth side surface (17-4 PH SS)	A	4.0 <sup>c</sup>	0.1 <sup>a</sup>	1.0 <sup>b</sup>	5.1
			B	2.0 <sup>c</sup>	0.0	1.5 <sup>b</sup>	3.5
			C	1.5 <sup>c</sup>	0.1 <sup>a</sup>	1.5 <sup>b</sup>	3.1
8 (close to top of the plenum assembly)	304.17 - 304.80	Thread top surface (17-4 PH SS)	A	8.0 <sup>b</sup>	0.0	12.0 <sup>c</sup>	20.0
			B	2.0 <sup>b</sup>	40.0 <sup>c</sup>	24.0 <sup>d</sup>	66.0
			C	3.0 <sup>b</sup>	48.0 <sup>c</sup>	12.0 <sup>d</sup>	63.0
		Thread face surface (17-4 PH SS)					

- a. Thin layer between inner and outer layer containing shiny deposits.
- b. Dense layer. A layer containing no pores.
- c. Porous layer. A layer containing pores.
- d. Loose layer.



(a) B8 sample 3



(b) B8 sample 8

INEL 4 0949

Figure 28. Macrographs of B8 surface Samples 3 and 8.

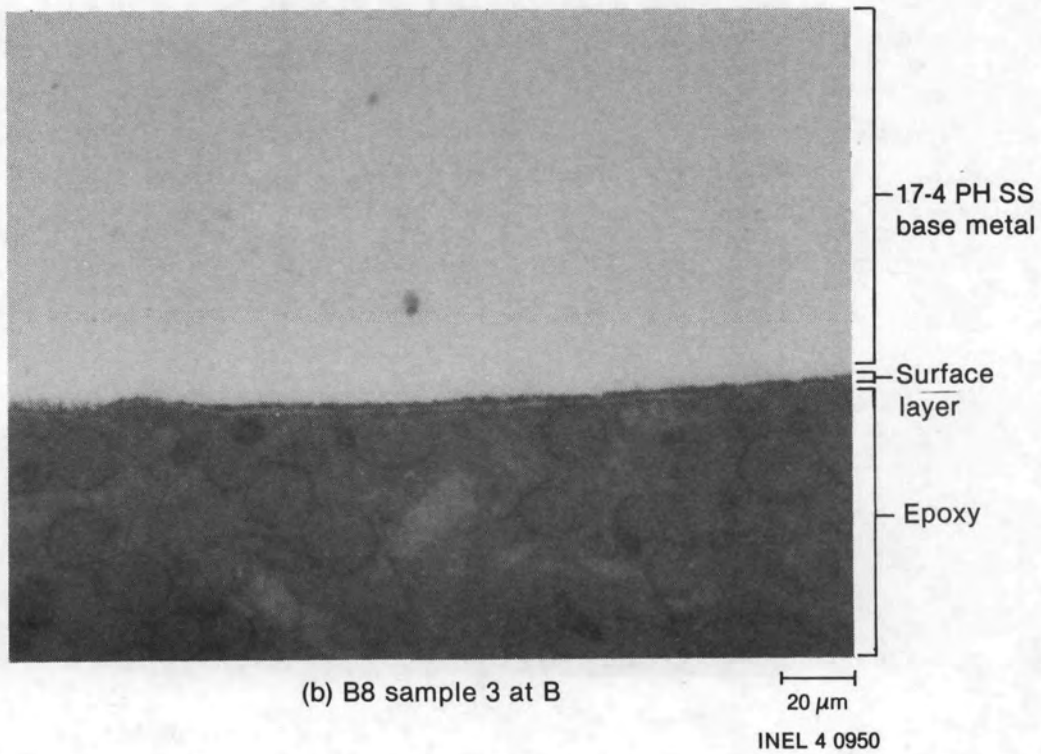
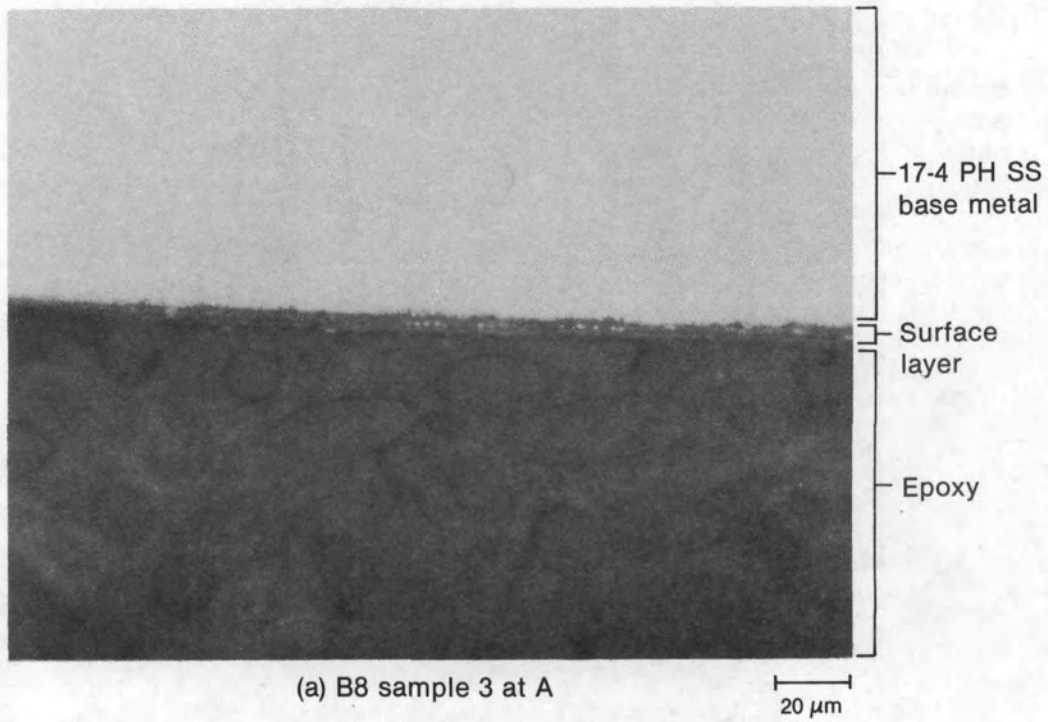
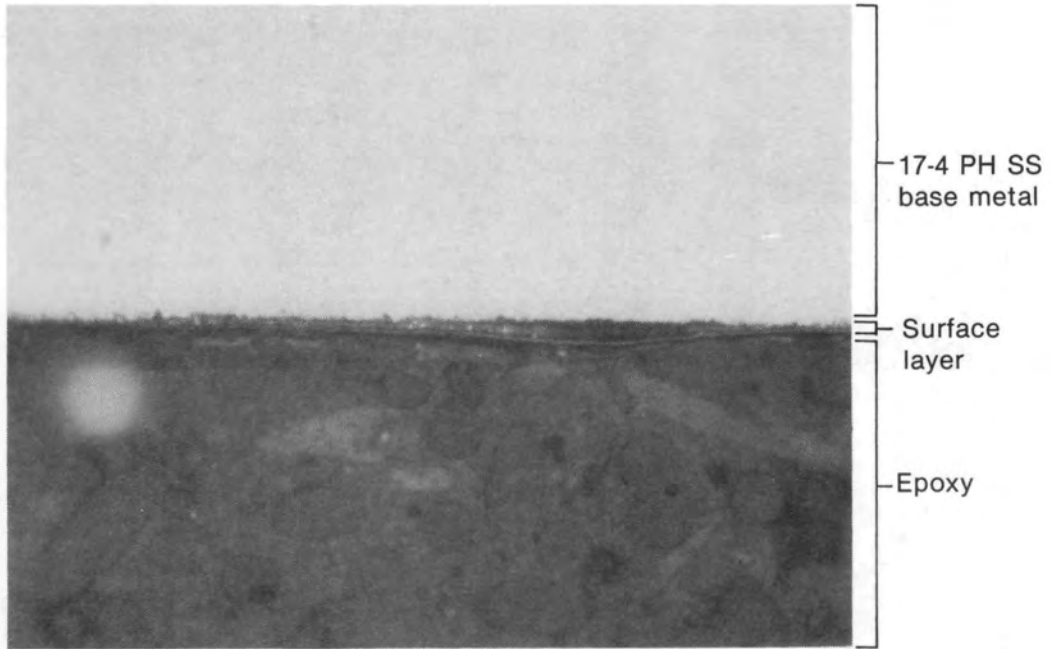


Figure 29. Micrographs of B8 Sample 3 showing surface layers.



(c) B8 sample 8 at C

20 $\mu$ m

INEL 4 0951

Figure 29. (continued)

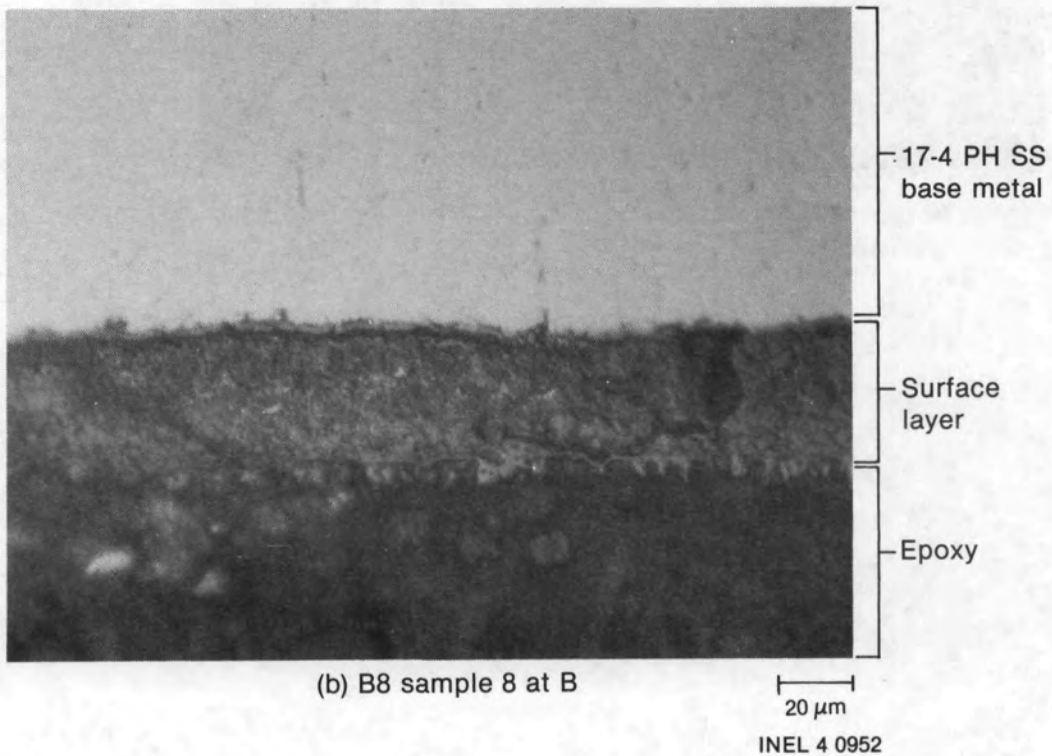
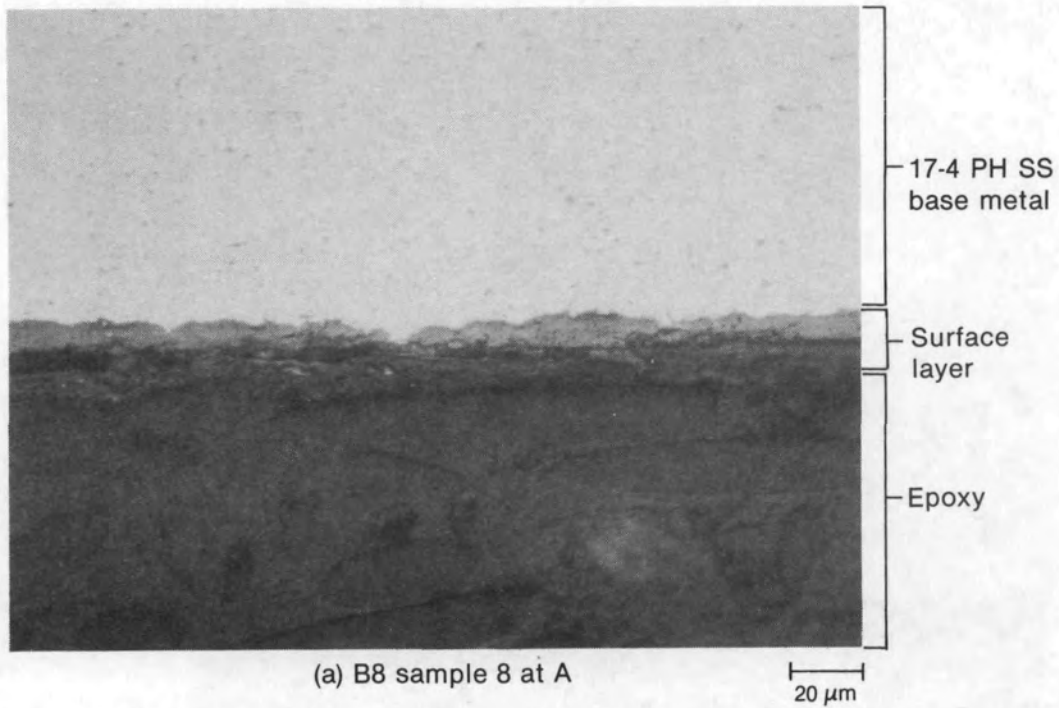
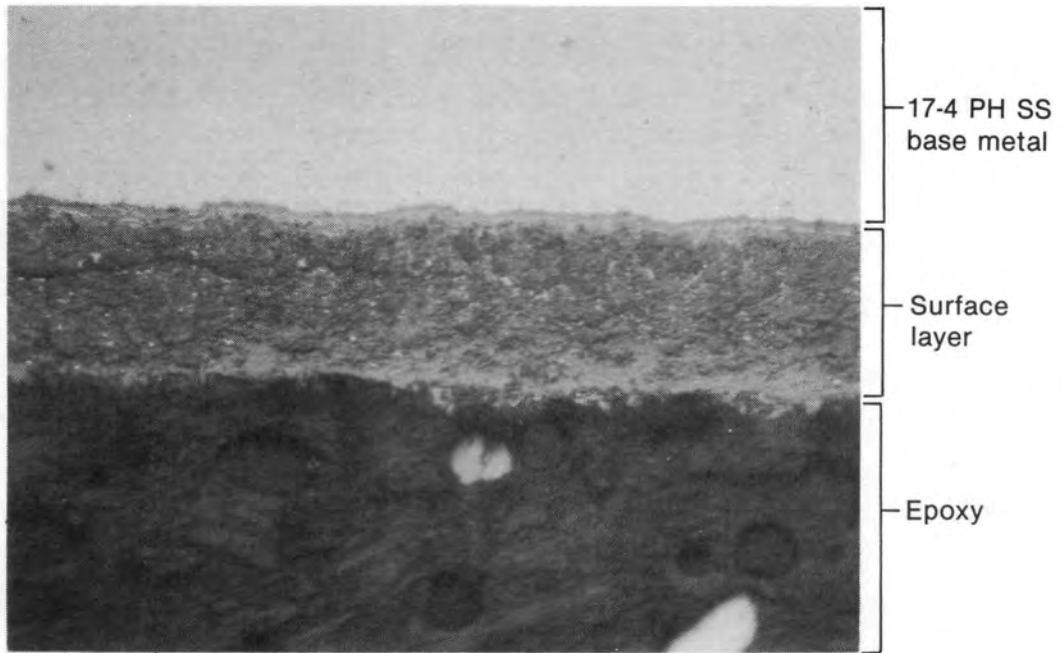


Figure 30. Micrographs of B8 Sample 8 showing surface layers.





(c) B8 sample 8 at C

20 $\mu$ m  
INEL 4 0953

Figure 30. (continued)

## Chemical Analyses

Chemical analyses were performed on samples obtained from the H8 and B8 leadscrews. The objective of these sample analyses is to aid in determining the extent and nature of fission product and core material deposition on the leadscrew surfaces. The samples analyzed are of four distinct types: brushoff debris; acidic solutions used to decontaminate the metallurgical samples; undissolved (insoluble) decontamination sample fractions (filtered solid material from the decontamination solution); and surface samples (lightly brushed leadscrew sections with the surface deposition left basically intact). Figures 2 and 3 and Table 1 identify the specific samples and outline the types of analyses performed on each sample.

The sample locations were chosen to identify possible radial and/or axial gradients in the elemental content or compounds present on the surfaces between the bottom and top of the plenum assembly. A comparison of elemental concentrations at the locations measured was performed, and an evaluation was made of the decontamination solution effectiveness on the leadscrew surfaces.

### H8 Leadscrew Chemical Analyses

The chemical analyses (i.e., ES, SEM/EDS and X-ray diffraction) were performed to determine elemental composition and the identity of chemical compounds deposited on the leadscrew surfaces. Debris brushed from the leadscrew surface, the soluble and insoluble portions of solutions used to decontaminate metallurgical samples, and lightly brushed leadscrew surfaces were examined. For comparison with the elemental analysis data, Table 6 lists the elemental composition (type and quantity) of the core structural materials.

Brushoff Debris. Table 7 lists the ES analysis results for the brushoff debris from the three lower leadscrew sections (H8-7, H8-8, and H8-9) and the probable sources of each element measured based on the Table 6 information. The principal observations made concerning the ES

TABLE 6. CORE MATERIAL COMPOSITION

<u>Material</u>	<u>Element</u>	<u>Weight %</u>	<u>Material</u>	<u>Element</u>	<u>Weight %</u>
UO <sub>2</sub> (93050 kg)	235U	2.265	Inconel-718 (1211 kg)	Ni	51.900
	238U	85.882		Cr	19.000
	O	11.853		Fe	18.000
Zircaloy-4 (23029 kg)	Zr	97.907		Nb	5.553
	Sn	1.60		Mo	3.000
	Fe	0.225		Ti	0.800
	Cr	0.125		Al	0.600
	O	0.095		Co	0.470
	C	0.0120		Si	0.200
	N	0.0080		Mn	0.200
	HF	0.0078		N	0.130
	S	0.0035		Cu	0.100
	Al	0.0024		C	0.040
	Ti	0.0020		S	0.007
	V	0.0020			
	Mn	0.0020			
	Ni	0.0020	ZrO <sub>2</sub> (331 kg)	Zr	74.0
	Cu	0.0020		O	26.0
	W	0.0020			
	H	0.0013			
Co	0.0010	Ag-In-Cd (2749 kg)	Ag	80.0	
B	0.000033		In	15.0	
Cd	0.000025		Cd	5.0	
U	0.000020				
Type 304 SS (676 kg)	Fe	68.635	B <sub>4</sub> C-Al <sub>2</sub> O <sub>3</sub> (626 kg)	Al	34.33
	Cr	19.000		O	30.53
Unidentified SS (3960 kg)	Ni	9.000		B	27.50
	Mn	2.000		C	7.64
	Si	1.000			
	N	0.130	Gd <sub>2</sub> O <sub>3</sub> -UO <sub>2</sub> (131.5 kg)	Gd	10.27
	C	0.080		U	77.72
	Co	0.080		O	12.01
	P	0.045			
	S	0.030			

TABLE 7. EMISSION SPECTROSCOPIC ANALYSIS OF THE BRUSHOFF DEBRIS FROM THE H8 LEADSCREW (wt%)

Element	H8-9 ( $5.4 \times 10^{-1}$ ) <sup>a</sup>	H8-8 ( $6.1 \times 10^{-2}$ ) <sup>a</sup>	H8-7 (35.6) <sup>a</sup>	Probable Source
Ag	0.1	0.2	0.002	Control rod
Al	0.2	0.2	0.05	B <sub>4</sub> C-Al <sub>2</sub> O <sub>3</sub>
B	0.3	1.0	0.5	Coolant water/ B <sub>4</sub> C-Al <sub>2</sub> O <sub>3</sub>
Ca	--b	0.7	--b	--
Cr	1.0	21.0	22.0	Stainless steel/Inconel
Cu	0.008	0.03	0.001	Inconel
Fe	6.0	33.0	37.0	Stainless steel/Inconel
Mg	--b	0.6	0.04	--
Mn	0.7	0.3	0.3	Stainless steel
Ni	0.1	4.0	0.02	Stainless Steel/Inconel
Si	0.02	4.0	5.0	Stainless steel
Ti	--b	0.6	0.02	Inconel
Zr	26.0	0.08	0.40	Zircaloy
U	45.0	--b	--b	Fuel

a. Weight of debris in g.

b. Not detected.

analysis results were: (a) fuel rod components account for most of the brushoff debris on the bottom leadscrew section (H8-9); (b) stainless steel and Inconel components (iron + chromium) account for most of the brushoff debris on the portion of the leadscrew near the top of the plenum assembly; (c) aluminum, possibly from the  $B_4C-Al_2O_3$  control rods, was found in debris removed from all three leadscrew sections examined, and the total amount was much greater near the top than near the bottom of the plenum assembly (~ a factor of 16); (d) silver from the silver-indium-cadmium (Ag-In-Cd) control rods was present in debris from all sample locations; and (e) although the aluminum and silver contents in the core materials are relatively similar, proportionally more aluminum than silver was found in the brushoff debris. ES analysis was not performed for indium and cadmium due to their location in the emission spectrum, which makes them not easily identifiable.

Decontamination Solutions. Elemental analyses were performed by ES on soluble and insoluble fractions of metallurgical sample decontamination solutions. The soluble and insoluble fractions were separated by filtering the decontamination solutions, composed of 40-wt%  $HNO_3$  + 0.12-M HF, with a 0.45- $\mu$ m vacuum filter system to collect the insoluble fractions. The solid and liquid fractions were independently analyzed. Table 8 lists the elemental analysis (in  $\mu$ g/mL) of the liquid (soluble) portion of the H8 decontamination solutions and the total quantity of each element removed. The volume of each solution varied, as noted in the table, due to the amount of wash solution used during the rinse; however, the total amount of each element present is quantitative, as the individual samples were decontaminated until radiologically clean. Table 9 lists the elemental analysis results for the insoluble fraction of each sample. These data are listed in percent of the total weight (wt%) and as the total weight of each element removed, which is quantitative for the sample.

The initial observation concerning these data is that silver was measured in the insoluble fractions but not in the soluble fractions. Silver, in its elemental form, is soluble in nitric acid. However, it was retained in the insoluble form while being stored at ambient temperature

TABLE 8. EMISSION SPECTROSCOPIC ANALYSIS OF THE SOLUBLE PORTIONS OF THE DECONTAMINATION SOLUTIONS FROM THE H8 LEADSCREW SAMPLES  
( $\mu\text{g/mL}$  and total weight removed in mg)

Element	2 (114 mL) <sup>a</sup>		7 (110 mL) <sup>a</sup>		11 (170 mL) <sup>a</sup>		14 (100 mL) <sup>a</sup>		15 (320 mL) <sup>a</sup>	
	$\mu\text{g/mL}$	mg	$\mu\text{g/mL}$	mg	$\mu\text{g/mL}$	mg	$\mu\text{g/mL}$	mg	$\mu\text{g/mL}$	mg
Ag	--b		--b		--b		--b		--b	
Al	37.0	4.2	45.0	4.9	39.0	6.6	47.8	4.8	38.4	12.3
B	195.0	22.2	249.0	27.4	256.0	43.5	269.0	26.9	229.0	73.3
Ca	3.3	0.4	6.1	0.7	6.0	1.0	18.0	1.8	15.8	5.1
Cr	89.1	10.2	190.0	20.9	130.0	22.1	186.0	18.6	120.0	38.4
Cu	28.4	3.2	17.2	1.9	36.1	6.1	54.1	5.4	35.0	11.2
Fe	520.0	59.3	819.0	90.1	837.0	142.3	1400.0	140.0	514.0	16.4
Mg	<0.5	--	0.8	0.1	<0.5	--	13.0	1.3	13.4	4.3
Mn	3.3	0.4	12.2	1.3	5.7	1.0	5.9	0.6	4.5	1.4
Na	100.0	11.4	102.0	11.2	81.0	13.8	123.0	12.3	122.0	39.0
Ni	109.0	12.4	71.9	7.9	43.3	7.4	60.6	6.1	44.4	14.2
Si	54.2	6.2	29.2	3.2	46.8	8.0	20.0	2.0	97.3	31.1
Zr	2.8	0.3	4.1	0.4	3.2	0.5	2.7	0.3	2.8	0.9

a. Volume of decontamination solutions.

b. Not detected.

TABLE 9. EMISSION SPECTROSCOPIC ANALYSIS OF THE INSOLUBLE MATERIALS FROM THE H8 DECONTAMINATION SOLUTIONS  
(wt% and total weight removed in mg)

Element	<sup>2</sup> (61.8 mg) <sup>g</sup>		<sup>7c<sup>a</sup></sup> (97.1 mg) <sup>g</sup>		<sup>7b<sup>b</sup></sup> (100.8 mg) <sup>g</sup>		<sup>7a<sup>c</sup></sup> (3.1 mg) <sup>g</sup>		<sup>11</sup> (100.9 mg) <sup>g</sup>		<sup>14.1<sup>d</sup></sup> (146.7 mg) <sup>g</sup>		<sup>14.2<sup>e</sup></sup> (9.6 mg) <sup>g</sup>		<sup>15</sup> (218.2 mg) <sup>g</sup>		Filter <sup>f</sup> wt%
	wt%	mg	wt%	mg	wt%	mg	wt%	mg	wt%	mg	wt%	mg	wt%	mg	wt%	mg	
Ag	9.0	--	0.606	<0.1	0.006	<0.1	0.01	<0.1	0.005	<0.1	0.003	<0.1	--h	--	--h	--h	0.0002
Al	9.0	--	0.06	<0.1	0.03	<0.1	--h	--h	--h	--h	--h	--	--h	--	--h	--h	5.0
B	16.0	9.9	0.3	0.29	0.2	0.2	1.0	<0.1	2.0	2.0	0.5	0.7	--h	--	--h	--h	2.0
Ca	6.0	3.7	0.2	0.19	--h	--h	8.0	0.25	10.0	10.1	5.0	7.3	22.0	2.1	16.0	34.9	4.0
Cr	13.0	8.0	16.0	15.5	32.0	32.3	21.0	0.65	12.0	12.1	16.0	23.5	22.0	2.1	32.0	69.8	0.3
Cu	--h	--h	0.0006	<0.1	0.003	<0.1	--h	--h	--h	--h	--h	--h	--h	--h	--h	--h	0.0001
Fe	9.0	5.6	46.0	44.7	33.0	33.3	28.0	0.87	25.0	25.2	4.0	5.9	42.0	4.0	16.0	34.9	1.0
Mg	--h	--h	0.06	<0.1	0.02	<0.1	0.8	<0.1	8.0	8.1	0.6	0.88	18.0	1.7	--h	--h	1.0
Mn	0.1	<0.1	0.02	<0.1	0.05	<0.1	3.0	<0.1	3.0	0.3	0.1	0.15	--h	--h	0.4	0.87	0.02
Ni	--h	--	0.01	<0.1	0.03	<0.1	0.03	<0.1	0.02	<0.1	0.01	<0.1	--h	--h	0.03	<0.1	--h
Si	4.0	2.5	4.0	3.9	2.0	2.0	3.0	<0.1	7.0	7.1	3.0	4.4	--h	--h	4.0	8.7	35.0
Ti	0.1	<0.1	0.06	<0.1	0.06	<0.1	0.1	<0.1	0.1	0.1	0.1	0.15	0.9	<0.1	--h	--h	0.08
Zr	--h	--h	0.2	0.19	0.3	0.30	0.1	<0.1	0.07	<0.1	0.1	0.15	--h	--h	--h	--h	0.01

73

- a. Outer sleeve from Sample 7.
- b. 410 SST pin from Sample 7.
- c. The 304 SST and 17-4 PH portions of Sample 7.
- d. Insoluble material in the first decontamination solution (40 wt% HNO<sub>3</sub> + 0.12-M HF).
- e. Insoluble material in the second decontamination solution (40 wt% HNO<sub>3</sub> + 0.12-M HF).
- f. The filter which was used to remove insoluble materials from the solution.
- g. Weight of insoluble material.
- h. Not detected.

for one to two months in a strong nitric acid solution prior to analysis. It is possible that the silver might have been encapsulated within an insoluble layer present on the leadscrew and may have been deposited before or at the same time as the insoluble adherent layer. SEM results showed silver globules near the surface of the leadscrew, which makes the insolubility of the silver surprising. Silver was also present in the brushoff debris, and a potassium bisulfate fusion was required for dissolution of that material. The data indicate that zirconium, although measurable in the solid fractions on Samples 7 to 14 but not on 2 or 15, was measured in all liquid fractions, indicating it was in a soluble form. Many forms of zirconium, including elemental zirconium and  $ZrO_2$ , are soluble in hydrofluoric acid, which was a component of the decontamination solutions used.

For comparison purposes, the elemental analysis data were converted to the quantity of each element removed per square centimeter of surface area for both soluble and insoluble fractions of the decontamination solutions. The comparisons are listed in Table 10. Consistent soluble surface concentrations were observed for aluminum, boron, manganese, and zirconium at all locations along the leadscrew, indicating a relatively uniform surface deposition for these elements. The boron would be expected to be evenly distributed, as it is present in the reactor coolant. The aluminum is a principal component of the  $B_4C-Al_2O_3$  poison rods, and the zirconium is only present in the cladding. These data indicate similar concentrations for these elements in the tightly adherent material. Aluminum and zirconium are also constituents of the brushoff debris. However, the relative concentrations are different and less consistent, indicating that the two types of sample material were not formed from material with the same elemental composition.

Comparison of Brushoff Debris and Decontamination Solutions. The concentrations (in atom ppm) of elements detected by ES in the brushoff debris and the decontamination solutions, both solid and liquid fractions, are compared in Table 11 for H8 Samples 2 and 15. The fraction of boron atoms deposited on Samples 2 through 15 is similar, as indicated by the sum for each sample shown in Table 12. However, the total boron deposition



TABLE 10. TOTAL ELEMENTAL CONTENT REMOVED BY DECONTAMINATION OF H8 SAMPLES  
(mg removed/cm<sup>2</sup>)

	Total Elemental Content (mg/cm <sup>2</sup> )					
	<sup>2</sup> (11.4 cm <sup>2</sup> ) <sup>a</sup>		<sup>11</sup> (22.7 cm <sup>2</sup> ) <sup>a</sup>		<sup>15</sup> (33.1 cm <sup>2</sup> ) <sup>a</sup>	
	Soluble <sub>b</sub> (114 mL) <sup>b</sup>	Insoluble <sub>c</sub> (61.8 mg) <sup>c</sup>	Soluble <sub>b</sub> (170 mL) <sup>b</sup>	Insoluble <sub>c</sub> (100.9 mg) <sup>c</sup>	Soluble <sub>b</sub> (320 mL) <sup>b</sup>	Insoluble <sub>c</sub> (218.2 mg) <sup>c</sup>
Ag	--d	--d	--d	2.2 x 10 <sup>-4</sup>	--d	--d
Al	0.37	--d	0.29	--d	0.37	--d
B	1.95	0.87	1.92	0.09	2.21	--d
Ca	0.03	0.33	0.04	0.44	0.15	1.05
Cr	0.89	0.70	0.97	0.53	1.16	2.11
Cu	0.028	--d	0.27	--d	0.34	--d
Fe	5.20	0.49	6.30	1.11	4.97	1.05
Mg	0.01	--d	<0.01	0.36	0.13	--d
Mn	0.03	0.01	0.04	0.01	0.04	0.03
Na	1.00	--d	0.61	--d	1.18	2.0 x 10 <sup>-3</sup>
Ni	1.09	--d	0.32	8.8 x 10 <sup>-4</sup>	0.43	2.0 x 10 <sup>-3</sup>
Si	0.54	0.22	0.35	0.31	0.94	0.26
Zr	0.03	--d	0.02	3.1 x 10 <sup>-3</sup>	0.03	--d

a. Surface area of sample.

b. Volume of decontamination solution.

c. Weight of insoluble material.

d. Not detected.

TABLE 11. ELEMENT CONTENT FROM H8 LEADSCREW SAMPLES AS DETERMINED FROM EMISSION SPECTROSCOPY  
(atom ppm)<sup>a</sup>

Element	Sample <sup>b</sup>	Brushoff Debris <sup>c</sup>		Soluble Decontamination Solution		Insoluble Material	
		Atom ppm	Percent	Atom ppm	Percent	Atom ppm	Percent
Ag	2	$1.1 \times 10^1$	100	--d	--	--d	--d
	15	$8.8 \times 10^{-2}$	100	--d	--	--d	--d
B	2	$3.5 \times 10^2$	$4.7 \times 10^{-2}$	$4.6 \times 10^5$	62.0	$2.8 \times 10^5$	38.0
	15	$2.3 \times 10^2$	$4.8 \times 10^{-2}$	$4.8 \times 10^5$	100.0	--d	--
Ca	2	--d	--	$2.0 \times 10^4$	42.5	$2.7 \times 10^4$	57.4
	15	--d	--	$8.6 \times 10^3$	6.7	$1.2 \times 10^5$	93.3
Cr	2	$2.3 \times 10^2$	0.3	$4.3 \times 10^4$	48.2	$4.6 \times 10^4$	51.5
	15	$2.0 \times 10^3$	--	$5.1 \times 10^4$	22.1	$1.8 \times 10^5$	77.9
Cu	2	1.5	$1.4 \times 10^{-2}$	$1.1 \times 10^4$	100.0	--d	--
	15	$7.5 \times 10^{-2}$	$6.3 \times 10^{-4}$	$1.2 \times 10^4$	100.0	--d	--
Fe	2	$1.3 \times 10^3$	0.5	$2.3 \times 10^5$	88.4	$2.9 \times 10^4$	11.1
	15	$3.2 \times 10^3$	1.1	$2.0 \times 10^5$	69.9	$8.3 \times 10^4$	29.0
Mg	2	--d	--	$5.0 \times 10^2$	100.0	--d	--
	15	8.0	$6.7 \times 10^{-2}$	$1.2 \times 10^4$	100.0	--d	--
Mn	2	$1.5 \times 10^2$	7.6	$1.5 \times 10^3$	75.8	$3.3 \times 10^2$	16.6
	15	$2.7 \times 10^1$	0.69	$1.8 \times 10^3$	45.8	$2.1 \times 10^3$	53.5
Ni	2	$2.0 \times 10^1$	$4.3 \times 10^{-2}$	$4.6 \times 10^4$	100.0	--d	--
	15	1.6	$1.0 \times 10^{-2}$	$1.6 \times 10^4$	99.9	$1.5 \times 10^1$	$9.4 \times 10^{-2}$

TABLE 11. (continued)

Element	Sample <sup>b</sup>	Brushoff Debris <sup>c</sup>		Soluble Decontamination Solution		Insoluble Material	
		Atom ppm	Percent	Atom ppm	Percent	Atom ppm	Percent
Si	2	8.7	$1.2 \times 10^{-2}$	$4.6 \times 10^4$	63.9	$2.6 \times 10^4$	36.1
	15	$8.5 \times 10^2$	$7.0 \times 10^{-1}$	$7.7 \times 10^4$	64.3	$4.2 \times 10^4$	35.0
Ti	2	--d	--	--d	--	$3.8 \times 10^2$	100.0
	15	2.0	100.0	--d	--	--d	--
Zr	2	$2.3 \times 10^3$	75.4	$7.5 \times 10^2$	24.6	--d	--
	15	$2.2 \times 10$	3.1	$6.8 \times 10^2$	96.9	--d	--
U	2	$2.3 \times 10^3$	100.0	--d	--d	--d	--
	15	--d	--d	--d	--d	--d	--

a. Atom ppm = number of atoms per million atoms deposited on the surface = N

$$= \frac{N_i \times 10^6}{N_T}$$

where

$$N_i = \frac{\text{weight (g)}}{\text{atomic weight (g)}} \times 6.02 \times 10^{23}$$

$$N_T = \sum N_i, i = \text{element.}$$

The total wt% in Tables 7 and 9 does not add to 100%. It is assumed that the remaining element is oxygen.

b. Sample 2 is close to the bottom and Sample 15 is close to top of the plenum assembly.

c. Brushoff debris elemental concentrations were calculated by averaging the total brushoff debris weight over the surface area of the leadscrew section.

d. Not measured.

TABLE 12. H8 BORON CONTENT  
(atom ppm)

Type of Sample	Sample Number (atom ppm)				
	2	7	11	14	15
Brushoff debris	$3.5 \times 10^2$	$3.5 \times 10^2$	$2.3 \times 10^2$	$2.3 \times 10^2$	$2.3 \times 10^2$
Soluble decontamination solution	$4.6 \times 10^5$	$4.6 \times 10^5$	$4.9 \times 10^5$	$4.20 \times 10^5$	$4.8 \times 10^5$
Insoluble material	$2.8 \times 10^5$	$2.7 \times 10^4$	$4.9 \times 10^4$	$9.4 \times 10^3$	--
Total	$2.40 \times 10^5$	$4.87 \times 10^5$	$4.9 \times 10^5$	$4.29 \times 10^5$	$4.80 \times 10^5$

is greater on the H8-7 section, as more brushoff debris was present. The average boron deposition is about  $5.3 \times 10^5$  atom ppm; i.e., about 53% of the atoms deposited on the leadscrew sample are due to boron. Greater than 62% of the boron was found in the decontamination solution. The majority of the remaining elements listed in Table 11 were found principally in the soluble portion of the decontamination solutions, with the exceptions of titanium, zirconium, and uranium. Although no silver was detected in H8 Samples 2 or 15 decontamination solutions, it was found in other decontamination samples.

Compound identification was performed by X-ray diffraction analysis on brushoff debris samples from the H8-9, H8-8, and H8-7 leadscrew sections, as well as the undissolved fractions from the decontamination solutions from Samples 2, 7A,<sup>a</sup> 7B,<sup>b</sup> 7C,<sup>c</sup> 11, 14.1,<sup>d</sup> 14.2,<sup>e</sup> and 15. The principal crystalline compound identified in all samples was magnetite ( $\text{Fe}_3\text{O}_4$ ). The only other compound identified was  $\text{UO}_2$ , found only in H8-9. These data indicate that most elements are present in the  $\text{Fe}_3\text{O}_4$  matrix, with the exception of the identified  $\text{UO}_2$ .

Surface Samples. Three surface samples from the H8 leadscrew were analyzed by SEM/EDS and ES. The samples were prepared by quartering the cylindrical surface samples and ranged in thickness from 0.25 to 1.0 cm. The samples are H8 Sample 3, from the bottom of the leadscrew, and H8 Samples 13 and 16, from the portion of the leadscrew near the top of the plenum assembly. The surface samples were analyzed as shown in Table 1. The metallographic examination of these samples was performed using SEM/EDS analysis for qualitative elemental identification. The unthreaded H8

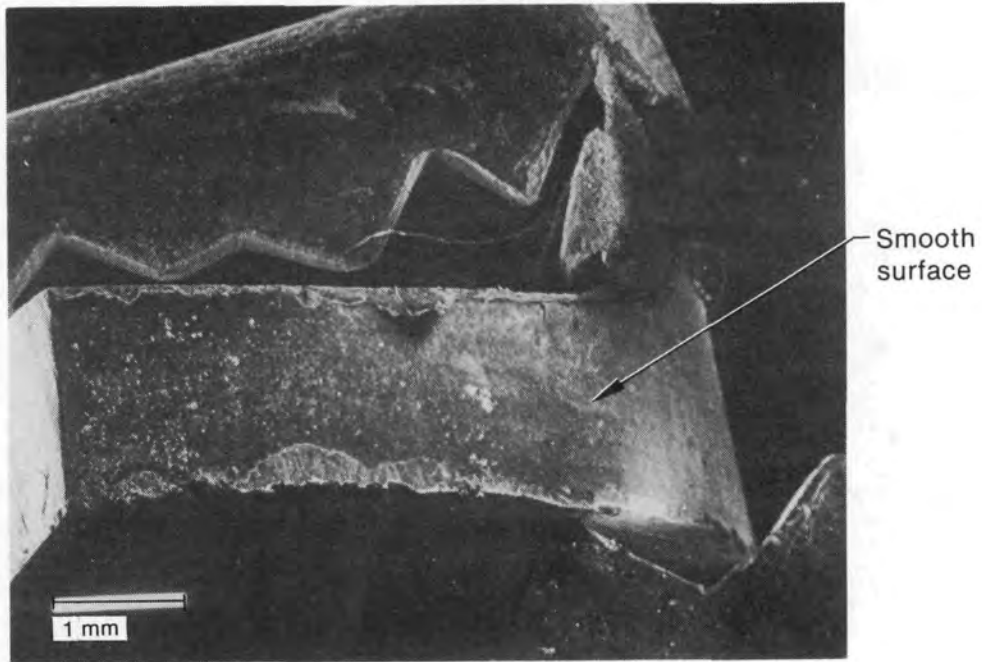
- 
- a. Outer 304 SS sleeve from H8 Sample 7.
  - b. 410 SS pin from H8 Sample 7.
  - c. The 304 SS and 17-4 PH portions of H8 Sample 7.
  - d. Sample 14 identification after first leaching.
  - e. Sample 14 identification after second leaching.

Sample 3 (17-4 PH SS) and the top and bottom threaded surfaces of H8 Samples 13 and 16 (17-4 PH SS) were specifically examined and analyzed by EDS. SEM micrographs of the smooth surface of Sample 3 and the top and bottom threaded surfaces of Sample 16 are shown in Figures 31, 32, and 33, respectively. The elements identified by EDS are listed in Table 13 for the H8 and B8 samples. (The B8 samples are discussed in a subsequent section.) The elements barium, chromium, copper, and iron were identified on H8 Sample 3. However, there are differences in the elements identified on H8 Samples 13 and 16 depending on where the examination was performed on the thread surface (i.e., top, face, or bottom). For example, cadmium and cesium were found only on the top of the thread and not on the bottom surface. (The B8 data do not conclusively support these data, as cadmium was observed on the bottom surface of B8 Sample 8.) The source of the cadmium is the control rods, whereas cesium is a fission product. Zirconium was observed only on the bottom thread surface, indicating the possibility of vapor disposition.

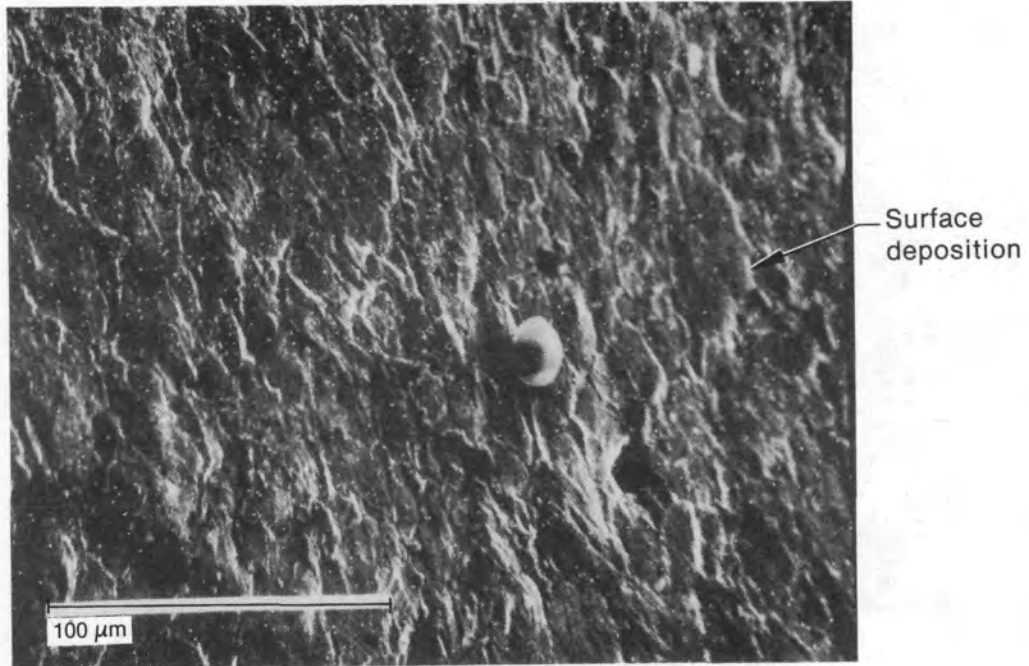
Barium was identified on all surfaces of all three surface samples. Barium oxide ( $BaO$ ) is readily formed when barium is released from fuel.  $BaO$  reacts with steam, and the more volatile barium hydroxide,  $Ba(OH)_2$  is formed, which is the dominant alkaline-earth vapor species.  $Ba(OH)_2$  readily condenses on surfaces whenever the vapor pressure is less than the equilibrium pressure.<sup>11</sup> During the TMI-2 accident, the steam pressure ranged from 8.2 to 15 MPa (82 to 150 bars); and the vapor pressure was less than the equilibrium pressure. In this pressure range,  $Ba(OH)_2$  will condense on exposed surfaces.

The EDS spectrum of one of the nodules in Figure 33c is shown in Figure 34. Silver is the major constituent. The aluminum peak is from the aluminum stub used to mount the sample. An X-ray spot map confirmed that the central portion of the nodule is silver.

The elemental composition of the surface layers on H8 Samples 3 and 16 was measured by EDS, and the data are presented in Table 14. SEM micrographs of H8 Sample 3 and H8 Sample 16 are shown in Figures 35 and 36,



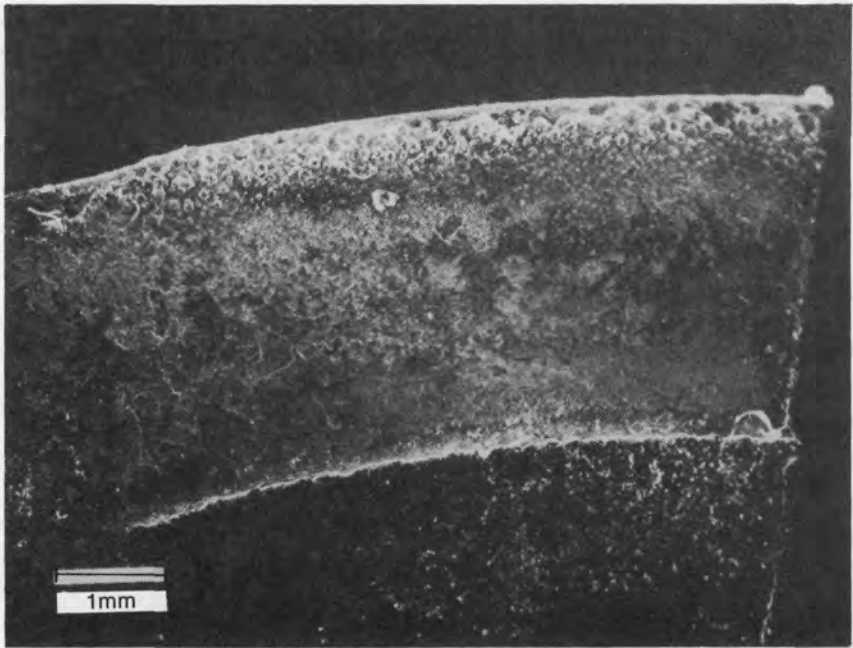
(a) SEM macrograph



(b) SEM micrograph

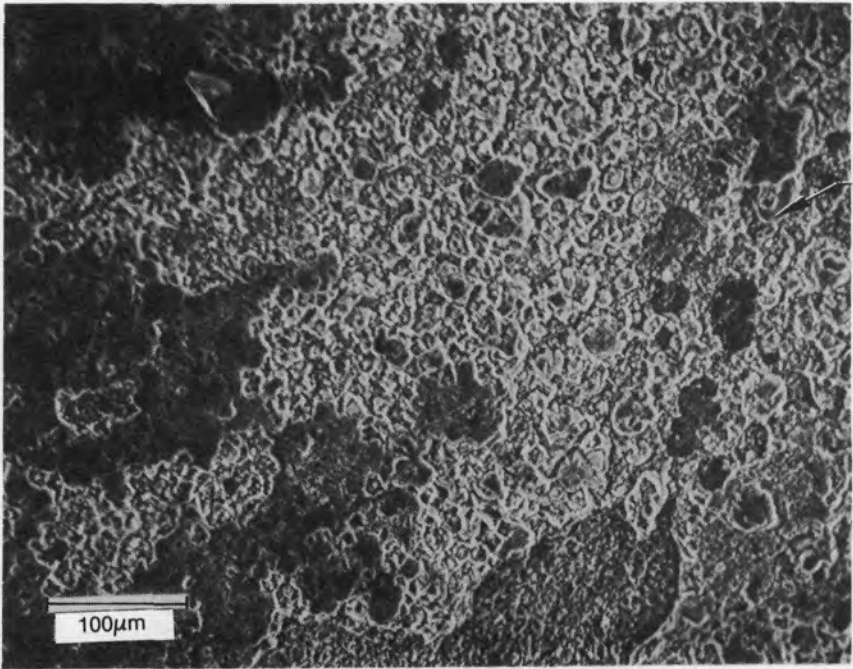
INEL 4 0954

Figure 31. SEM photographs of the smooth surface on H8 Sample 3 (close to the bottom of the plenum assembly).



Top of  
the threaded  
surface (17-4 PH SS)

(a) SEM macrograph



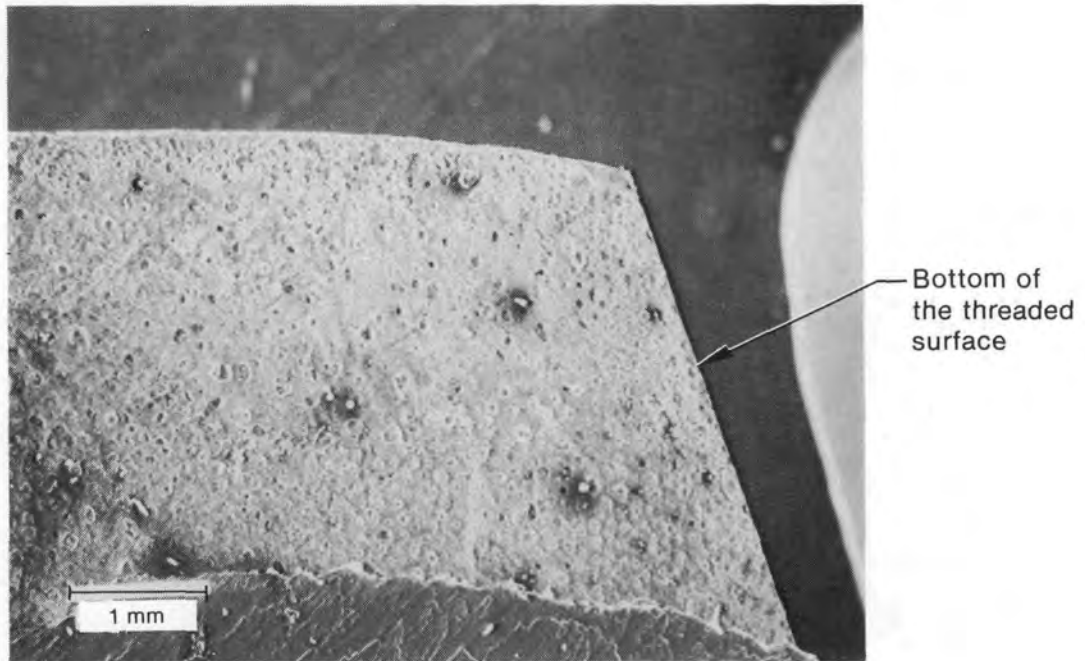
Surface  
deposition

(b) SEM micrograph

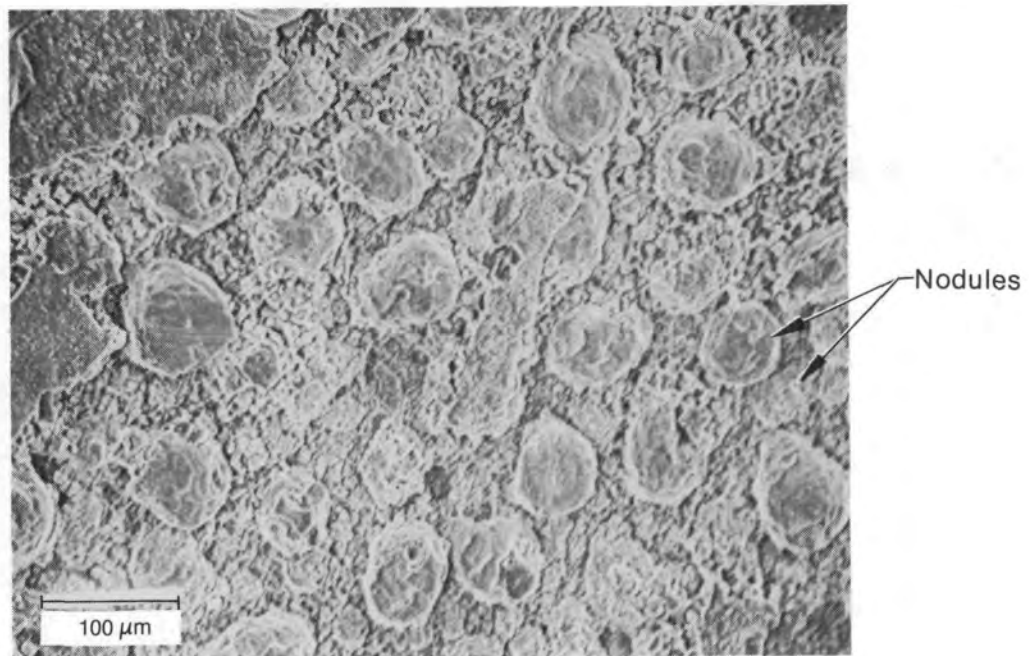
INEL 4 0955

Figure 32. SEM photographs of the top threaded surface of H8 Sample 16 (close to top of the plenum assembly).





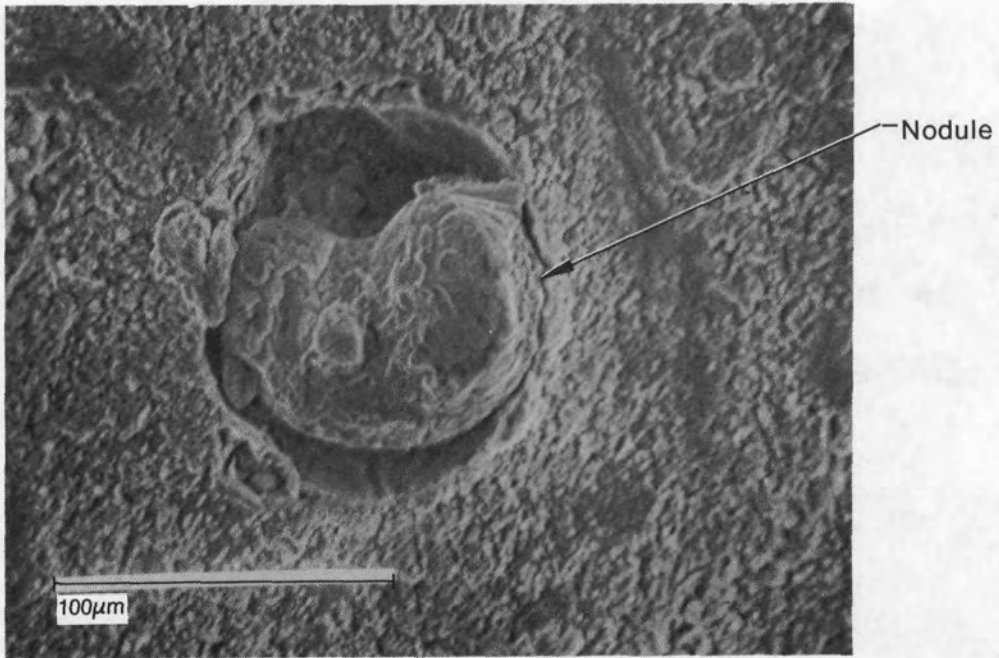
(a) SEM macrograph



(b) SEM micrograph

INEL 4 0956

Figure 33. SEM photographs of the bottom threaded surface of H8 Sample 16 (close to the top of the plenum assembly).



(c) SEM micrograph of a nodule

INEL 4 0957

Figure 33. (continued)

TABLE 13. QUALITATIVE ELEMENTAL IDENTIFICATION OF H8 AND B8 LEADSCREW SURFACE SAMPLES<sup>a</sup>

Sample	Distance From Bottom of Leadscrew		Elemental Constituents		
	cm	in.	Top of the Threaded Leadscrew Sample	Bottom of the Threaded Leadscrew Sample	Smooth Side Surface of the Leadscrew Sample
H8 Sample 3	4.45	1.75	--b	--b	Ba, Cr, Cu, and Fe
H8 Sample 13	233.00	91.75	Ag, Ba, Cd, Cr, Cs, Cu, Fe, In, Ni, and Te	Ag, Ba, Cr, Cu, Fe, In, Ni, and Te	--c
H8 Sample 16	302.90	119.25	Ag, Ba, Cr, Cu, Fe, In, Ni, and Te	Ag, Ba, Cr, Cu, Fe, Ni, and Zr	--c
B8 Sample 3	4.45	1.75	--b	--b	Ba, Cd, Cr, Cu, Fe, Ni, Si, and Zr
B8 Sample 8	304.17	119.75	Ag, Ba, Cr, Cu, Fe, In, Ni, and Te	Ag, Ba, Cd, Cr, Cu, Fe, In, Ni, Te, Zr, and U	--c

a. Elements were identified by SEM equipped with Energy-Dispersive-Spectrometer (EDS).

b. H8 Sample 3 and B8 Sample 3 are smooth-surfaced (304 SS) samples near the bottom of the plenum assembly.

c. H8 Sample 13, H8 Sample 16, and B8 Sample 8 are threaded 17-4 PH stainless steel samples near the top of the plenum assembly.

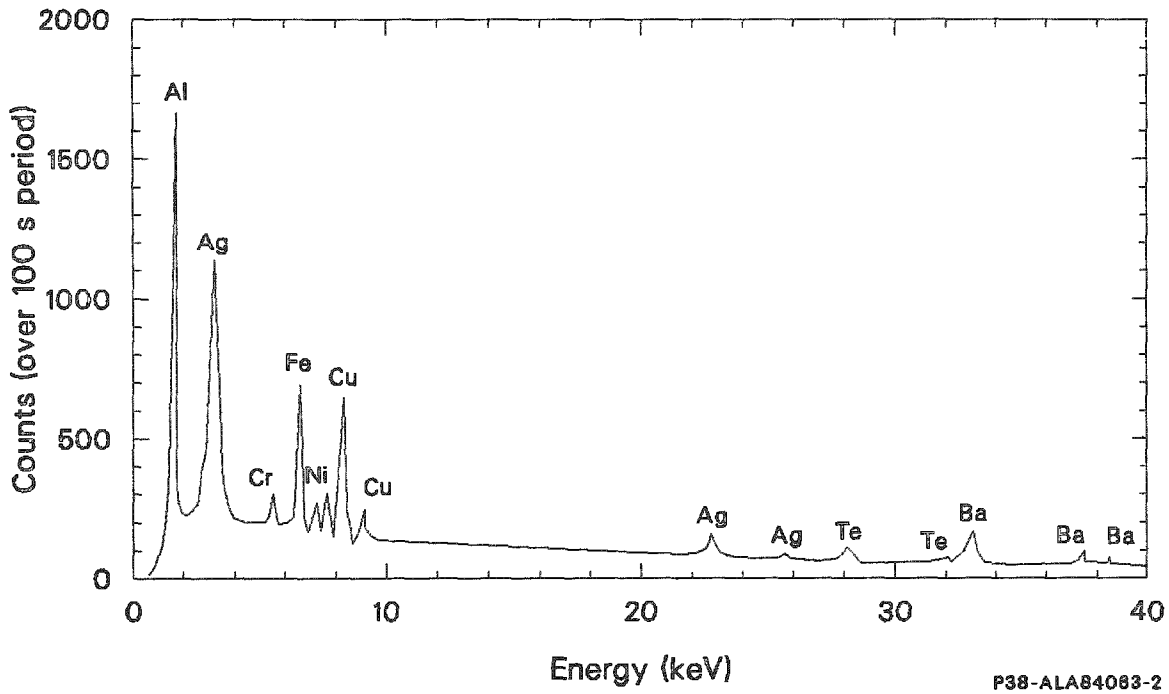


Figure 34. EDS spectrum of the nodule shown in Figure 33(c).

TABLE 14. ELEMENTAL COMPOSITION OF H8 LEADSCREW SURFACE LAYERS ON SAMPLES 3 AND 16 (wt%)

Element	Elemental Composition (wt%)									
	Base Metal <sup>a</sup>		Inner Layer		Mid Layer		Outer Layer		Outer Edge <sup>b</sup>	
	3 <sup>c</sup>	16 <sup>c</sup>	3 <sup>c</sup>	16 <sup>c</sup>	3 <sup>c</sup>	16 <sup>c</sup>	3 <sup>c</sup>	16 <sup>c</sup>	3 <sup>c</sup>	16 <sup>c</sup>
Ag	--d	--d	--d	--d	--e	--d	--d	--e	--d	14.3
Al	--d	--d	--d	--d	--e	12.1	0.9	--e	1.2	--d
Ca	--d	--d	--d	--f	--e	--d	--d	--e	--d	--d
Cd	--d	--d	--d	--d	--e	--d	--d	--e	--d	--d
Cr	16.2	16.0	39.2	37.4	--e	31.9	3.9	--e	1.7	1.0
Cu	3.3	3.2	8.1	3.4	--e	--f	--d	--e	--f	--f
Fe	75.9	76.8	48.5	54.0	--e	56.0	94.4	--e	92.6	83.4
In	--d	--d	--d	--d	--e	--d	--d	--e	--d	--d
Nb	--f	--f	--d	--d	--e	--d	--d	--e	--d	--d
Ni	3.7	4.0	2.4	4.2	--e	--f	--d	--e	3.2	1.3
Si	0.8	--d	1.7	1.0	--e	--d	0.8	--e	1.3	--d
Ti	--d	--d	--d	--d	--e	--d	--d	--e	--d	--d
Zr	--d	--d	--d	--d	--e	--d	--d	--e	--d	--d

a. Base metal = 17-4 PH SS. Composition: Fe (76 to 80 wt%), Cr (15.5 to 17.5 wt%), Ni (3 to 5 wt%), Si (maximum 1 wt%), Nb (0.15 to 0.45 wt%), C (maximum 0.07 wt%), Cu (3 to 5 wt%).

b. Outer edge: Outer edge of the outer layer next to the epoxy.

c. Sample 3 is close to the bottom of the plenum assembly. Sample 16 is close to the top of the plenum assembly. The surface examined was the top of the thread surface.

d. Not identified.

e. Not analyzed.

f. Below detection limit.

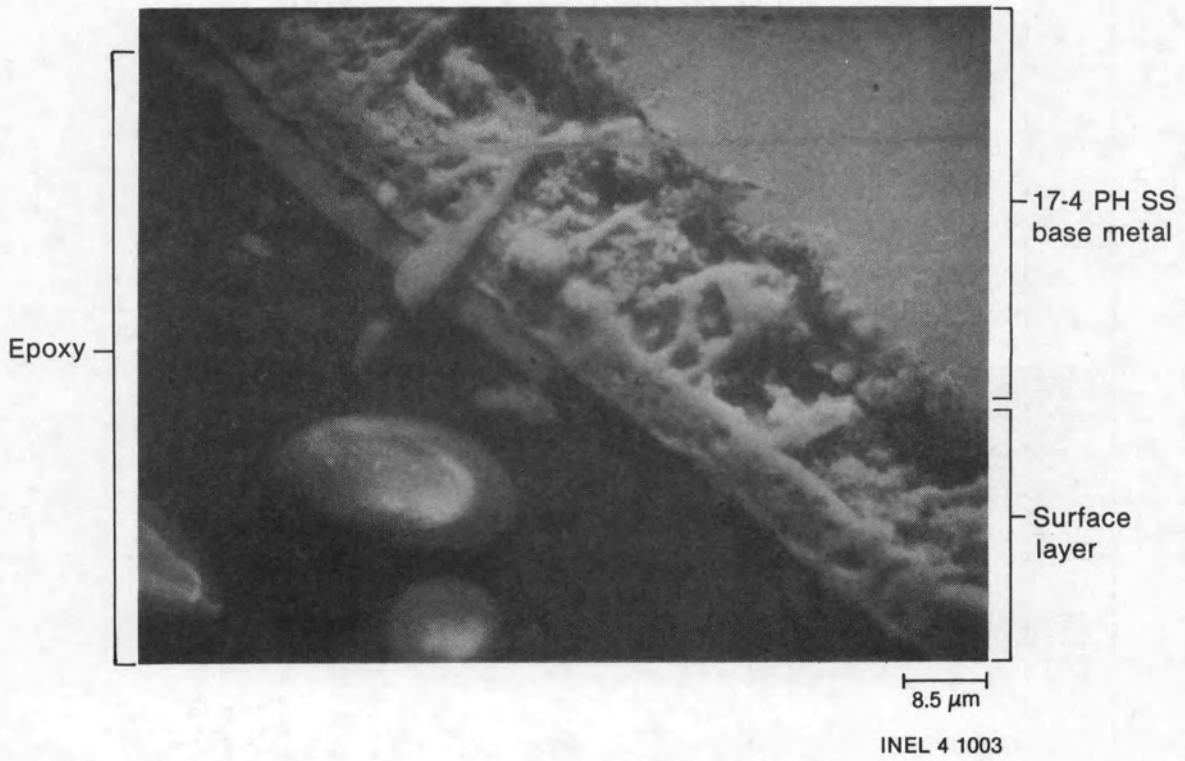


Figure 35. SEM micrograph of the smooth surface of H8 Sample 3.

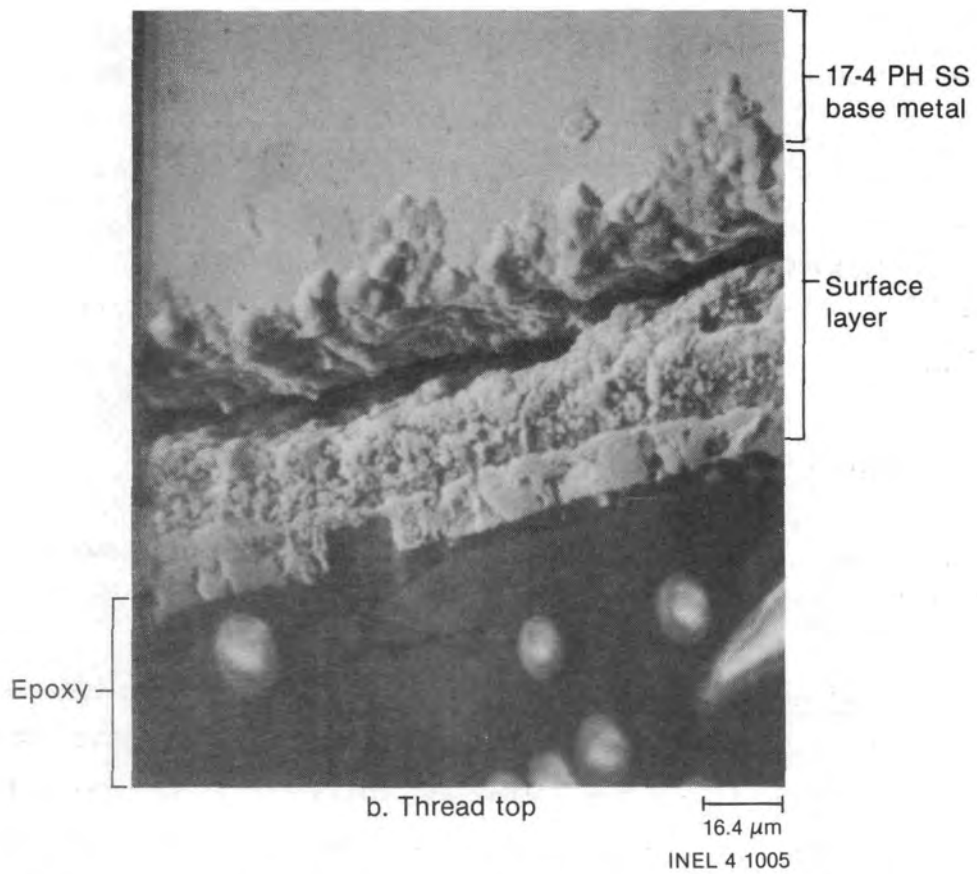
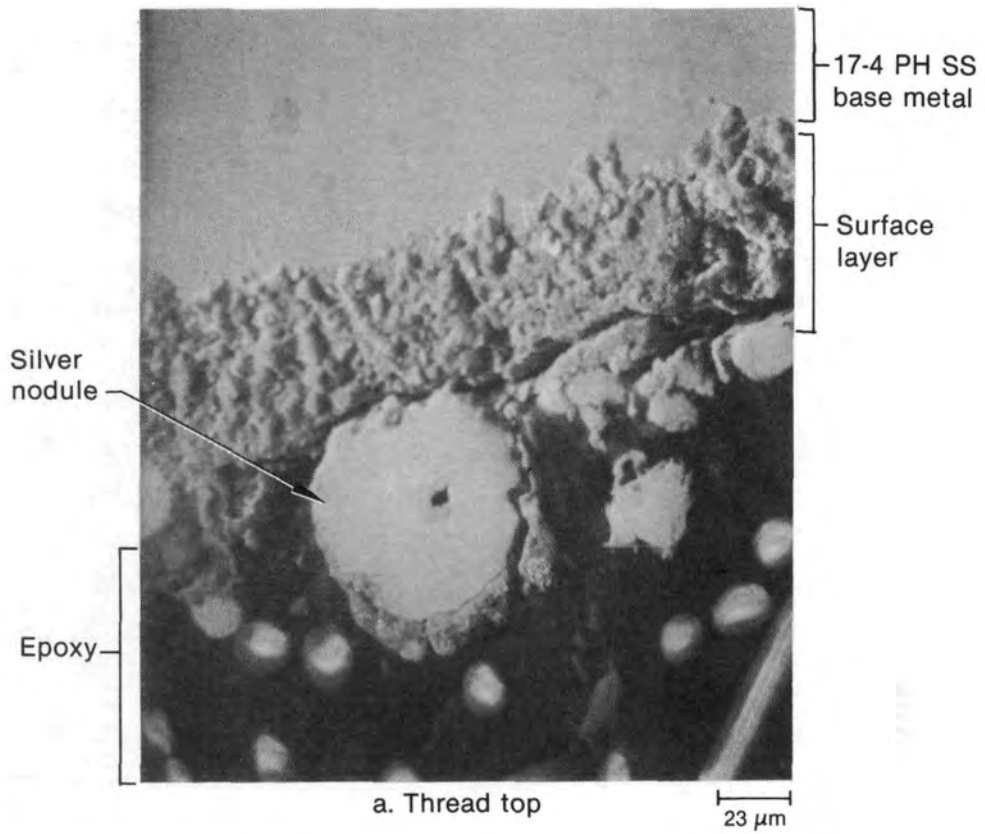


Figure 36. SEM micrographs of the top threaded surface from H8 Sample 16.

respectively. The major elements (iron, chromium, nickel, and copper) of 17.4 PH SS were identified. The iron content of the inner layer (next to base metal) was lower than that of the 17-4 PH SS base metal. In contrast, the iron content in the outer layer was higher than the base metal. The chromium content in the inner and outer layers was opposite to the iron. Deposition of silver on the Sample 16 thread top surface was observed.

In addition to the above qualitative analysis, semiquantitative elemental analyses were performed using ES on portions of surface Samples 3, 13, and 16. The results of these analyses are shown in Table 15. The elements present are components of the 17-4 PH SS surface sample; however, the measured weight percent of each elemental component does not agree with the listed composition of stainless steel (see Table 6). For example, the iron component is much greater than expected (>80%). These analytical results are semiquantitative, and the results are within the uncertainty of the analysis (plus or minus a factor of 2). Some elements (silver, barium, cadmium, indium, and tellurium) not detected by ES were identified by EDS. Tellurium, barium, and cesium are not listed as core component materials; however, they may be present as unlisted trace amounts or, more likely, fission products. The ORIGEN2<sup>18</sup> code-calculated core inventory of stable tellurium fission products (<sup>126</sup>Te, <sup>128</sup>Te and <sup>130</sup>Te) is about 3650 g, and the inventories of radioactive <sup>125m</sup>Te and <sup>137m</sup>Ba five years after the accident are  $5.2 \times 10^3$  and  $6.7 \times 10^5$  Ci, respectively. The inventory of fission product elemental cesium is about 20.7 kg.

### B8 Leadscrew Chemical Analyses

The chemical analyses performed on the B8 leadscrew samples were similar to those performed on the H8 samples.

Brushoff Debris. The results from ES analysis of the B8 brushoff debris from Sections B8-3 (close to the bottom of the plenum assembly) and B8-1 (close to the top of the plenum assembly) are listed in Table 16. Two major components of the debris collected from B8-3 are uranium (10 wt%)



TABLE 15. ELEMENTAL ANALYSIS OF H8 AND B8 LEADSCREW SURFACE SAMPLES  
(wt%)

Element	Surface Sample (wt%)				
	H8 Sample Number			B8 Sample Number	
	3	13	16	3	8
Al	0.02	0.02	0.08	0.02	0.02
Cr	12	10	7	8	7
Cu	2	3	3	2	3
Fe	90	80	90	90	80
Mg	0.02	0.01	0.01	0.02	0.02
Mn	0.2	0.3	0.2	0.2	0.4
Mo	0.2	0.3	0.1	0.2	0.1
Ni	4	6	6	3	6
Nb	1.0	0.8	0.4	0.4	0.4

TABLE 16. EMISSION SPECTROSCOPIC ANALYSIS OF THE BRUSHOFF DEBRIS FROM THE B8 LEADSCREW (wt%)

Element	Leadscrew Section (wt%) <sup>a</sup>	
	B8-3 (0.75 g) <sup>b</sup>	B8-1 (18.75 g) <sup>b</sup>
Ag	0.10	0.10
Al	0.20	0.06
B	0.10	0.10
Cr	2.00	11.00
Cu	0.02	0.05
Fe	30.00	30.00
Mg	2.00	0.30
Mn	0.20	0.10
Mo	0.40	0.10
Nb	0.04	0.02
Ni	0.40	1.00
Si	0.10	0.08
Sn	0.20	0.05
Ti	0.02	0.03
Zr	8.00	2.00
U	10.00	1.00

a. Sample B8-3 is located close to the bottom, and B8-1 is located close to the top of the plenum assembly.

b. Weight of brushoff debris.

and zirconium (8 wt%). In contrast, the uranium and zirconium concentrations on B8-1 (near the top of the plenum assembly) are lower; 1 wt% and 2 wt%, respectively. Gradients are present for other elements. The chromium, copper, and nickel concentrations increase from the bottom of the leadscrew to top of the plenum assembly, whereas the silver, boron, iron, manganese, silicon, and titanium concentrations are constant within a factor of 2. The remaining elements present (aluminum, magnesium, molybdenum, niobium, and tin) generally decrease in concentration from the bottom to the top of the plenum assembly.

A comparison of the H8 and B8 data was made, resulting in the following observations:

1. Much more brushoff debris was available and collected from the leadscrew regions near the top than from regions near the bottom of the plenum assembly.
2. The debris composition at both B8 locations was predominantly iron, whereas at H8 Section 9 (near the bottom of the plenum assembly) the debris was dominated by uranium and zirconium.
3. Although uranium and zirconium constitute larger fractions of the debris near the bottom of the plenum assembly, the total amount of these elements collected was greater near the top of the plenum assembly.
4. Chromium is a large constituent of the debris near the top of the plenum assembly.
5. Molybdenum, niobium, and tin were found in the B8 brushoff debris but not in the H8 brushoff debris (Table 7). Molybdenum and niobium are unique components of Inconel-718. These data indicate that the B8 brushoff debris had a significant fraction of Inconel-718 present, rather than being composed primarily of stainless steel as was indicated at the H8 location.

6. Tin is a component of the zircaloy cladding (1.6 wt%); however, these data indicate that tin was not transported with the zirconium. No tin was measured in the H8 samples, although quantitatively more zirconium was measured. This could be due to a temperature effect, as tin has a lower melting and boiling point than does zirconium.
7. Chromium and silicon concentrations are lower at the B8 location.
8. The silver concentration on the B8 samples is approximately the same as the H8 samples, indicating there may be a similar deposition mechanism for silver at both locations.

In general, these data indicate a wide range of elemental concentrations at the measured leadscrew locations, which may mean that the formation mechanism for the brushoff debris was dependent on core location.

Decontamination Solutions. The elemental analysis data for the B8 Samples 2 and 7 decontamination solutions (soluble and insoluble fractions) are listed in Tables 17 and 18, respectively. Sample 2 was decontaminated using a 40-wt%  $\text{HNO}_3$  and 0.12-M HF solution, whereas Sample 7 was decontaminated using a serial decontamination technique with progressively stronger agents. The solutions in order of use are: (a) 10-wt% sodium hydroxide ( $\text{NaOH}$ ) + 3-wt% potassium permanganate ( $\text{KMnO}_4$ ), (b) 25-g/L oxalic acid ( $\text{H}_2\text{C}_2\text{O}_4$ ) + 50-g/L dibasic ammonium citrate ( $(\text{NH}_4)_2\text{HC}_6\text{H}_5\text{O}_7$ ), and (c) 40-wt% nitric acid ( $\text{HNO}_3$ ) and 0.12-M hydrofluoric acid (HF). These decontamination agents were used at the recommendation of GPU Nuclear for comparison purposes with decontamination studies performed at other facilities. The decontaminations were performed at  $\sim 363 \text{ K}$  (194°F).

Table 17 lists the elemental concentration data and total mass removed for the soluble fractions of the B8 decontamination solutions. Again, as with the H8 decontamination solutions, the volume of solution is variable due to the amount of rinse solution used; however, the total quantity of

TABLE 17. EMISSION SPECTROSCOPIC ANALYSIS OF THE SOLUBLE PORTIONS OF THE B8 LEADSCREW DECONTAMINATION SOLUTIONS ( $\mu\text{g/mL}$  and total weight removed in mg)

Element	<sup>2a</sup> (226 mL) <sup>e</sup>		<sup>7b</sup> (250 mL) <sup>e</sup>		<sup>7c</sup> (176 mL) <sup>e</sup>		<sup>7d</sup> (198 mL) <sup>e</sup>	
	$\mu\text{g/mL}$	mg	$\mu\text{g/mL}$	mg	$\mu\text{g/mL}$	mg	$\mu\text{g/mL}$	mg
Ag	0.2	0.05	1.4	0.4	6.0	1.1	480.0	95.0
Al	3.0	0.68	22.0	5.5	3.0	0.5	4.8	0.9
B	5.0	1.1	86.0	22.0	6.0	1.1	12.0	2.4
Ca	5.0	1.1	--f	--f	--f	--	2.4	0.5
Cr	8.0	1.8	108.0	27.0	12.0	2.1	18.0	3.6
Cu	3.0	0.7	6.0	1.5	18.0	3.2	24.0	4.8
Fe	40.0	9.0	--f	--	240.0	42.2	330.0	65.3
K	0.5	0.1	--g	--	4.2	0.7	0.5	0.1
Mg	0.2	<0.1	--f	--	--f	--	--f	--
Mn	0.6	0.1	--g	--	24.0	4.2	6.0	1.2
Na	8.0	1.8	--g	--	36.2	6.4	12.0	2.4
Nb	0.5	0.1	8.0	2.0	3.0	0.5	2.4	0.5
Ni	6.0	1.4	--f	--	36.0	6.4	48.0	9.5
Pb	10.0	2.3	--f	--	--f	--	24.0	4.8
Si	15.0	3.4	1120.0	280	12.0	2.1	30.0	5.9
Sn	13.0	2.9	--f	--	60.0	10.6	126.0	25.0
Zr	1.0	0.2	10.0	2.5	6.0	1.1	42.0	8.5
U	--f	--	--f	--	6.0	1.1	--f	--

- a. Decontamination solution  $\text{HNO}_3 + \text{HF}$ .
- b. First decontamination solution,  $\text{NaOH} + \text{KMnO}_4$ .
- c. Second decontamination solution,  $\text{H}_2\text{C}_2\text{O}_4 + (\text{NH}_4)\text{HC}_6\text{H}_5\text{O}_7$ .
- d. Third decontamination solution,  $\text{HNO}_3 + \text{HF}$ .
- e. Volume of decontamination solution.
- f. Not measured.
- g. Component of decontamination solution.

TABLE 18. EMISSION SPECTROSCOPIC ANALYSIS OF INSOLUBLE MATERIALS FROM THE B8 LEADSCREW DECONTAMINATION SOLUTIONS (wt% and total wt removed in mg)

Element	<sup>2a</sup> (4 mg) <sup>e</sup>		<sup>7b</sup> (57 mg) <sup>e</sup>		<sup>7c</sup> (64 mg) <sup>e</sup>		<sup>7d</sup> (28 mg) <sup>e</sup>	
	wt%	mg	wt%	mg	wt%	mg	wt%	mg
Ag	0.20	<0.01	0.10	<0.1	0.20	0.1	0.10	<0.1
Al	3.00	0.12	0.30	0.2	0.07	<0.1	0.30	<0.1
B	--f	--	--f	--	0.01	<0.1	0.10	<0.1
Cr	20.00	0.80	4.00	2.3	5.00	3.2	29.00	8.1
Cu	0.10	<0.1	0.10	<0.1	0.01	<0.1	0.01	<0.1
Fe	6.00	0.24	16.00	9.1	33.00	21.1	18.00	5.0
Mg	2.00	<0.1	0.10	<0.1	2.00	1.3	0.03	<0.1
Mn	3.00	0.12	15.00	8.6	0.20	<0.1	0.20	<0.1
Mo	--f	--	--f	--	0.10	<0.1	0.03	<0.1
Nb	--f	--	--f	--	0.04	<0.1	0.03	<0.1
Ni	0.80	<0.1	0.40	0.2	0.20	0.1	0.50	0.1
Si	2.00	<0.1	0.20	0.1	0.03	<0.1	0.20	<0.1
Sn	2.00	<0.1	0.40	0.2	0.30	0.2	0.20	<0.1
Ti	7.00	0.3	--f	--	0.04	<0.1	--f	--
Zr	0.40	<0.1	5.00	2.8	5.00	3.2	3.00	0.8
U	--f	--	--f	--	4.00	2.6	--f	--

- a. Decontamination solution HNO<sub>3</sub> + HF.
- b. First decontamination solution, NaOH + KMnO<sub>4</sub>.
- c. Second decontamination solution, H<sub>2</sub>C<sub>2</sub>O<sub>4</sub> + (NH<sub>4</sub>)HC<sub>6</sub>H<sub>5</sub>O<sub>7</sub>.
- d. Third decontamination solution, HNO<sub>3</sub> + HF.
- e. Weight of insoluble material.
- f. Not measured.

each element measured is quantitative. The first and most important observation that may be made concerning these data is that a large amount of silver (480  $\mu\text{g/mL}$ ) was measured in the  $\text{HNO}_3 + \text{HF}$  solution, whereas lesser amounts were measured in the weaker decontamination solutions. Table 18 lists the concentrations and total amounts of the insoluble fractions contained in the decontamination solutions. It should be noted that silver is present in all insoluble sample fractions. The second observation based on these data is that significantly larger amounts of material ( $\sim$  a factor of 10) were present on B8 Sample 7 than on Sample 2. Third, the  $\text{NaOH} + \text{KMnO}_4$  decontamination solution is relatively effective for some elements. A large amount of silicon ( $\sim 1120 \mu\text{g/mL}$ ) was found in this decontamination fraction. Other elements effectively dissolved by this solution were aluminum, boron, chromium, and niobium.

The percentage of each element removed from B8 Sample 7 by each decontamination solution was calculated. The calculations are listed in Table 19 and indicate a large fraction of soluble material present in the initial solution ( $\text{NaOH} + \text{KMnO}_4$ ) for most elements. Only a small fraction of the available iron was present in the  $\text{NaOH} + \text{KMnO}_4$  decontamination solution. The uranium content was dissolved only in the oxalic acid/ammonium citrate solution, whereas the zirconium was measured in all three solutions, with  $>50\%$  being soluble in the  $\text{HNO}_3 + \text{HF}$  solution.

The total elemental quantities removed by each solution per square centimeter of surface area were calculated. The calculated weights of each element removed ( $\text{mg/cm}^2$ ) are listed on Table 20. The data suggest that very little of the metal content, including iron, was soluble in the  $\text{NaOH} + \text{KMnO}_4$  solution, with increasing amounts dissolving in the subsequent solutions. There are relatively large quantities of insoluble debris near the top of the plenum assembly and lesser quantities of soluble material near the bottom.

The concentrations (in atom ppm) for the decontamination solutions as compared to the brushoff debris for B8 Samples 2 and 7 are listed in Table 21. Also presented is the percentage of total atom content

TABLE 19. PERCENTAGES OF TOTAL ELEMENTAL CONTENT REMOVED FROM  
B8 SAMPLE 7  
(%)

Element	Total Elemental Content Removed (%)					
	NaOH + KMnO <sub>4</sub>		H <sub>2</sub> C <sub>2</sub> O <sub>4</sub> + (NH <sub>4</sub> ) <sub>2</sub> HC <sub>6</sub> H <sub>5</sub> O <sub>7</sub>		HNO <sub>3</sub> + HF	
	Soluble	Insoluble	Soluble	Insoluble	Soluble	Insoluble
Ag	0.3	0.06	1.0	0.1	98.4	0.03
Al	73.9	2.3	8.7	0.6	13.0	1.1
B	86.6	-- <sup>a</sup>	4.0	0.03	9.3	0.1
Cr	58.6	5.0	4.3	7.10	7.9	17.1
Cu	14.2	0.6	35.5	0.07	49.6	0.03
Fe	-- <sup>a</sup>	6.5	29.6	14.8	45.6	3.5
Mg	-- <sup>a</sup>	4.0	-- <sup>a</sup>	95.4	-- <sup>a</sup>	0.6
Nb	65.5	-- <sup>a</sup>	22.2	0.9	11.1	0.3
Ni	-- <sup>a</sup>	1.4	38.0	0.8	58.0	0.8
Si	97.2	0.04	0.7	0.01	2.1	0.02
Ti	-- <sup>a</sup>	-- <sup>a</sup>	-- <sup>a</sup>	100.0	-- <sup>a</sup>	-- <sup>a</sup>
Sn	-- <sup>a</sup>	0.6	29.6	0.5	69.4	0.2
Zr	16.3	18.4	6.1	20.4	51.0	4.1
U	-- <sup>a</sup>	-- <sup>a</sup>	27.3	72.7	-- <sup>a</sup>	-- <sup>a</sup>

a. Not detected.



TABLE 20. TOTAL ELEMENTAL CONTENT REMOVED BY DECONTAMINATION OF B8 SAMPLES 2 AND 7  
(mg removed/cm<sup>2</sup>)

Element	2 (11.4 cm <sup>2</sup> ) <sup>a</sup>		7 (33.1 cm <sup>2</sup> ) <sup>a</sup>						Total	
	Soluble <sup>b</sup> (270 mL) <sup>e</sup>	Insoluble <sup>h</sup> (4 mg) <sup>f</sup>	Soluble <sup>c</sup> (250 mL) <sup>e</sup>	Insoluble <sup>c</sup> (57 mg) <sup>f</sup>	Soluble <sup>d</sup> (176 mL) <sup>e</sup>	Insoluble <sup>d</sup> (64 mg) <sup>f</sup>	Soluble <sup>b</sup> (198 mL) <sup>e</sup>	Insoluble <sup>h</sup> (28 mg) <sup>f</sup>	Soluble	Insoluble
Ag	4.0 x 10 <sup>-3</sup>	7.0 x 10 <sup>-4</sup>	0.01	1.7 x 10 <sup>-3</sup>	0.03	3.9 x 10 <sup>-3</sup>	2.87	8.5 x 10 <sup>-4</sup>	2.91	6.4 x 10 <sup>-3</sup>
Al	0.06	0.01	0.17	5.2 x 10 <sup>-3</sup>	0.02	1.4 x 10 <sup>-3</sup>	0.03	2.5 x 10 <sup>-3</sup>	0.22	0.01
B	0.10	--g	0.65	--g	0.03	1.9 x 10 <sup>-4</sup>	0.07	8.5 x 10 <sup>-4</sup>	0.75	1.0 x 10 <sup>-3</sup>
Ca	0.10	--g	--g	--g	--g	--g	0.01	--g	--g	0.01
Cr	0.15	0.07	0.82	0.07	0.06	0.10	0.11	0.24	0.99	0.41
Cu	0.06	3.5 x 10 <sup>-4</sup>	0.04	1.7 x 10 <sup>-3</sup>	0.10	1.9 x 10 <sup>-4</sup>	0.14	8.5 x 10 <sup>-5</sup>	0.28	2.0 x 10 <sup>-3</sup>
Fe	0.77	0.02	--g	0.28	1.28	0.64	1.97	0.15	3.25	1.07
K	0.01	--g	--h	--g	0.02	--g	3.0 x 10 <sup>-3</sup>	--g	0.02	--g
Mg	3.9 x 10 <sup>-3</sup>	7.0 x 10 <sup>-3</sup>	--g	1.7 x 10 <sup>-3</sup>	--g	0.04	--g	2.5 x 10 <sup>-4</sup>	--g	0.04
Mn	0.01	0.01	--h	0.26	0.13	3.9 x 10 <sup>-3</sup>	0.03	1.7 x 10 <sup>-3</sup>	0.16	0.27
Na	0.15	--g	--h	--g	0.19	1.9 x 10 <sup>-3</sup>	0.07	2.5 x 10 <sup>-4</sup>	0.26	2.2 x 10 <sup>-3</sup>
Nb	9.6 x 10 <sup>-3</sup>	--g	0.06	--g	0.02	7.7 x 10 <sup>-4</sup>	0.01	2.5 x 10 <sup>-4</sup>	0.03	1.0 x 10 <sup>-3</sup>
Ni	0.11	2.8 x 10 <sup>-3</sup>	--g	6.9 x 10 <sup>-3</sup>	0.19	3.9 x 10 <sup>-3</sup>	0.29	4.2 x 10 <sup>-3</sup>	0.48	0.02
Pb	0.19	--g	--g	--g	--g	--g	0.14	--g	0.14	--g
Si	0.29	7.0 x 10 <sup>-3</sup>	8.5	3.4 x 10 <sup>-3</sup>	0.06	5.8 x 10 <sup>-4</sup>	0.18	1.7 x 10 <sup>-3</sup>	8.74	5.7 x 10 <sup>-3</sup>
Ti	--g	0.02	--g	--g	--g	7.7 x 10 <sup>-4</sup>	--g	--g	--g	7.7 x 10 <sup>-3</sup>
Sn	0.25	7.0 x 10 <sup>-3</sup>	--g	6.9 x 10 <sup>-3</sup>	0.32	5.8 x 10 <sup>-3</sup>	0.75	1.7 x 10 <sup>-3</sup>	1.07	0.01
Zr	0.02	1.4 x 10 <sup>-3</sup>	0.08	0.09	0.03	0.10	0.25	0.02	0.28	0.21
U	--g	--g	--g	--g	0.03	0.08	--g	--g	0.03	0.08

a. Surface area of sample.

b. HNO<sub>3</sub> + HF.

c. NaOH + KMnO<sub>4</sub>.

d. H<sub>2</sub>C<sub>2</sub>O<sub>4</sub> + (NH<sub>4</sub>)<sub>2</sub>HC<sub>6</sub>H<sub>5</sub>O<sub>7</sub>.

e. Volume of decontamination solution.

f. Weight of insoluble material.

g. Not detected.

h. Component of decontamination solution.

TABLE 21. ELEMENT CONTENT FROM B8 LEADSCREW SAMPLES AS DETERMINED FROM EMISSION SPECTROSCOPY (atom ppm)

Element	Sample <sup>a</sup>	Brushoff Debris <sup>b</sup>		Soluble Decontamination Solution		Insoluble Material	
		Atom ppm	Percent	Atom ppm	Percent	Atom ppm	Percent
Ag	2	3.51	0.15	$7.28 \times 10^2$	31.22	$1.60 \times 10^3$	68.63
	7	3.30	0.03	$8.66 \times 10^3$	83.81	$1.67 \times 10^3$	16.16
B	2	$3.59 \times 10^1$	0.019	$1.88 \times 10^5$	99.98	--c	--c
	7	$3.63 \times 10^1$	0.14	$2.31 \times 10^4$	89.30	$2.73 \times 10^3$	10.55
Cr	2	$1.40 \times 10^2$	0.02	$6.09 \times 10^4$	15.57	$3.30 \times 10^5$	84.39
	7	$8.00 \times 10^2$	0.44	$6.11 \times 10^3$	3.33	$1.76 \times 10^5$	96.22
Fe	2	$1.98 \times 10^3$	0.78	$1.65 \times 10^5$	63.95	$9.10 \times 10^4$	35.27
	7	$2.00 \times 10^3$	0.145	$8.46 \times 10^5$	61.39	$5.30 \times 10^5$	38.46
Nb	2	1.60	0.08	$2.12 \times 10^3$	99.92	--c	--c
	7	0.83	0.13	$3.13 \times 10^2$	50.17	$3.10 \times 10^2$	49.69
Ni	2	$2.59 \times 10^1$	0.50	$4.03 \times 10^4$	78.20	$1.10 \times 10^4$	22.30
	7	$2.5 \times 10^1$	0.26	$2.60 \times 10^3$	26.73	$7.10 \times 10^3$	73.01
Si	2	$1.34 \times 10^1$	0.005	$2.11 \times 10^5$	77.85	$6.00 \times 10^4$	22.14
	7	$1.06 \times 10^1$	0.010	$9.71 \times 10^4$	94.45	$5.70 \times 10^3$	5.54
Sn	2	$6.4 \times 10^1$	0.011	$4.32 \times 10^4$	75.50	$1.40 \times 10^4$	24.47
	7	1.50	0.116	$2.90 \times 10^3$	46.02	$3.40 \times 10^4$	53.96
Zr	2	$3.3 \times 10^2$	3.90	$4.35 \times 10^3$	51.90	$3.70 \times 10^3$	44.20
	7	$8.30 \times 10^1$	0.13	$1.27 \times 10^3$	1.94	$6.40 \times 10^4$	97.93
U	2	$1.56 \times 10^1$	100	--c	--c	--c	--c
	7	$1.50 \times 10^2$	1.61	$4.32 \times 10^1$	0.460	$9.10 \times 10^3$	97.93

a. Sample 2 is close to the bottom and Sample 7 is close to top of plenum assembly.

b. The brushoff debris contribution is based on the average deposition of the total brushoff debris retained from the individual leadscrew sections.

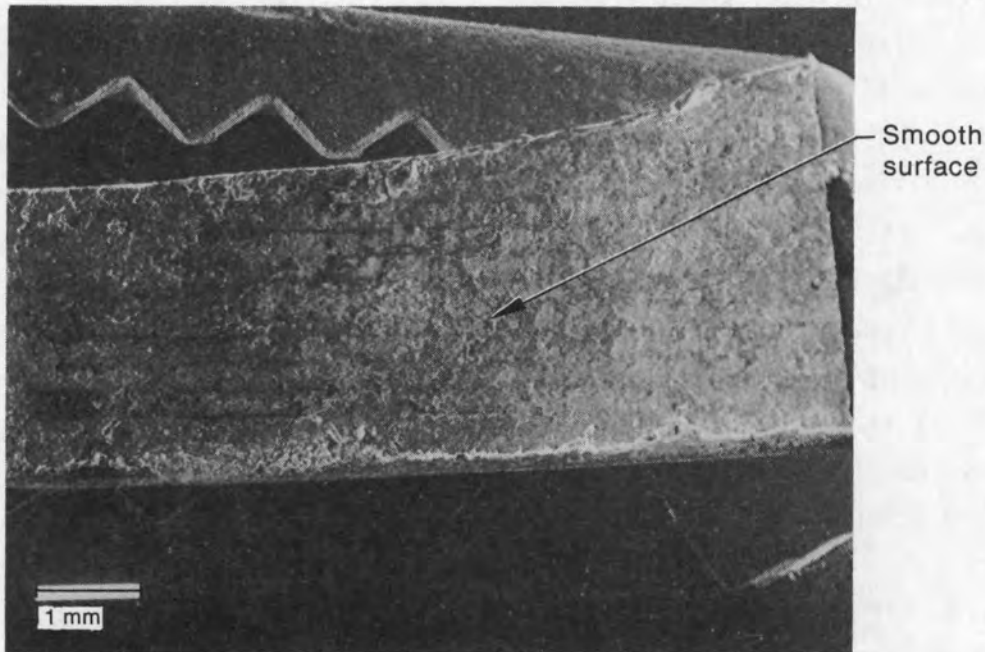
c. Not measured.

attributable to each sample fraction. The solubility of silver is much lower ( $\sim$  a factor of 5) on B8 Sample 2 than on B8 Sample 7, indicating that silver is less soluble near the bottom of the plenum assembly. The elemental constituents are mainly found in the soluble portion of the decontamination solutions, with the brushoff debris contributing a lesser fraction. These data generally indicate differences in the solubility characteristics between the B8 Samples 2 and 7 locations, with solubility decreasing towards the top of the leadscrew. B8 Samples 2 and 7 have boron depositions of about  $1.9 \times 10^5$  and  $2.3 \times 10^4$  atom ppm, which are 19% and 2.3% of the total atoms present, respectively. This is much less than was measured at the H8 locations ( $\sim$ 53%). The boron in both B8 samples is primarily soluble ( $\geq$ 89%), and at H8 the boron is  $\geq$ 62% soluble.

X-ray diffraction analyses were performed on brushoff debris samples from B8 Sections 1 and 3, soluble and insoluble fractions of the decontamination solutions from B8 Samples 2 and 7, and B8 surface Samples 3 and 8. The principal crystalline compound identified in all samples was  $\text{Fe}_3\text{O}_4$ . No other compounds were identified.

Surface Samples. Surface examinations of B8 Samples 3 and 8 were performed by SEM and analyzed by EDS for qualitative elemental identification. The data are presented in Table 13. SEM micrographs of the smooth surface on B8 Sample 3 and the top and bottom threaded surfaces of B8 Sample 8 are presented in Figures 37, 38, and 39, respectively. On B8 Sample 3, barium, cadmium, chromium, copper, iron, nickel, silicon, and zirconium were observed. Cadmium, nickel, silicon, and zirconium were not observed on H8 Sample 3, a comparable axial location on the H8 leadscrew.

Silver, barium, chromium, copper, iron, indium, nickel, and tellurium were identified on the top and bottom thread surfaces of B8 Sample 8. In addition, cadmium, zirconium, and uranium were identified on the bottom thread surface, indicating that these materials probably were not deposited by gravitational settling of the particles. It is interesting to note that cadmium, a control rod element, is deposited with the uranium and zirconium although not found with these elements in the H8 leadscrew samples. Some



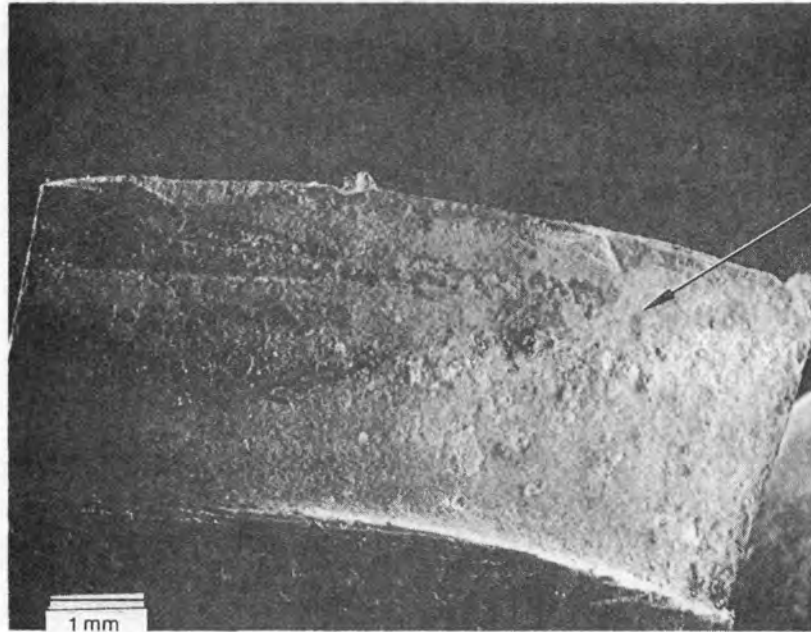
(a) SEM macrograph



(b) SEM micrograph

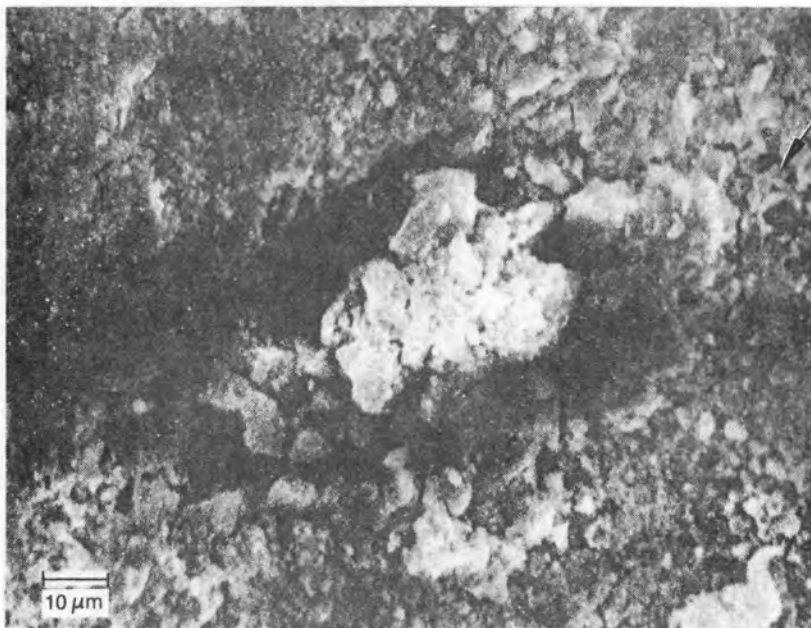
INEL 4 0958

Figure 37. SEM photographs of the smooth surface on B8 Sample 3 (close to the bottom of the plenum assembly).



Top threaded surface (17-4 PH SS)

(a) SEM macrograph

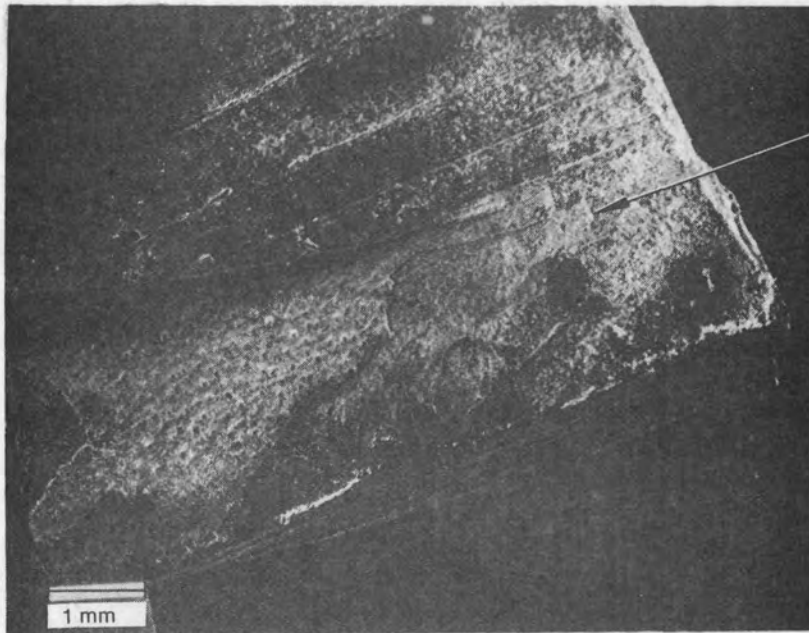


Surface deposition

(b) SEM micrograph

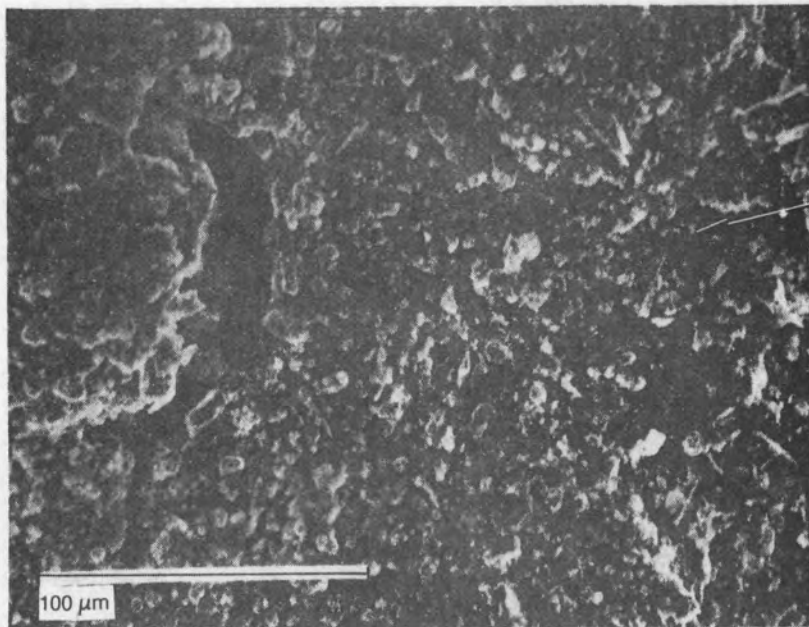
INEL 4 0959

Figure 38. SEM photographs of the top threaded surface of B8 Sample 8 (close to the top of the plenum assembly).



Bottom threaded surface (17-4 PH SS)

(a) SEM macrograph



Surface deposition

(b) SEM micrograph

INEL 4 0960

Figure 39. SEM photographs of the bottom threaded surface of B8 Sample 8 (close to the top of the plenum assembly).

of the above-listed elements were not identified by ES analysis, possibly because the amounts of material present are below the detection limits.

Elemental composition of the surface layers on B8 Samples 3 and 8 were measured by EDS, and the data are presented in Table 22. SEM micrographs of Sample 3 and the Sample 8 thread top, thread face, and thread bottom are shown in Figures 40 and 41, respectively. The behavior of iron and chromium in the inner and outer debris layers is similar to that of the H8 leadscrew samples, although there is no correlation between iron and chromium. Silver was detected on the outer edge of the top threaded surface on Sample 8.

Table 15 shows the results of the ES analysis of the B8 surface samples. Considering the uncertainty of the analysis, the elemental analyses of these samples are similar to the H8 sample analyses.

#### Radiological Analyses

Radiological analyses were performed on samples obtained from the H8 and B8 leadscrews. The objective of the analyses was to aid in determining the extent and nature of fission product and core material deposition on the leadscrew surfaces. The samples analyzed are of four distinct types; brushoff debris, acidic solutions used to decontaminate the metallurgical samples, undissolved (insoluble) decontamination sample fractions (filtered solid material from the decontamination solution), and surface samples (lightly brushed leadscrew sections with the surface deposition left intact). Figures 2 and 3 and Table 1 identify the specific samples used for radiological analyses and outline the types of analyses performed on each sample.

The sample locations were chosen to identify possible radial and/or axial gradients in the fission product content on the surfaces between the bottom and the top of the plenum assembly. A comparison of the measured radionuclide concentrations from the various locations was performed, and an evaluation was made of the effects of the decontamination solutions on the leadscrew surface deposits.

TABLE 22. ELEMENTAL COMPOSITION OF B8 LEADSCREW SURFACE LAYERS ON SAMPLES 3 AND 8 (wt%)

Element	Elemental Composition (wt%)										
	Base Metal <sup>a</sup>		Inner Layer		Mid Layer		Outer Layer		Outer Edge		
	3 <sup>b</sup>	8 <sup>b</sup>	3 <sup>b</sup>	8 <sup>b</sup>	3 <sup>b</sup>	8 <sup>b</sup>	3 <sup>b</sup>	8 <sup>b</sup>	3 <sup>b</sup>	8 <sup>b</sup>	8 <sup>c</sup>
Ag	--d	--e	--d	--d	--e	--e	--d	--d	--d	44.1	--d
Al	--d	--e	--d	5.3	--e	--e	5.9	--d	0.4	16.3	7.3
Ca	--d	--e	3.4	--d	--e	--e	3.2	--f	1.5	--d	--d
Cd	--d	--e	2.1	--d	--e	--e	--d	--d	--d	--d	--d
Cr	16.5	16.2	25.5	28.4	--e	--e	29.1	28.1	28.2	2.0	2.1
Cu	3.4	2.7	3.5	2.4	--e	--e	1.8	1.4	2.1	5.2	--f
Fe	75.9	76.8	57.0	56.2	--e	--e	40.0	65.7	45.2	28.6	90.7
In	--d	--e	--f	--f	--e	--e	--d	--f	--d	--d	--d
Nb	--f	--d	--f	--d	--e	--e	--d	--d	--d	--d	--d
Ni	4.1	4.2	6.8	7.1	--e	--e	11.7	3.7	15.4	3.7	--f
Si	--d	--e	1.7	0.5	--e	--e	8.3	1.1	2.0	--d	--d
Ti	--d	--e	--d	--d	--e	--e	--d	--d	3.7	--d	--d
Zr	--d	--e	--d	--d	--e	--e	--d	--d	1.5	--d	--d

a. Base metal = 17-4 pH SS. Composition: Fe (76 to 80 wt%), Cr (15.5 to 17.5 wt%), Ni (3 to 5 wt%), Cu (3 to 5 wt%), Si (maximum 1 wt%), Nb (0.15 to 0.45 wt%), C (maximum 0.07 wt%).

b. B8 Sample 3 is close to the bottom of the plenum assembly. B8 Sample 8 is close to the top of the plenum assembly. The surface examined was the top of the thread surface.

c. The very outside edge of Sample 8 contained a high concentration of iron.

d. Not identified.

e. Not analyzed.

f. Below detection limit.



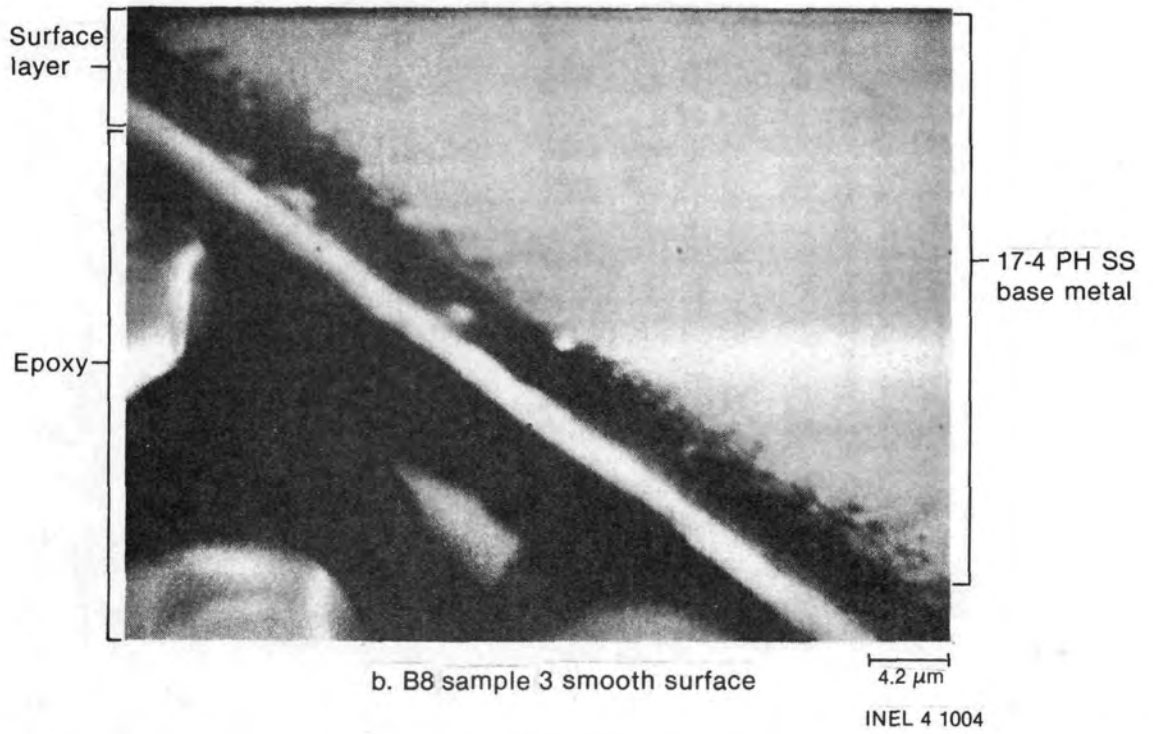
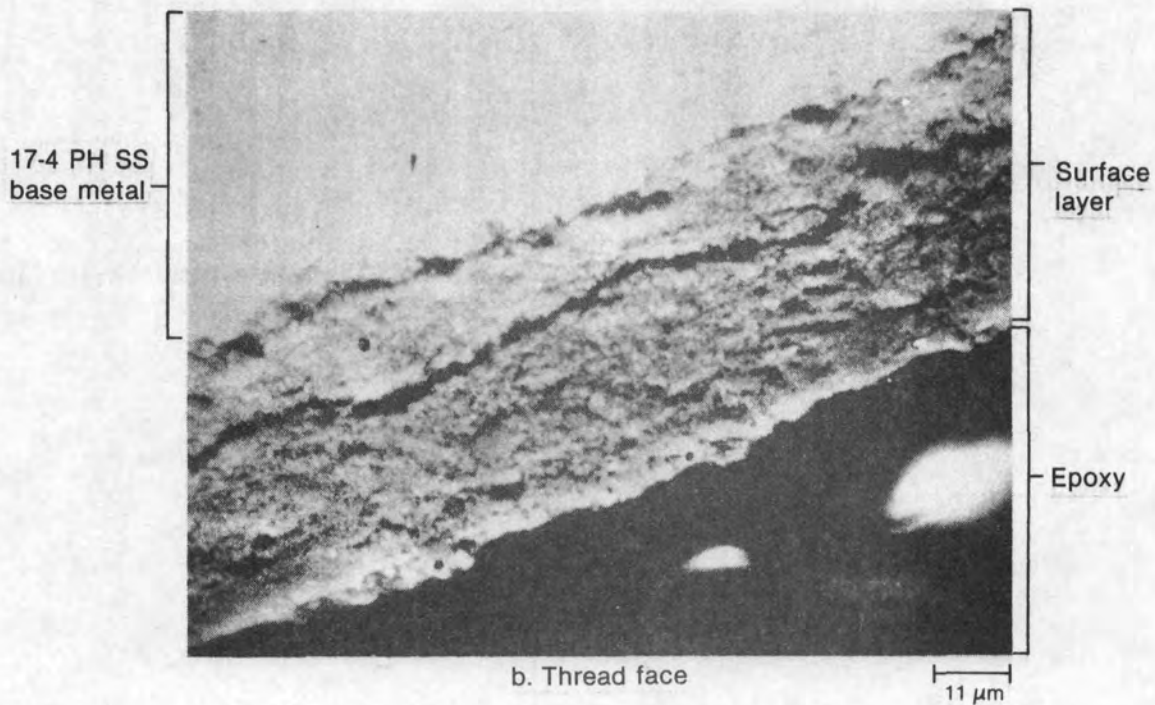
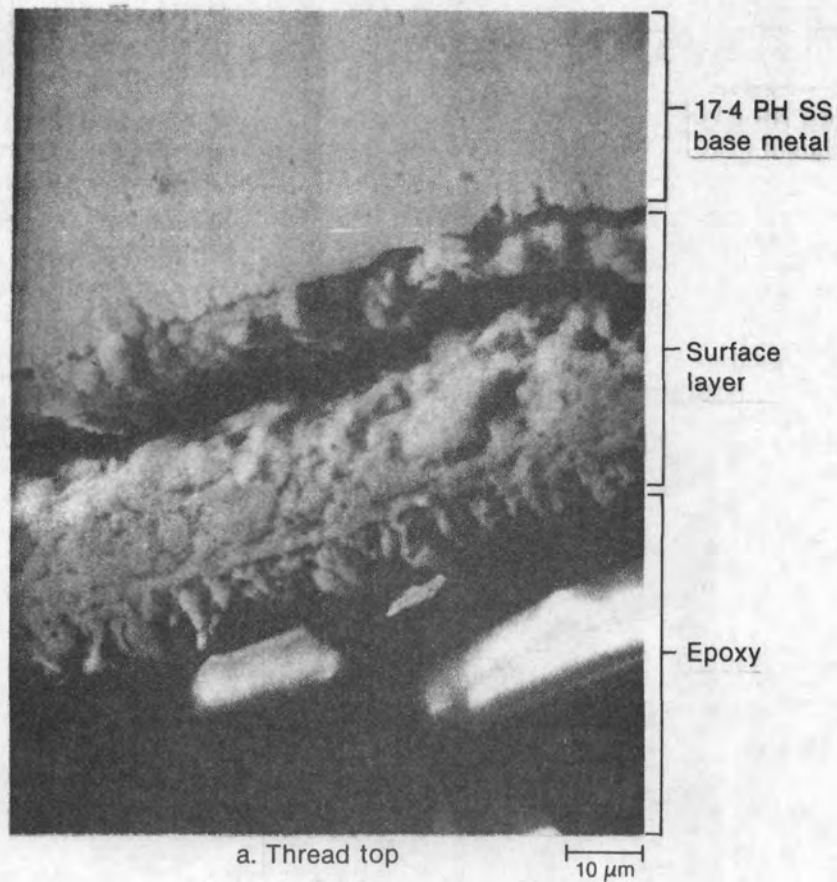
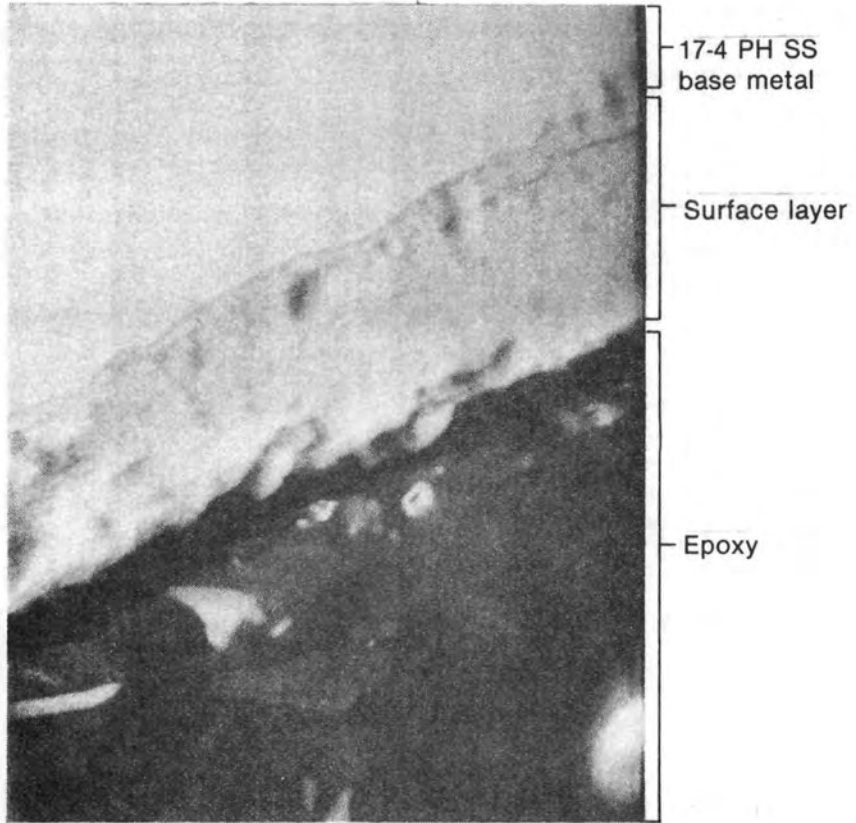


Figure 40. SEM micrograph of B8 Sample 3 surface layer on smooth surface.



INEL 4 1006

Figure 41. SEM micrographs of B8 Sample 8 surface layers on (a) the thread top surface, (b) the thread face, and (c) the thread bottom surface.



c. Thread bottom

INEL 4 1007

Figure 41. (continued)

## H8 Leadscrew Radiological Analyses

Radiological analyses were performed on the H8 leadscrew samples to determine fission and activation product deposition on the leadscrew surfaces. The data were used to characterize the radionuclide deposition between the bottom and top of the plenum assembly. The samples analyzed are portions of the samples used for chemical analysis.

Brushoff Debris Analysis. The results of GS analysis for the brushoff debris from H8 leadscrew sections H8-9, H8-8, and H8-7 are listed in Table 23. The concentrations of some radionuclides,  $^{54}\text{Mn}$ ,  $^{60}\text{Co}$ ,  $^{106}\text{Ru}$ ,  $^{125}\text{Sb}$ ,  $^{134}\text{Cs}$ ,  $^{137}\text{Cs}$ , and  $^{144}\text{Ce}$ , are relatively consistent between H8-7 and H8-9. The H8-8<sup>a</sup> data indicate lesser radionuclide concentrations for  $^{60}\text{Co}$ ,  $^{106}\text{Ru}$ , and  $^{144}\text{Ce}$ . Gradients exist for  $^{110\text{m}}\text{Ag}$  and  $^{125}\text{Sb}$  from the bottom (H8-9) to the top of the plenum assembly (H8-7), with the higher concentrations at the top. In general, the fission product concentrations for sections H8-9 and H8-7 are similar (within a factor of 2). A much higher uranium concentration is indicated by the elemental analysis results for the H8-9 debris (~70%) than was measured for the H8-7 debris. Therefore, fission product concentrations in the brushoff debris appear to be independent of uranium content. These data are supported by the fissile material analysis results to be discussed.

A particle size distribution analysis was performed on small quantities (<0.5 g) of the H8-7 and H8-9 brushoff debris to evaluate the radionuclide content of individual particle size groups. The particle size distribution analyses were performed using a wet (Freon wash) particle sizing method. A vacuum was applied to the bottom of a series of particle sizing sieves, and the sample was washed through the sieves.

---

a. Section H8-8 was not brushed. The H8-8 debris contained in the plastic wrapping during unpackaging was collected for analysis. Therefore, the results may not be representative of this leadscrew section.

TABLE 23. RADIONUCLIDE CONTENT OF THE H8 BRUSHOFF DEBRIS  
( $\mu\text{Ci}/\text{mg}$ )

Radionuclide	Half Life	Radionuclide Content ( $\mu\text{Ci}/\text{mg}$ ) <sup>a</sup>		
		H8-9 (539.6 mg) <sup>b</sup>	H8-8 (61.3 mg) <sup>b</sup>	H8-7 (35.6 x 10 <sup>3</sup> mg) <sup>b</sup>
<sup>54</sup> Mn	3.12 x 10 <sup>2</sup>	3.80 ± 1.20 x 10 <sup>-3</sup>	--c	3.00 ± 1.00 x 10 <sup>-3</sup>
<sup>60</sup> Co	1.93 x 10 <sup>3</sup>	2.27 ± 0.06 x 10 <sup>-1</sup>	5.80 ± 0.60 x 10 <sup>-3</sup>	2.28 ± 0.05 x 10 <sup>-1</sup>
<sup>106</sup> Ru	3.68 x 10 <sup>2</sup>	6.80 ± 0.03 x 10 <sup>-1</sup>	2.60 ± 0.80 x 10 <sup>-2</sup>	7.60 ± 0.20 x 10 <sup>-1</sup>
<sup>110m</sup> Ag	2.53 x 10 <sup>2</sup>	--c	1.90 ± 0.40 x 10 <sup>-3</sup>	3.60 ± 1.40 x 10 <sup>-3</sup>
<sup>125</sup> Sb	9.89 x 10 <sup>2</sup>	4.80 ± 0.10 x 10 <sup>-1</sup>	4.28 ± 0.07 x 10 <sup>-1</sup>	6.97 ± 0.09 x 10 <sup>-1</sup>
<sup>134</sup> Cs	7.48 x 10 <sup>2</sup>	1.06 ± 0.04 x 10 <sup>-1</sup>	1.18 ± 0.03 x 10 <sup>-1</sup>	1.18 ± 0.03 x 10 <sup>-1</sup>
<sup>137</sup> Cs	1.04 x 10 <sup>4</sup>	1.98 ± 0.01	1.96 ± 0.01	2.16 ± 0.01
<sup>144</sup> Ce	2.84 x 10 <sup>2</sup>	1.56 ± 0.02	1.40 ± 0.40 x 10 <sup>-2</sup>	1.44 ± 0.20
<sup>154</sup> Eu	3.10 x 10 <sup>3</sup>	1.50 ± 0.20 x 10 <sup>-2</sup>	--c	--c

a. Decay corrected to 11/1/1983.

b. Weight of brushoff debris.

c. Not detected.

The H8-7 and H8-9 particle size distribution and associated radionuclide concentration data are listed in Table 24. The radionuclide concentrations are listed in percent of total radionuclide activity in each particle size fraction. The data are presented in this form because: (a) the visible presence of metal turnings from the cutting operation would bias the data if presented as radionuclide concentrations ( $\mu\text{Ci/g}$ ), and (b) only small quantities ( $\sim 0.5$  g) are available for this analysis. Significant losses were incurred during sieving ( $\leq 100$  mg), making the data semiquantitative.

Observations were made concerning the particle size distribution and associated radionuclide concentration. They are: (a) 63 wt% of the H8-9 sample is in the particle size range between 1000 to 125  $\mu\text{m}$ , compared to only 23 wt% for the H8-7 sample, and (b) the largest fraction of the H8-7 sample (62 wt%) is within the 45-60  $\mu\text{m}$  size range. There is a gradient in the particle sizes between the H8-7 and H8-9 leadscrew sections, with a predominance of the smaller sizes concentrated on H8-7 (near the top of the plenum assembly). Steel slivers from the leadscrew cutting operation were visibly present only in the 500- to 1000- $\mu\text{m}$  size fraction.

An analysis of the radionuclide concentration data for both H8-9 and H8-7 leadscrew locations indicates that: (a) greater than 93% of the radionuclide content is associated with particle sizes  $\leq 212$   $\mu\text{m}$ , and (b) greater than 50% of the radionuclide content is associated with particle sizes  $\leq 60$   $\mu\text{m}$ . Indeed, significant quantities of individual radionuclides (16 to 34% on H8-9 and 4 to 10% on H8-7) are associated with the smallest particle size range ( $\leq 0.45$   $\mu\text{m}$ ), suggesting that the radionuclides in these particle size fractions, 38 to 60 and  $\leq 0.45$   $\mu\text{m}$ , may have been transported primarily as hydrosols or aerosols, respectively.

Strontium-90,  $^{129}\text{I}$ , tellurium, and fissile material analyses were performed on the brushoff debris. The data listed in Table 25 indicate several trends. The  $^{90}\text{Sr}$  concentrations are consistent within 50% for H8-7 and H8-9. The  $^{129}\text{I}$  and tellurium concentrations decreased towards the top of the plenum assembly, as no  $^{129}\text{I}$  and tellurium could be detected in the H8-7 brushoff debris. There is a gradient in the quantity

TABLE 24. RADIONUCLIDE CONCENTRATION BY PARTICLE SIZE ON H8-9 AND H8-7 BRUSHOFF DEBRIS  
 (% of total radionuclide content/gram of sample)

Radionuclide	Brushoff Debris Particle Size ( $\mu\text{m}$ )															
	>1000		500-1000		212-500		125-212		60-125		45-60	38-45	0.45-38		<0.45	
	H8-9 (46.1) <sup>a</sup> %/g	H8-7 (9) <sup>a</sup> %/g	H8-9 (63.5) <sup>d</sup> %/g	H8-7 (17) <sup>a</sup> %/g	H8-9 (133.8) <sup>a</sup> %/g	H8-7 (42) <sup>a</sup> %/g	H8-9 (86.6) <sup>a</sup> %/g	H8-7 (55) <sup>a</sup> %/g	H8-9 (90.5) <sup>a</sup> %/g	H8-7 (99) <sup>a</sup> %/g	H8-9 (229) <sup>a</sup> %/g	H8-7 (15) <sup>a</sup> %/g	H8-9 (22.7) <sup>a</sup> %/g	H8-7 (42) <sup>a</sup> %/g	H8-9 (79.4) <sup>a</sup> %/g	H8-7 (22.8) <sup>a</sup> %/g
<sup>54</sup> Mn	--b	--b	--b	--b	--b	--b	--b	--b	--b	--b	--b	--b	--b	--b	100	--b
<sup>60</sup> Co	--b	0.94	1.1	2.1	11.6	5.6	25.3	10.1	7.2	28.9	31.8	3.2	34.1	10.3	20.7	7.0
<sup>106</sup> Ru	--b	1.1	--b	2.3	15.0	8.8	26.0	12.0	9.1	27.9	28.2	2.8	24.2	10.4	25.7	6.6
<sup>110m</sup> Ag	--h	--b	1.6	--b	20.2	--b	26.4	--b	6.9	--b	--b	--b	18.1	--b	26.8	--b
<sup>125</sup> Sb	<0.01	0.83	1.3	4.6	17.0	14.4	29.2	20.6	4.8	29.1	18.3	1.9	16.3	6.2	31.4	4.0
<sup>134</sup> Cs	0.2	1.2	0.8	4.6	9.7	9.0	29.0	13.6	8.8	31.7	22.8	2.0	33.5	9.1	18.0	6.1
<sup>137</sup> Cs	0.2	1.3	0.8	3.4	9.9	10.6	29.4	16.1	8.6	27.7	23.4	2.4	33.1	8.9	18.1	6.1
<sup>144</sup> Ce	--b	1.2	6.6	2.4	19.4	8.3	19.6	13.7	5.7	28.2	28.1	2.6	29.3	8.6	19.4	6.8

a. Debris weight in mg.

b. Not detected.

TABLE 25. H8 BRUSHOFF DEBRIS  $^{90}\text{Sr}$ ,  $^{129}\text{I}$  (BETA EMITTERS), TELLURIUM,  
AND  $^{235}\text{U}$  CONCENTRATIONS<sup>a</sup>

Radionuclide	H8-9 (bottom of the plenum assembly, 0.54 g) <sup>b</sup>	H8-7 (top of the plenum assembly, 35.6 g) <sup>b</sup>
$^{90}\text{Sr}$ ( $\mu\text{Ci/g}$ )	$6.0 \pm 2 \times 10^1$	$3.9 \pm 1.3 \times 10^1$
$^{129}\text{I}$ ( $\mu\text{Ci/g}$ )	$8.0 \pm 3 \times 10^{-3}$	--c
Te <sup>d</sup>	$1.3 \times 10^4$	--c
$^{235}\text{U}$ ( $\mu\text{g/g}$ )	$7.6 \pm 0.4 \times 10^3$	$5.0 \pm 0.1 \times 10^1$

a. Decay date for  $^{90}\text{Sr}$  is 6/15/84.

b. Debris weight.

c. Small sample-below detection limit.

d. Stable tellurium analysis was performed using ICP spectroscopy. The concentration is in  $\mu\text{g/sample}$ .

e. Fissile analysis was performed by neutron activation and delayed neutron counting. The concentration is in  $\mu\text{g/g}$ .



of fissile material content present from the bottom to the top of the plenum assembly (a factor of  $1.5 \times 10^2$ ), with the largest amount at the bottom (H8-9). Most fuel materials in the brushoff debris are retained near the bottom of the plenum assembly, with a small fraction being present at the top. When the gamma spectroscopy data in Table 23 and the  $^{90}\text{Sr}$  data in Table 25 are compared with the fissile material content, the fission-product concentrations are relatively consistent at both locations, whereas the fissile material content is significantly different ( $1.5 \times 10^2$ ). These data support the chemical data which indicates that uranium content is independent of fission-product concentration.

The total radionuclide concentrations present on the leadscrew surfaces were calculated using data from the brushoff debris and decontamination solutions. These results are discussed in the following section.

Decontamination Solutions. Analysis of the tightly adherent layer (AD) deposited on the leadscrews was performed to determine its radionuclide content. That layer was removed using a 40 wt%  $\text{HNO}_3$  + 0.12-M HF decontamination solution. Metallurgical samples were soaked in the solution for 1 to 2 h at elevated temperatures [approximately 363 K (194°F)]. Following the initial decontamination attempt, insoluble material was observed in all solutions. In some instances, a second decontamination was required to completely remove all measurable radionuclides from the surfaces of the samples. The individual decontamination solutions were filtered using a 0.45  $\mu\text{m}$  vacuum filtration system to separate the insoluble material. The soluble and insoluble fractions were analyzed independently.

Gamma spectroscopy was the initial analysis performed on decontamination sample fractions from the solution. The radionuclide content of the insoluble material and soluble fractions is listed in Table 26. The data are presented as  $\mu\text{Ci/sample}$ , as the presence of insoluble components not associated with the surface materials (metal turnings) would bias the data if reported as radionuclide concentrations ( $\mu\text{Ci/g}$ ). Where two decontaminations were required to fully remove all activity from the leadscrew sample, the data for both are shown.

TABLE 26. GAMMA SPECTRAL ANALYSIS OF THE H8 DECONTAMINATION SOLUTIONS<sup>a</sup>

116

Leadscrew Sample	Distance from Bottom of Leadscrew (cm)	Radionuclide	Soluble Radionuclide ( $\mu\text{Ci/sample}$ )		Insoluble Radionuclide ( $\mu\text{Ci/sample}$ )	
			Leach 1 (mL)	Leach 2 (mL)	Leach 1 (mg)	Leach 2 (mg)
2	2.5	<sup>54</sup> Mn	--b	--b	$1.40 \pm 0.40 \times 10^{-2}$	--b
		<sup>60</sup> Co	$4.30 \pm 0.90 \times 10^{-5}$	$7.70 \pm 2.10 \times 10^{-8}$	$2.70 \mp 0.50 \times 10^{-2}$	--b
		<sup>106</sup> Ru	--b	--b	$3.90 \mp 0.80 \times 10^{-1}$	--b
		<sup>125</sup> Sb	--b	$3.90 \pm 1.20 \times 10^{-7}$	$1.30 \mp 0.40 \times 10^{-1}$	--b
		<sup>134</sup> Cs	$5.39 \pm 0.09 \times 10^{-3}$	$1.78 \mp 0.09 \times 10^{-6}$	$1.27 \mp 0.03$	$2.70 \pm 0.10 \times 10^{-2}$
		<sup>137</sup> Cs	$8.57 \mp 0.03 \times 10^{-2}$	$2.76 \mp 0.03 \times 10^{-5}$	$2.01 \mp 0.01 \times 10^1$	$4.45 \mp 0.06 \times 10^{-1}$
4	13.3	<sup>54</sup> Mn	--b	$3.90 \pm 1.20 \times 10^{-8}$	$9.10 \pm 0.80 \times 10^{-3}$	$2.71 \pm 0.07 \times 10^{-3}$
		<sup>60</sup> Co	$4.10 \pm 0.03 \times 10^{-5}$	$2.00 \mp 0.70 \times 10^{-8}$	$5.20 \mp 1.20 \times 10^{-3}$	$1.50 \mp 0.50 \times 10^{-3}$
		<sup>106</sup> Ru	--b	--b	$4.40 \mp 1.20 \times 10^{-2}$	--b
		<sup>125</sup> Sb	--b	--b	$2.90 \mp 0.60 \times 10^{-2}$	--b
		<sup>134</sup> Cs	$3.35 \pm 0.01 \times 10^{-4}$	$1.04 \pm 0.05 \times 10^{-6}$	$1.67 \mp 0.04 \times 10^{-1}$	$7.00 \pm 0.30 \times 10^{-2}$
		<sup>137</sup> Cs	$5.40 \mp 0.02 \times 10^{-3}$	$1.69 \mp 0.02 \times 10^{-5}$	$2.65 \mp 0.02$	$1.11 \mp 0.01$
5	15.2	<sup>54</sup> Mn	$7.00 \pm 3.30 \times 10^{-6}$	$7.80 \pm 1.50 \times 10^{-8}$	$1.38 \pm 0.08 \times 10^{-1}$	--b
		<sup>60</sup> Co	$1.40 \mp 0.10 \times 10^{-4}$	$8.80 \mp 2.00 \times 10^{-8}$	$6.40 \mp 0.70 \times 10^{-2}$	--b
		<sup>106</sup> Ru	--b	--b	$2.70 \mp 1.20 \times 10^{-1}$	--b
		<sup>110m</sup> Ag	--b	--b	$2.5 \mp 0.70 \times 10^{-3}$	--b
		<sup>125</sup> Sb	$1.60 \pm 0.20 \times 10^{-4}$	$5.10 \pm 0.90 \times 10^{-7}$	$3.50 \mp 0.60 \times 10^{-1}$	--b
		<sup>134</sup> Cs	$1.44 \mp 0.03 \times 10^{-3}$	$1.31 \mp 0.07 \times 10^{-6}$	$3.48 \mp 0.04$	$1.30 \pm 0.20 \times 10^{-2}$
		<sup>137</sup> Cs	$2.28 \mp 0.01 \times 10^{-2}$	$2.12 \mp 0.02 \times 10^{-5}$	$5.48 \mp 0.01 \times 10^1$	$2.19 \mp 0.08 \times 10^{-1}$
		<sup>144</sup> Ce	$1.80 \mp 0.50 \times 10^{-4}$	--b	--b	--b

TABLE 26. (continued)

Leadscrew Sample	Distance from Bottom of Leadscrew (cm)	Radionuclide	Soluble Radionuclide ( $\mu\text{Ci/sample}$ )		Insoluble Radionuclide ( $\mu\text{Ci/sample}$ )	
			Leach 1 (110 mL)	Leach 2 (144 mL)	Leach 1 (97.1 mg)	Leach 2 (6.9 mg)
7c (304 and 17-4 PH)	20.3	$^{54}\text{Mn}$	--b	$4.30 + 2.10 \times 10^{-7}$	$1.60 + 0.20 \times 10^{-1}$	$1.10 + 0.10 \times 10^{-2}$
		$^{60}\text{Co}$	$2.70 \pm 0.30 \times 10^{-4}$	$2.10 \mp 0.50 \times 10^{-5}$	$1.70 \mp 0.20 \times 10^{-1}$	$1.70 \mp 0.20 \times 10^{-2}$
		$^{110m}\text{Ag}$	--b	--b	$1.90 \mp 0.90 \times 10^{-1}$	$3.90 \mp 1.20 \times 10^{-3}$
		$^{125}\text{Sb}$	$2.60 + 0.30 \times 10^{-3}$	$6.00 + 0.30 \times 10^{-5}$	$2.10 \mp 0.40$	$9.10 \mp 1.10 \times 10^{-2}$
		$^{134}\text{Cs}$	$1.03 \mp 0.02 \times 10^{-2}$	$8.90 \mp 2.00 \times 10^{-5}$	$3.18 \mp 0.03 \times 10^1$	$5.58 \mp 0.09 \times 10^{-1}$
		$^{137}\text{Cs}$	$1.67 \mp 0.01 \times 10^{-1}$	$1.45 \mp 0.01 \times 10^{-3}$	$5.02 \mp 0.01 \times 10^2$	$8.78 \mp 0.04$
		$^{144}\text{Ce}$	$6.50 \mp 2.70 \times 10^{-4}$	$5.50 \mp 0.40 \times 10^{-5}$	--b	--b
7b (410 SS)	20.3		Leach 1 (126 mL)	--b	Leach 1 (100.8 mg)	--b
		$^{54}\text{Mn}$	--b		$6.10 + 0.30 \times 10^{-2}$	
		$^{60}\text{Co}$	$6.40 \pm 0.40 \times 10^{-5}$		$4.20 \mp 0.30 \times 10^{-2}$	
		$^{106}\text{Ru}$	--b		$5.10 \mp 0.20 \times 10^{-1}$	
		$^{110m}\text{Ag}$	--b		$6.60 \mp 1.20 \times 10^{-3}$	
		$^{125}\text{Sb}$	$2.00 + 0.10 \times 10^{-4}$		$1.17 \mp 0.01$	
		$^{134}\text{Cs}$	$3.81 \mp 0.07 \times 10^{-4}$		$9.10 \mp 0.30 \times 10^{-2}$	
		$^{137}\text{Cs}$	$6.12 \mp 0.03 \times 10^{-3}$		$1.47 \mp 0.01$	
		$^{144}\text{Ce}$	$7.60 \mp 1.30 \times 10^{-5}$		$5.00 \mp 0.40 \times 10^{-1}$	
		7a (thin 304 SS clad)	20.3		Leach 1 (86 mL)	--b
$^{54}\text{Mn}$	$1.10 + 0.02 \times 10^{-5}$				$7.70 + 1.20 \times 10^{-3}$	
$^{60}\text{Co}$	$3.40 \mp 0.40 \times 10^{-7}$				$7.70 \mp 1.30 \times 10^{-3}$	
$^{125}\text{Sb}$	$5.40 \mp 0.30 \times 10^{-6}$				--b	
$^{134}\text{Cs}$	$1.10 \mp 0.02 \times 10^{-5}$				$2.10 + 0.60 \times 10^{-1}$	
$^{137}\text{Cs}$	$1.70 \mp 0.01 \times 10^{-4}$				$3.28 \mp 0.02$	
$^{144}\text{Ce}$	$7.90 \mp 2.80 \times 10^{-7}$				--b	

TABLE 26. (continued)

Leadscrew Sample	Distance from Bottom of Leadscrew (cm)	Radionuclide	Soluble Radionuclide ( $\mu\text{Ci/sample}$ )		Insoluble Radionuclide ( $\mu\text{Ci/sample}$ )	
			Leach 1 (340 mL)	--b	Leach 1 (146.7 mg)	--b
10	205.7					
		$^{60}\text{Co}$	$4.70 \pm 0.60 \times 10^{-4}$	--b	$5.90 \pm 0.08 \times 10^{-1}$	--b
		$^{106}\text{Ru}$	--b		$5.80 \mp 1.30$	
		$^{125}\text{Sb}$	$2.80 \pm 0.50 \times 10^{-3}$		$3.50 \mp 0.60$	
		$^{134}\text{Cs}$	$1.68 \mp 0.04 \times 10^{-2}$		$2.55 \mp 0.04 \times 10^1$	
		$^{137}\text{Cs}$	$2.70 \mp 0.01 \times 10^{-1}$		$4.05 \mp 0.02 \times 10^2$	
		$^{144}\text{Ce}$	$1.50 \mp 0.50 \times 10^{-3}$		$1.50 \mp 0.10 \times 10^{-1}$	
11	229.2		Leach 1 (170 mL)	Leach 2 (104 mL)	Leach 1 (100.9 mg)	Leach 2 (6.4 mg)
		$^{60}\text{Co}$	$1.10 \pm 0.30 \times 10^{-4}$	$4.00 \pm 1.00 \times 10^{-7}$	$2.60 \pm 0.50 \times 10^{-1}$	$1.20 \pm 0.20 \times 10^{-2}$
		$^{110\text{m}}\text{Ag}$	--b	--b	$1.90 \mp 0.70 \times 10^{-1}$	--b
		$^{125}\text{Sb}$	$2.80 \pm 0.40 \times 10^{-3}$	$1.30 \pm 0.10 \times 10^{-5}$	$3.50 \mp 0.60$	$1.60 \pm 0.20 \times 10^{-1}$
		$^{134}\text{Cs}$	$1.41 \mp 0.03 \times 10^{-2}$	$2.10 \mp 0.06 \times 10^{-5}$	$2.33 \mp 0.04 \times 10^1$	$9.20 \mp 0.10 \times 10^1$
		$^{137}\text{Cs}$	$2.27 \mp 0.01 \times 10^{-1}$	$3.41 \mp 0.02 \times 10^{-4}$	$3.73 \mp 0.02 \times 10^2$	$1.53 \mp 0.05 \times 10^1$
12	231.1		Leach 1 (404 mL)	Leach 2 (99 mL)	Leach 1 (182.5 mg)	Leach 2 (2.6 mg)
		$^{54}\text{Mn}$	--b	--b	$7.90 \pm 1.10 \times 10^{-1}$	--b
		$^{60}\text{Co}$	$8.60 \pm 1.10 \times 10^{-4}$	$2.60 \pm 0.90 \times 10^{-8}$	$1.40 \mp 0.20$	$2.10 \pm 1.30 \times 10^{-4}$
		$^{106}\text{Ru}$	--b	--b	$2.20 \mp 0.20 \times 10^1$	$6.60 \mp 3.20 \times 10^{-3}$
		$^{110\text{m}}\text{Ag}$	--b	--b	$6.70 \mp 2.50 \times 10^{-1}$	--b
		$^{125}\text{Sb}$	$5.70 \pm 0.10 \times 10^{-2}$	$1.30 \pm 0.10 \times 10^{-6}$	$2.50 \mp 0.10 \times 10^1$	$1.00 \pm 0.20 \times 10^{-2}$
		$^{134}\text{Cs}$	$4.68 \mp 0.08 \times 10^{-2}$	$1.82 \mp 0.08 \times 10^{-6}$	$3.43 \mp 0.06 \times 10^1$	$7.70 \mp 0.90 \times 10^{-3}$
		$^{137}\text{Cs}$	$7.61 \mp 0.01 \times 10^{-1}$	$2.84 \mp 0.03 \times 10^{-5}$	$5.41 \mp 0.02 \times 10^2$	$1.16 \mp 0.04 \times 10^{-1}$

TABLE 26. (continued)

Leadscrew Sample	Distance from Bottom of Leadscrew (cm)	Radionuclide	Soluble Radionuclide ( $\mu\text{Ci}/\text{sample}$ )		Insoluble Radionuclide ( $\mu\text{Ci}/\text{sample}$ )			
			Leach 1 (368 mL)	Leach 2 (70 mL)	Leach 1 (146.7 mg)	Leach 2 (9.6 mg)		
14	266.7	$^{54}\text{Mn}$	--b	$3.20 \pm 0.90 \times 10^{-7}$	$4.40 \pm 0.80 \times 10^{-1}$	$2.60 \pm 0.20 \times 10^{-2}$		
		$^{60}\text{Co}$	$8.30 \pm 1.10 \times 10^{-4}$	$9.60 \pm 1.2 \times 10^{-7}$	$1.00 \pm 0.10$	$3.80 \pm 0.30 \times 10^{-2}$		
		$^{106}\text{Ru}$	$4.40 \pm 2.00 \times 10^{-3}$	$1.90 \pm 0.20 \times 10^{-5}$	$2.60 \pm 0.20 \times 10^1$	$2.20 \pm 0.40 \times 10^{-1}$		
		$^{110m}\text{Ag}$	$4.00 \pm 1.10 \times 10^{-4}$	--b	$4.00 \pm 1.00 \times 10^{-1}$	$3.00 \pm 1.70 \times 10^{-3}$		
		$^{125}\text{Sb}$	$5.40 \pm 0.10 \times 10^{-2}$	$5.60 \pm 0.10 \times 10^{-5}$	$1.48 \pm 0.08 \times 10^1$	$4.90 \pm 0.20 \times 10^{-1}$		
		$^{134}\text{Cs}$	$3.99 \pm 0.06 \times 10^{-2}$	$3.46 \pm 0.06 \times 10^{-5}$	$2.70 \pm 0.05 \times 10^1$	$1.55 \pm 0.02$		
		$^{137}\text{Cs}$	$6.54 \pm 0.02 \times 10^{-1}$	$5.64 \pm 0.02 \times 10^{-4}$	$4.40 \pm 0.02 \times 10^2$	$2.50 \pm 0.01 \times 10^1$		
		$^{144}\text{Ce}$	$3.50 \pm 0.90 \times 10^{-3}$	$5.50 \pm 1.00 \times 10^{-6}$	--b	--b		
		15	302.3	$^{54}\text{Mn}$	--b	--b	$6.40 \pm 1.60 \times 10^{-1}$	$2.70 \pm 0.60 \times 10^{-3}$
				$^{60}\text{Co}$	$1.20 \pm 0.10 \times 10^{-3}$	$3.40 \pm 0.50 \times 10^{-7}$	$2.10 \pm 0.30$	$3.60 \pm 0.70 \times 10^{-3}$
$^{106}\text{Ru}$	$4.90 \pm 2.00 \times 10^{-3}$			--b	$5.30 \pm 0.20 \times 10^1$	$4.10 \pm 1.20 \times 10^{-2}$		
$^{110m}\text{Ag}$	--b			--b	$3.40 \pm 1.60 \times 10^{-1}$	--b		
$^{125}\text{Sb}$	$4.50 \pm 0.10 \times 10^{-2}$			$1.12 \pm 0.04 \times 10^{-5}$	$2.60 \pm 0.20 \times 10^1$	$1.83 \pm 0.08 \times 10^{-1}$		
$^{134}\text{Cs}$	$4.88 \pm 0.07 \times 10^{-2}$			$1.10 \pm 0.02 \times 10^{-5}$	$4.20 \pm 0.10 \times 10^1$	$2.17 \pm 0.05 \times 10^{-1}$		
$^{137}\text{Cs}$	$8.12 \pm 0.03 \times 10^{-1}$			$1.75 \pm 0.01 \times 10^{-4}$	$6.80 \pm 0.04 \times 10^2$	$3.51 \pm 0.02$		
$^{144}\text{Ce}$	$1.10 \pm 0.10 \times 10^{-2}$			$3.10 \pm 0.30 \times 10^{-6}$	$4.20 \pm 1.5$	--b		

a. Decay corrected to 9-15-1983.

b. Not measured.

An evaluation of the data in Table 26 indicates that 95 to 99% of the total sample radionuclide content was retained in the insoluble fraction of the first decontamination solution for all samples, indicating that the majority of the radionuclide content is in an extremely insoluble form. Table 26 lists three subsamples for Sample 7 (7a, 7b, and 7c). This sample is the connection between the 304 SS lower extension and the 17-4 PH SS threaded section. Sample 7a is a 304 SS sleeve portion of the leadscrew; 7b is a 410 SS pin; and 7c is a 304 SS and 17-4 PH SS combination piece of the leadscrew. The majority of the activity present on Sample 7 was deposited on 7c, with lesser fractions of the total radionuclide content deposited on the other components (7a and 7b).

A comparison of the radionuclide concentrations listed in Table 26 was performed to define the axial concentration gradients. Table 27 ratios the radionuclide concentration for each sample to the radionuclide concentrations measured at H8 Sample 15 location (the location with the highest general radionuclide concentrations). The data are listed in percent of total radionuclide content present at H8 Sample 15. There is a well defined concentration gradient along the length of the leadscrew in the tightly adherent surface material, with radionuclide concentrations increasing at different rates for different radionuclides. (The majority of the brushoff debris had been previously removed from these sample locations by brushing.) The deposited radionuclides increase significantly in concentration starting at H8 Sample 7, 0.51 m (20 in.) from the bottom of the leadscrew. Concentrations above this point are relatively consistent, within a factor of 3-4, for  $^{54}\text{Mn}$ ,  $^{110\text{m}}\text{Ag}$ ,  $^{134}\text{Cs}$ , and  $^{137}\text{Cs}$ . Other radionuclides ( $^{60}\text{Co}$ ,  $^{106}\text{Ru}$ ,  $^{125}\text{Sb}$  and  $^{144}\text{Ce}$ ) have less consistent relative concentrations until near the top of the plenum assembly. At the bottom (bayonet area) of the leadscrew, the radionuclide concentrations on Samples 2 and 3 may be uncharacteristic of the exposed leadscrew environment. These samples may have been protected by the control rod spider assembly, since it is not known for certain when the control rod spider fell from the leadscrew (during the accident or afterward).

TABLE 27. COMPARISON OF TOTAL RADIONUCLIDE CONCENTRATIONS IN THE H8 DECONTAMINATION SOLIDS (INSOLUBLES) IN % OF SAMPLE 15

Radionuclide	Radionuclide Concentrations (%)								
	2	4	5	7	10	11	12	14	15
<sup>54</sup> Mn	2.2	1.4	21.6	35.7	--a	41.0	123.0	68.8	100
<sup>60</sup> Co	1.3	0.25	3.0	10.5	28.1	12.4	66.7	47.6	100
<sup>106</sup> Ru	0.74	<0.1	0.51	0.96	10.9	--a	41.5	49.1	100
<sup>110m</sup> Ag	--a	--a	0.7	57.8	--a	55.9	197.0	118.0	100
<sup>125</sup> Sb	0.5	0.1	1.4	12.6	13.5	13.5	96.2	56.9	100
<sup>134</sup> Cs	3.0	0.4	8.3	76.4	60.7	55.5	81.7	67.9	100
<sup>137</sup> Cs	2.9	0.4	8.1	74.5	59.6	54.8	79.6	64.7	100
<sup>144</sup> Ce	--a	--a	--a	--a	11.9	3.6	--a	--a	100

a. Not detected.

Table 28 lists the  $^{90}\text{Sr}$ ,  $^{129}\text{I}$ , tellurium, and fissile material concentrations for the H8 Samples 2 and 15 decontamination solutions (soluble and insoluble). The second decontamination solution is a small contributor (<1%) to the total radionuclide content except for the  $^{235}\text{U}$  concentration on Sample 15. The  $^{90}\text{Sr}$  is >99% soluble for H8 Samples 2 and 15; this is in contrast to most other radionuclides (Table 26), which are principally insoluble. The  $^{129}\text{I}$  is 75 to 90% soluble on H8 Samples 2 and 15. A comparison of the  $^{90}\text{Sr}$  and  $^{129}\text{I}$  data for H8 Samples 2 and 15 indicates a large axial gradient in the deposition characteristics, with the highest concentrations at the top of the plenum assembly. The  $^{90}\text{Sr}$  and  $^{129}\text{I}$  concentrations on H8 Sample 15 are factors of 68 and  $1.1 \times 10^3$  greater respectively than those measured on H8 Sample 2. The fissile material content measured at both locations is uniform (within a factor of 2) and much less than the concentrations measured in the brushoff debris ( $\sim 10^2$  to  $10^3$ ). The  $^{235}\text{U}$  present in the decontamination solutions may be from the small amounts of surface debris not removed during the brushing operation. Tellurium was not detected.

Summed Brushoff Debris and Decontamination Solution Surface Concentrations. To calculate the radionuclide concentrations on the leadscrew surfaces, the radionuclide content of each sample was converted to  $\mu\text{Ci}/\text{cm}^2$ . Table 29 lists the calculated surface radionuclide concentrations based on the radionuclide content from the brushoff debris removed from the two leadscrew Sections H8-7 and H8-9. These surface radionuclide concentrations are probably no better than a factor of 2 of the actual undisturbed brushoff debris surface concentration, as some brushoff debris may have been lost during the leadscrew cutting operation and subsequent handling. Based on these data, there is an obvious axial gradient in the radionuclide deposition along the leadscrew for most radionuclides. The gradients in these radionuclide concentrations from the top of the plenum assembly range from 36-66 times the amount deposited at the H8-9 location (near the bottom). The exceptions are  $^{129}\text{I}$ , tellurium,  $^{154}\text{Eu}$  and  $^{235}\text{U}$ , which indicate reductions in surface radionuclide concentration from locations H8-9 to H8-7. These data indicate specific radionuclide gradients in the brushoff debris composition.



TABLE 28. H8 LEADSCREW SAMPLE DECONTAMINATION DATA FOR  $^{90}\text{Sr}$ ,  $^{129}\text{I}$  (BETA EMITTERS), TELLURIUM and  $^{235}\text{U}$

Leadscrew	Sample	Distance from the Bottom of Leadscrew (cm)	Radionuclide	Insoluble Radionuclide ( $\mu\text{Ci/sample}$ )	Soluble Radionuclide ( $\mu\text{Ci/Sample}$ )	
				Leach 1 (61.8 mg)	Leach 1 (114 mL)	Leach 2 (110 mL)
H8	2 <sup>a</sup> ( $\text{HNO}_3$ + HF decontamination solution)	2.5	$^{90}\text{Sr}^{\text{b}}$	$1.27 \pm 0.06 \times 10^{-2}$	$2.2 \pm 0.3 \times 10^1$	$6.8 \pm 0.8 \times 10^{-2}$
			$^{129}\text{I}$	$5.2 \pm 1.9 \times 10^{-7}$	$1.6 \pm 0.6 \times 10^{-6}$	--c
			$\text{Te}^{\text{d}}$	--c	$1.1 \times 10^2$	--c
			$^{235}\text{U}^{\text{d}}$	$3.4 \pm 0.6$	$4.3 \pm 0.4$	--c
	15 <sup>a</sup> ( $\text{HNO}_3$ + HF decontamination solution)	302.3	$^{90}\text{Sr}^{\text{b}}$	Leach 1 (218.2 mg) $6.5 \pm 0.2$	Leach 1 (320 mL) $1.51 \pm 0.01 \times 10^3$	Leach 2 (122 mL) $4.0 \pm 0.2 \times 10^{-1}$
			$^{129}\text{I}$	$2.4 \pm 0.4 \times 10^{-4}$	$2.0 \pm 0.3 \times 10^{-3}$	$<1.4 \times 10^{-8}^{\text{b}}$
			$\text{Te}^{\text{d}}$	--c	$1.14 \times 10^2$	--c
			$^{235}\text{U}^{\text{d}}$	$1.8 \pm 0.8$	$1.9 \pm 0.1$	$9.8 \pm 1.2 \times 10^{-1}$

a. Sample 2 is close to the bottom and Sample 15 is close to top of the plenum assembly.

b.  $^{90}\text{Sr}$  decay corrected to 6/15/84.

c. Not detected.

d. Te and  $^{235}\text{U}$  data are listed in  $\mu\text{g/sample}$ .

TABLE 29. SURFACE RADIONUCLIDE CONCENTRATIONS OF LEADSCREW H8 BRUSHOFF DEBRIS ( $\mu\text{Ci}/\text{cm}^2$ )

<u>Radionuclide</u>	<u>H8-9<sup>a</sup></u> <u>(<math>\mu\text{Ci}/\text{cm}^2</math>)</u>	<u>H8-7<sup>b</sup></u> <u>(<math>\mu\text{Ci}/\text{cm}^2</math>)</u>
<sup>54</sup> Mn	$1.5 \times 10^{-3}$	$5.4 \times 10^{-2}$
<sup>60</sup> Co	$9.1 \times 10^{-2}$	4.1
<sup>90</sup> Sr	$2.4 \times 10^{-2}$	$7.0 \times 10^{-1}$
<sup>106</sup> Ru	$2.7 \times 10^{-1}$	13.7
<sup>110m</sup> Ag	-- <sup>c</sup>	$6.5 \times 10^{-2}$
<sup>125</sup> Sb	$1.9 \times 10^{-1}$	12.6
<sup>129</sup> I	$3.2 \times 10^{-6}$	-- <sup>c</sup>
Te <sup>d</sup>	9.3	-- <sup>e</sup>
<sup>134</sup> Cs	$4.3 \times 10^{-2}$	2.1
<sup>137</sup> Cs	$7.9 \times 10^{-1}$	38.8
<sup>144</sup> Ce	$6.9 \times 10^{-1}$	25.9
<sup>154</sup> Eu	$6.0 \times 10^{-3}$	-- <sup>c</sup>
<sup>235</sup> Ud	3.05	0.9

a. Surface area of Section H8-9 = 1347  $\text{cm}^2$ .

b. Surface area of Section H8-7 = 1981  $\text{cm}^2$ .

c. Not detected.

d. Concentration in  $\mu\text{g}/\text{cm}^2$

e. Below detection limit.

Tables 30 and 31 list the surface radionuclide concentrations based on the insoluble and soluble decontamination solution data. The principal contributor to the total surface radionuclide concentrations listed is the insoluble decontamination solution fraction (95 to 99%), with the exceptions of the  $^{129}\text{I}$  and  $^{90}\text{Sr}$  concentrations as was previously discussed. It is interesting to note that the  $^{137}\text{Cs}$  and  $^{90}\text{Sr}$  concentrations are similar at the bottom of the leadscrew and are within a factor of 2 at the top of the plenum assembly, although the  $^{137}\text{Cs}$  is insoluble and the  $^{90}\text{Sr}$  is soluble. These data indicate that both radionuclides may have been transported by a common mechanism.

The brushoff debris and decontamination sample data were compared to determine the fraction of total surface radionuclide concentrations attributable to the brushoff debris. Table 32 lists the brushoff debris contributions to the total surface radionuclide concentration (%). For some radionuclides ( $^{54}\text{Mn}$ ,  $^{60}\text{Co}$ ,  $^{106}\text{Ru}$ ,  $^{125}\text{Sb}$ ,  $^{144}\text{Ce}$ , and  $^{235}\text{U}$ ), the brushoff debris contributes >90% of the total radionuclide deposition. Other radionuclides ( $^{90}\text{Sr}$ ,  $^{134}\text{Cs}$ ,  $^{137}\text{Cs}$ ) are associated to a greater extent with the tightly adherent layer.

Table 33 lists the total measured surface radionuclide concentrations ( $\mu\text{Ci}/\text{cm}^2$ ), based on both the brushoff debris and decontamination solutions and the ORIGEN2-calculated radionuclide inventories<sup>17</sup> decay-corrected to the time of sample analysis. The uncertainty in the total surface concentration data is no better than a factor of 2. The radionuclide concentrations for  $^{60}\text{Co}$ ,  $^{106}\text{Ru}$ ,  $^{125}\text{Sb}$ , and  $^{144}\text{Ce}$  are comparable with those reported by other laboratories.<sup>18</sup> However, the surface concentrations for  $^{54}\text{Mn}$ ,  $^{110\text{m}}\text{Ag}$ ,  $^{134}\text{Cs}$ , and  $^{137}\text{Cs}$ , are a factor of 10 lower than the values reported from other laboratories.<sup>18</sup> This may be partially due to the uncertainty in the amounts of brushoff debris collected and/or plateout of some radionuclides during the decontaminations.

Surface Sample Analysis Results. Table 1 identifies the H8 surface samples (Samples 3, 13, and 16) and lists the analyses performed on each sample. The surface areas of the individual sample fractions are based on

TABLE 30. H8 SURFACE RADIONUCLIDE CONCENTRATIONS FROM INSOLUBLE RADIONUCLIDES  
( $\mu\text{Ci}/\text{cm}^2$ )

Radionuclide	Surface Radionuclide Concentrations ( $\mu\text{Ci}/\text{cm}^2$ )								
	Section H8-9				Section H8-7				
	$^{2a}$ (2.5) <sup>d</sup>	$^{4a}$ (13.3) <sup>d</sup>	$^{5b}$ (15.2) <sup>d</sup>	$^{7b}$ (20.3) <sup>d</sup>	$^{10b}$ (205.7) <sup>d</sup>	$^{11c}$ (229.2) <sup>d</sup>	$^{12c}$ (31.1) <sup>d</sup>	$^{14c}$ (266.7) <sup>d</sup>	$^{15c}$ (302.3) <sup>d</sup>
$^{54}\text{Mn}$	$1.23 \times 10^{-3}$	$1.04 \times 10^{-3}$	$6.08 \times 10^{-3}$	$7.53 \times 10^{-3}$	--e	--e	$2.39 \times 10^{-2}$	$1.41 \times 10^{-2}$	$1.94 \times 10^{-2}$
$^{60}\text{Co}$	$2.37 \times 10^{-3}$	$5.88 \times 10^{-4}$	$2.82 \times 10^{-3}$	$8.24 \times 10^{-3}$	$2.60 \times 10^{-2}$	$8.22 \times 10^{-3}$	$4.23 \times 10^{-2}$	$3.14 \times 10^{-2}$	$6.36 \times 10^{-2}$
$^{90}\text{Sr}$	$1.07 \times 10^{-3}$	--f	--f	--f	--f	--f	--f	--f	$1.96 \times 10^{-1}$
$^{106}\text{Ru}$	$3.42 \times 10^{-2}$	$3.86 \times 10^{-3}$	$1.19 \times 10^{-2}$	--e	$2.56 \times 10^{-1}$	--e	$6.65 \times 10^{-1}$	$7.92 \times 10^{-1}$	1.60
$^{110m}\text{Ag}$	--e	--e	$1.10 \times 10^{-4}$	$8.39 \times 10^{-2}$	--e	$5.74 \times 10^{-3}$	$2.02 \times 10^{-2}$	$1.21 \times 10^{-2}$	$1.03 \times 10^{-2}$
$^{125}\text{Sb}$	$1.14 \times 10^{-2}$	$2.54 \times 10^{-3}$	$1.54 \times 10^{-2}$	$9.65 \times 10^{-2}$	$1.54 \times 10^{-1}$	$1.11 \times 10^{-1}$	$7.56 \times 10^{-1}$	$1.53 \times 10^1$	$7.91 \times 10^{-1}$
$^{129}\text{I}$	$4.56 \times 10^{-8}$	--f	--f	--f	--f	--f	--f	--f	$7.25 \times 10^{-6}$
$^{129}\text{Te}$	--e	--f	--f	--f	--f	--f	--f	--f	--e
$^{134}\text{Cs}$	$1.14 \times 10^{-1}$	$2.08 \times 10^{-2}$	$1.54 \times 10^{-1}$	1.43	1.12	$7.32 \times 10^{-1}$	1.04	$8.63 \times 10^{-1}$	1.28
$^{137}\text{Cs}$	1.80	$3.30 \times 10^{-1}$	2.42	$2.25 \times 10^1$	$1.78 \times 10^1$	$1.17 \times 10^1$	$1.63 \times 10^1$	$1.40 \times 10^1$	$2.06 \times 10^1$
$^{144}\text{Ce}$	--e	--e	--e	--e	$6.61 \times 10^{-3}$	--e	--e	--e	--e
$^{235}\text{U}$	$2.98 \times 10^{-1}$	--f	--f	--f	--f	--f	--f	--f	$5.44 \times 10^{-2}$

a. Bayonet diameter = 1.9 cm. Sample surface area = 11.4  $\text{cm}^2$ .

b. Sample diameter = 3.8 cm. Sample surface area = 22.7  $\text{cm}^2$ .

c. Surface area of threaded sample = 33.1  $\text{cm}^2$ .

d. Distance from bottom of leadscrew (cm).

e. Not detected.

f. Not analyzed.

g. Te and  $^{235}\text{U}$  concentrations in  $\mu\text{g}/\text{cm}^2$ .

TABLE 31. H8 SURFACE RADIONUCLIDE CONCENTRATIONS FROM SOLUBLE RADIONUCLIDES  
( $\mu\text{Ci}/\text{cm}^2$ )

Radionuclide	Surface Radionuclide Concentrations ( $\mu\text{Ci}/\text{cm}^2$ )								
	Section H8-9				Section H8-7				
	( $2.5^a$ ) <sup>d</sup>	( $13.3^a$ ) <sup>d</sup>	( $15.2^b$ ) <sup>d</sup>	( $20.3^b$ ) <sup>d</sup>	( $205.7^b$ ) <sup>d</sup>	( $229.2^c$ ) <sup>d</sup>	( $231.1^c$ ) <sup>d</sup>	( $266.7^c$ ) <sup>d</sup>	( $302.3^c$ ) <sup>d</sup>
$^{54}\text{Mn}$	--e	--e	$3.08 \times 10^{-7}$	--e	--e	--e	--e	--e	--e
$^{60}\text{Co}$	$3.77 \times 10^{-6}$	$3.60 \times 10^{-6}$	$1.17 \times 10^{-6}$	$1.19 \times 10^{-5}$	$2.07 \times 10^{-5}$	$3.32 \times 10^{-6}$	$2.60 \times 10^{-5}$	$2.51 \times 10^{-5}$	$3.63 \times 10^{-5}$
$^{90}\text{Sr}$	1.93	--f	--f	--f	--f	--f	--f	--f	$4.56 \times 10^1$
$^{106}\text{Ru}$	--e	--e	--e	--e	--e	--e	--e	$1.33 \times 10^{-4}$	$1.48 \times 10^{-4}$
$^{110\text{m}}\text{Ag}$	--e	--e	--e	--e	--e	--e	--e	$1.21 \times 10^{-5}$	--e
$^{125}\text{Sb}$	--e	--e	$7.05 \times 10^{-6}$	$1.15 \times 10^{-4}$	$1.23 \times 10^{-4}$	$8.46 \times 10^{-5}$	$1.72 \times 10^{-3}$	$1.63 \times 10^{-3}$	$1.36 \times 10^{-3}$
$^{129}\text{I}$	$1.40 \times 10^{-7}$	--f	--f	--f	--f	--f	--f	--f	$6.04 \times 10^{-5}$
Te <sup>g</sup>	$1.00 \times 10^{-1}$	--f	--f	--f	--f	--f	--f	--f	9.06
$^{134}\text{Cs}$	$4.73 \times 10^{-4}$	$2.95 \times 10^{-5}$	$6.34 \times 10^{-5}$	$4.54 \times 10^{-4}$	$9.11 \times 10^{-4}$	$4.26 \times 10^{-4}$	$1.41 \times 10^{-3}$	$1.21 \times 10^{-3}$	$1.47 \times 10^{-3}$
$^{137}\text{Cs}$	$7.52 \times 10^{-3}$	$4.75 \times 10^{-4}$	$1.00 \times 10^{-3}$	$7.36 \times 10^{-3}$	$1.48 \times 10^{-2}$	$6.86 \times 10^{-3}$	$2.30 \times 10^{-2}$	$1.98 \times 10^{-2}$	$2.45 \times 10^{-2}$
$^{144}\text{Ce}$	--e	--e	$7.93 \times 10^{-6}$	$2.86 \times 10^{-5}$	$6.61 \times 10^{-5}$	--e	--e	$1.06 \times 10^{-4}$	$3.32 \times 10^{-4}$
$^{235}\text{U}$	$3.77 \times 10^{-1}$	--f	--f	--f	--f	--f	--f	--f	$8.7 \times 10^{-2}$

a. Bayonet diameter = 1.9 cm. Sample surface area =  $11.4 \text{ cm}^2$ .

b. Sample diameter = 3.8 cm. Sample surface area =  $22.7 \text{ cm}^2$ .

c. Surface area of threaded sample =  $33.1 \text{ cm}^2$ .

d. Distance from bottom of leadscrew (cm).

e. Not detected.

f. Not analyzed.

g. Te and  $^{235}\text{U}$  concentrations in  $\mu\text{g}/\text{cm}^2$ .

TABLE 32. H8 BRUSHOFF DEBRIS CONTRIBUTIONS TO TOTAL SURFACE RADIONUCLIDE CONCENTRATIONS (%)<sup>a</sup>

Radionuclide	2	4	5	7	10	11	12	14	15
<sup>54</sup> Mn	55	74	20	17	100	100	69	79	74
<sup>60</sup> Co	98	99.7	97	92	99	99	99	99	98
<sup>90</sup> Sr	1.2	--b	--b	--b	--b	--b	--b	--b	1.5
<sup>106</sup> Ru	89	99	96	--c	98	--c	95	94	90
<sup>110m</sup> Ag	--c	--c	0.0	0.0	--a	92	76	84	86
<sup>125</sup> Sb	94	99	92	66	99	99	94	45	94
<sup>129</sup> I	99	--b	--b	--b	--b	--b	--b	--b	0
<sup>134</sup> Cs	27	80	22	29	65	74	67	71	62
<sup>137</sup> Cs	30	83	25	34	69	77	70	74	65
<sup>144</sup> Ce	100	100	100	100	100	--c	--c	--c	--c
<sup>235</sup> U	93	--b	--b	--b	--b	--b	--b	--b	87

a. Percent of radionuclide surface concentration in brushoff debris compared to the total concentration (sum of concentrations in brushoff debris, decontamination solution and insoluble solid fractions).

b. Not measured.

c. Not detected.

TABLE 33. TOTAL H8 SURFACE RADIONUCLIDE CONCENTRATIONS AND RADIONUCLIDE CORE INVENTORY ( $\mu\text{Ci}/\text{cm}^2$ )<sup>a</sup>

Radionuclide	Radionuclide Concentrations ( $\mu\text{Ci}/\text{cm}^2$ )		Core Inventory <sup>c</sup> ( $\mu\text{Ci}$ )
	H8-9	H8-7	
<sup>54</sup> Mn	$5.6 \times 10^{-3}$	$7.3 \times 10^{-2}$	--d
<sup>60</sup> Co	$9.5 \times 10^{-2}$	4.1 <sup>e</sup>	--d
<sup>90</sup> Sr	2.0	46.5	$7.5 \times 10^{11}$
<sup>106</sup> Ru	$2.9 \times 10^{-1}$	14.5 <sup>e</sup>	$2.2 \times 10^{11}$
<sup>110m</sup> Ag	$4.2 \times 10^{-2}$	$7.8 \times 10^{-2}$	$2.2 \times 10^7$
<sup>125</sup> Sb	$2.2 \times 10^{-1}$	13.1 <sup>e</sup>	$3.9 \times 10^{10}$
<sup>129</sup> I	$3.4 \times 10^{-6}$	$6.8 \times 10^{-5}$	$2.5 \times 10^{11}$
Te <sup>f</sup>	$1.9 \times 10^1$	9.06	$4.5 \times 10^9$
<sup>134</sup> Cs	$5.1 \times 10^{-1}$	3.2	$3.3 \times 10^{10}$
<sup>137</sup> Cs	7.4	56.0	$7.9 \times 10^{11}$
<sup>144</sup> Ce	$6.2 \times 10^{-1}$	26.1 <sup>e</sup>	$3.9 \times 10^{11}$
<sup>235</sup> U <sup>f</sup>	3.7	1.0	$2.2 \times 10^{12}$

a. Sum of surface activities from brushoff debris, decontamination solutions, and insoluble fractions. The average surface activities of four samples from H8-9 section and five samples from H8-7 section in Tables 30 and 31 are added to the values in Table 29 to obtain the value in Table 33 for each radionuclide.

b. Gamma spectral analyses for decontamination solutions and insoluble fractions from Section H8-8 were not performed, and therefore the total surface activities are not listed.

c. ORIGEN2-calculated core radionuclide inventories at 1705 days after the accident.

d. Activation product.

e. The surface activities for these radionuclides are in agreement with values reported by other laboratories (Reference 19).

f. Te and <sup>235</sup>U concentrations in  $\mu\text{g}/\text{cm}^2$  and inventories in  $\mu\text{g}$ .

micrometer measurements of the individual leadscrew fraction subsamples. The radionuclide concentrations for these samples in  $\mu\text{Ci}/\text{cm}^2$  are shown in Table 34. These data were obtained by measuring the total radionuclide content present on the surface sample.

A comparison of the summed radionuclide concentration and surface sample data in Tables 33 and 34 indicates that the concentrations are higher by factors of 5-30 for  $^{60}\text{Co}$ ,  $^{90}\text{Sr}$ ,  $^{129}\text{I}$ ,  $^{134}\text{Cs}$ , and  $^{137}\text{Cs}$  for H8 Sample 3 than for the summed concentrations calculated for section H8-9. The data for H8 Samples 13 and 16 are also higher ( $\sim$  a factor of 10) when compared with the H8-7 section data from Table 33. The data from H8 Samples 13 and 16 are comparable with the data reported by other laboratories.<sup>19</sup> The most likely cause for the lower concentrations calculated from the summed brushoff debris and decontamination solution measurements is losses of brushoff debris during collection (for H8-9, only  $\sim 0.54$  g could be collected by brushing).

In addition to the samples removed from the plenum assembly region, Sample 18 was removed from section H8-2 which was located between the top of the plenum assembly and the reactor head. Table 35 lists the surface radionuclide concentrations for this sample measured by gamma spectroscopy.

Core Inventory Deposition Fractions. The fraction of the core inventory deposited on the plenum assembly surfaces has been extrapolated from the H8 analysis data. The extrapolated radionuclide content (in percent of core inventory) deposited on the plenum assembly surfaces is listed in Table 36. The deposition fractions in percent were calculated as follows:

$$DF = \frac{100 CA}{I} \quad (2)$$

where

DF = deposition fraction (%)



TABLE 34. H8 LEADSCREW SURFACE SAMPLE RADIONUCLIDE CONTENT  
( $\mu\text{Ci}/\text{cm}^2$ )

Radionuclide	Radionuclide Content ( $\mu\text{Ci}/\text{cm}^2$ )		
	H8 Sample 3 <sup>a</sup> (0.24) <sup>c</sup>	H8 Sample 13 <sup>b</sup> (2.45) <sup>c</sup>	H8 Sample 16 <sup>b</sup> (1.65) <sup>c</sup>
<sup>60</sup> Co	$1.2 \pm 0.2 \times 10^{-1}$	$1.5 \pm 0.1$	$5.7 \pm 0.9 \times 10^{-1}$
<sup>90</sup> Sr	$2.9 \pm 0.3$	$1.01 \pm 0.01$	$7.4 \pm 0.4$
<sup>129</sup> I	$2.4 \pm 0.9 \times 10^{-5}$	$1.6 \pm 0.3 \times 10^{-4}$	$3.9 \pm 0.9 \times 10^{-4}$
<sup>125</sup> Sb	--d	$3.5 \pm 0.1 \times 10^1$	$3.2 \pm 0.1 \times 10^1$
<sup>134</sup> Cs	$1.15 \pm 0.02 \times 10^1$	$4.4 \pm 0.6 \times 10^1$	$3.9 \pm 0.2 \times 10^1$
<sup>137</sup> Cs	$2.27 \pm 0.02 \times 10^2$	$8.89 \pm 0.03 \times 10^2$	$7.92 \pm 0.04 \times 10^2$
<sup>144</sup> Ce	--d	--d	--d
<sup>235</sup> Ue	$5.1 \pm 0.1$	$1.03 \pm 0.01 \times 10^1$	--f

- a. H8 Sample 3 is close to the bottom of the plenum assembly.
- b. H8 Samples 13 and 16 are close to the top of plenum assembly.
- c. Measured surface area ( $\text{cm}^2$ ) of the individual subsamples analyzed.
- d. Not detected.
- e. Fissile material concentration in  $\mu\text{g}/\text{cm}^2$ .
- f. Not measured.

TABLE 35. SURFACE RADIONUCLIDE CONCENTRATIONS OF H8 SAMPLE 18 NEAR THE TOP OF THE REACTOR HEAD ( $\mu\text{Ci}/\text{cm}^2$ )

Distance From Bottom of Leadscrew (cm)	Radionuclide	Surface Activity ( $\mu\text{Ci}/\text{cm}^2$ )
528.3	$^{60}\text{Co}^a$	$5.9 \pm 0.2 \times 10^{-1}$
	$^{106}\text{Ru}$	$7.5 \pm 1.0 \times 10^{-1}$
	$^{125}\text{Sr}$	$2.4 \pm 0.10$
	$^{134}\text{Cs}$	$1.3 \pm 0.02$
	$^{137}\text{Cs}$	$2.9 \pm 0.01 \times 10^1$
	$^{144}\text{Ce}$	$2.0 \pm 0.5$

a. Activation product.

TABLE 36. RADIONUCLIDE DEPOSITION FRACTIONS (%) ON PLENUM ASSEMBLY SURFACES FROM THE H8 DATA<sup>a</sup>

Radionuclide	Brushoff Debris		Soluble Radionuclides		Insoluble Radionuclides		Total Deposition Fraction <sup>b</sup>	
	H8-9 <sup>c</sup>	H8-7 <sup>d</sup>	H8-9 <sup>c</sup>	H8-7 <sup>d</sup>	H8-9 <sup>c</sup>	H8-7 <sup>d</sup>	H8-9 <sup>c</sup>	H8-7 <sup>d</sup>
<sup>90</sup> Sr	1.54 x 10 <sup>-5</sup>	4.49 x 10 <sup>-4</sup>	1.24 x 10 <sup>-3</sup>	2.93 x 10 <sup>-2</sup>	6.87 x 10 <sup>-7</sup>	1.26 x 10 <sup>-4</sup>	1.26 x 10 <sup>-3</sup>	2.99 x 10 <sup>-2</sup>
<sup>106</sup> Ru	5.34 x 10 <sup>-4</sup>	2.68 x 10 <sup>-2</sup>	-- <sup>e</sup>	2.75 x 10 <sup>-7</sup>	3.13 x 10 <sup>-5</sup>	1.62 x 10 <sup>-3</sup>	5.65 x 10 <sup>-4</sup>	2.84 x 10 <sup>-2</sup>
<sup>110m</sup> Ag	-- <sup>e</sup>	1.25	-- <sup>e</sup>	2.34 x 10 <sup>-4</sup>	8.09 x 10 <sup>-1</sup>	2.34 x 10 <sup>-1</sup>	8.09 x 10 <sup>-1</sup>	1.48
<sup>125</sup> Sb	2.10 x 10 <sup>-3</sup>	1.41 x 10 <sup>-1</sup>	-- <sup>e</sup>	1.09 x 10 <sup>-5</sup>	3.43 x 10 <sup>-4</sup>	4.34 x 10 <sup>-3</sup>	2.44 x 10 <sup>-3</sup>	1.45 x 10 <sup>-1</sup>
<sup>129</sup> I	5.55 x 10 <sup>-3</sup>	-- <sup>e</sup>	2.43 x 10 <sup>-4</sup>	1.05 x 10 <sup>-1</sup>	7.91 x 10 <sup>-5</sup>	1.26 x 10 <sup>-2</sup>	5.87 x 10 <sup>-3</sup>	1.18 x 10 <sup>-1</sup>
Te <sup>f</sup>	8.8 x 10 <sup>-3</sup>	-- <sup>g</sup>	9.54 x 10 <sup>-3</sup>	8.7 x 10 <sup>-3</sup>	-- <sup>g</sup>	-- <sup>g</sup>	1.83 x 10 <sup>-2</sup>	-- <sup>g</sup>
<sup>134</sup> Cs	5.52 x 10 <sup>-4</sup>	2.70 x 10 <sup>-2</sup>	3.23 x 10 <sup>-6</sup>	1.39 x 10 <sup>-5</sup>	5.50 x 10 <sup>-3</sup>	1.29 x 10 <sup>-2</sup>	6.06 x 10 <sup>-3</sup>	3.99 x 10 <sup>-2</sup>
<sup>137</sup> Cs	4.25 x 10 <sup>-4</sup>	2.09 x 10 <sup>-2</sup>	2.16 x 10 <sup>-6</sup>	9.57 x 10 <sup>-6</sup>	3.62 x 10 <sup>-3</sup>	8.65 x 10 <sup>-3</sup>	4.05 x 10 <sup>-3</sup>	2.96 x 10 <sup>-2</sup>
<sup>144</sup> Ce	6.81 x 10 <sup>-4</sup>	1.70 x 10 <sup>-2</sup>	2.00 x 10 <sup>-8</sup>	2.40 x 10 <sup>-7</sup>	-- <sup>e</sup>	7.26 x 10 <sup>-6</sup>	5.38 x 10 <sup>-4</sup>	2.86 x 10 <sup>-2</sup>
<sup>154</sup> Eu	9.51 x 10 <sup>-4</sup>	-- <sup>e</sup>	-- <sup>e</sup>	-- <sup>e</sup>	-- <sup>e</sup>	-- <sup>e</sup>	9.51 x 10 <sup>-4</sup>	-- <sup>e</sup>
<sup>155</sup> Eu	-- <sup>e</sup>	-- <sup>e</sup>	-- <sup>e</sup>	-- <sup>e</sup>	-- <sup>e</sup>	-- <sup>e</sup>	-- <sup>e</sup>	-- <sup>e</sup>
<sup>235</sup> Uf	5.89 x 10 <sup>-4</sup>	1.74 x 10 <sup>-4</sup>	7.28 x 10 <sup>-5</sup>	1.68 x 10 <sup>-5</sup>	5.76 x 10 <sup>-5</sup>	1.05 x 10 <sup>-5</sup>	7.19 x 10 <sup>-4</sup>	2.01 x 10 <sup>-4</sup>

a. The H8 data used was from the brushoff debris and the decontamination solution. Deposition fraction (%) = calculated surface radionuclide concentration ( $\mu\text{Ci}/\text{cm}^2$ ) x plenum assembly surface area ( $4.25 \times 10^6 \text{ cm}^2$ ) x 100 ÷ core inventory ( $\mu\text{Ci}$ ).

b. Sum of deposition fractions from brushoff debris, soluble and insoluble radionuclides.

c. Section H8-9 is close to the bottom of the plenum assembly.

d. Section H8-7 is close to the top of the plenum assembly.

e. Not measured.

f. Deposition fraction (%) = calculated surface radionuclide concentration ( $\mu\text{g}/\text{cm}^2$ ) x plenum assembly surface area ( $4.25 \times 10^6 \text{ cm}^2$ ) x 100 ÷ core inventory ( $\mu\text{g}$ ).

g. Below detection limit.

- C = calculated surface radionuclide concentration ( $\mu\text{Ci}/\text{cm}^2$   
or  $\mu\text{g}/\text{cm}^2$ )
- A = plenum assembly surface area =  $4.25 \times 10^6 \text{ cm}^2$
- I = core inventory ( $\mu\text{Ci}$  or  $\mu\text{g}$ ).

The plenum surface area ( $4.25 \times 10^6 \text{ cm}^2$ ) was reported in Reference 20, and the ORIGEN2 code-calculated radionuclide inventories were obtained from Reference 18. The data in Table 36 indicate that very small fractions of the core inventory were deposited on the plenum assembly surfaces--<0.2% for all radionuclides except  $^{110\text{m}}\text{Ag}$  and tellurium, which are less than 2.0%.

For comparison purposes, the fraction of core radionuclide inventory deposited on the plenum surfaces based on the surface sample data has also been calculated. These data are listed in Table 37, and the calculated deposition fractions based on these data are less than 0.7% for all radionuclides. No  $^{110\text{m}}\text{Ag}$  was measurable on these samples, and therefore no deposition fraction could be calculated. The fraction of core inventory deposited on the plenum surfaces is quite small, whether the summed sample or the surface sample data are used.

#### B8 Leadscrew Radiological Analyses

The radiological analyses performed on the B8 samples are the same as those performed on the H8 samples (see Table 1) with the exception that fewer samples were examined. The B8 samples were examined so that axial and radial comparisons could be made between the bottom and top of the plenum assembly at the H8 and B8 locations.

Brushoff Debris. The radionuclide concentrations measured by gamma spectroscopy for the B8 brushoff debris are presented in Table 38. The quantities of brushoff debris listed are only fractions of the total amount present, as only portions of the leadscrew were brushed. These data

TABLE 37. RADIONUCLIDE DEPOSITION FRACTIONS (%) ON THE PLENUM ASSEMBLY SURFACES FROM THE H8 SURFACE SAMPLES

Radionuclide	H8-3	H8-13	H8-16	Core Inventory <sup>a</sup> ( $\mu$ Ci)
$^{60}\text{Co}$	--b	--b	--b	--b
$^{90}\text{Sr}$	$7.7 \times 10^{-5}$	$9.6 \times 10^{-4}$	$3.6 \times 10^{-4}$	$6.62 \times 10^{11}$
$^{125}\text{Sb}$	--c	$4.2 \times 10^{-1}$	$3.9 \times 10^{-1}$	$3.51 \times 10^{10}$
$^{129}\text{I}$	$4.2 \times 10^{-2}$	$2.8 \times 10^{-1}$	$6.8 \times 10^{-1}$	$2.45 \times 10^5$
Te <sup>d</sup>	--c	--c	1.15	$4.45 \times 10^9$
$^{134}\text{Cs}$	$1.6 \times 10^{-1}$	$6.2 \times 10^{-1}$	$5.5 \times 10^{-1}$	$2.99 \times 10^{10}$
$^{137}\text{Cs}$	$1.3 \times 10^{-1}$	$5.0 \times 10^{-1}$	$4.5 \times 10^{-1}$	$7.52 \times 10^{11}$
$^{144}\text{Ce}$	--c	--c	--c	$2.99 \times 10^9$
$^{235}\text{Ud}$	$9.9 \times 10^{-4}$	$2.0 \times 10^{-3}$	--e	$2.2 \times 10^{12}$

- a. The core inventory is calculated at  $1.81 \times 10^3$  days after the accident.
- b. Activation product.
- c. Not detected.
- d. Core inventory in  $\mu\text{g}$  for Te or  $^{235}\text{U}$ .
- e. Not measured.

TABLE 38. RADIONUCLIDE CONTENT OF THE B8 BRUSHOFF DEBRIS  
( $\mu\text{Ci}/\text{mg}$ )<sup>a</sup>

Radionuclide	Radionuclide Content ( $\mu\text{Ci}/\text{mg}$ )	
	B8-3 <sup>b</sup> (0.75 g) <sup>d</sup>	B8-1 <sup>c</sup> (18.75 g) <sup>d</sup>
<sup>60</sup> Co	$2.24 \pm 0.06 \times 10^{-1}$	$2.50 \pm 0.5 \times 10^{-2}$
<sup>106</sup> Ru	$6.30 \pm 0.20 \times 10^{-1}$	--
<sup>125</sup> Sb	$4.00 \pm 0.10 \times 10^{-1}$	$1.99 \pm 0.08$
<sup>134</sup> Cs	$1.89 \pm 0.04 \times 10^{-1}$	$2.65 \pm 0.05$
<sup>137</sup> Cs	$3.53 \pm 0.03$	$4.74 \pm 0.02 \times 10^1$
<sup>144</sup> Ce	$7.50 \pm 0.10 \times 10^{-1}$	--e
<sup>154</sup> Eu	$1.20 \pm 0.20 \times 10^{-2}$	--e
<sup>155</sup> Eu	$2.45 \pm 0.02 \times 10^{-2}$	--e

- a. Decay corrected date 3/15/84.  
b. Section B8-3 is close to bottom of plenum assembly.  
c. Section B8-1 is close to top of the plenum assembly.  
d. Weight of brushoff debris.  
e. Not detected.

indicate a gradient in radionuclide concentrations from the bottom to the top of the plenum assembly, with higher concentrations at the B8-1 location (top of the plenum assembly) for  $^{125}\text{Sb}$ ,  $^{134}\text{Cs}$ , and  $^{137}\text{Cs}$ . Some radionuclides ( $^{106}\text{Ru}$ ,  $^{144}\text{Ce}$ ,  $^{154}\text{Eu}$ , and  $^{155}\text{Eu}$ ) were measured at the bottom of the leadscrew (B8-3) but not at the top of the plenum assembly (B8-1). The axial gradients in the radionuclide concentrations measured are approximately a factor of 14 for  $^{134}\text{Cs}$  and  $^{137}\text{Cs}$ , and a factor of 4.8 for  $^{125}\text{Sb}$ . Table 39 lists the  $^{90}\text{Sr}$ ,  $^{129}\text{I}$ , tellurium, and  $^{235}\text{U}$  concentrations in the B8 brushoff debris. These data also indicate an axial gradient with factors of 4-5 higher concentrations measured at the top of the plenum assembly. For  $^{235}\text{U}$ , the highest concentration was at the bottom (B8-3); and for tellurium, it was at the top. No tellurium was measurable in brushoff debris from the B8-3 section (bottom of plenum assembly).

Decontamination Solutions. Table 40 lists the radionuclide concentrations present in the B8 decontamination solutions. These samples were brushed prior to decontamination of the metallurgical samples to remove some of the debris. The data indicate that significant fractions of the total radionuclide content are soluble; at comparable H8 sample locations, smaller fractions of the total sample are soluble. The data also indicate a difference in the chemical composition of the leadscrew surface deposits between the B8 and H8 leadscrew locations. The B8 Sample 7 data indicate that solubility generally increases with the strength of the decontamination agent.

Table 41 lists the  $^{90}\text{Sr}$ ,  $^{129}\text{I}$ , tellurium, and  $^{235}\text{U}$  concentrations for the B8 decontamination solutions. The data indicate similar behavior to the Table 40 data with large soluble material fractions. Table 42 lists the total activity removed, fraction insoluble (%), and the percentage of total activity removed by each solution. The data indicate that  $^{90}\text{Sr}$ ,  $^{125}\text{Sb}$ ,  $^{134}\text{Cs}$ , and  $^{137}\text{Cs}$  are principally soluble. The ammonium citrate solution had the highest overall removal effectiveness. The radionuclides  $^{144}\text{Ce}$ ,  $^{154}\text{Eu}$ , and  $^{155}\text{Eu}$  were soluble without use of the nitric acid solution. Cerium, ruthenium, and

TABLE 39. B8 BRUSHOFF DEBRIS  $^{90}\text{Sr}$ ,  $^{129}\text{I}$  (BETA EMITTERS), TELLURIUM, AND  $^{235}\text{U}$  CONCENTRATION ( $\mu\text{Ci/g}$ )<sup>a</sup>

Radionuclide	Section B8-3 (bottom of the plenum assembly, 0.75 g <sup>b</sup> )	Section B8-1 (top of the plenum assembly, 18.75 g <sup>b</sup> )
$^{90}\text{Sr}$ ( $\mu\text{Ci/g}$ )	$4.8 \pm 0.2$	$2.2 \pm 0.9 \times 10^1$
$^{129}\text{I}$ ( $\mu\text{Ci/g}$ )	$1.7 \pm 0.2 \times 10^{-3}$	$9.1 \pm 0.9 \times 10^{-3}$
Te <sup>c</sup>	--d	$1.05 \times 10^1$
$^{235}\text{Ue}$	$8.8 \pm 0.2 \times 10^3$	$6.8 \pm 0.9 \times 10^2$

a. Decay date 6/15/84.

b. Debris weight.

c. Stable tellurium analysis was performed ICP detection spectroscopy. The concentration is in  $\mu\text{g/sample}$ .

d. Below detection limit.

e. Fissile analysis was performed by neutron activation and delayed neutron counting. The  $^{235}\text{U}$  concentration is in  $\mu\text{g/g}$ .



TABLE 40. B8 LEADSCREW DECONTAMINATION SOLUTION RADIONUCLIDE CONCENTRATIONS<sup>a</sup>

Leadscrew Sample	Distance from Bottom of Leadscrew (cm)	Radionuclide	Soluble Radionuclides ( $\mu\text{Ci/sample}$ )	Insoluble Radionuclides ( $\mu\text{Ci/sample}$ )	Insoluble Fraction (%)
2 ( $\text{HNO}_3$ + HF)	2.5	$^{60}\text{Co}$	$7.21 \pm 0.02$	$4.2 \pm 0.2 \times 10^{-1}$	5.5
		$^{106}\text{Ru}$	--b	--b	--b
		$^{125}\text{Sb}$	$4.84 \pm 0.01$	$1.54 \pm 0.01 \times 10^{-1}$	3.1
		$^{134}\text{Cs}$	$1.74 \pm 0.01 \times 10^1$	$2.21 \pm 0.02$	55.9
		$^{137}\text{Cs}$	$3.21 \pm 0.09 \times 10^2$	$4.11 \pm 0.03 \times 10^1$	11.4
		$^{144}\text{Ce}$	$1.41 \pm 0.04$	--b	0
7 ( $\text{NaOH}$ + $\text{KMnO}_4$ )	302.3	$^{60}\text{Co}$	--b	$4.78 \pm 0.05$	100
		$^{106}\text{Ru}$	--b	$7.3 \pm 0.2$	100
		$^{125}\text{Sb}$	$3.9 \pm 0.1 \times 10^{-1}$	$1.19 \pm 0.01 \times 10^1$	96.8
		$^{134}\text{Cs}$	$1.18 \pm 0.04 \times 10^1$	$1.23 \pm 0.02$	9.4
		$^{137}\text{Cs}$	$2.2 \pm 0.6 \times 10^2$	$2.15 \pm 0.01 \times 10^1$	8.9
		$^{144}\text{Ce}$	--b	$2.08 \pm 0.01 \times 10^1$	100
		$^{154}\text{Eu}$	--b	$3.0 \pm 0.2 \times 10^{-1}$	100
		$^{155}\text{Eu}$	--b	$6.8 \pm 0.1 \times 10^{-1}$	100
7 [ $\text{H}_2\text{C}_2\text{O}_4$ + ( $\text{NH}_4$ ) $_2\text{HC}_6\text{H}_5\text{O}_7$ ]	302.3	$^{60}\text{Cs}$	$7.6 \pm 0.2 \times 10^{-1}$	$1.01 \pm 0.02 \times 10^1$	93
		$^{106}\text{Ru}$	--b	$2.78 \pm 0.08 \times 10^1$	100
		$^{125}\text{Sb}$	$1.50 \pm 0.04 \times 10^1$	$8.3 \pm 0.2$	35.6
		$^{134}\text{Cs}$	$1.15 \pm 0.03 \times 10^2$	$4.59 \pm 0.08$	3.8
		$^{137}\text{Cs}$	$2.1 \pm 0.6 \times 10^3$	$8.43 \pm 0.05 \times 10^1$	3.9
		$^{144}\text{Ce}$	$9.5 \pm 0.3$	$1.40 \pm 0.02 \times 10^1$	59.6
		$^{154}\text{Eu}$	--b	$2.41 \pm 0.05 \times 10^{-1}$	100
		$^{155}\text{Eu}$	--b	$5.06 \pm 0.05 \times 10^{-1}$	100
7 ( $\text{HNO}_3$ + HF)	302.3	$^{60}\text{Co}$	$1.32 \pm 0.04$	$5.6 \pm 0.6 \times 10^{-1}$	29.8
		$^{106}\text{Ru}$	--b	$1.37 \pm 0.09 \times 10^1$	100
		$^{125}\text{Sb}$	$5.4 \pm 0.2 \times 10^1$	$5.62 \pm 0.05 \times 10^1$	50.9
		$^{134}\text{Cs}$	$1.13 \pm 0.03 \times 10^2$	$1.87 \pm 0.01 \times 10$	14.2
		$^{137}\text{Cs}$	$2.0 \pm 0.6 \times 10^3$	$3.19 \pm 0.01 \times 10^2$	13.8
		$^{144}\text{Ce}$	--b	--b	

a. Decay date corrected to 3/15/84.

b. Not detected.

TABLE 41. B8 LEADSCREW SAMPLE DECONTAMINATION DATA FOR  $^{90}\text{Sr}$ ,  $^{129}\text{I}$  (BETA EMITTERS), TELLURIUM, and  $^{235}\text{U}$

Sample (Leaching Solution)	Distance from the Bottom of Leadscrew (cm)	Radionuclide	Insoluble	Soluble Radionuclides		Insoluble Fraction (%)
			Radionuclides ( $\mu\text{Ci/sample}$ )	( $\mu\text{Ci/Sample}$ )		
2a ( $\text{HNO}_3 + \text{HF}$ )	2.5	$^{90}\text{Sr}$ $^{129}\text{I}$ $^{129}\text{I}$ $^{235}\text{U}$	Leach 1 (4 mg)	Leach 1 (226 mL)		
			$2.0 \pm 0.8 \times 10^{-1}$	$1.9 \pm 0.1 \times 10^1$	--b	1.0
			$4.0 \pm 0.2 \times 10^{-6}$	$2.5 \pm 0.2 \times 10^{-5}$	--b	13.8
			--d	--d	--d	--d
7a ( $\text{NaOH} + \text{KMnO}_4$ )	302.3	$^{90}\text{Sr}$ $^{129}\text{I}$ $^{129}\text{I}$ $^{235}\text{U}$	Leach 1 (57 mg)	Leach 1 (250 mL)		
			$4.7 \pm 0.2 \times 10$	$2.6 \pm 0.2 \times 10^{-2}$	--b	99.9
			$3.4 \pm 0.3 \times 10^{-5}$	--d	--b	100.0
			$2.4 \pm 0.6 \times 10^1$	$1.2 \pm 0.1 \times 10^2$	--d	16.7
7a [ $\text{H}_2\text{C}_2\text{O}_4 + (\text{NH}_4)_2$ $\text{HC}_6\text{H}_5\text{O}_7$ ]	302.3	$^{90}\text{Sr}$ $^{129}\text{I}$ $^{129}\text{I}$ $^{235}\text{U}$	Leach 1 (64 mg)	Leach 1 (176 mL)		
			$7.7 \pm 0.4 \times 10^1$	$5.4 \pm 0.2 \times 10^2$	--b	12.0
			$4.1 \pm 0.3 \times 10^{-4}$	--d	--b	100.0
			--d	--d	--d	--d
7a ( $\text{HNO}_3 + \text{HF}$ )	302.3	$^{90}\text{Sr}$ $^{129}\text{I}$ $^{129}\text{I}$ $^{235}\text{U}$	Leach 1 (28 mg)	Leach 1 (198 mL)		
			$4.4 \pm 0.1$	$3.3 \pm 0.1 \times 10^2$	--b	1.3
			$7.0 \pm 0.1 \times 10^{-4}$	$6.4 \pm 0.6 \times 10^{-4}$	--b	52.2
			$2.1 \pm 0.1 \times 10^1$	$6.5 \pm 1.4 \times 10^1$	--d	--d

- a. Sample 2 is close to the bottom and Sample 7 is close to top of the plenum assembly.
- b. No second leach performed.
- c. Te and  $^{235}\text{U}$  concentrations in  $\mu\text{g/sample}$ .
- d. Below detection limit - no data.

TABLE 42. B8 SAMPLE 7 DECONTAMINATION SOLUTION REMOVAL EFFICIENCIES

Radionuclide	Total Activity Removed From the B8 Sample 7 ( $\mu\text{Ci}$ ) <sup>a</sup>		Radionuclide Content Removed by Each Decontamination Solution (%)			
	Soluble	Insoluble	Percent <sup>b</sup>	Potassium Permanganate Solution	Ammonium Citrate Solution	Nitric Acid Solution
<sup>60</sup> Co	2.1	$1.5 \times 10^1$	88	28	61.5	11
<sup>90</sup> Sr	$8.70 \times 10^2$	$1.28 \times 10^2$	13	4.7	61.8	33.5
<sup>106</sup> Ru	--c	$4.9 \times 10^1$	100	14.9	56.7	28
<sup>125</sup> Sb	$6.9 \times 10^1$	$7.6 \times 10^1$	52	8.5	16.1	76
<sup>129</sup> I	$6.4 \times 10^{-4}$	$1.14 \times 10^{-3}$	64	1.9	23.0	75.3
<sup>134</sup> Cs	$2.4 \times 10^2$	$2.4 \times 10^1$	9.1	4.9	45.3	49.9
<sup>137</sup> Cs	$4.3 \times 10^3$	$4.2 \times 10^2$	8.9	5.1	46.3	49.1
<sup>144</sup> Ce	9.5	$3.5 \times 10^1$	79	46.7	52.8	--c
<sup>154</sup> Eu	--b	$5.4 \times 10^{-1}$	100	55.6	44.4	--c
<sup>155</sup> Eu	--b	1.2	100	56.7	42.5	--c
<sup>235</sup> Ud	$2.69 \pm 10^2$	$7.40 \times 10^1$	22	42.0	32.9	25.1

a. Activity removed by all decontamination solutions from Tables 40 and 41.

b. Listed is the total percentage of insoluble material.

c. Not detected.

d. In  $\mu\text{g}/\text{gram}$  of material.

europium are in a less soluble form than the cesium and antimony radionuclides for these decontamination solutions. The  $^{235}\text{U}$  is more soluble than  $^{129}\text{I}$ . The data indicate the presence of two groups of radionuclides with different solubility characteristics.

Summed Brushhoff Debris and Decontamination Solution Surface Concentrations. Table 43 lists the calculated surface radionuclide concentrations based on the brushhoff debris obtained from the B8 leadscrew. Not all of the brushhoff debris was obtained; however, the remainder would be present in the decontamination solutions. Table 44 lists the calculated surface radionuclide concentrations based on the decontamination solution analysis results from B8 Samples 2 and 7. The data from Tables 43 and 44 indicate that, with one exception ( $^{60}\text{Co}$ ), axial gradients exist (4.5-21) in the surface concentrations from the bottom of the leadscrew to the top of the plenum assembly. Interestingly,  $^{134}\text{Cs}$  and  $^{137}\text{Cs}$  exhibit the smallest gradient ( $\sim 4.5$ ), with  $^{129}\text{I}$  exhibiting the largest gradient (21).

Table 45 lists the total surface radionuclide concentrations for the B8 leadscrew. These data are based on both the brushhoff debris and decontamination solution analysis results. The gradients between the bottom of the leadscrew and top of the plenum assembly range from 2.6 to 47. The radionuclides with gradients of about a factor of 2.6 are  $^{154}\text{Eu}$ ,  $^{155}\text{Eu}$ ,  $^{144}\text{Ce}$ , and  $^{235}\text{U}$ . Tellurium was not detected in the decontamination solution samples. Interestingly,  $^{129}\text{I}$  exhibits the largest gradient, with a factor of 47. The gradients for  $^{134}\text{Cs}$  and  $^{137}\text{Cs}$  were about 16. No gradient was observed for the  $^{60}\text{Co}$  concentrations.

Table 46 lists the percentages of total radionuclide concentration contributed by the brushhoff debris. There is a large difference in the principal source of the surface radionuclide concentrations at the two locations. At B8-3, the decontamination solution is the principal contributor for  $^{60}\text{Co}$ ,  $^{90}\text{Sr}$ ,  $^{125}\text{Sb}$ ,  $^{129}\text{I}$ ,  $^{134}\text{Cs}$ , and  $^{137}\text{Cs}$ ; whereas  $^{106}\text{Ru}$ ,  $^{144}\text{Ce}$ ,  $^{154}\text{Eu}$ ,  $^{155}\text{Eu}$ , and  $^{235}\text{U}$ , which are >70%,

TABLE 43. SURFACE RADIONUCLIDE CONCENTRATIONS OF THE B8 BRUSHOFF DEBRIS  
( $\mu\text{Ci}/\text{cm}^2$ )

<u>Radionuclide</u>	<u>Surface Radionuclide Concentrations</u> ( $\mu\text{Ci}/\text{cm}^2$ )	
	<u>B8-3<sup>a</sup></u>	<u>B8-1<sup>a</sup></u>
$^{60}\text{Co}$	$1.15 \times 10^{-1}$	$2.16 \times 10^{-1}$
$^{90}\text{Sr}$	$2.46 \times 10^{-3}$	$1.90 \times 10^{-1}$
$^{106}\text{Ru}$	$3.23 \times 10^{-1}$	--b
$^{125}\text{Sb}$	$2.04 \times 10^{-1}$	$1.72 \times 10^1$
$^{129}\text{I}$	$8.70 \times 10^{-7}$	$7.87 \times 10^{-5}$
$^{134}\text{Cs}$	$9.68 \times 10^{-2}$	$2.29 \times 10^1$
$^{137}\text{Cs}$	1.81	$4.10 \times 10^2$
$^{144}\text{Ce}$	$3.83 \times 10^{-1}$	--b
$^{154}\text{Eu}$	$6.14 \times 10^{-3}$	--b
$^{155}\text{Eu}$	$1.26 \times 10^{-2}$	--b
$^{235}\text{Uc}$	4.52	5.88

a. Surface area of Sections B8-3 (close to the bottom of the plenum assembly) =  $1460 \text{ cm}^2$  and that of B8-1 (close to top of the plenum assembly) =  $2168 \text{ cm}^2$ .

b. Not detected.

c.  $^{235}\text{U}$  concentration in  $\mu\text{g}/\text{cm}^2$ .

TABLE 44. SURFACE RADIONUCLIDE CONCENTRATIONS OF B8 SAMPLES FROM DECONTAMINATION SOLUTIONS  
(SOLUBLE AND INSOLUBLE FRACTIONS)  
( $\mu\text{Ci}/\text{cm}^2$ )

Sample (Leaching Solution)	Distance From Bottom of Leadscrew (cm)	Radionuclide	Insoluble Radionuclide ( $\mu\text{Ci}/\text{cm}^2$ )	Soluble Radionuclide ( $\mu\text{Ci}/\text{cm}^2$ )	Total
2a ( $\text{HNO}_3 + \text{HF}$ )	2.5	$^{60}\text{Co}$	$3.68 \times 10^{-2}$	$6.32 \times 10^{-1}$	$6.69 \times 10^{-1}$
		$^{90}\text{Sr}$	$1.75 \times 10^{-2}$	1.67	1.69
		$^{125}\text{Sb}$	$1.35 \times 10^{-2}$	$4.25 \times 10^{-1}$	$4.39 \times 10^{-1}$
		$^{129}\text{I}$	$3.51 \times 10^{-7}$	$2.19 \times 10^{-6}$	$2.54 \times 10^{-6}$
		$^{134}\text{Cs}$	1.94	1.53	1.72
		$^{137}\text{Cs}$	3.61	$2.82 \times 10^1$	$3.18 \times 10^1$
		$^{144}\text{Ce}$	--b	$1.24 \times 10^{-1}$	$1.24 \times 10^{-1}$
		$^{235}\text{U}$	$1.32 \times 10^{-1}$	1.40	1.53
		$^{99}\text{Tc}$	--b	--b	--b
		$^{134}\text{Cs}$	$1.94 \times 10^{-1}$	1.53	1.72
7d (Total)	302.3	$^{60}\text{Co}$	$4.66 \times 10^{-1}$	$6.29 \times 10^{-2}$	$5.29 \times 10^{-1}$
		$^{90}\text{Sr}$	3.77	9.99	$1.38 \times 10^1$
		$^{106}\text{Ru}$	1.48	--b	1.48
		$^{125}\text{Sb}$	2.31	2.09	4.40
		$^{129}\text{I}$	$3.45 \times 10^{-5}$	$1.93 \times 10^{-5}$	$5.38 \times 10^{-5}$
		$^{99}\text{Tc}$	--b	--b	--b
		$^{134}\text{Cs}$	$7.36 \times 10^{-1}$	7.24	7.98
		$^{137}\text{Cs}$	$1.28 \times 10^1$	$1.30 \times 10^2$	$1.43 \times 10^2$
		$^{144}\text{Ce}$	1.05	$2.87 \times 10^{-1}$	1.34
		$^{154}\text{Eu}$	$1.63 \times 10^{-2}$	--b	$1.63 \times 10^{-2}$
		$^{155}\text{Eu}$	$3.58 \times 10^{-2}$	--b	$3.58 \times 10^{-2}$
		$^{235}\text{U}$	2.24	8.13	$1.04 \times 10^1$

a. Sample 2 surface area =  $11.4 \text{ cm}^2$ .

b. Not detected.

c. Te and  $^{235}\text{U}$  concentrations in  $\mu\text{g}/\text{cm}^2$ .

d. Sample 7 surface area =  $33.1 \text{ cm}^2$  and includes all subsamples (7a, 7b, and 7c). Total concentration = sum of concentrations in  $\text{NaOH} + \text{KMnO}_4 + (\text{NH}_4)_2 \text{HC}_6\text{H}_5\text{O}_7$ , and  $\text{HNO}_3 + \text{HF}$ .

TABLE 45. TOTAL RADIONUCLIDE CONCENTRATIONS ON THE B8 LEADSCREW  
( $\mu\text{Ci}/\text{cm}^2$ )<sup>a</sup>

Radionuclide	Surface Radionuclide Concentration ( $\mu\text{Ci}/\text{cm}^2$ )		Core Inventory <sup>b</sup> ( $\mu\text{Ci}$ )
	B8-3 (bottom)	B8-1 (top)	
<sup>60</sup> Co <sup>c</sup>	$7.84 \times 10^{-1}$	$7.45 \times 10^{-1}$	--d
<sup>90</sup> Sr	1.69	$1.40 \times 10^1$	$6.62 \times 10^{11}$
<sup>106</sup> Ru	$3.23 \times 10^{-1}$	1.48	$1.10 \times 10^{11}$
<sup>125</sup> Sb	$6.43 \times 10^{-1}$	$1.83 \times 10^1$	$3.51 \times 10^{10}$
<sup>129</sup> I	$2.82 \times 10^{-6}$	$1.33 \times 10^{-4}$	$2.45 \times 10^5$
Te <sup>e</sup>	--d	5.46	$4.45 \times 10^9$
<sup>134</sup> Cs	1.82	$3.09 \times 10^1$	$2.99 \times 10^{10}$
<sup>137</sup> Cs	$3.36 \times 10^1$	$5.53 \times 10^2$	$7.52 \times 10^{11}$
<sup>144</sup> Ce	$5.07 \times 10^{-1}$	1.34	$2.99 \times 10^9$
<sup>154</sup> Eu	$6.14 \times 10^{-3}$	$1.63 \times 10^{-2}$	$5.20 \times 10^9$
<sup>155</sup> Eu	$1.26 \times 10^{-2}$	$3.58 \times 10^{-2}$	$1.56 \times 10^{10}$
<sup>235</sup> U <sup>e</sup>	6.05	$1.63 \times 10^1$	$2.22 \times 10^{12}$

a. Sum of surface radionuclide concentrations from brushoff debris decontamination solutions and insoluble fractions.

b. ORIGEN2-calculated core activity at  $1.81 \times 10^3$  days after the accident.

c. Activation product.

d. Not detected.

e. Te and <sup>235</sup>U concentrations in  $\mu\text{g}/\text{cm}^2$  and core inventories in  $\mu\text{g}$ .

TABLE 46. B8 BRUSHOFF DEBRIS CONTRIBUTION TO TOTAL SURFACE RADIONUCLIDE CONCENTRATION (%)

<u>Radionuclide</u>	<u>Leadscrew Section</u>	
	<u>B8-3 (bottom)</u>	<u>B8-1 (top)</u>
<sup>60</sup> Co	14	--a
<sup>90</sup> Sr	0.1	1.4
<sup>106</sup> Ru	100	--a
<sup>125</sup> Sb	31.7	94
<sup>129</sup> I	30.9	59.2
Te	--a	100.0
<sup>134</sup> Cs	5.3	74.1
<sup>137</sup> Cs	5.0	74.0
<sup>144</sup> Ce	75.5	0
<sup>154</sup> Eu	100	0
<sup>155</sup> Eu	100	0
<sup>235</sup> U	74.7	36

a. Not detected.



are associated with the brushoff debris. At the B8-1 location,  $^{60}\text{Co}$ ,  $^{90}\text{Sr}$ ,  $^{106}\text{Ru}$ , and  $^{235}\text{U}$  are principally associated with the decontamination solution, and  $^{125}\text{Sb}$ ,  $^{129}\text{I}$ ,  $^{134}\text{Cs}$ , tellurium, and  $^{137}\text{Cs}$  are largely associated with the brushoff debris. This may be due to retained brushoff debris on the decontamination sample surfaces, as only portions of the leadscrew were brushed clean.

Surface Samples. Two B8 surface samples, numbers 3 and 8, were examined, as shown in Table 1. The data are listed in Table 47. Large surface radionuclide concentration gradients are apparent between B8 Samples 3 and 8, ranging between factors of 5 and  $1.22 \times 10^3$  for all radionuclides, with  $^{137}\text{Cs}$  at  $3.7 \times 10^2$ . The B8 Sample 3 surface radionuclide concentrations are significantly lower when compared with the summed total surface radionuclide concentrations (Table 45). The B8 Sample 3 measured  $^{90}\text{Sr}$  concentration is 20% of the summed total surface concentrations, and the  $^{129}\text{I}$  concentration is 94% of the summed total surface concentrations. Losses may have occurred from B8 Sample 3 during the cutting operation, as the surface area for this sample is quite small ( $0.48 \text{ cm}^2$ ). In contrast, the B8 Sample 8 (surface sample with area  $2.62 \text{ cm}^2$ ) radionuclide concentrations are about a factor of 2 higher than the concentrations calculated from the brushoff debris and decontamination solutions at the same location. This is within the uncertainty of the analysis. For calculational purposes, the highest surface radionuclide concentration will be used, whether based on the summed radionuclide concentrations or the surface sample radionuclide data.

For comparison purposes, the radionuclide concentrations measured on the leadscrew surfaces have been extrapolated to the surface area of the plenum assembly. The core deposition fractions based on the summed brushoff debris and decontamination sample data are listed in Table 48. These data indicate core inventory fractions less than 1.0% at the B8 Samples 2 and 7 locations. The deposition fractions for the B8 surface samples have also been calculated and are listed in Table 49. These data again indicate small core inventory fractions of <1% for all radionuclides, with the highest calculated concentration for  $^{134}\text{Cs}$  (0.81%) at the B8 Sample 8 location.

TABLE 47. SURFACE RADIONUCLIDE CONCENTRATIONS BASED ON B8 SURFACE SAMPLES ( $\mu\text{Ci}/\text{cm}^2$ )

Radionuclide	Surface Radionuclide Concentrations ( $\mu\text{Ci}/\text{cm}^2$ )	
	B8 Sample 3 ( $0.48 \text{ cm}^2$ ) <sup>a</sup>	B8 Sample 8 ( $2.62 \text{ cm}^2$ ) <sup>a</sup>
$^{60}\text{Co}$	$5.20 \pm 0.03 \times 10^{-2}$	$2.6 \pm 0.6 \times 10^{-1}$
$^{90}\text{Sr}$	$3.3 \pm 0.1 \times 10^{-1}$	$8.0 \pm 0.8$
$^{125}\text{Sb}$	$4.4 \pm 0.7 \times 10^{-2}$	$5.36 \pm 0.07 \times 10^1$
$^{129}\text{I}$	$2.6 \pm 0.2 \times 10^{-6}$	$2.8 \pm 0.7 \times 10^{-4}$
Te	--b	--b
$^{134}\text{Cs}$	$1.52 \pm 0.04 \times 10^{-1}$	$5.67 \pm 0.07 \times 10^1$
$^{137}\text{Cs}$	$3.01 \pm 0.01$	$1.10 \pm 0.03 \times 10^3$
$^{144}\text{Ce}$	$2.1 \pm 0.6 \times 10^{-2}$	--b
$^{235}\text{U}$	--c	$1.36 \pm 9 \times 10^{-3}$

a. Sample surface area.  
b. Not detected.  
c. Not analyzed.

TABLE 48. RADIONUCLIDE DEPOSITION FRACTIONS (%) ON PLENUM THE ASSEMBLY SURFACES FROM THE B8 DATA<sup>a</sup>

Radionuclide	Deposition Fraction From Brushoff Debris		Deposition Fraction From Insoluble Radionuclides		Deposition Fraction From Soluble Radionuclides		Total Deposition Fraction <sup>b</sup>	
	2 <sup>c</sup>	7 <sup>d</sup>	2 <sup>c</sup>	7 <sup>d</sup>	2 <sup>c</sup>	7 <sup>d</sup>	2 <sup>c</sup>	7 <sup>d</sup>
<sup>90</sup> Sr	1.59 x 10 <sup>-6</sup>	1.22 x 10 <sup>-4</sup>	1.12 x 10 <sup>-5</sup>	2.42 x 10 <sup>-3</sup>	1.07 x 10 <sup>-3</sup>	6.42 x 10 <sup>-3</sup>	1.08 x 10 <sup>-3</sup>	8.96 x 10 <sup>-3</sup>
<sup>106</sup> Ru	1.25 x 10 <sup>-3</sup>	--e	--e	5.70 x 10 <sup>-3</sup>	--e	--e	1.25 x 10 <sup>-3</sup>	5.70 x 10 <sup>-3</sup>
<sup>110m</sup> Ag	--e	--e	--e	--e	--e	--e	--e	--e
<sup>125</sup> Sb	2.47 x 10 <sup>-3</sup>	2.08 x 10 <sup>-1</sup>	1.64 x 10 <sup>-4</sup>	2.80 x 10 <sup>-2</sup>	5.15 x 10 <sup>-3</sup>	2.54 x 10 <sup>-2</sup>	7.78 x 10 <sup>-3</sup>	2.61 x 10 <sup>-1</sup>
<sup>129</sup> I	1.51 x 10 <sup>-3</sup>	1.36 x 10 <sup>-1</sup>	6.09 x 10 <sup>-4</sup>	6.00 x 10 <sup>-2</sup>	3.80 x 10 <sup>-3</sup>	3.35 x 10 <sup>-2</sup>	5.92 x 10 <sup>-3</sup>	2.30 x 10 <sup>-1</sup>
Te <sup>f</sup>	--g	5.2 x 10 <sup>-1</sup>	--g	--g	--g	--g	--g	5.2 x 10 <sup>-1</sup>
<sup>134</sup> Cs	1.38 x 10 <sup>-3</sup>	3.26 x 10 <sup>-3</sup>	2.75 x 10 <sup>-3</sup>	1.52 x 10 <sup>-2</sup>	2.16 x 10 <sup>-2</sup>	1.03 x 10 <sup>-1</sup>	2.58 x 10 <sup>-2</sup>	1.21 x 10 <sup>-1</sup>
<sup>137</sup> Cs	1.02 x 10 <sup>-3</sup>	2.32 x 10 <sup>-1</sup>	2.04 x 10 <sup>-3</sup>	7.26 x 10 <sup>-3</sup>	1.59 x 10 <sup>-2</sup>	7.37 x 10 <sup>-2</sup>	1.89 x 10 <sup>-2</sup>	3.13 x 10 <sup>-1</sup>
<sup>144</sup> Ce	5.45 x 10 <sup>-2</sup>	--e	--e	1.49 x 10 <sup>-1</sup>	1.76 x 10 <sup>-2</sup>	4.07 x 10 <sup>-2</sup>	7.21 x 10 <sup>-2</sup>	1.90 x 10 <sup>-1</sup>
<sup>154</sup> Eu	5.02 x 10 <sup>-4</sup>	--e	--e	1.34 x 10 <sup>-3</sup>	--e	--e	5.02 x 10 <sup>-4</sup>	1.34 x 10 <sup>-3</sup>
<sup>155</sup> Eu	3.42 x 10 <sup>-4</sup>	--e	--e	9.75 x 10 <sup>-4</sup>	--e	--e	3.42 x 10 <sup>-4</sup>	9.75 x 10 <sup>-4</sup>
<sup>235</sup> U <sup>h</sup>	8.70 x 10 <sup>-4</sup>	1.14 x 10 <sup>-3</sup>	2.55 x 10 <sup>-5</sup>	4.32 x 10 <sup>-4</sup>	2.70 x 10 <sup>-4</sup>	1.57 x 10 <sup>-3</sup>	1.17 x 10 <sup>-3</sup>	3.14 x 10 <sup>-3</sup>

- a. Deposition fraction (%) = calculated surface activity ( $\mu\text{Ci}/\text{cm}^2$ )  $\times$  upper plenum surface area ( $\text{cm}^2$ )  $\times$  100  $\div$  core inventory in ( $\mu\text{Ci}$ ).
- b. Sum of extrapolated release fractions from brushoff debris, and soluble and insoluble radionuclides.
- c. Sample 2 is close to the bottom of the plenum assembly.
- d. Sample 7 is close to the top of the plenum assembly.
- e. Not measured.
- f. Stable tellurium measured by ICP technique.
- g. Below detection limit.
- h. Measured by neutron activation and delayed neutron counting.

TABLE 49. RADIONUCLIDE DEPOSITION FRACTIONS ON THE PLENUM ASSEMBLY SURFACES FROM THE B8 SURFACE SAMPLES (%)

Radionuclide	3	8	Core Inventory <sup>a</sup> ( $\mu\text{Ci}$ )
$^{60}\text{Co}$	--b	--b	
$^{90}\text{Sr}$	$2.1 \times 10^{-4}$	$5.1 \times 10^{-3}$	$6.62 \times 10^{11}$
$^{125}\text{Sb}$	$5.3 \times 10^{-4}$	$6.5 \times 10^{-1}$	$3.51 \times 10^{10}$
$^{129}\text{I}$	$4.5 \times 10^{-3}$	$4.9 \times 10^{-1}$	$2.45 \times 10^5$
$^{134}\text{Cs}$	$2.1 \times 10^{-3}$	$8.1 \times 10^{-1}$	$2.99 \times 10^{10}$
$^{137}\text{Cs}$	$1.7 \times 10^{-3}$	$6.2 \times 10^{-1}$	$7.52 \times 10^{11}$
$^{144}\text{Ce}$	$1.2 \times 10^{-5}$	--c	$2.99 \times 10^9$
$^{235}\text{Ud}$	--e	$2.6 \times 10^{-4}$	$2.20 \times 10^{12}$

a. Core inventory is calculated at  $1.81 \times 10^3$  days after the accident.

b. Activation product.

c. Not detected.

d. Core inventory in  $\mu\text{g}$ .

e. Not analyzed.

## COMPARISON OF TEMPERATURES, ELEMENTAL BEHAVIOR, AND RADIONUCLIDE BEHAVIOR IN THE PLENUM REGION

In this section, the H8 and B8 leadscrew data are used to provide a profile of the temperatures to which the leadscrews have been exposed and the chemical and fission product behavior in the plenum assembly region. This is a limited profile, as only the data for the two leadscrews are available for extrapolation purposes. The chemical and radiological analysis data are compared at four measured locations, near the bottom and top of the plenum assembly at the H8 and B8 positions. The H8 and B8 radionuclide surface concentrations are compared in order of the brushoff debris, decontamination solutions, surface samples, and total surface radionuclide concentrations. Other comparisons performed on the radiological data are of the fission product-to-fissile-material ratios,  $^{137}\text{Cs}$ -to- $^{129}\text{I}$  ratios, and the calculated total core inventory fractions retained on the plenum assembly region based on both the H8 and B8 data.

### Temperature Comparisons

The preliminary temperatures, estimated and based on metallurgical examination of leadscrews H8 and B8, are compared in Figure 42. Hardness measurements and metallographic and SEM examinations of microstructure and 13-h heat-treatment of 17-4 PH standards suggest that H8 and B8 samples close to the top of the plenum assembly experienced temperatures of about 700 and 755 K (800 and 900°F), respectively.

Comparison of the microstructures of the H8 sample with the B8 samples near the bottom of the plenum assembly suggests that the H8 leadscrew was cooled faster than the B8 leadscrew. The H8 and B8 temperature estimates are presented in Table 50. Comparison of microstructure and hardness of the H8 sample (near the bottom of the plenum assembly) with 17-4 PH standard A<sub>27</sub> [heat treated at 1255 K (1800°F) for 1 h and air-quenched] and TEM examination of copper precipitates suggest that the H8 sample

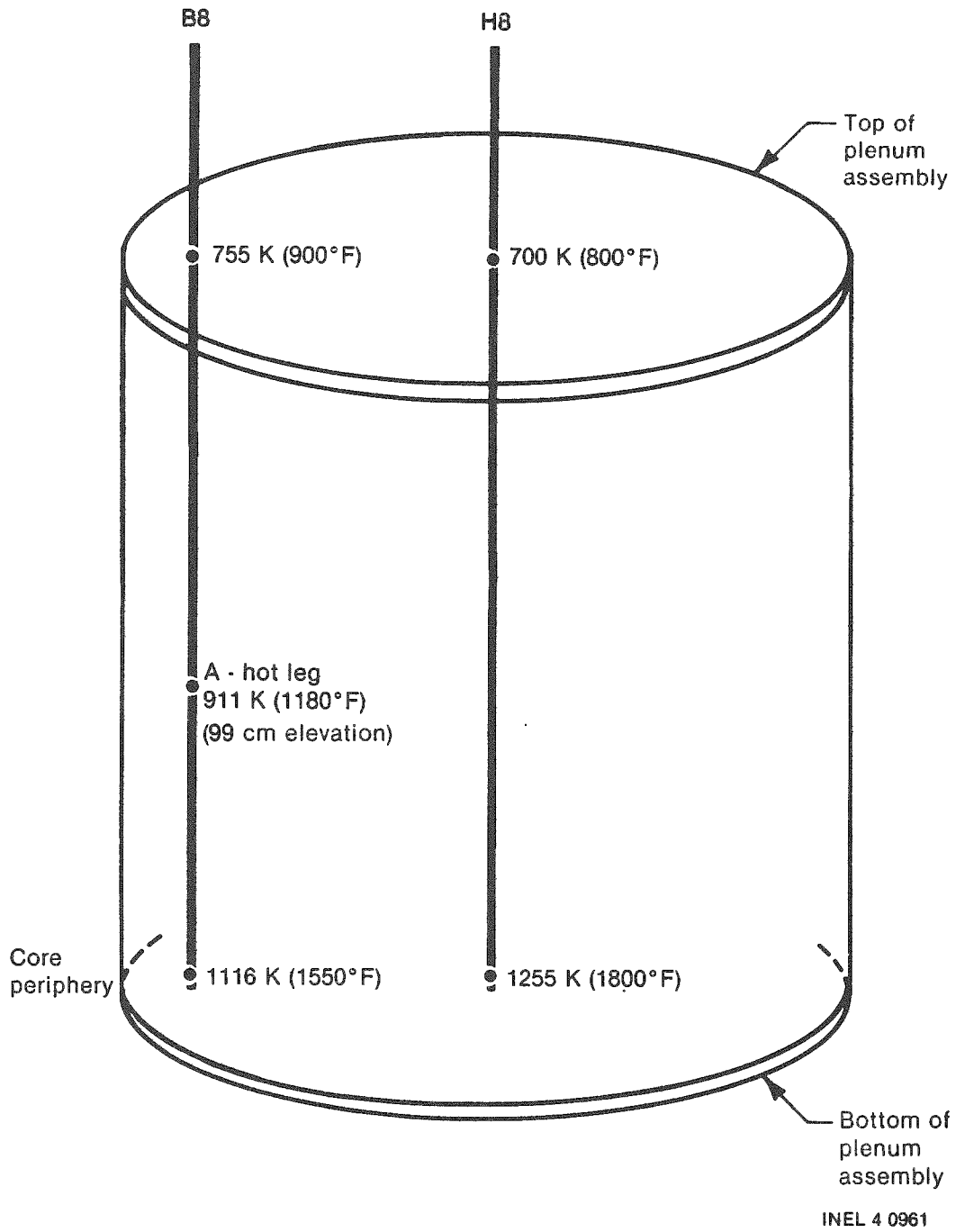


Figure 42. Surface temperatures on H8 and B8 leadscrews.

TABLE 50. ESTIMATED TEMPERATURES ON H8 AND B8 LEADSCREWS

<u>Sample or Standard</u>	<u>As-Received Hardness</u>	<u>Hardness After Heat Treatment at the H900 Condition</u>	<u>Microstructure</u>	<u>Lamellar Spacing (<math>\mu\text{m}</math>)</u>	<u>Oxide Layer Thickness (<math>\mu\text{m}</math>)</u>	<u>TEM Examination</u>
H8 Sample 2	34.0 <sup>a</sup>	47.0 <sup>a</sup>	Quenched martensite	--	48	Small Cu precipitates
17-4 PH standard A <sub>27</sub>	35.0	--	Quenched martensite	--	--	--
Estimated H8 temperature K (°F)	1255 (1800)	1089-1477 <sup>b</sup> (1500-2200)	1255 (1800)	--	--	1089-1477 (1500-2200)
B8 Sample 2	35.0 <sup>c</sup>	38.0 <sup>c</sup>	Lamellar	0.24	5	No Cu precipitates
17-4 PH standard A <sub>24</sub>	35.4	--	Lamellar	0.20	--	--
Estimated B8 temperature K (°F)	1116 (1550)	1089-1477 <sup>d</sup> (1500-2200)	1116 (1550)	1116 (1550)	1080 (1485) <sup>e</sup>	1089-1477 (1500-2200)

a. Increase in hardness from 34 to 47 when heat-treated at the H900 condition suggests that H8 Sample 2 experienced the estimated temperature in fully solutionized condition.

b. Temperature range of fully solutionized condition = 1089-1477 K.

c. Increase in hardness from 35 to 38 when heat-treated at the H900 condition suggests that B8 Sample 2 experienced the estimated temperature in partially solutionized condition.

d. Partially solutionized temperature = lower end of 1089-1477 K (1500-2200°F).

e. Estimated from relative oxide thicknesses of H8 and B8 Samples and the H8 estimated temperature.

close to the bottom of the plenum assembly experienced a temperature of 1255 K (1800°F). A similar comparison of the microstructure, hardness, and lamellar spacing of the B8 sample (close to the bottom of the plenum assembly) with standard A<sub>24</sub> [annealed at 1116 K (1550°F) for 1 h and air-quenched], comparison of oxide layer thickness with B8 measured thickness, and TEM examination of copper precipitates suggest that the B8 sample close to the bottom of the plenum assembly experienced a temperature of about of 1116 K (1550°F). In both cases, the grain sizes of the H8 and B8 samples were not used to estimate the temperatures, mainly due to difficulties experienced in measuring the grain sizes of transformation microstructures.

Also, a number of 304L SS standards were heat-treated for 1 h at different temperatures, and the microstructure and hardness were compared with the 304 SS Sample 7a from H8 and Sample 5 from B8 at the A-hot leg axial location. The 1-h transient time was chosen based on the microstructural and hardness match between H8 and B8 (H8-2, B8-2) with the standards (A<sub>27</sub> and A<sub>24</sub>). The details of the annealing study are discussed in Appendix A. The estimated temperatures of H8 Sample 7a and B8 Sample 5 at the A-hot leg are 1189 and 911 K (1670 and 1180°F), respectively. The axial temperature profiles of leadscrews H8 and B8 are shown in Figure 43. The uncertainty in the temperature estimates is about  $\pm 28$  to 56 K ( $\pm 50$  to 100°F). The uncertainties in temperature estimates were established on the basis of uncertainties in Rockwell-C hardness measurements and the temperature intervals used in the time-temperature matrix (see Figure A-1).

#### Surface Layer Thickness Analysis

The surface layer thicknesses on H8 and B8 samples are compared in Figure 44. The surface layer near the top of the plenum assembly (H8 position) was the thickest (114  $\mu\text{m}$ ), and that near the bottom of the plenum assembly (B8 position) was the thinnest (5  $\mu\text{m}$ ). The surface layer near the bottom of the plenum assembly at the H8 and B8 positions may be composed of oxide layers formed as a result of high-temperature oxidation. The thickest surface layer is near the top of the plenum assembly, which is



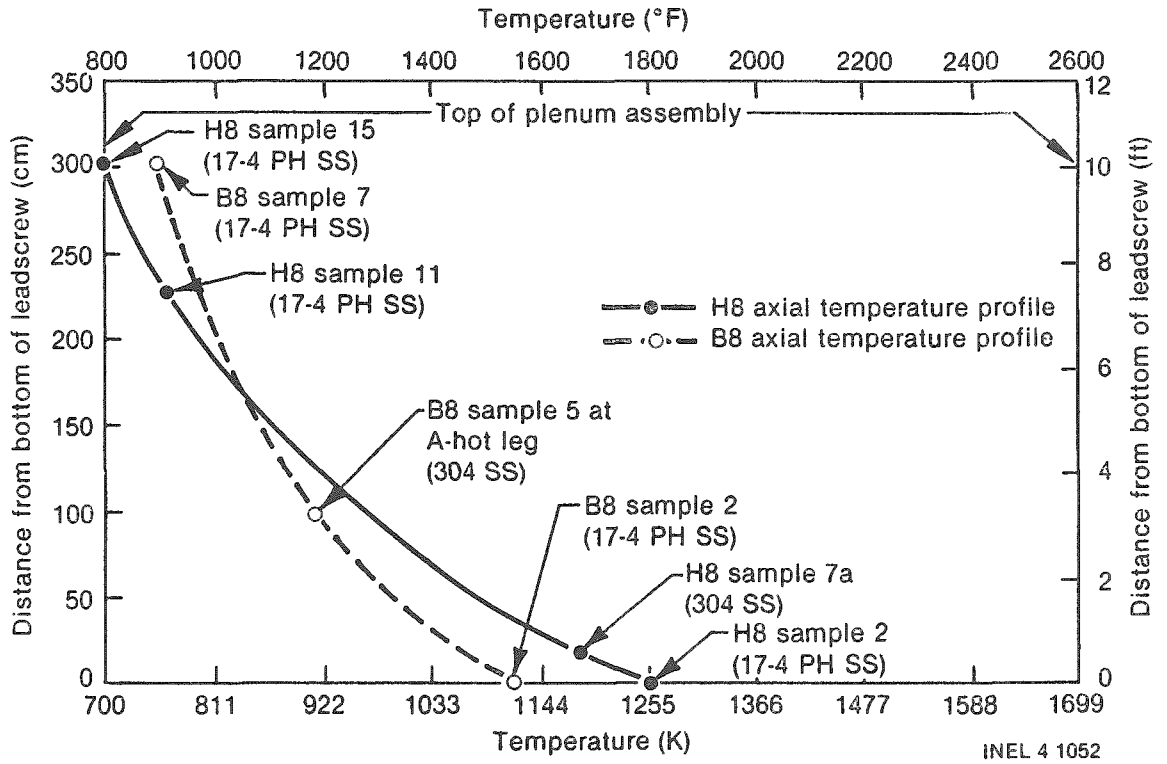
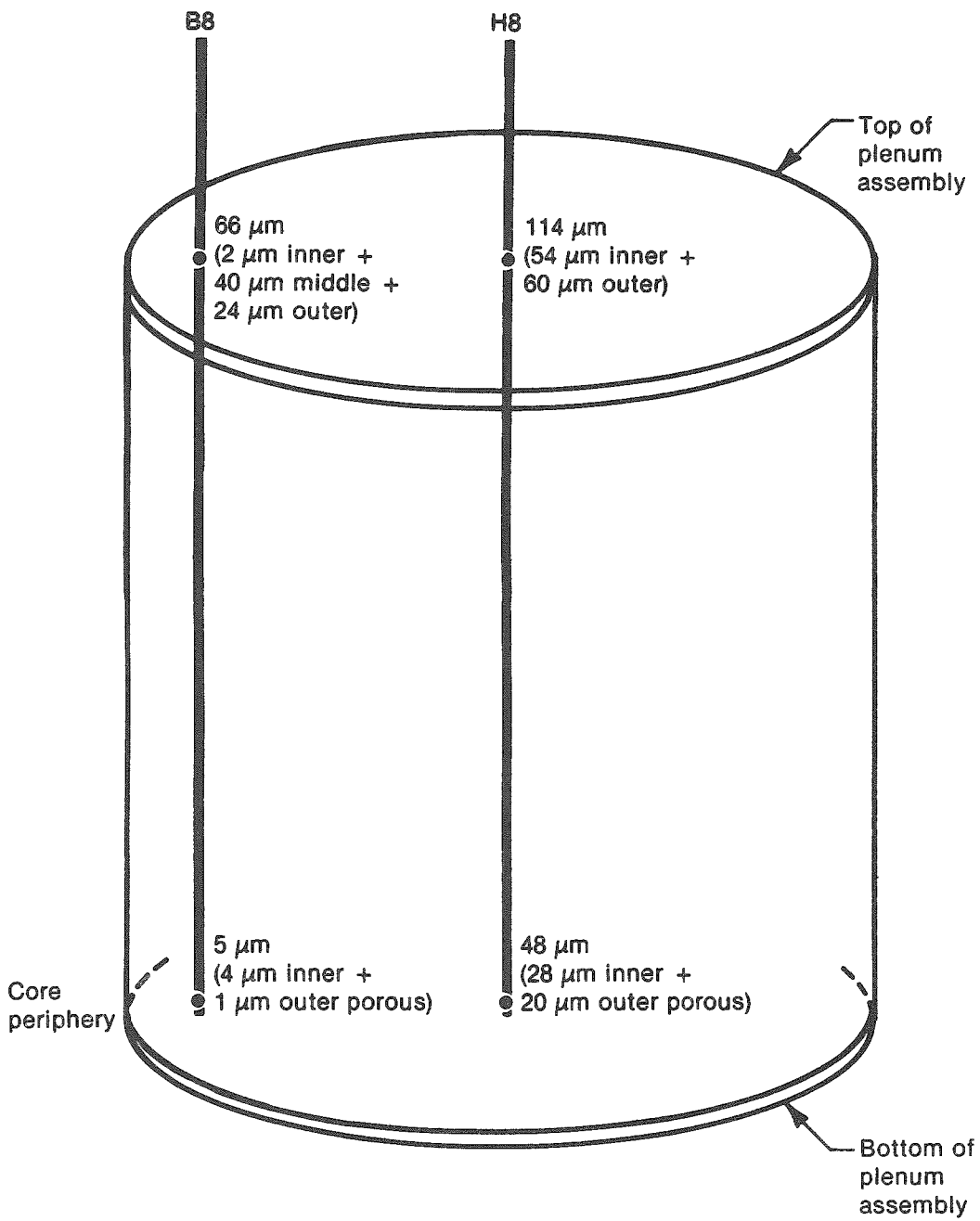


Figure 43. Axial temperature profiles of the H8 and B8 leadscrews.



INEL 4 0962

Figure 44. The thickness of the surface layers on the H8 and B8 leadscrews.

colder than the bottom, suggesting that these surface layers might have formed primarily as a result of deposition, rather than oxidation of the base metal.

### Chemical Analyses

The chemical analysis data obtained from the examination of H8 and B8 leadscrews provides information on the elemental composition and chemical forms of the materials deposited on surfaces of the plenum assembly. Figure 45 shows the elemental compositions of the brushoff debris at the top and the bottom of the plenum assembly. The elements of principal interest are uranium, zirconium, boron, and silver. The uranium concentration indicates a definite gradient (decreased by a factor of 10) from the bottom to the top of the plenum assembly. The data indicate both axial and radial gradients in concentration in the brushoff debris. The behavior of the zirconium is similar to that of uranium. The silver is uniformly distributed in the brushoff debris at three locations, with a smaller amount at the top of the plenum assembly on H8. Boron is uniformly distributed at H8 and B8 locations.

In contrast to the brushoff debris, very little uranium was measured in either the soluble or insoluble fractions of the decontamination solutions, as shown in Figures 46 and 47. The only uranium found was at the top of the plenum assembly location on B8, with 4 wt% in the insoluble fraction and 0.2 wt% in the soluble solution. The uranium content of the decontamination solutions could be from brushoff debris not removed during the sample cutting and brushing operation. The zirconium concentrations are also quite low ( $\leq 4.3$  wt%) at all measured locations. The highest silver concentration found in the decontamination solutions was at the top of the plenum assembly on the B8 leadscrew (14.5 wt%). From these data, the plenum assembly surface deposition of silver is estimated to be 1% of the total silver content in the control rods. Very little ( $< 0.2$  wt%) was found at any of the other locations.

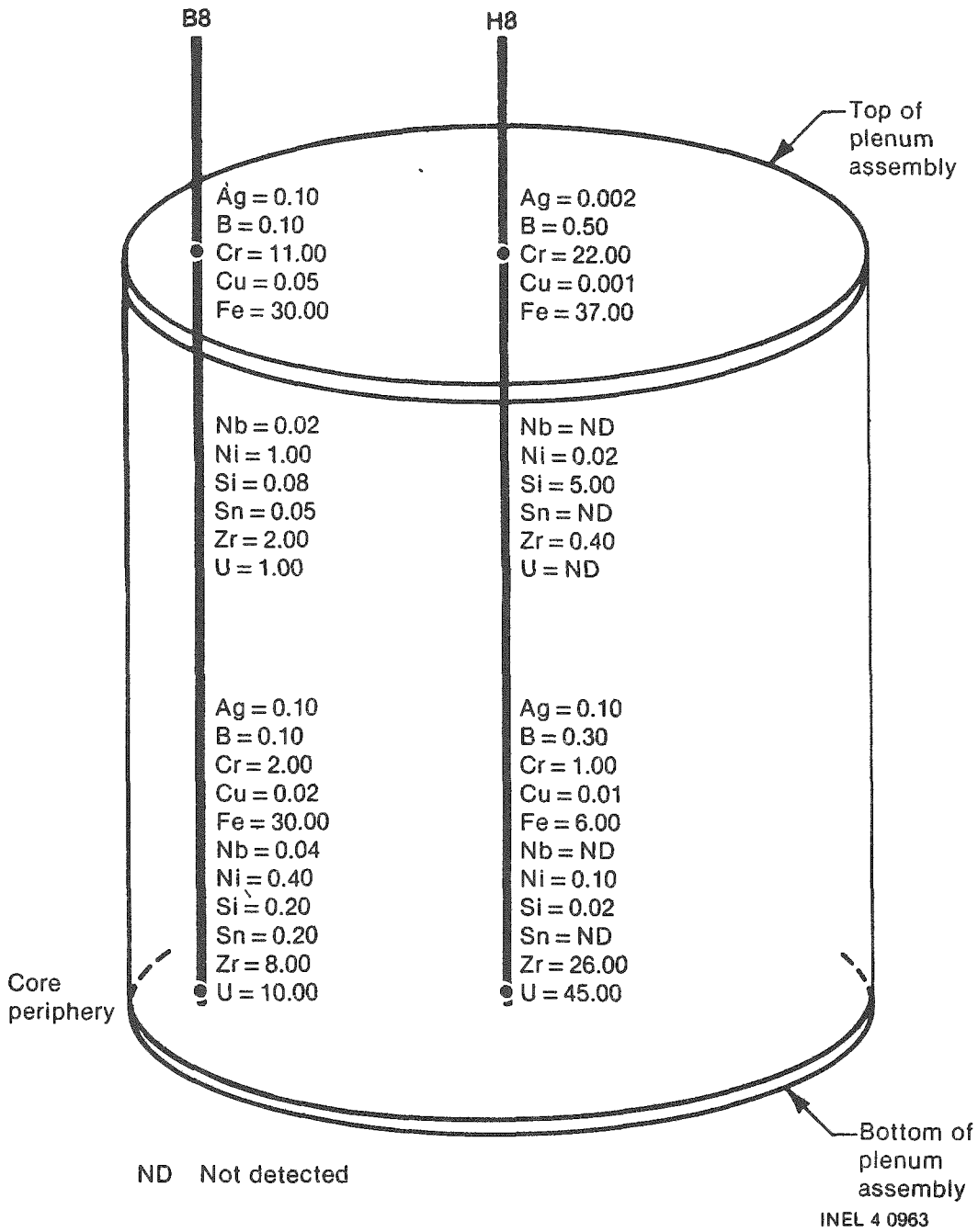


Figure 45. The concentrations of elements identified in the brushoff debris at the H8 and B8 leadscrew locations (wt%).

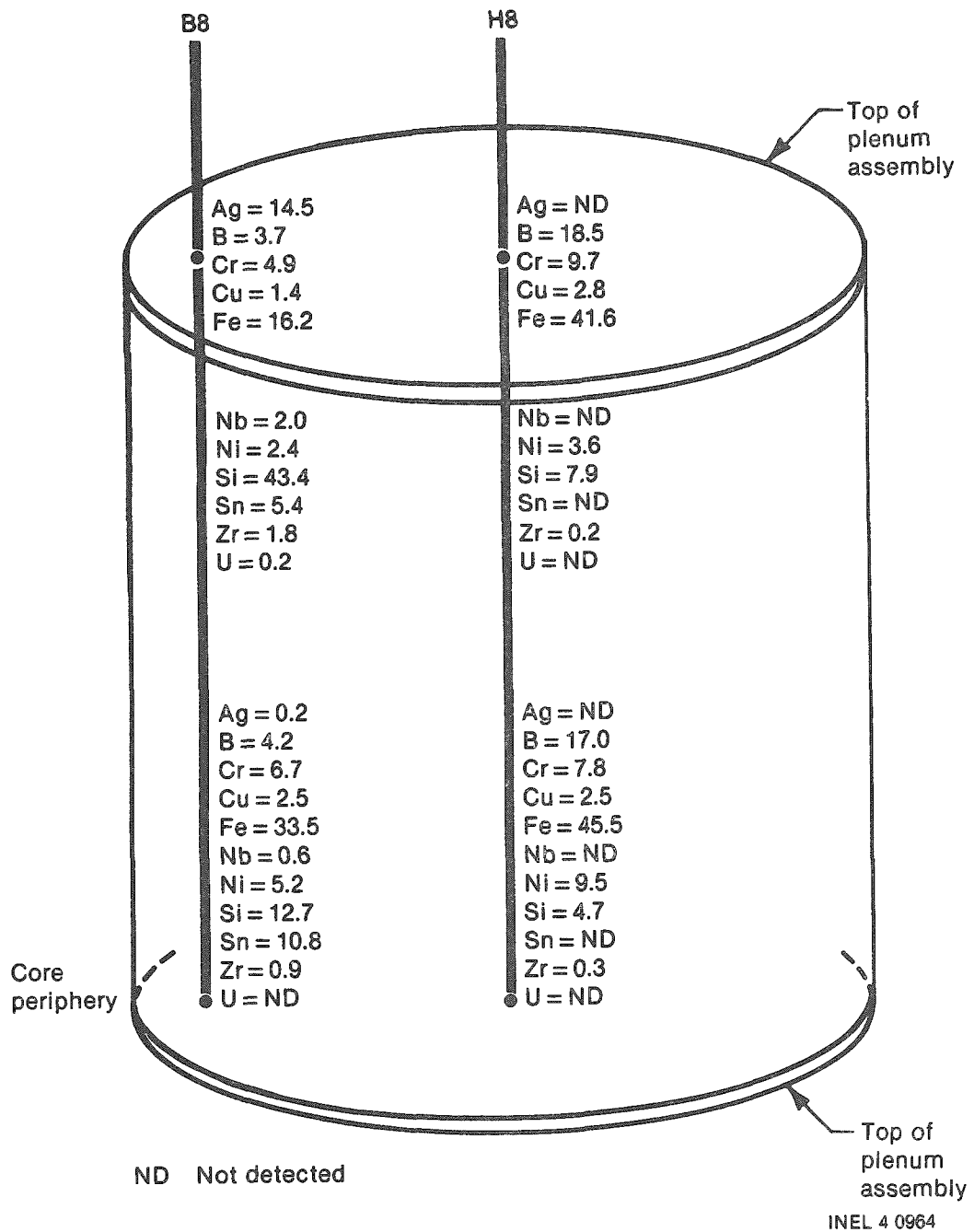


Figure 46. The concentrations of soluble elements identified in the decontamination solutions (wt%).

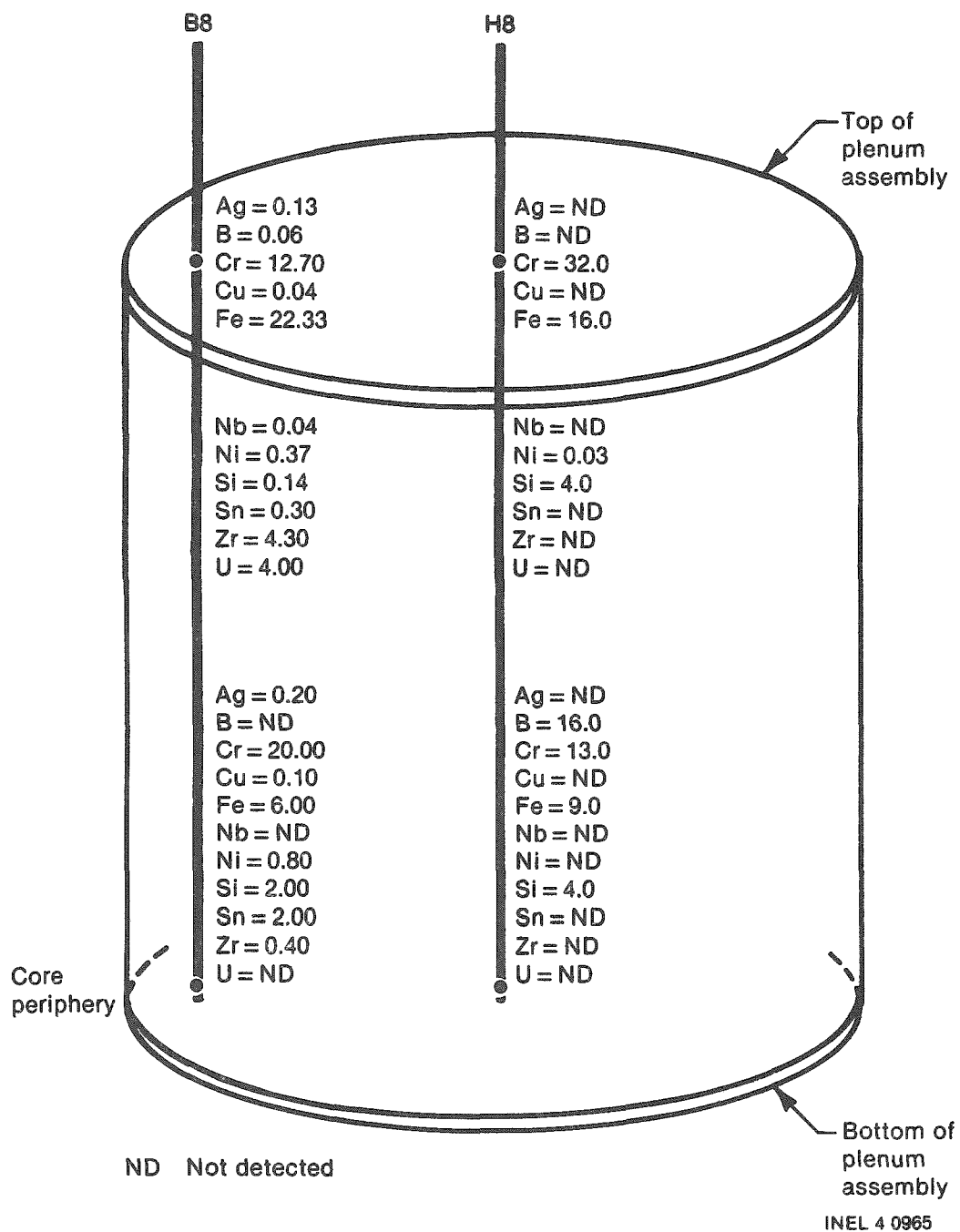


Figure 47. The concentrations of insoluble elements identified in the decontamination solutions (wt%).

These data allow a number of observations concerning the chemical behavior of core materials present on the plenum surfaces. They are: (a) the uranium and zirconium are deposited at similar locations; (b) there is a gradient (decrease) in uranium deposition from the bottom to the top of the plenum assembly; (c) the uranium and zirconium are principally present in the brushoff debris, with significantly lower fractions present in the tightly adherent material; and (d) the silver appears to be evenly distributed in the brushoff debris at ~0.1 wt%, but is less consistently deposited in the tightly adherent layer with some high and low concentrations.

Figure 48 lists the concentrations ( $\mu\text{g}/\text{cm}^2$ ) of elements removed during decontamination of the samples from the four plenum assembly locations. The principal elements of interest are silver, boron, zirconium, and uranium. The silver was detected only in the B8 decontamination solutions, and there is a gradient of a factor of ~600 from the bottom to the top of the plenum assembly, with the highest at the top. The concentrations of boron are within a factor of 3 at all locations, with the exception of the bottom of the plenum assembly (B8 location) which is a factor of 20 to 40 less than the other locations. Higher zirconium and uranium concentrations were measured at the B8 location at the top of the plenum assembly. The zirconium concentration is a factor of 20 greater than the other measured locations, and uranium was measurable only at this location. In general, the quantities of elements removed during decontamination were higher at the top of the plenum assembly.

#### Comparison of Radionuclide Analysis Results

Figure 49 shows the comparison of the brushoff debris radionuclide concentrations at the H8 and B8 locations. The axial gradient for the H8 leadscrew ranges from 29 to 66 for the principal radionuclides, whereas the axial gradient at the B8 location ranges from 77 to 227, about a factor of 3 greater than the gradient at the H8 leadscrew. The data indicate large axial gradients which change based on leadscrew location. The  $^{235}\text{U}$

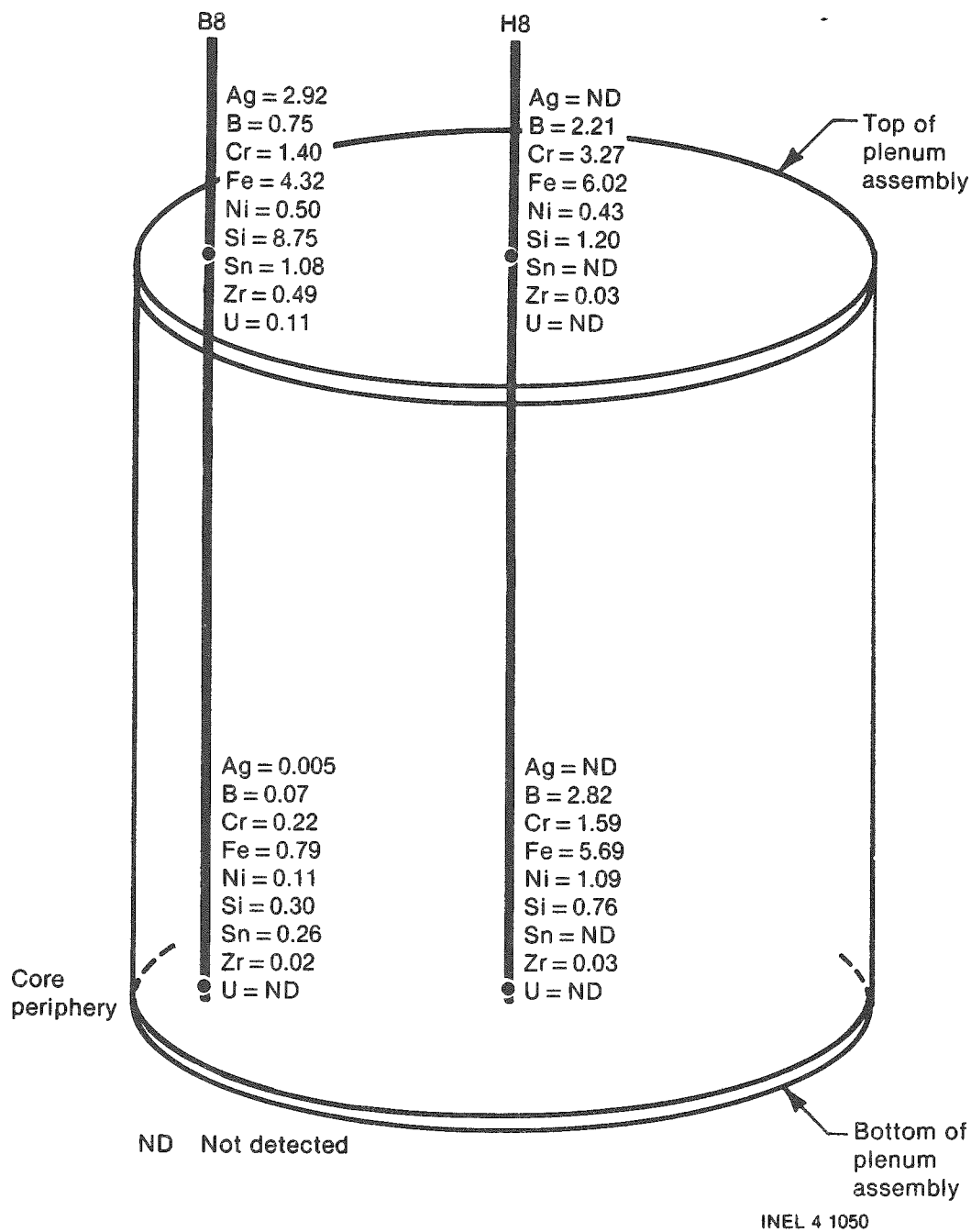


Figure 48. The total concentrations removed by decontamination ( $\mu\text{g}/\text{cm}^2$ ).



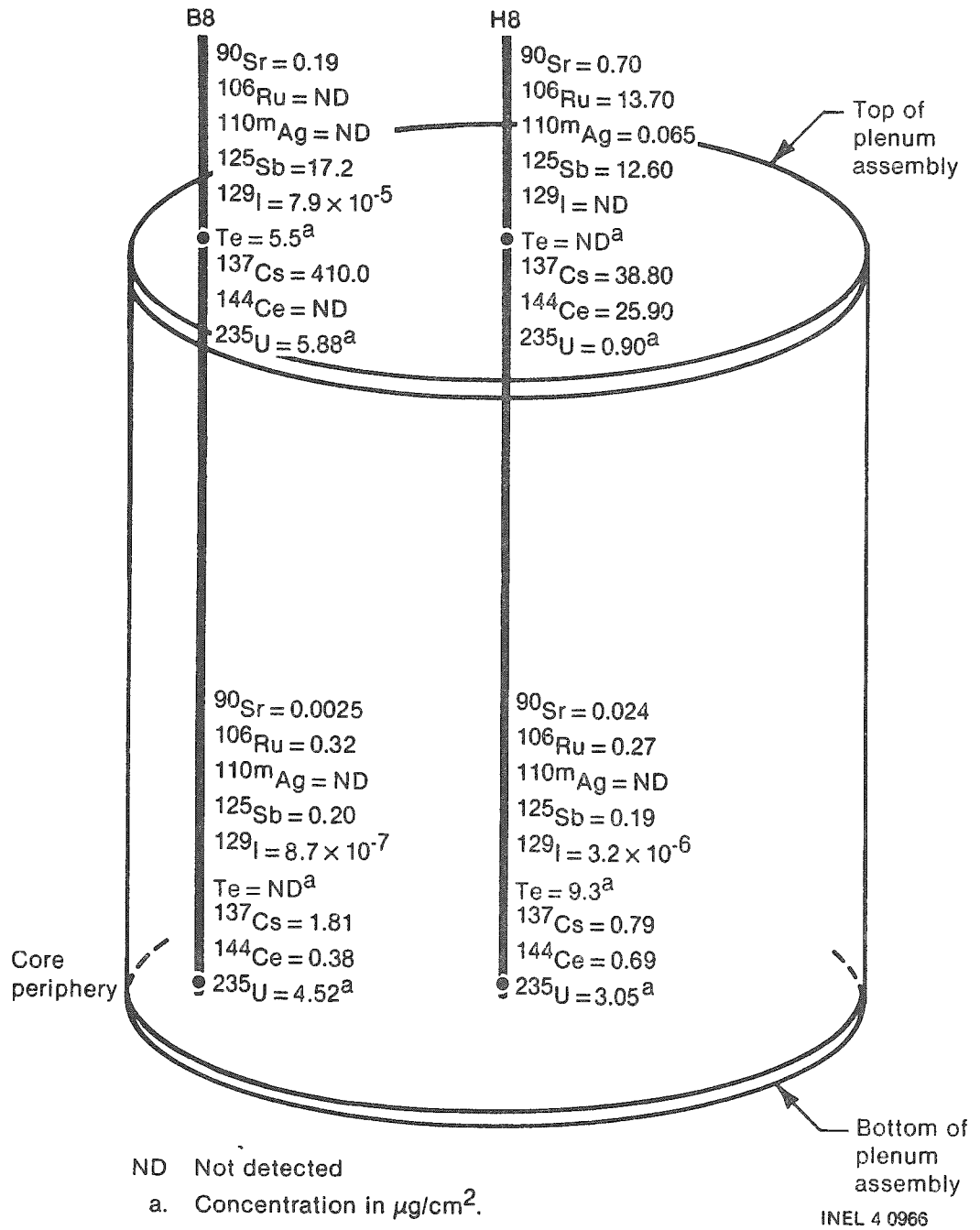
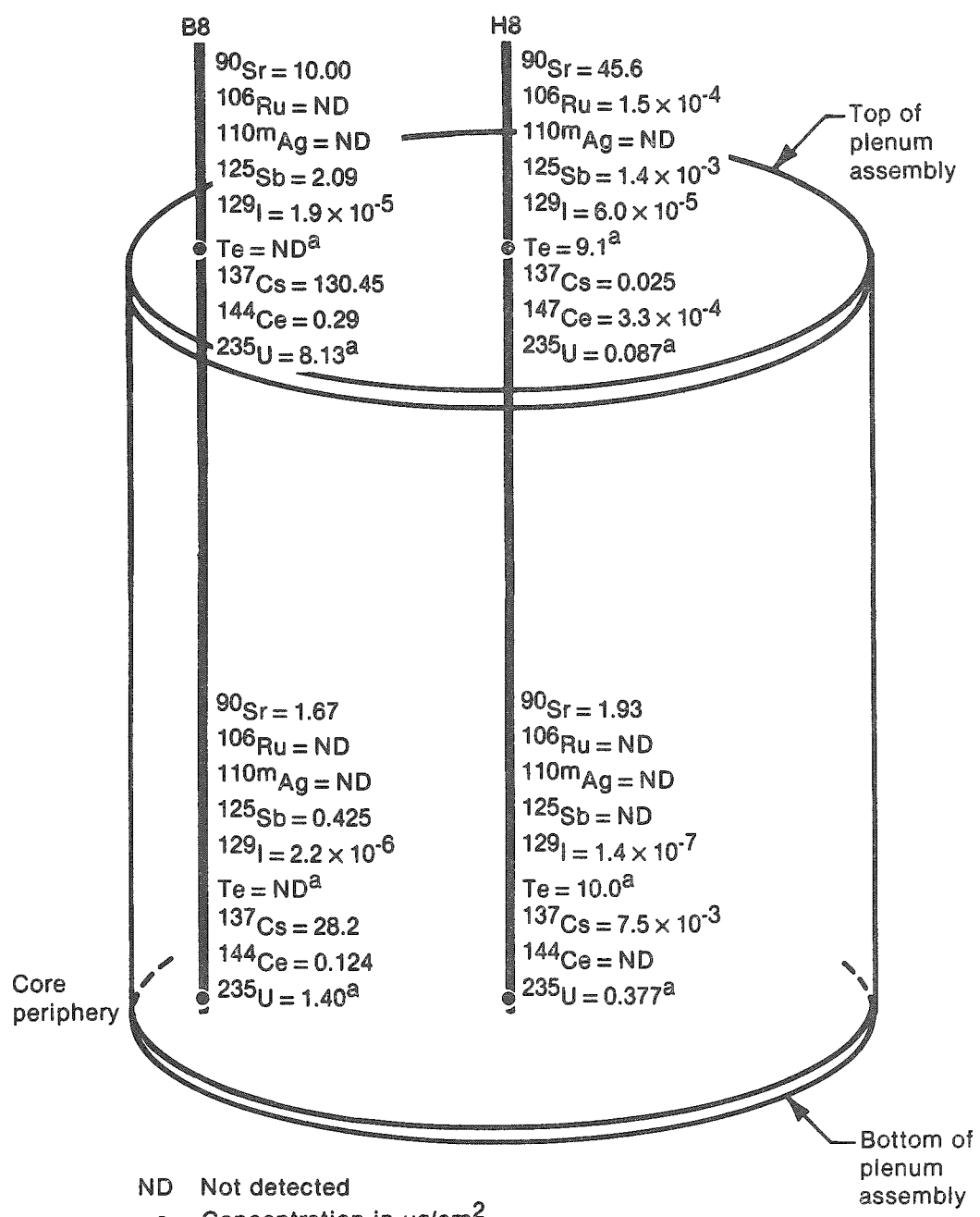


Figure 49. The surface radionuclide concentrations in the brushoff debris ( $\mu\text{Ci}/\text{cm}^2$ ).

analyses indicate a relatively small concentration gradient in the brushoff debris, with the highest concentrations at the bottom of the leadscrew (bottom of the plenum assembly). The radial gradients in the brushoff debris concentrations are within a factor of 2 for most radionuclides at the bottom of the plenum assembly; but at the top of the plenum assembly, the radionuclide concentration gradients range to a factor of 10, with high and low concentrations at both core locations.

The comparisons of the soluble and insoluble radionuclide concentrations in the decontamination solutions are shown in Figures 50 and 51, respectively. Axial gradients are present for the majority of the radionuclides, with the higher concentrations at the top of the plenum assembly. The soluble radionuclide with the largest axial gradients is  $^{129}\text{I}$ , which is higher at the top of the plenum assembly than the bottom at H8 and B8 locations by factors of 159 and 100, respectively. The  $^{137}\text{Cs}$  exhibits smaller axial gradients by factors of 11.4 and 3.6 for H8 and B8, respectively. The data indicate a wide range of radial gradients also. At the top of the plenum assembly, the  $^{129}\text{I}$  gradient is a factor of 4.8, with the highest concentration at the B8 location. At the bottom of the plenum assembly, the gradient is a factor of 7.6. The  $^{129}\text{I}$  is representative of all other radionuclides and indicates a radial gradient in the insoluble material in the decontamination solutions.

The decontamination solution radionuclide concentration data in percentages of soluble material are presented in Figure 52. The  $^{90}\text{Sr}$  is highly soluble at all locations, and a gradient in solubility is present for other radionuclides. The radionuclides deposited at the H8 locations have the lowest solubility fractions, being <1% for  $^{106}\text{Ru}$ ,  $^{110\text{m}}\text{Ag}$ ,  $^{125}\text{Sb}$ , and  $^{137}\text{Cs}$ , whereas at the B8 locations the solubility fractions are higher (>89% for  $^{137}\text{Cs}$  and >48% for  $^{125}\text{Sb}$ ). The data indicate a gradient in the chemical behavior of fission products in the plenum assembly area, as shown by the variable radionuclide behavior at the measured locations. The remaining radionuclides,  $^{129}\text{I}$ , and  $^{235}\text{U}$ , are principally soluble, >56% at most locations.



INEL 4 0968

Figure 50. The soluble radionuclide concentrations in the decontamination solutions ( $\mu\text{Ci}/\text{cm}^2$ ).

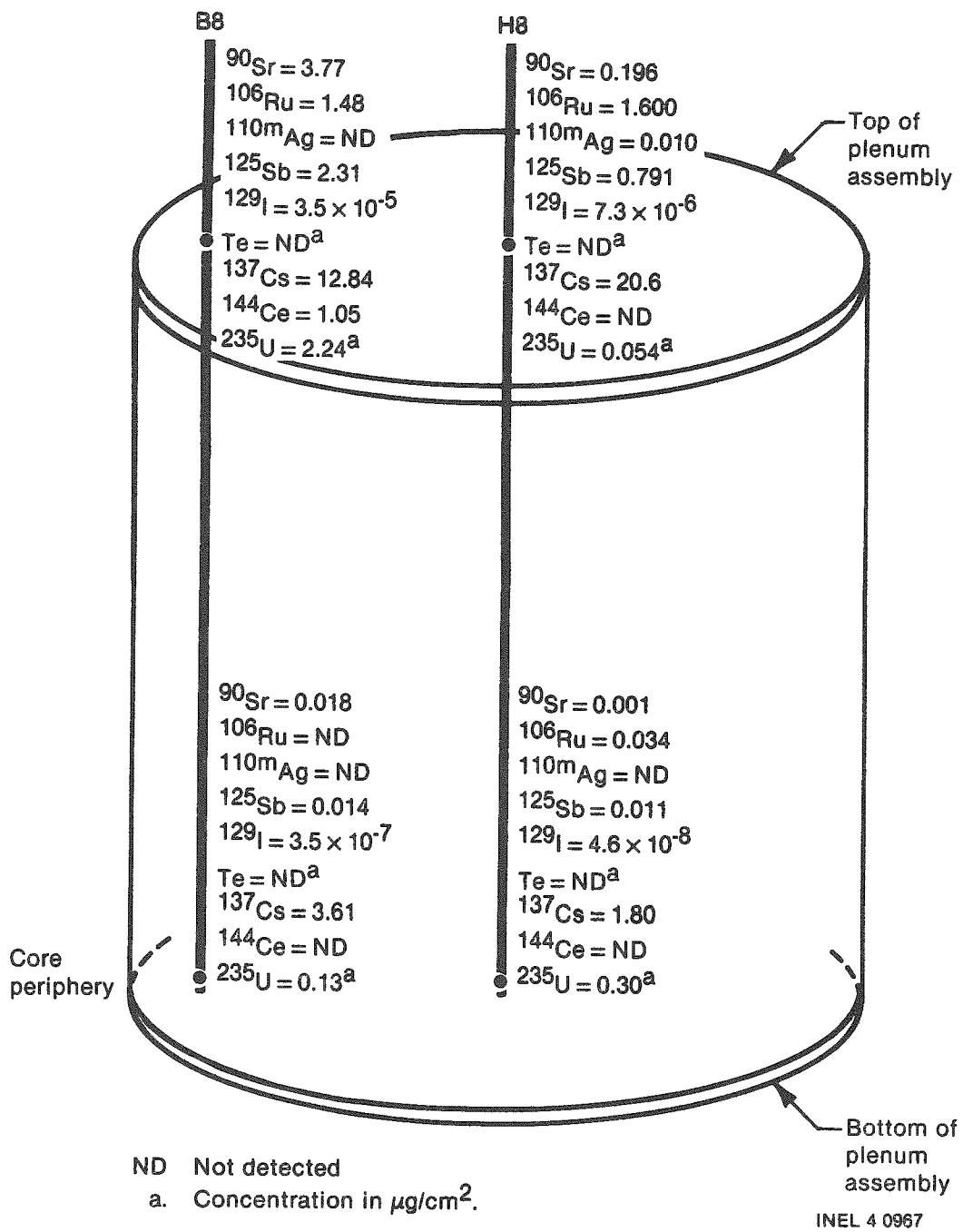


Figure 51. The insoluble surface radionuclide concentrations in the decontamination solutions (μCi/cm<sup>2</sup>).

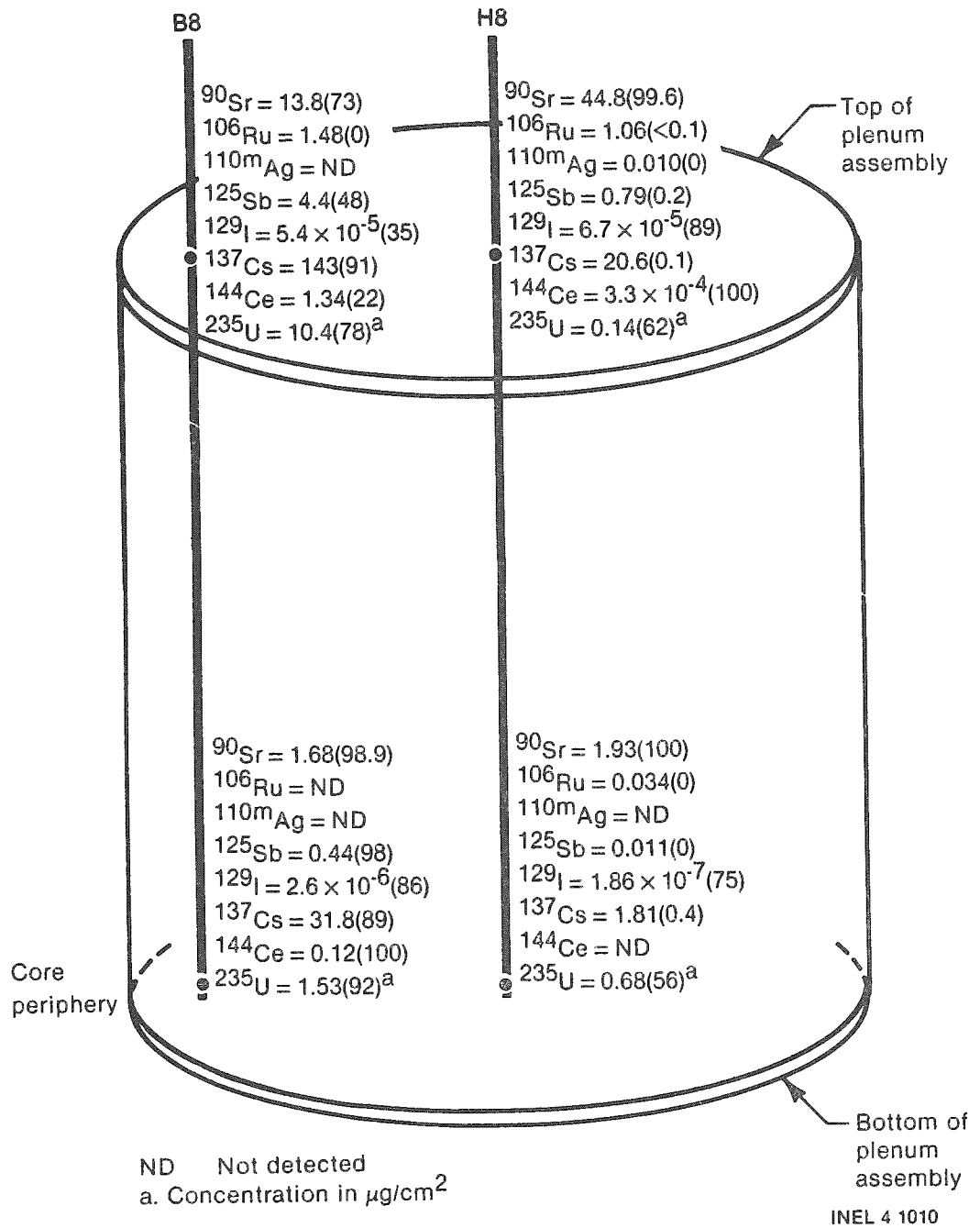
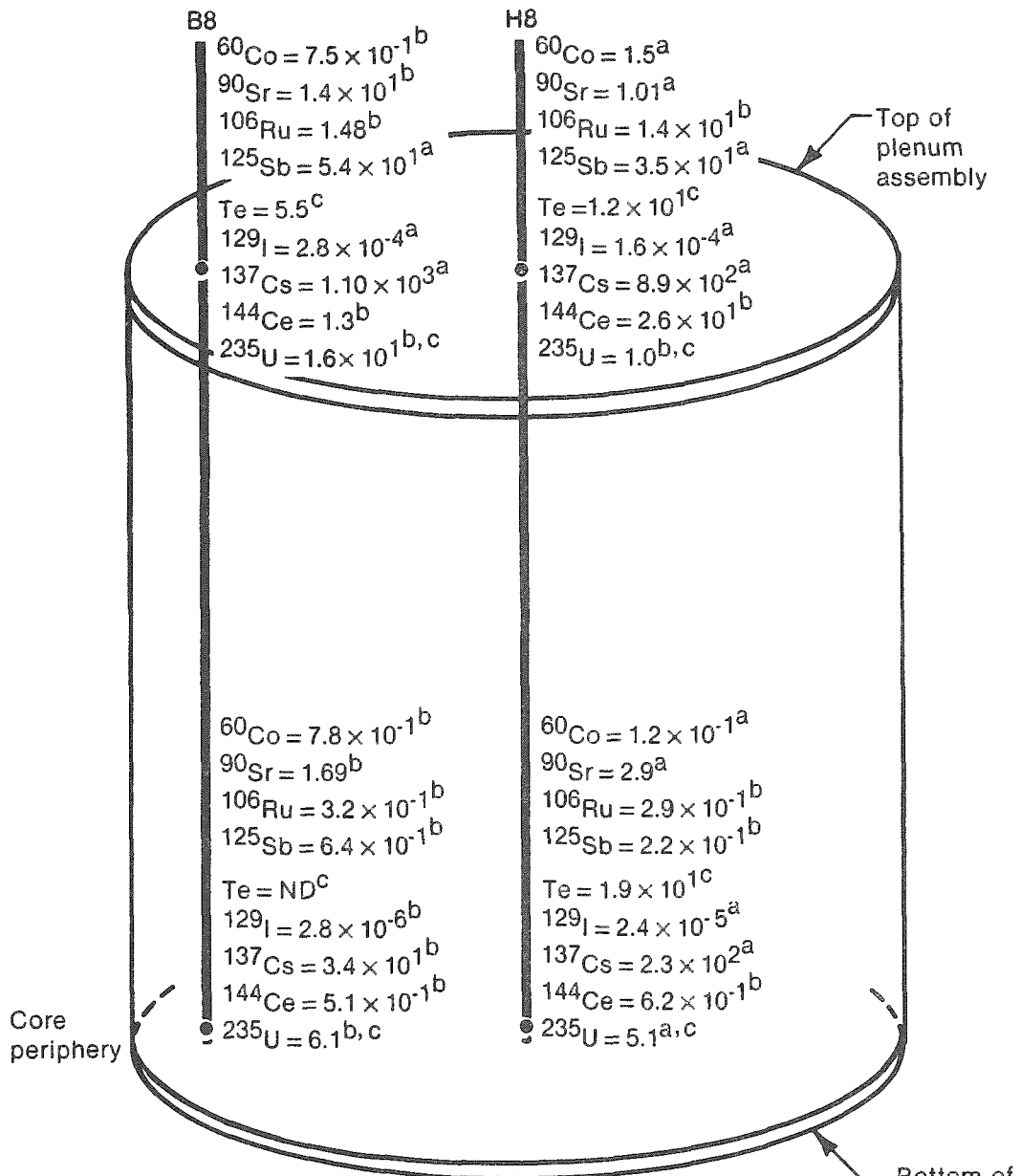


Figure 52. Total decontamination solution surface radionuclide concentrations in  $\mu\text{Ci}/\text{cm}^2$  (soluble fraction in %).

The radionuclide concentrations in the brushoff debris and decontamination solutions allow a number of observations concerning fission product behavior in the plenum assembly. They are: (a) there is a wide range of radionuclide compositions in the brushoff debris that are location dependent; (b) the solubility of the brushoff debris is radionuclide dependent; (c)  $^{129}\text{I}$  exhibits one of the wider ranges of concentrations in the plenum assembly; (d) axial gradients in fission product concentrations are more pronounced than the radial gradients; (e) the solubility of the measured radionuclides are generally in two groups, with one group being less soluble than the other; and (f) the presence of an insoluble chemical compound matrix for which there are radial and axial gradients in the deposition is indicated. The axial gradients may result from higher temperatures, resuspension, and/or washout experienced by leadscrew surfaces near the bottom of the plenum assembly. Also, fractions of the lower 7.5 to 10.2 cm (3 to 4 in.) of the leadscrew near the bottom of the plenum assembly may not have been directly exposed to the reactor environment, but were protected by the control rod spider for a portion of the accident.

Figure 53 shows the comparison of the total surface radionuclide concentrations at all four leadscrew locations. These data are based on the higher concentration of either the summed brushoff and decontamination solution data or the surface sample concentrations. The surface sample concentrations are used at three locations. These data indicate relatively similar concentrations at the bottom of the plenum assembly locations, except for  $^{137}\text{Cs}$  and  $^{129}\text{I}$ , which are factors of 6.4 and 8.6 higher at the H8 location. At the top of the plenum assembly, the concentrations are diverse, with the concentrations of  $^{60}\text{Co}$  and  $^{90}\text{Sr}$  a factor of 5 higher at the B8 location. The  $^{235}\text{U}$  concentration is a factor of 16 higher. The concentrations of  $^{125}\text{Sb}$ ,  $^{129}\text{I}$ , and  $^{137}\text{Cs}$  are within a factor of 2 at the two locations, indicating similar deposition.

Similar elemental concentrations of tellurium (within a factor of 2) were measurable at three of the four locations shown in Figure 53; however, there are uncertainties associated with these data for the following reasons:



- a. Surface sample concentrations.
- b. Based on summed concentrations.
- c. Concentration in  $\mu\text{g}/\text{cm}^2$ .

ND Not detected

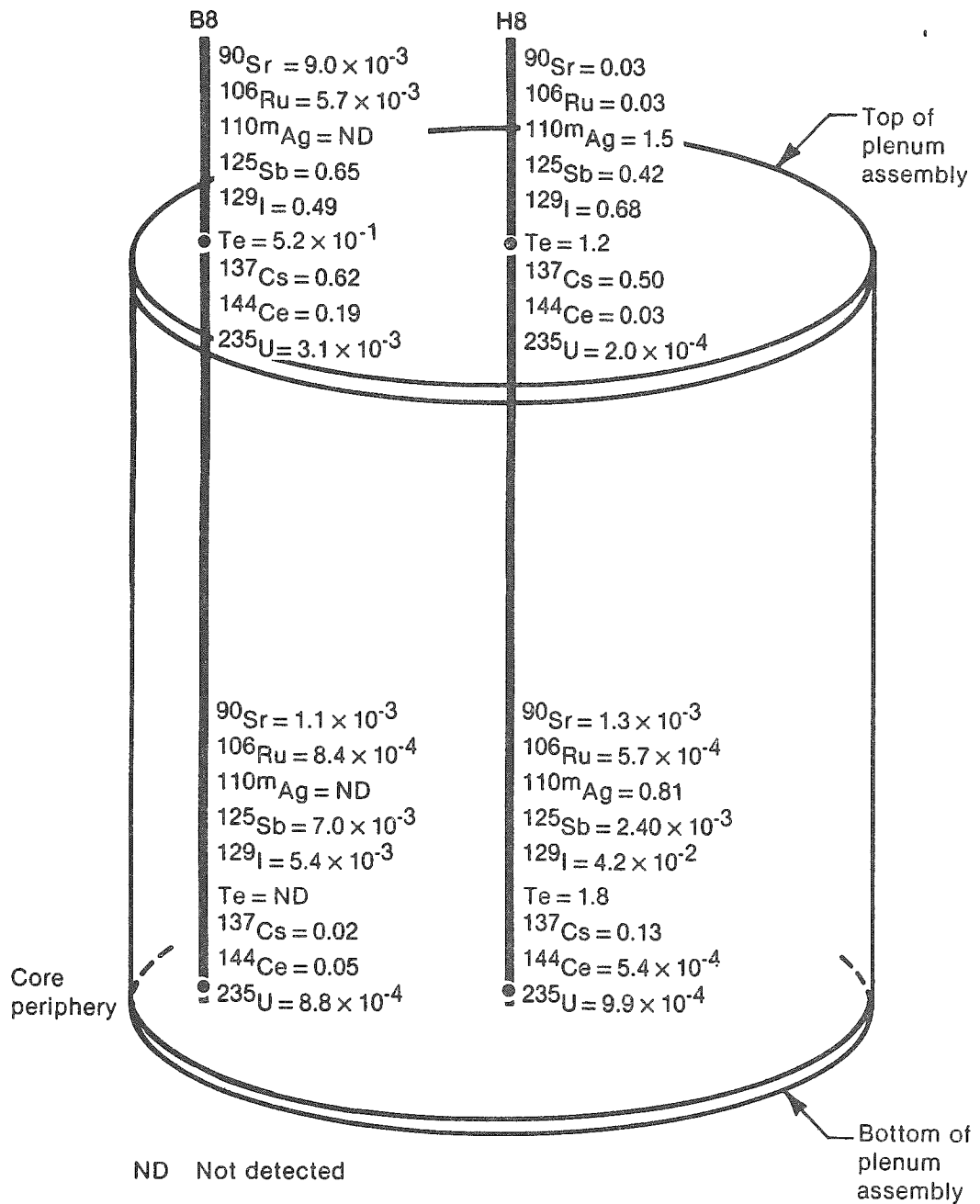
INEL 4 1011

Figure 53. The total surface radionuclide concentrations based on highest surface or summed surface concentrations ( $\mu\text{Ci}/\text{cm}^2$ ).

1. The majority of the analytical results are near the lower limit of the detecting system.
2. Although all types of samples were analyzed for tellurium, it was only detected on those samples noted below.
3. At the H8 location, the data for the bottom end of H8 are based on brushoff debris and H8 Sample 2 decontamination solution analysis; whereas the data near the top of the plenum assembly are based only on H8 Sample 16 surface sample analysis.
4. At the top of the plenum assembly on B8, the concentration is based only on the brushoff debris analysis. Therefore, the similarity of the measurable surface concentrations may be coincidental.

Figure 54 shows the calculated fraction of core fission product inventory retained on the plenum assembly surfaces. These data are based on the highest radionuclide concentrations (either summed brushoff debris and decontamination solutions or surface samples) extrapolated to plenum assembly surface area and normalized to the core inventories. There are significant axial and radial gradients in the fission-product deposition. The axial gradient at the H8 location ranges from factors of 1.85 for  $^{110m}\text{Ag}$  to 175 for  $^{125}\text{Sb}$ , with most radionuclides having gradients of 16-55. For B8, the axial ranges are smaller, with minimum ranges for  $^{144}\text{Ce}$  and  $^{235}\text{U}$ , at 3.8 and 3.6 respectively, and the widest range for  $^{125}\text{Sb}$  with a factor of 93. The radial gradients are generally significantly less. At the bottom of the plenum assembly, the maximum gradient is for  $^{144}\text{Ce}$ , with the higher concentration at the B8 location by a factor of 92. The radionuclide concentrations for  $^{90}\text{Sr}$ ,  $^{106}\text{Ru}$ , and  $^{125}\text{Sb}$  are within a factor of 3. The  $^{129}\text{I}$  and  $^{137}\text{Cs}$  have gradients of 7.8 and 6.5 respectively, with the higher concentration at the H8 location.





INEL 4 0969

Figure 54. The comparison of retained radionuclides on plenum assembly surfaces (core fraction in %).

The remaining comparisons are of the fission-product-to-fissile-material ratios and the cesium-to-iodine ratios. Table 51 lists the fission product-to-<sup>235</sup>U ratios for the H8 and B8 brushoff debris. The data have been decay-corrected to the time of the accident for comparison purpose. Listed below is the equation used to calculate the fraction of each fission product concentration carried with the <sup>235</sup>U:

$$\text{Fission Products carried with fuel (\%)} = \frac{\text{Measured fission product to } ^{235}\text{U ratio}}{\text{Calculated fission product to } ^{235}\text{U ratio}} \times 100$$

The data in Table 51 indicate that the quantity of fission products measured is much greater for all samples than would be predicted from the ORIGEN2<sup>18</sup> code-calculated fission product inventory for the amount of <sup>235</sup>U present in the core. At the H8 location close to the bottom of the plenum assembly, measured fission product concentrations are from 0.8 to 11 times the ORIGEN2-predicted fission product concentration; however, the concentrations of <sup>106</sup>Ru, <sup>137</sup>Cs, <sup>144</sup>Ce, and <sup>154</sup>Eu are close to the expected concentration within a factor of 3. The <sup>125</sup>Sb, however, is much higher than predicted. At the top of the plenum assembly, the ratios are much greater. At the H8-7 location, the concentrations are 10<sup>2</sup>-10<sup>3</sup> higher than would be expected. At B8-3, close to the bottom of the plenum assembly, there is a range between 0.3 and 8.8 times the predicted fission product concentration, which is similar to the H8-9 data. At the B8-1 location, the measured radionuclide concentrations are generally 10<sup>2</sup> greater than the predicted fission product concentrations and are similar to the H8-7 data. These data indicate both radionuclide- and location-dependent differences in the fission-product-to-fissile-material ratios.

Table 52 lists the measured fission-product-to-fissile-material ratios for the decontamination solution data and the comparison with the ORIGEN2 code-calculated fission-product-to-fissile-material ratios. The behavior is similar to the brushoff debris, with much higher radionuclide concentrations than would be predicted based on the amount of fissile material present.

TABLE 51. FISSION-PRODUCT-TO-<sup>235</sup>U RATIOS FOR THE H8 AND B8 BRUSHOFF DEBRIS.

Radionuclide	Calculated Fission-Product- To- <sup>235</sup> U Ratio	Measured Fission-Product-to- <sup>235</sup> U-Ratio				Percent Carried with <sup>235</sup> U <sup>a</sup>			
		H8-9 <sup>b</sup>	H8-7 <sup>c</sup>	B8-3 <sup>b</sup>	B8-1 <sup>c</sup>	H8-9 <sup>b</sup>	H8-7 <sup>c</sup>	B8-3 <sup>b</sup>	B8-1 <sup>c</sup>
<sup>106</sup> Ru	$4.2 \times 10^{-4}$	$6.3 \times 10^{-4}$	$1.1 \times 10^{-1}$	$6.5 \times 10^{-4}$	--d	$1.5 \times 10^2$	$2.6 \times 10^4$	$1.6 \times 10^2$	--d
<sup>125</sup> Sb	$1.7 \times 10^{-5}$	$1.9 \times 10^{-4}$	$4.3 \times 10^{-2}$	$1.5 \times 10^{-4}$	$9.8 \times 10^{-3}$	$1.1 \times 10^3$	$2.5 \times 10^5$	$8.8 \times 10^2$	$5.8 \times 10^4$
<sup>137</sup> Cs	$4.3 \times 10^{-3}$	$3.3 \times 10^{-3}$	$5.6 \times 10^{-1}$	$5.2 \times 10^{-3}$	$9.1 \times 10^{-1}$	$7.7 \times 10^1$	$1.3 \times 10^4$	$1.2 \times 10^2$	$2.1 \times 10^4$
<sup>144</sup> Ce	$3.3 \times 10^{-3}$	$3.9 \times 10^{-3}$	$5.5 \times 10^{-1}$	$2.2 \times 10^{-3}$	--d	$1.2 \times 10^2$	$1.7 \times 10^4$	$6.7 \times 10^1$	--d
<sup>154</sup> Eu	$3.8 \times 10^{-6}$	$1.1 \times 10^{-3}$	--d	$7.4 \times 10^{-6}$	--d	$2.9 \times 10^2$	--d	$2.0 \times 10^2$	--d
<sup>155</sup> Eu	$4.4 \times 10^{-5}$	--d	--d	$1.4 \times 10^{-5}$	--d	--d	--d	$3.2 \times 10^1$	--d

a. (Measured/calculated) x 100.

b. Close to the bottom of the plenum assembly.

c. Close to the top of the plenum assembly.

d. Not detected.

TABLE 52. FISSION-PRODUCT-TO-<sup>235</sup>U RATIOS FROM THE H8 AND B8 DECONTAMINATION SOLUTIONS

Radionuclide	Calculated Fission-Product- To- <sup>235</sup> U Ratio	Measured Fission-Product-to- <sup>235</sup> U Ratio				Percent Carried with <sup>235</sup> U <sup>a</sup>			
		H8 Sample 2 <sup>b</sup>	H8 Sample 15 <sup>c</sup>	B8 Sample 2 <sup>b</sup>	B8 Sample 7 <sup>c</sup>	H8 Sample 2 <sup>b</sup>	H8 Sample 15 <sup>c</sup>	B8 Sample 2 <sup>b</sup>	B8 Sample 7 <sup>c</sup>
<sup>106</sup> Ru	4.2 x 10 <sup>-4</sup>	3.5 x 10 <sup>-4</sup>	8.4 x 10 <sup>-2</sup>	6.4 x 10 <sup>-4</sup>	1.65 x 10 <sup>-3</sup>	8.30 x 10 <sup>2</sup>	2.00 x 10 <sup>4</sup>	1.52 x 10 <sup>2</sup>	4.00 x 10 <sup>2</sup>
<sup>125</sup> Sb	1.7 x 10 <sup>-5</sup>	4.5 x 10 <sup>-5</sup>	1.8 x 10 <sup>-2</sup>	1.7 x 10 <sup>-4</sup>	1.02 x 10 <sup>-3</sup>	2.67 x 10 <sup>2</sup>	1.10 x 10 <sup>5</sup>	1.00 x 10 <sup>2</sup>	6.00 x 10 <sup>2</sup>
<sup>137</sup> Cs	4.3 x 10 <sup>-3</sup>	3.4 x 10 <sup>-2</sup>	1.9	2.0 x 10 <sup>-2</sup>	6.80 x 10 <sup>-1</sup>	7.90 x 10 <sup>2</sup>	4.40 x 10 <sup>4</sup>	4.65 x 10 <sup>2</sup>	1.60 x 10 <sup>4</sup>
<sup>144</sup> Ce	3.3 x 10 <sup>-3</sup>	--d	4.3 x 10 <sup>-5</sup>	2.2 x 10 <sup>-3</sup>	3.40 x 10 <sup>-3</sup>	--d	--d	6.70 x 10 <sup>1</sup>	1.03 x 10 <sup>2</sup>
<sup>154</sup> Eu	3.8 x 10 <sup>-6</sup>	--d	--d	--d	--d	--d	--d	--d	--d
<sup>155</sup> Eu	4.4 x 10 <sup>-5</sup>	--d	--d	--d	--d	--d	--d	--d	--d

a. (Measured/calculated) x 100.

b. Close to the bottom of the plenum assembly.

c. Close to the top of the plenum assembly.

d. Not detected.

Table 53 lists the  $^{137}\text{Cs}$ -to- $^{129}\text{I}$  atom ratios present at each sample location, based on the data listed in Figure 53 and ORIGEN2 code-calculated inventories of  $^{137}\text{Cs}$  and  $^{129}\text{I}$  at the time of the accident. The cesium-to-iodine ratios are consistent on the H8 leadscrew within a factor of 1-1.15 and on the B8 leadscrew within a factor of 2 from top to bottom. The data indicate a similarity in transport mechanisms due to the very similar concentration ratios. During the TMI-2 accident, the estimated  $\text{I}/\text{H}_2\text{O}$ ,  $\text{H}/\text{O}$ , and  $\text{Cs}/\text{I}$  ratios were about  $2 \times 10^{-7}$ , 2.5 and 10, respectively. Under these conditions and at a pressure of about 15 MPa (150 bars), the estimated concentrations of  $\text{CsI}$  were<sup>21</sup> 100% (at 873 K), 90% (at 1073 K), 45% (at 1273 K), and 10% (at 1473 K). The estimated temperature range experienced on the upper plenum region was 1116-1255 K (1550-1800°F). The concentration of  $\text{CsI}$  in this temperature range is 50 to 75%. The fission-product-to-fissile-material ratios and the  $^{137}\text{Cs}$ -to- $^{129}\text{I}$  ratios indicate the following concerning the behavior of fission products: (a) the fission-product-to-fissile-material ratios are not similar to the ORIGEN2-calculated fission-product-to- $^{235}\text{U}$  ratios; (b) there is a gradient, with higher fission-product-to-fissile-material ratios at the bottom of the plenum assembly; and (c) the  $^{137}\text{Cs}$ -to- $^{129}\text{I}$  ratios are similar at all locations, indicating the possibility of similar transport methods.

TABLE 53. COMPARISON OF  $^{137}\text{Cs}$ -TO- $^{129}\text{I}$  ATOM RATIOS

Sample	$^{137}\text{Cs}$ To $^{129}\text{I}$ Atom Ratio			
	Loose Brushoff Debris	Decontamination Solution	Surface Sample <sup>a</sup>	Calculated <sup>a</sup>
H8 Sample 2 <sup>b</sup>	$1.42 \times 10^{11}$	-- <sup>c</sup>	$4.41 \times 10^{11}$	$1.83 \times 10^{12}$
H8 Sample 15 <sup>d</sup>	-- <sup>c</sup>	$1.76 \times 10^{11}$	$5.09 \times 10^{11}$	
B8 Sample 2 <sup>b</sup>	$1.24 \times 10^{12}$	$7.00 \times 10^{12}$	$5.58 \times 10^{12}$	
B8 Sample 7	$2.98 \times 10^{12}$	$1.52 \times 10^{12}$	$2.39 \times 10^{12}$	

a. Calculated from ORIGEN-2 code-calculated  $^{137}\text{Cs}$  and  $^{129}\text{I}$  discharge inventories.

b. Close to the bottom of the plenum assembly.

c. Not detected.

d. Close to the top of the plenum assembly.

## PRINCIPAL OBSERVATIONS AND RECOMMENDATIONS

### Observations

A number of samples from leadscrews H8 and B8 were subjected to a series of analyses, including metallography, SEM, TEM, ES, X-ray diffraction, gamma ray spectroscopy, chemical separation for  $^{90}\text{Sr}$  analysis, neutron activation analysis for  $^{129}\text{I}$ , ICP for tellurium analysis, and delayed neutron counting for fissile material content. The observations made are:

1. The lower portions of the H8 and B8 leadscrews near the bottom of the plenum assembly experienced temperatures of 1255 and 1116 K (1800 and 1550°F), respectively; and the upper portions of H8 and B8 near the top of the plenum assembly experienced temperatures of 700 and 755 K (800 and 900°F), respectively. The uncertainty in temperature measurement estimates is  $\pm 28$  to 56 K (50 to 100°F).
2. Axial temperature differences of 555 K (1000°F) and 361 K (650°F) exist near the core center (H8 position) and core periphery (B8 position) of the plenum assembly. A radial temperature difference of 139 K (250°F) exists between H8 and B8 near the bottom of the plenum assembly. A small radial temperature difference of 56 K (100°F) exists near the top of the plenum assembly.
3. The temperature estimates are preliminary, and additional analyses will be performed to confirm or revise these temperatures.
4. Significantly higher concentrations of uranium and zirconium were found deposited near the bottom than were found near the top of the plenum assembly.
5. Very little silver (1%) is deposited on plenum assembly surfaces from control rod material.

6. From 62 to 89% of the boron deposited on the surface may be soluble in a strong acidic solution (40-wt%  $\text{HNO}_3$  + 0.12-M HF).
7. The specific radionuclide concentrations of the H8 brushoff debris ( $\mu\text{Ci/g}$ ) were relatively uniform along the axial length of the leadscrew. A gradient was observed on the B8 leadscrew, with the highest radionuclide concentrations near the top of the plenum assembly. The radionuclides  $^{144}\text{Ce}$ ,  $^{154}\text{Eu}$ , and  $^{155}\text{Eu}$  were not measurable near the top of the plenum assembly at the B8 position.
8. Much of the H8 surface deposition layer containing  $^{125}\text{Sb}$  and  $^{137}\text{Cs}$  radionuclides is insoluble in strong acidic solutions. In contrast, the deposition layer containing these radionuclides on B8 is significantly more soluble in strong acidic solutions, indicating a radial gradient in chemical behavior of fission products.
9. In general, highest surface radionuclide concentrations ( $\mu\text{Ci}/\text{cm}^2$ ) were found in the region near the top of the plenum assembly, which was also the lowest in temperature (700 to 755 K).
10. Significant fractions (<50%) of the radionuclide content of the brushoff debris at the bottom and top of the plenum assembly (H8 position) are associated with particle sizes  $\leq 60 \mu\text{m}$ , indicating that many radionuclides may have been transported as aerosols or hydrosols. (Sixteen to 34% of the particle sizes are  $\leq 0.45 \mu\text{m}$ .)
11. The fractions of the total core inventory of  $^{90}\text{Sr}$ ,  $^{106}\text{Ru}$ ,  $^{110\text{m}}\text{Ag}$ ,  $^{125}\text{Sb}$ ,  $^{129}\text{I}$ , tellurium,  $^{137}\text{Cs}$ ,  $^{144}\text{Ce}$ , and  $^{235}\text{U}$  retained on the plenum assembly surfaces are very small (<2%), based on the extrapolation of the leadscrew analysis results to the entire plenum assembly surface area.



12. Small radial gradients in radionuclide concentrations are present between the H8 and B8 locations, with the highest at the top of the plenum assembly.
13. The measured ratios of fission product concentration to fissile material content are much higher than would be expected from ORIGEN2 calculations. This discrepancy is much greater at the top of the plenum assembly ( $\sim 10^2$  to  $10^3$ ) than at the bottom.
14. The  $^{137}\text{Cs}$ -to- $^{129}\text{I}$  atom ratios suggest that the transport mechanisms for both radionuclides are similar.

#### Recommendations

A technical review committee (M. L. Picklesimer, metallurgical consultant, PIC Products; H. W. Garvin, metallurgical consultant, ARMCO; and G. O. Hayner, Supervisor, Failure Analysis, B&W) has reviewed the temperature estimates section of the report and recommended that the following work be done on both 17-4 PH SS and 304 SS in order to complete the present examination in an orderly and acceptable fashion. The essential elements for completion of a basic temperature study of 17-4 PH SS and 304 SS standards are as follows:

1. Incorporate the results of the low-temperature study of leadscrew 17-4 PH samples into Figure 14 of the report. (These data were obtained since the preparation of the draft report.)
2. Complete the test matrix listed in Appendix A (Figure A-1); make hardness, optical, and SEM comparisons of the control samples from the test matrix with the unknowns from the leadscrews based on an H900 and quenched heat-treated condition for the control samples. The H900 heat-treated condition will provide a larger range of hardness values for comparison with the unknowns and a more reliable interpretation of their history.

3. Perform STEM work, including selected area X-ray diffraction and elemental analyses as appropriate. This work should be performed on at least the following test matrix specimens: A<sub>11</sub>, A<sub>31</sub>, A<sub>41</sub> (1300°F), A<sub>17</sub>, A<sub>27</sub>, A<sub>37</sub> (1800°F), A<sub>24</sub>, A<sub>25</sub>, A<sub>26</sub> (60 min. isochronal). Based on the results obtained from the samples indicated above, STEM work on additional specimens from the completed test matrix may be required. The objective of this work is to more fully characterize key samples in the test matrix in the following areas: substructure, selected area X-ray diffraction, and selected area elemental analyses. These data will be used to more fully understand and characterize phase, microstructural, and hardness changes observed in the specimens.
4. An X-ray diffraction study should be performed on the unknown samples and all controls from the completed Appendix A test matrix specimens in the as-received and as-quenched conditions, respectively. The objective of this study is to qualitatively determine the reaction products and approximate reaction kinetics (from the crystal structures) present in the controls and unknowns. These data would provide support for comparison with hardness and microstructural data to further verify temperatures attained by the leadscrew unknowns.
5. Based on the additional work to be performed and described previously, establish revised estimates of peak temperatures for the unknowns.
6. Complete the 1°F/min cooling rate study. Determine the microstructures and hardness values in the H900 condition. If a lamellar structure is not seen in this work, a reheat study should be performed. A 1°F/min specimen which was not reheated to either the H900 or H1100 condition should be subdivided into seven separate specimens. These seven specimens should be reheated, one each to 1300, 1350, 1400, 1450, 1500, 1550, and

1600°F, respectively, and held for one hour at each temperature. The microstructures from these specimens should be compared to that of B8-2. If a lamellar structure is produced which is comparable to the B8-2 unknown, then a hardness comparison should be made in the H900 condition. The lamellar spacing of this specimen should be determined and compared to the B8-2 specimen. The reasons for this study are to determine the B8-2 unknown temperature from lamellar spacing measurements and to determine if the previous temperature prediction may be low.

7. Perform a microstructural examination of a longitudinal section of the leadscrew specimens. This will indicate if differences exist between the transverse and longitudinal structures.
8. Repeat the hardness measurements performed on the H8-2 sample in the H900 condition. If these measurements are close to Rc47, then repeat the hardness test using the H8-3 specimen in the H900 condition.
9. Determine the bulk chemistry of H8-15 and B8-7 by suitable techniques. These data will further assist the interpretation of the microstructures, since the microstructure and hardness of the alloy are sensitive to the exact balance of the elemental composition.
10. Perform a microprobe line scan analysis of at least one specimen showing a lamellar microstructure to determine any compositional differences between the plates composing the structure.
11. A strong effort should be made to obtain higher and more uniform contrast for the photomicrographs used in the final report. It is suggested that Polaroid P/N film be used to produce slightly underexposed negatives which will allow much more control and variation in printing.

The following recommendations apply to 304 SS samples:

1. Archive 304 SS material (if available) should be used for all control specimens for comparison with the lower extension piece specimens of the leadscrews. The 304L upper extension piece material should not be used for control samples, since it has a much lower carbon content. If archive material is not available, then 1-1/2 to 2-in. OD commercial 304 SS rod with hardness in the range of 80-95 Rb (88-92 Rb preferred) should be used for the control specimens. The interpretation of the microstructures to allow an estimate of peak temperatures will depend to a very large extent on the presence or absence of carbides and their type, size, and concentration.
2. Determine the bulk chemistry of the upper and low extension pieces by suitable techniques. This will provide assurances that the materials are actually 304 SS.
3. Repeat the work already performed with the 304 SS material as noted above (to replace that done with the 304L SS). This should include, as a minimum, the comparison of control and leadscrew specimens with regard to hardness and microstructure for the temperature range of interest.

The authors recommend that additional leadscrews be examined in order to characterize the axial and radial profiles for temperatures and radionuclide and core material plateout in the entire plenum assembly. The H8 and B8 leadscrew examination task demonstrated the feasibility of the analytical techniques; however, the data obtained are too limited to adequately characterize the plenum assembly as a whole. Additional data from several strategic leadscrew locations within the plenum assembly region are needed for an adequate characterization.

Garry Thomas, EPRI,<sup>22</sup> suggests several reasons why characterization of the plenum assembly is critical and why the leadscrews can provide the data needed to accomplish the characterization. They include the following:

1. The plenum assembly acts as a major buffer for the reactor primary system by moderating the temperature of the core exit gases. It alters the thermodynamic and thermochemical states of fission products leaving the core. Therefore, its real effect should be characterized.
2. The strategic placement of leadscrews allows for three-dimensional sampling of the entire (~70 ton) plenum assembly.
3. The leadscrews are the most accessible components in the plenum assembly.
4. Visual examination and temperature estimates of the leadscrews indicate no visible sign of damage to the plenum assembly in contrast to modeling predictions. The temperature characterization of several leadscrews across the plenum assembly will spatially define core boundary temperatures to benchmark core degradation codes.
5. Characterization of the plenum assembly as a whole will help understand the convection recirculation between the degraded core and the plenum assembly. If recirculation occurs to the magnitude indicated by models, then (a) the plenum assembly has a major impact on the development of core damage and fission product movement and (b) it should be traceable at TMI-2 via temperature mapping of the plenum assembly.
6. The closed-circuit television examinations of the core void region indicates asymmetric damage to the core and the underside of the plenum assembly.

## 6. REFERENCES

1. J. O. Carlson, TMI-2 Core Examination Plan, EGG-TMI-6169, July 1969.
2. R. R. Hobbins, P. E. MacDonald and D. E. Owen, "TMI-2 Core Examination," International Meeting on Light Water Reactor Severe Accident Evaluation, August 28 to September 1, 1983, Cambridge, MA, Volume 1, p. 1.6-1.
3. D. E. Owen et al., "TMI-2 Core Damage: A Summary of Present Knowledge," International Meeting on Light Water Reactor Severe Accident Evaluation, August 28 to September 1, 1983, Cambridge, MA, Volume 1, p. 1.5-1.
4. GPU Technical Plan, H8 Leadscrew Characterization, TPO/TMI-041, March 1983.
5. H. Jordan et al., TRAP-MELT Users Manual, NUREG/CR-0632, February 1979.
6. R. L. Clark et al., TMI-2 Leadscrew Debris Pyrophoricity Study, GEND-INF-044, April 1984.
7. G. M. Bain and G. O. Hayner, Initial Examination of the Surface Layer of a 9-Inch Leadscrew Section Removed From Three Mile Island-2, EPRI-NP-3407, January 1984.
8. K. J. Hofstetter et al., Chemical Analyses and Test Results for Sections of the TMI-2 H8 Leadscrews, TPO/TMI-103, Revision 0, February 1984.
9. K. J. Hofstetter et al., "Adherent Activity on TMI-2 Leadscrew," ANS Transactions, 45, November 1983, p. 278.
10. K. J. Hofstetter et al., "Decontamination Barrier on TMI-2 Leadscrew," ANS Transactions, 46, June 1984, p. 384.
11. R. P. Wichner and R. D. Spence, Quantity and Nature of LWR Aerosols Produced in the Pressure Vessel During Core Heatup Accidents--A Chemical Equilibrium Estimate, NUREG/CR-3181, March 1984.
12. Interoffice correspondence by D. R. Buchanan to H. M. Burton, GPU Nuclear Corporation, July 5, 1983.
13. Three Mile Island Nuclear Station, Unit 2 License Application, FSAR, Volume 5, Metropolitan Edison Co., 1974.
14. Analysis of Three Mile Island-Unit 2 Accident, NSAC-1, Revised, March 1980, Figure TH20.
15. Vendor's Handbook, ARMCO 17-4 PH Stainless Steel, ARMCO Steel Corporation, 1966.

16. C. O. Smith, The Science of Engineering Materials, Prentice-Hall Inc., Englewood Cliffs, New Jersey, 1977, p. 322.
17. M. D. Gorman, Influence of Isothermal Holding of ARMCO 17-4 PH During Cooling from Solution Treatment, ARMCO Research and Technology, 703 Curtis Street, Middletown, Ohio 45043, December 18, 1984.
18. J. C. Cunnane and S. L. Nicolosi, Characterization of the Contamination in the TMI-2 Reactor Coolant System, EPRI NP-2722, November 1982.
19. J. A. Daniel et al., Analyses of the H8, B8, and E9 Leadscrews from the TMI-2 Reactor Vessel, SAI-83/1083, August 31, 1983.
20. R. J. Davis et al., Radionuclide Mass Balance for the TMI-2 Accident: Data Through 1979 and Preliminary Assessment of Uncertainties, NUS-4432, Volume 2, September 1982.
21. Technical Bases for Estimating Fission Product Behavior During LWR Accidents, NUREG-0772, P. C-6, June 1981.
22. Letter, Garry R. Thomas, EPRI, to J. O. Carlson, EG&G Idaho, Inc., subject: "Need for Additional TMI-2 Leadscrew Metallurgical Sampling," September 14, 1984.





APPENDIX A  
ANNEALING STUDY OF 17-4 PH AND 304L SS STANDARDS



APPENDIX A  
ANNEALING STUDY OF 17-4 PH AND 304L SS STANDARDS

The annealing study was performed on 17-4 PH SS standards obtained from leadscrew sections H8-19 (26 cm) and H8-20 (11.4 cm) (Figure 2 of the text) located near the top of the reactor head. These sections were cut into a number of 1.5-cm-thick slices, and then each slice was cut into quarters (standards). One standard from each slice was annealed as per the time-temperature matrix given in Figure A-1. Rockwell-C hardness measurements, optical microscopy, and SEM were performed on as-received and annealed standards. The results are listed in Table A-1. The hardness of the as-received standards ranged from 34.6 to 36.4. Subsequent heat-treatment of a standard at the H900 condition did not significantly increase the hardness (34.6 to 35.1), confirming that the leadscrew at this location is still at the H1100 condition (as fabricated condition). The optical and SEM micrographs of the annealed standards from Sections H8-19 and -20 are shown in Figures A-2 through A-7 and A-8 through A-13, respectively

Several attempts were made to measure the grain sizes from the optical and SEM micrographs. Because of the complicated microstructures and difficulty in measuring the grain sizes, only a few micrographs were measured for grain sizes. Due to the difficulties encountered, the grain sizes were not used to estimate the peak temperature of the leadscrew.

The microstructures and the hardness numbers of the annealed standards were compared with H8 Sample 2 and B8 Sample 2. As shown in Figure A-14, the hardness numbers and SEM micrographs of the annealed standards  $A_{27}$  and  $A_{24}$  compare closely with H8 Sample 2 and B8 Sample 2, suggesting that these samples have experienced temperatures of about 1255 K (1800°F) and 1116 K (1550°F), respectively. The uncertainty in temperature was  $\pm 28$  to 56 K (50 to 100°F). In addition, heat treatment of H8 Sample 2 and B8 Sample 2 at H900 condition increased the hardness from 34 to 47 and from 35 to 38, respectively, suggesting that H8 Sample 2 is at fully solutionized condition and B8 Sample 2 is at partially solutionized condition. In general, the temperature range for the solutionized condition is 1089 to 1477 K (1500 to 2200°F), with the partially solutionized condition expected to be near the

A <sub>11</sub>	* A <sub>12</sub>	* A <sub>13</sub>	* A <sub>14</sub>	A <sub>15</sub>	A <sub>16</sub>	A <sub>17</sub>	* A <sub>18</sub>	* A <sub>19</sub>
A <sub>21</sub>	A <sub>22</sub>	A <sub>23</sub>	A <sub>24</sub>	A <sub>25</sub>	A <sub>26</sub>	A <sub>27</sub>	A <sub>28</sub>	A <sub>29</sub>
A <sub>31</sub>	* A <sub>32</sub>	* A <sub>33</sub>	* A <sub>34</sub>	A <sub>35</sub>	A <sub>36</sub>	A <sub>37</sub>	* A <sub>38</sub>	* A <sub>39</sub>
A <sub>41</sub>	* A <sub>42</sub>	* A <sub>43</sub>	* A <sub>44</sub>	A <sub>45</sub>	A <sub>46</sub>	A <sub>47</sub>	* A <sub>48</sub>	* A <sub>49</sub>

Time (min)

1. 30
2. 60
3. 120
4. 240

Temperature K (°F)

- |                |                |                |
|----------------|----------------|----------------|
| 1. 977 (1300)  | 4. 1116 (1550) | 7. 1255 (1800) |
| 2. 1033 (1400) | 5. 1144 (1600) | 8. 1311 (1900) |
| 3. 1059 (1500) | 6. 1200 (1700) | 9. 1477 (2200) |

Sample identification: A<sub>ij</sub>

where: i (1 to 4) = time in minutes

j (1 to 9) = temperature in K (°F)

\* not annealed

P38-ALA84063-4

Figure A-1. The time-temperature matrix for 17-4 PH SS annealing study.

TABLE A-1. ROCKWELL-C HARDNESS MEASUREMENTS FROM AS-RECEIVED AND ANNEALED 17-4 PH SS STANDARDS

Section	17-4 PH SS Standards	Annealing History		Rockwell-C Hardness (RC)
		Time (min)	Temperature K (°F)	
H8-20	A <sub>00</sub> (one end)	As received	As received	34.6
H8-19	A <sub>00</sub> (one end)	As received	As received	37.0
H8-20	A <sub>11</sub>	30	977 (1300)	31.3
H8-20	A <sub>15</sub>	30	1144 (1600)	34.2
H8-20	A <sub>16</sub>	30	1200 (1700)	35.1
H8-20	A <sub>17</sub>	30	1255 (1800)	34.6
H8-20	A <sub>21</sub>	60	977 (1300)	31.4
H8-19	A <sub>22</sub>	60	1033 (1400)	33.7
H8-19	A <sub>23</sub>	60	1089 (1500)	34.4
H8-19	A <sub>24</sub>	60	1116 (1550)	35.4
H8-20	A <sub>25</sub>	60	1144 (1600)	33.8
H8-20	A <sub>26</sub>	60	1200 (1700)	35.0
H8-20	A <sub>27</sub>	60	1255 (1800)	35.0
H8-20	A <sub>28</sub>	60	1311 (1900)	34.3
H8-20	A <sub>29</sub>	60	1477 (2220)	33.9
H8-20	A <sub>31</sub>	120	977 (1300)	29.3
H8-20	A <sub>35</sub>	120	1144 (1600)	34.3
H8-20	A <sub>36</sub>	120	1200 (1700)	34.3
H8-20	A <sub>37</sub>	120	1255 (1800)	34.4
H8-20	A <sub>41</sub>	240	977 (1300)	29.3
H8-20	A <sub>45</sub>	240	1255 (1600)	34.5
H8-20	A <sub>46</sub>	240	1200 (1700)	34.2
H8-20	A <sub>47</sub>	240	1255 (1800)	34.5
H8-20	A <sub>00</sub> (Other end)	As received	As received	36.4
H8-19	A <sub>00</sub> (Other end)	H900 <sup>a</sup>		37.4
H8-20	A <sub>00</sub> (Same as prior heat treatment)	As received	As received	34.6
H8-20	A <sub>15</sub> A <sub>00</sub> (Same as A <sub>15</sub> prior to heat treatment)	As received + H900 <sup>b</sup>		35.1

TABLE A-1. (continued)

---

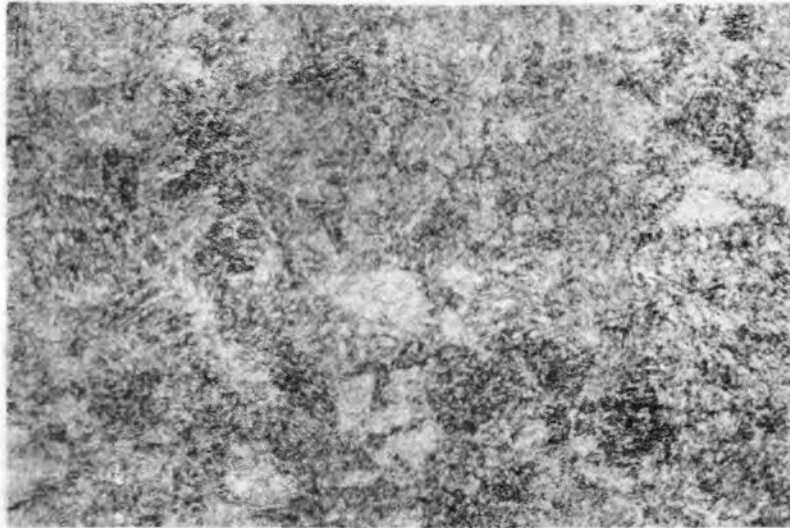
---

a. Heat treatment of standard A<sub>00</sub> from H8-19 section at H900 condition (heated for one hour at 900°F and air-quenched) increased the hardness from 37.0 to 37.4, indicating that standard A<sub>00</sub> is at the H1100 condition (as-fabricated condition).

b. Heat treatment of standard A<sub>15</sub> from Section H8-20 at H900 increased the hardness from 34.2 to 35.1, indicating that standard A<sub>15</sub> is at the H1100 condition (as-fabricated condition).

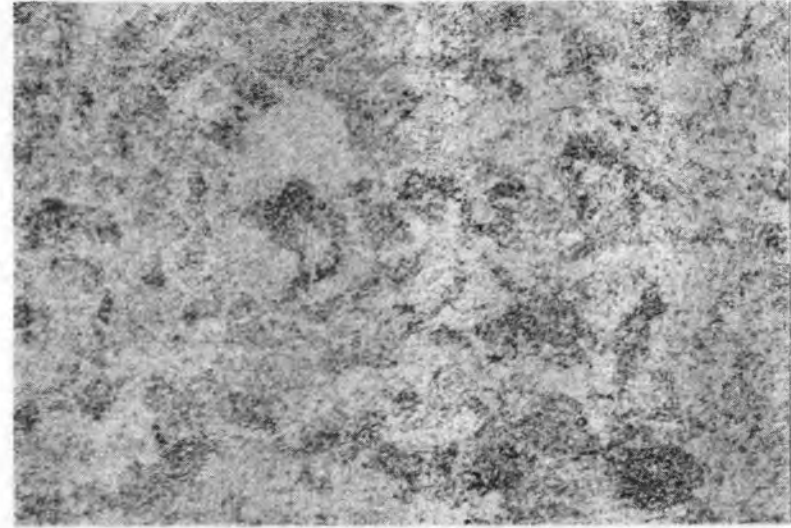
---

A-7



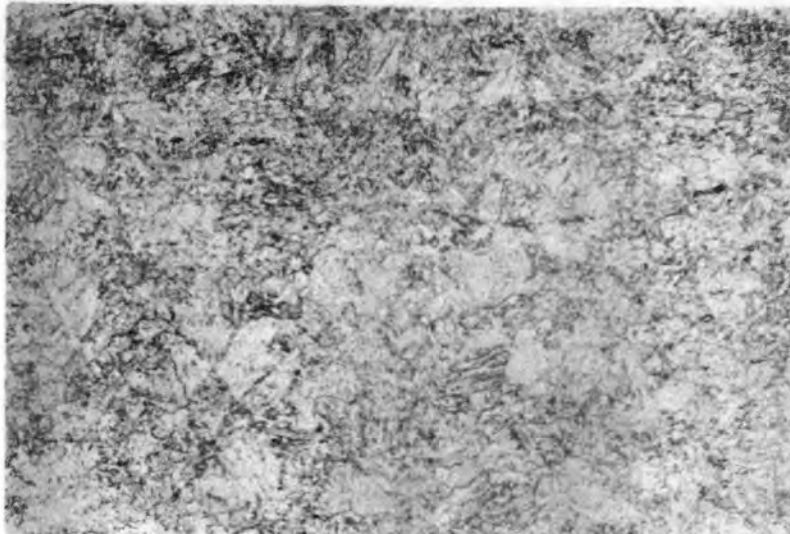
A<sub>11</sub>, 30 min., 977 K (1300°F)

25 μm



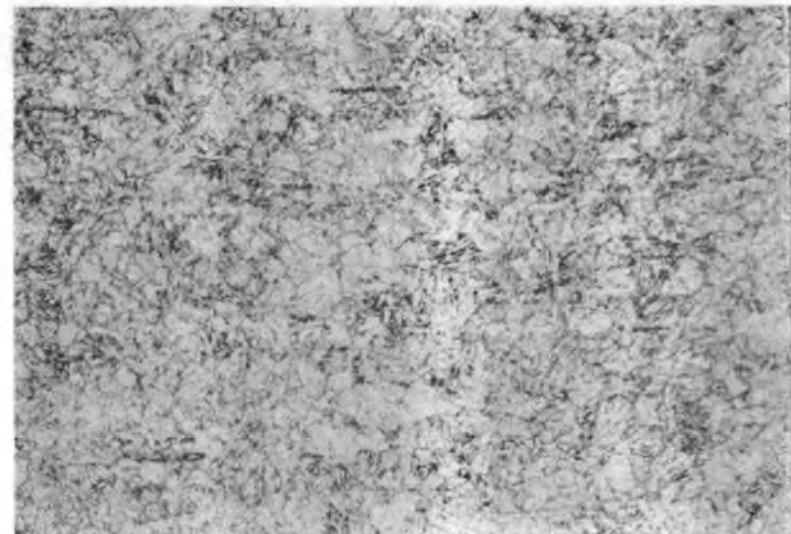
A<sub>15</sub>, 30 min., 1144 K (1600°F)

25 μm



A<sub>16</sub>, 30 min., 1200 K (1700°F)

25 μm



A<sub>17</sub>, 30 min., 1255 K (1800°F)

25 μm

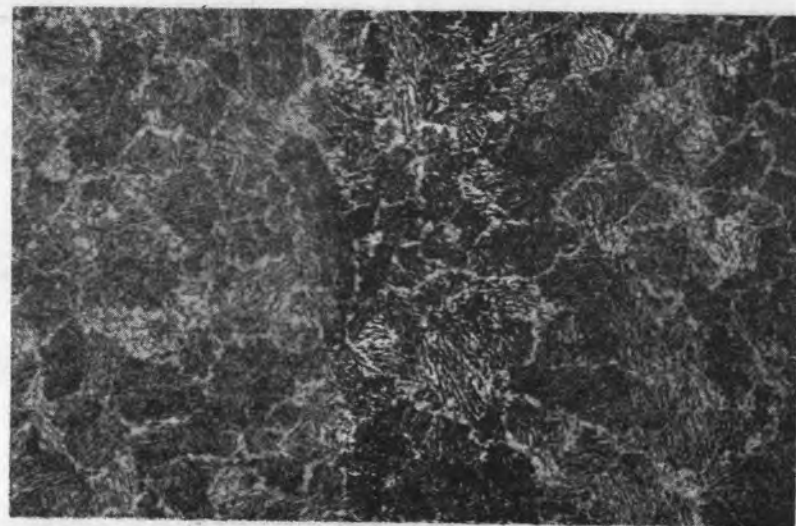
INEL 4 0970

Figure A-2. Optical micrographs of 17-4 PH SS Standards A<sub>11</sub>, A<sub>15</sub>, A<sub>16</sub> and A<sub>17</sub>.



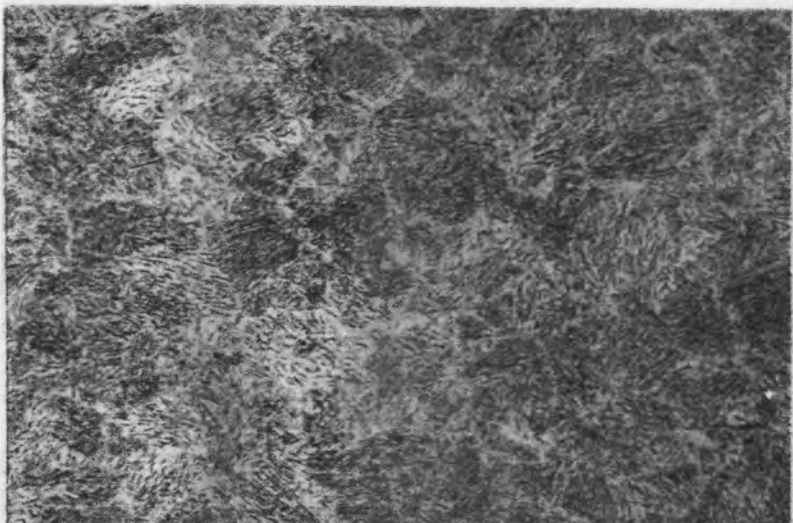
(a) A<sub>21</sub>, 60 min., 977 K (1300°F)

20 μm



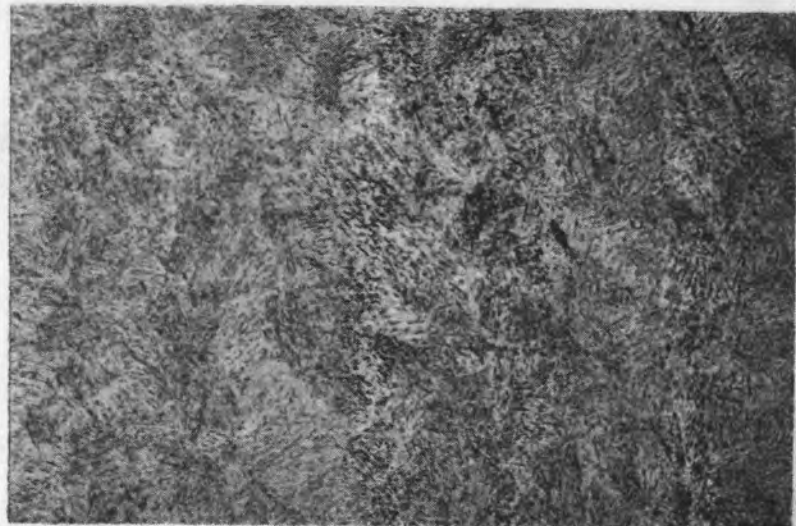
(b) A<sub>22</sub>, 60 min., 1033 K (1400°F)

25 μm



(c) A<sub>23</sub>, 60 min., 1089 K (1500°F)

25 μm



(d) A<sub>24</sub>, 60 min., 1116 K (1550°F)

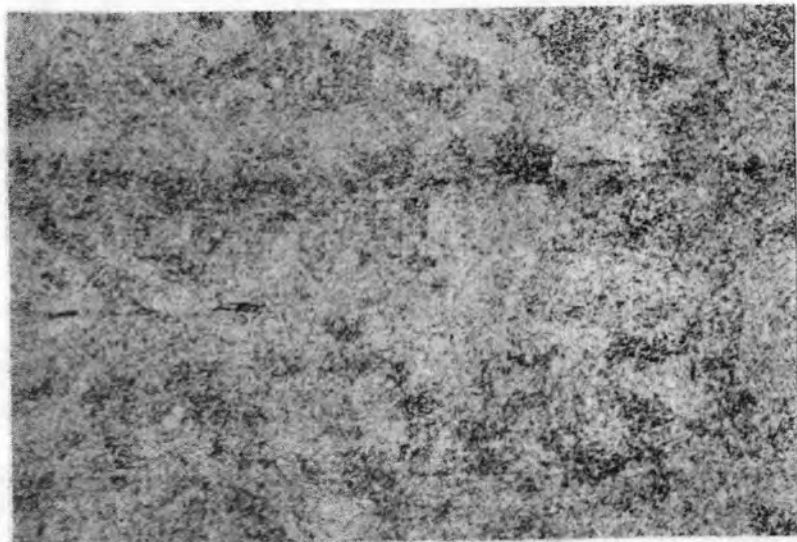
25 μm

INEL 4 0971

Figure A-3. Optical micrographs of 17-4 PH SS Standards A<sub>21</sub>, A<sub>22</sub>, A<sub>23</sub>, and A<sub>24</sub>.



A-9



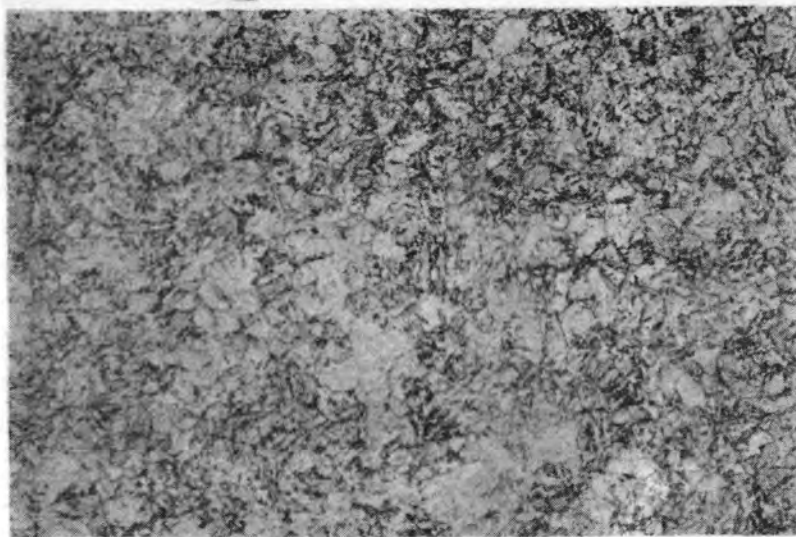
A<sub>25</sub>, 60 min., 1144 K (1600°F)

20 μm



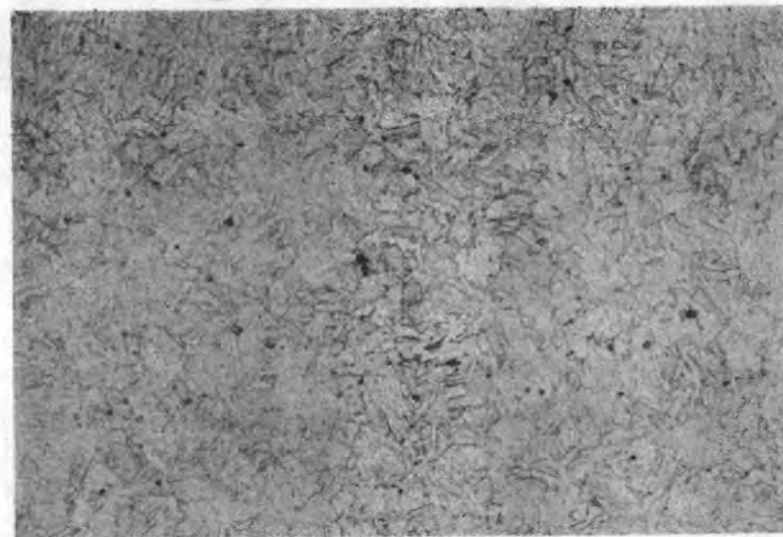
A<sub>26</sub>, 60 min., 1200 K (1700°F)

20 μm



A<sub>27</sub>, 60 min., 1255 K (1800°F)

20 μm

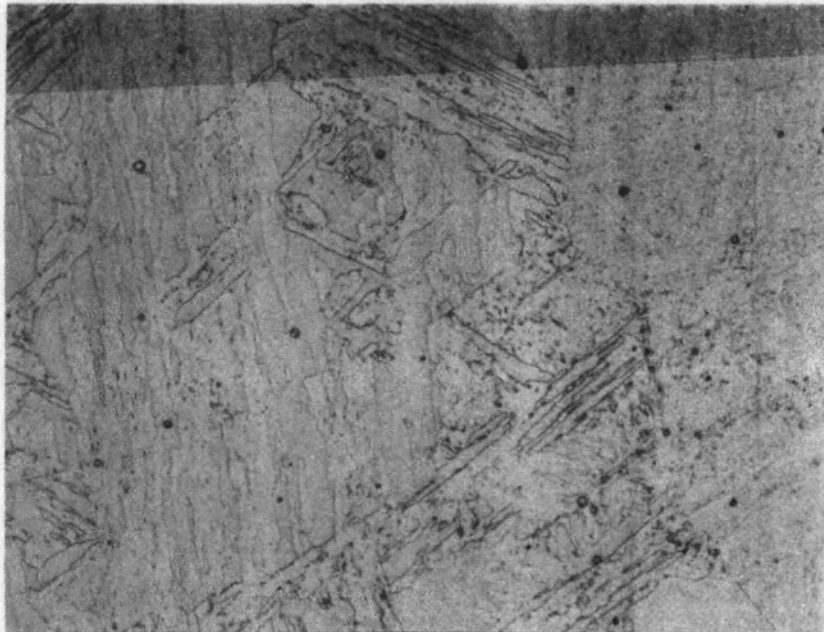


A<sub>28</sub>, 60 min., 1311 K (1900°F)

20 μm

INEL 4 0972

Figure A-4. Optical micrographs of 17-4 PH Standards A<sub>25</sub>, A<sub>26</sub>, A<sub>27</sub> and A<sub>28</sub>.

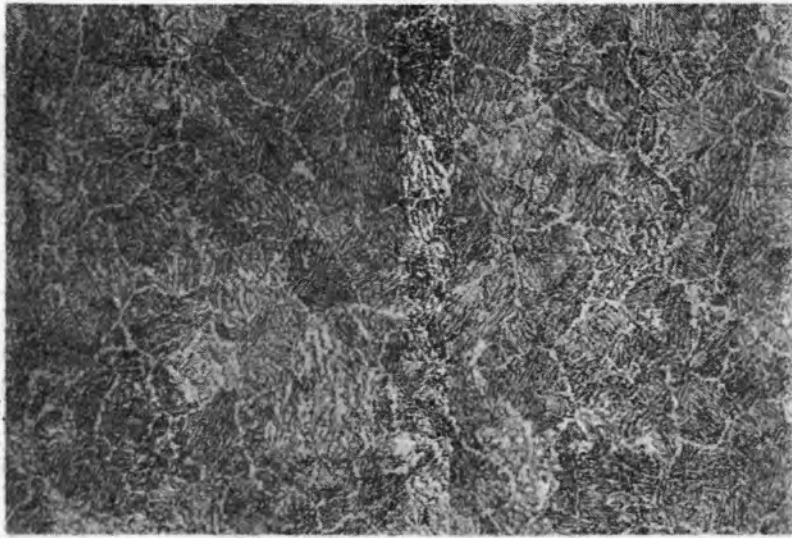


A29, 60 min., 1477 K (2200°F)

20  $\mu$ m  
INEL 4 0973

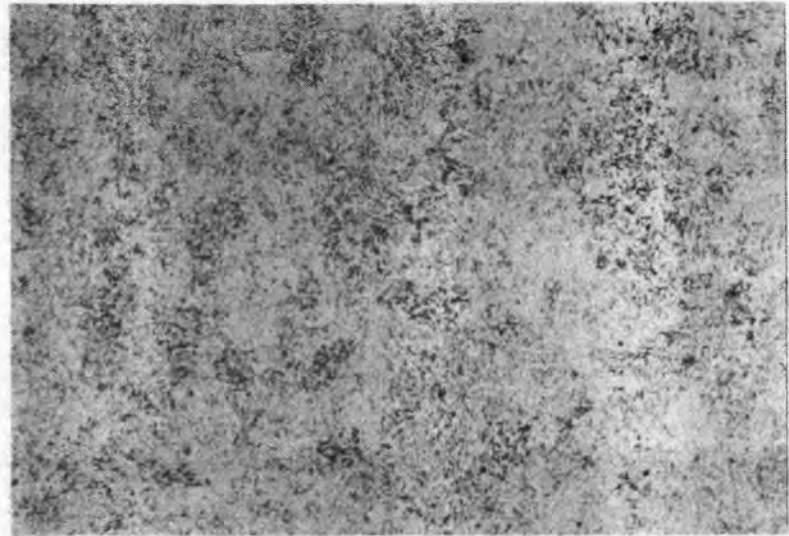
Figure A-5. Optical micrograph of 17-4 PH SS Standard A29.

A-11



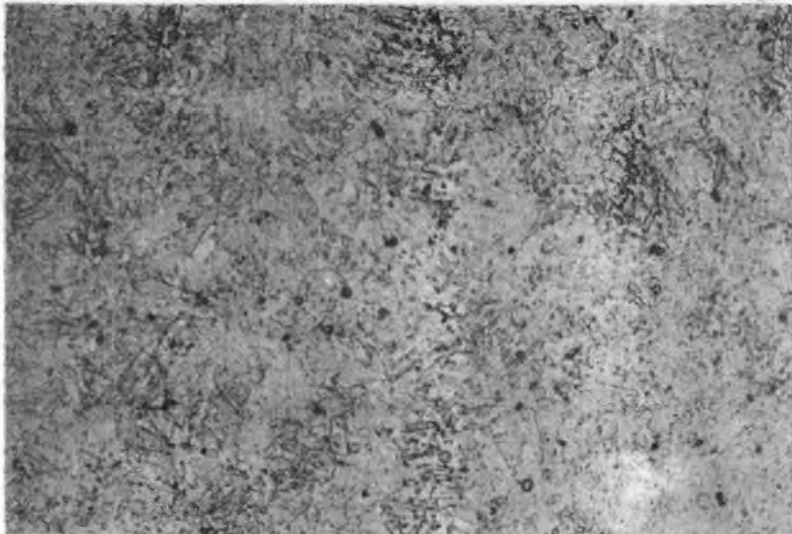
A<sub>31</sub>, 120 min., 977 K (1300°F)

20 μm



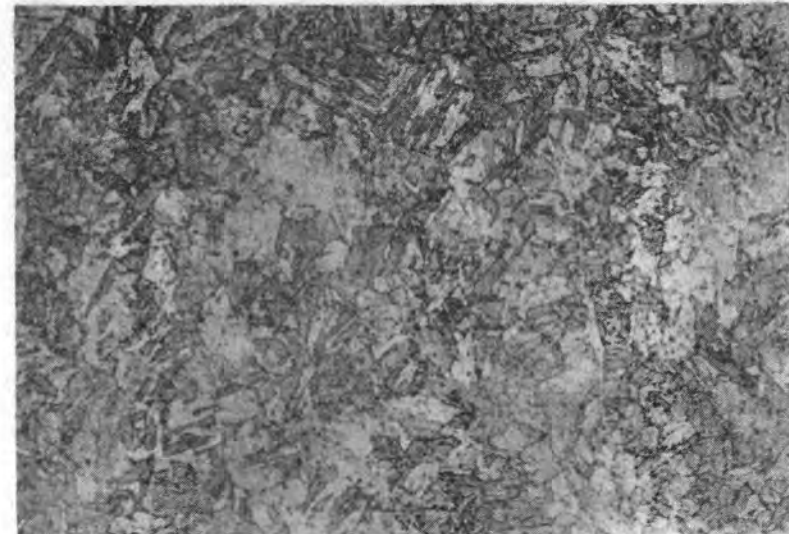
A<sub>35</sub>, 120 min., 1144 K (1600°F)

20 μm



A<sub>36</sub>, 120 min., 1200 K (1700°F)

20 μm



A<sub>37</sub>, 120 min., 1255 K (1800°F)

20 μm

INEL 4 0974

Figure A-6. Optical micrographs of 17-4 PH SS Standards A<sub>31</sub>, A<sub>35</sub>, A<sub>36</sub>, and A<sub>37</sub>.

A-12



A<sub>41</sub>, 240 min., 977 K (1300°F)

20 μm



A<sub>45</sub>, 240 min., 1144 K (1600°F)

20 μm



A<sub>46</sub>, 240 min., 1200 K (1700°F)

20 μm

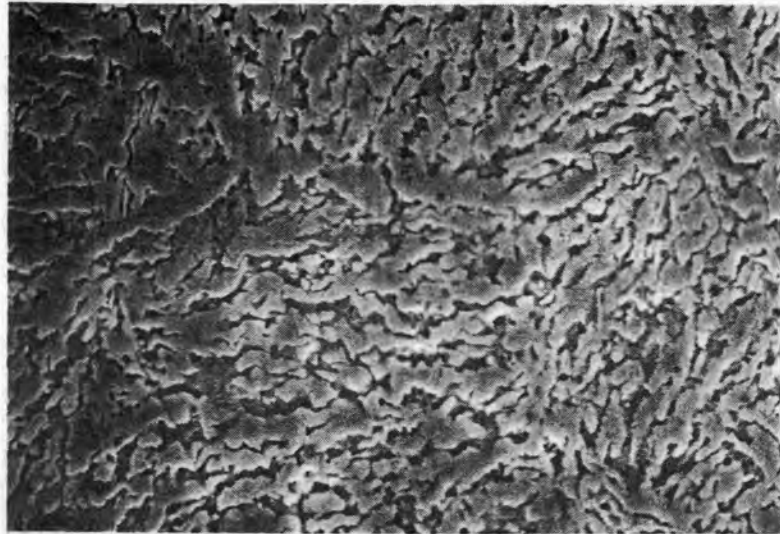


A<sub>47</sub>, 240 min., 1255 K (1800°F)

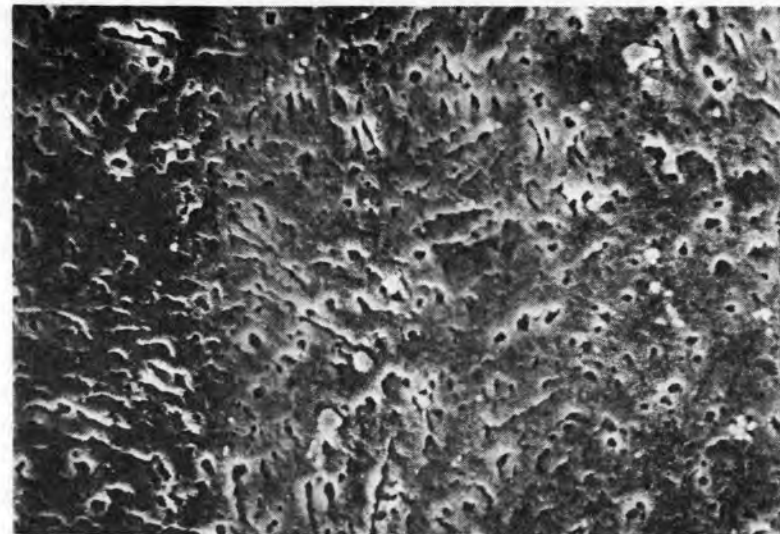
20 μm

INEL 4 0975

Figure A-7. Optical micrographs of 17-4 PH SS Standards A<sub>41</sub>, A<sub>45</sub>, A<sub>46</sub> and A<sub>47</sub>.

A<sub>11</sub>, 30 min., 977 K (1300°F)

2 μm

A<sub>15</sub>, 30 min., 1144 K (1600°F)

2 μm

A<sub>16</sub>, 30 min., 1200 K (1700°F)

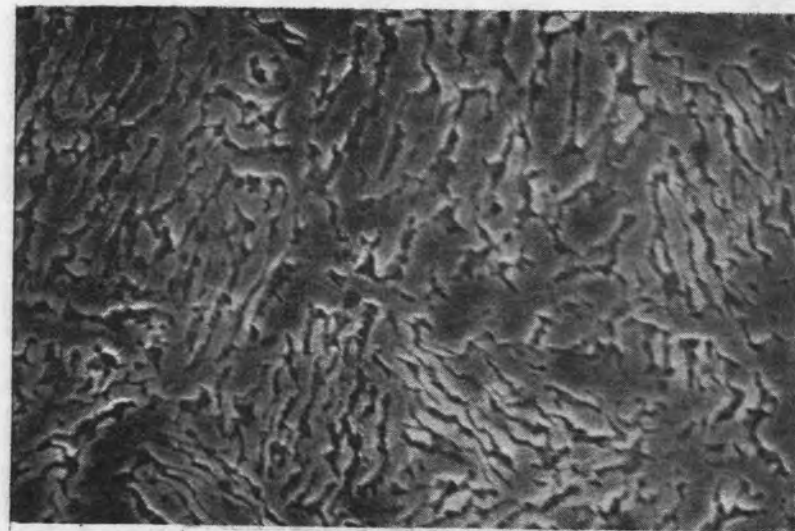
2 μm

A<sub>17</sub>, 30 min., 1255 K (1800°F)

2 μm

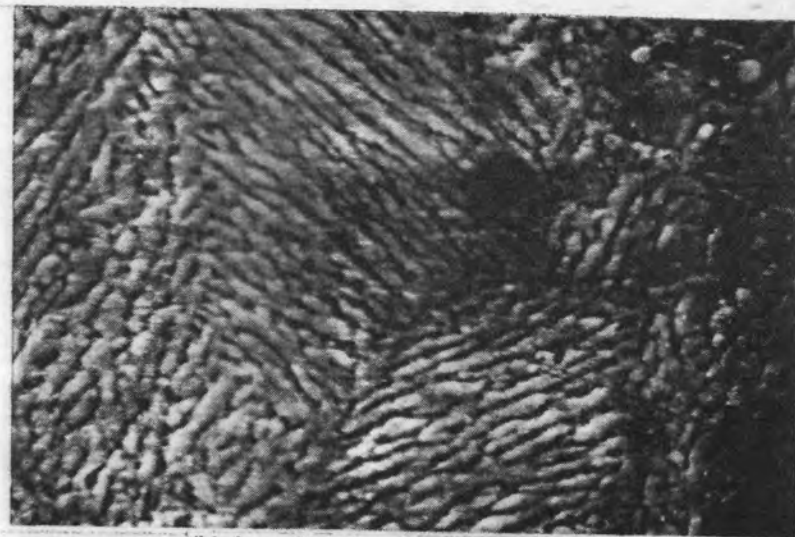
INEL 4 0976

Figure A-8. SEM micrographs of 17-4 PH SS Standards A<sub>11</sub>, A<sub>15</sub>, A<sub>16</sub>, and A<sub>17</sub>.



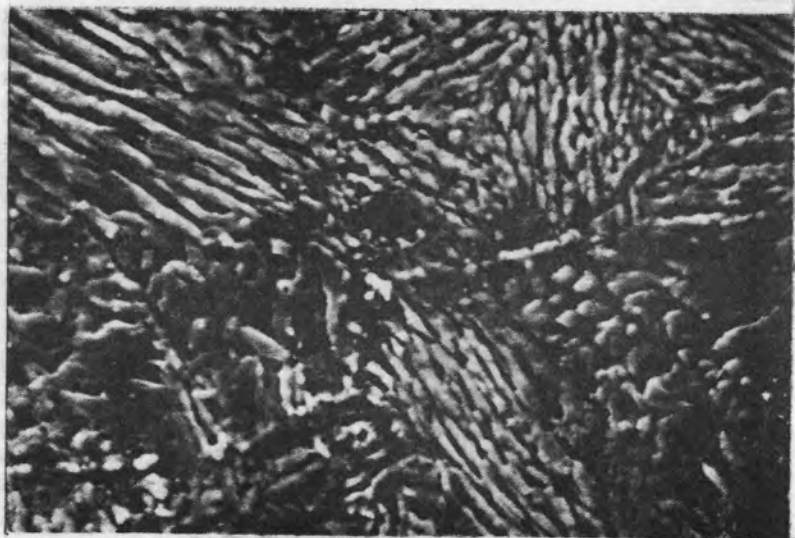
(a) A<sub>21</sub>, 60 min., 977 K (1300°F)

2 μm



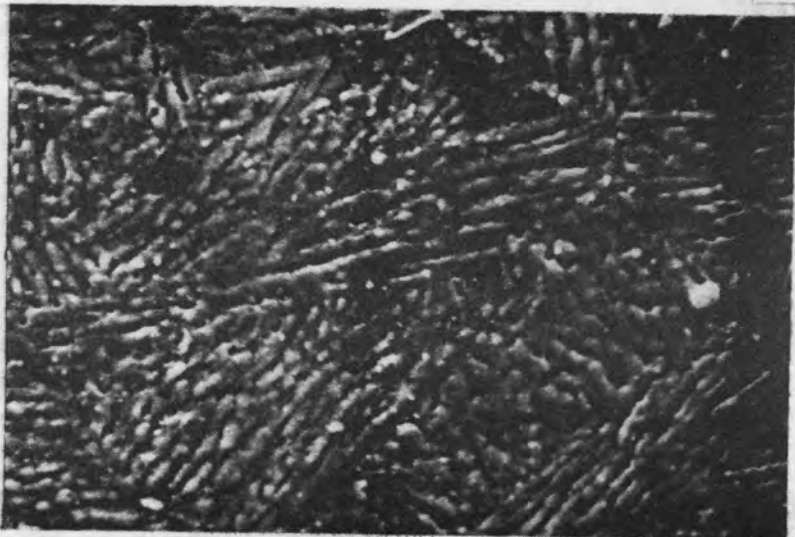
(b) A<sub>22</sub>, 60 min., 1033 K (1400°F)

2 μm



(c) A<sub>23</sub>, 60 min., 1116 K (1500°F)

2 μm

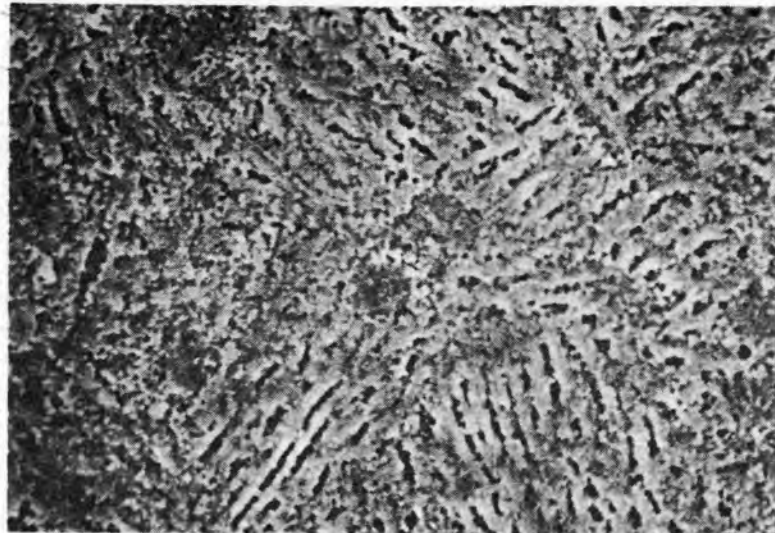


(d) A<sub>24</sub>, 60 min., 1116 K (1550°F)

2 μm

INEL 4 0977

Figure A-9. SEM micrographs of 17-4 PH SS Standards A<sub>21</sub>, A<sub>22</sub>, A<sub>23</sub> and A<sub>24</sub>.



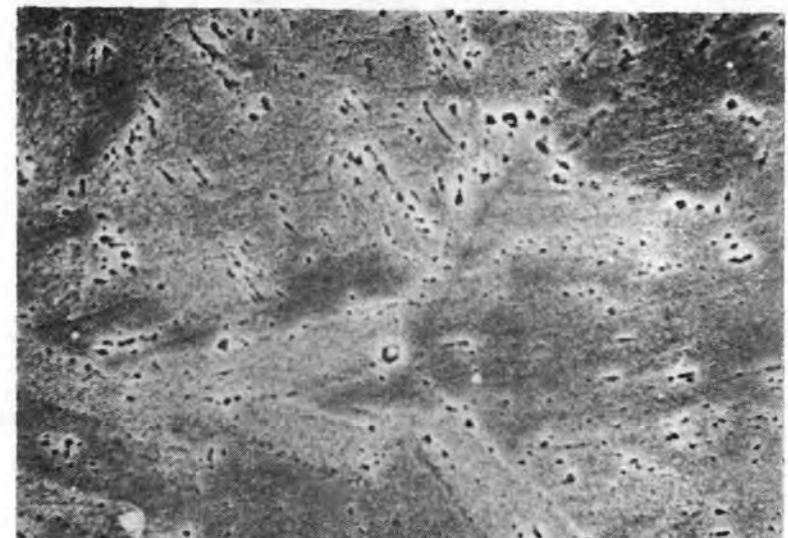
A<sub>25</sub>, 60 min., 1144 K (1600°F) 2μm



A<sub>26</sub>, 60 min., 1200 K (1700°F) 2μm



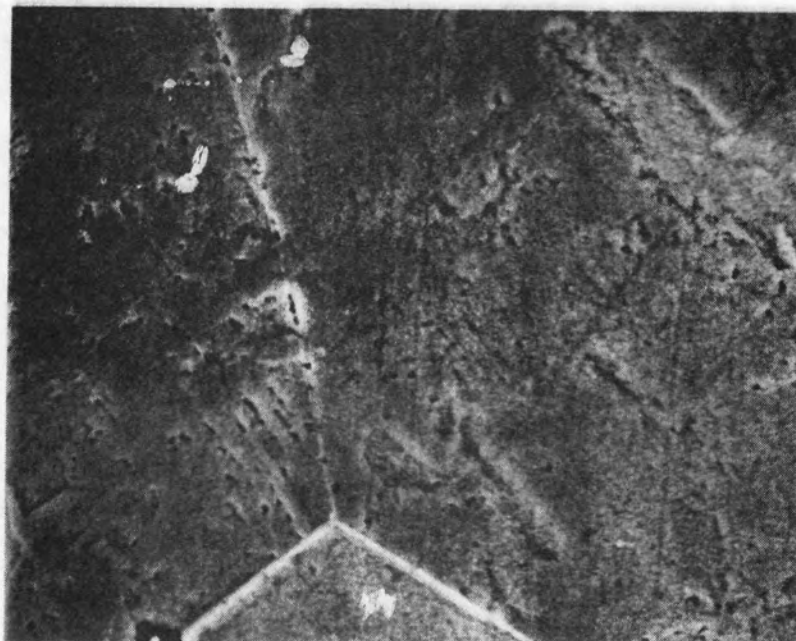
A<sub>27</sub>, 60 min., 1255 K (1800°F) 2μm



A<sub>28</sub>, 60 min., 1311 K (1900°F) 2μm

INEL 4 0978

Figure A-10. SEM micrographs of 17-4 PH SS Standards A<sub>25</sub>, A<sub>26</sub>, A<sub>27</sub> and A<sub>28</sub>.



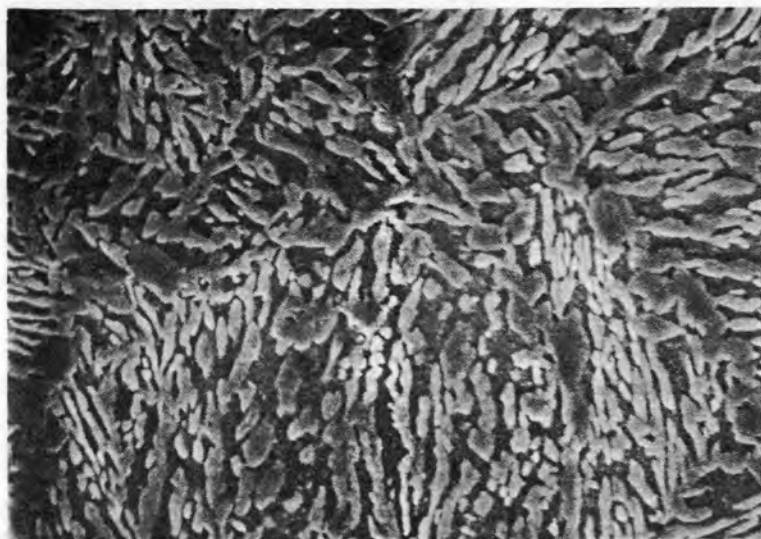
A<sub>29</sub>, 60 min., 1477 K (2200°F)

2 μm

INEL 4 0979

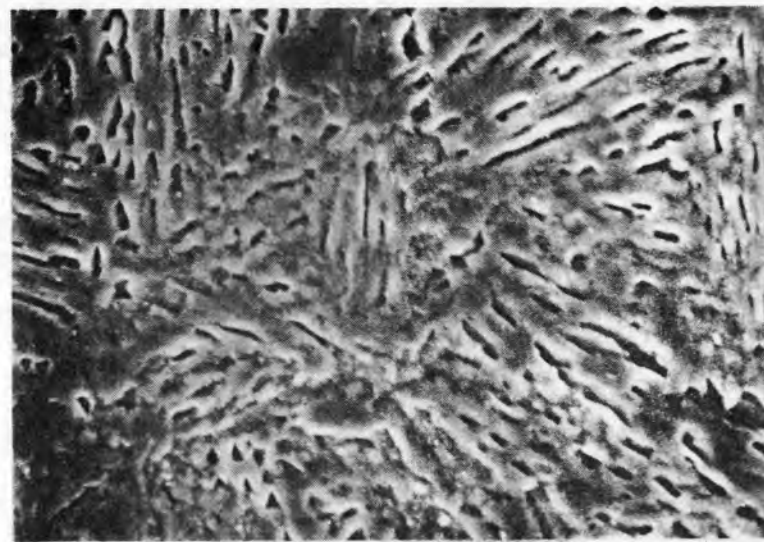
Figure A-11. SEM micrograph of 17-4 PH SS Standard A<sub>29</sub>.





A<sub>31</sub>, 120 min., 977 K (1300°F)

2 μm



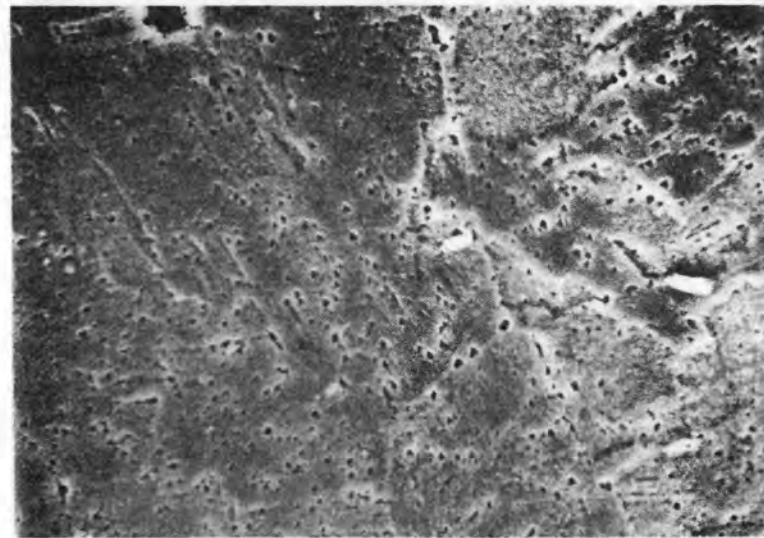
A<sub>35</sub>, 120 min., 1144 K (1600°F)

2 μm



A<sub>36</sub>, 120 min., 1200 K (1700°F)

2 μm

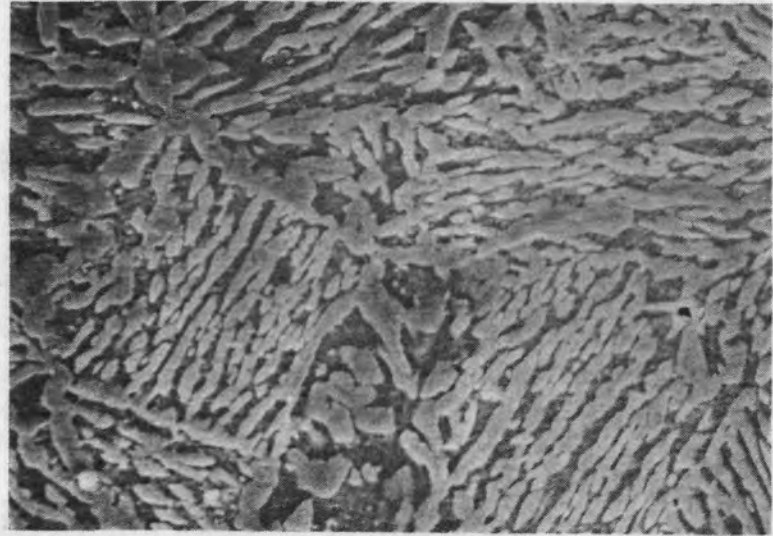


A<sub>37</sub>, 120 min., 1255 K (1800°F)

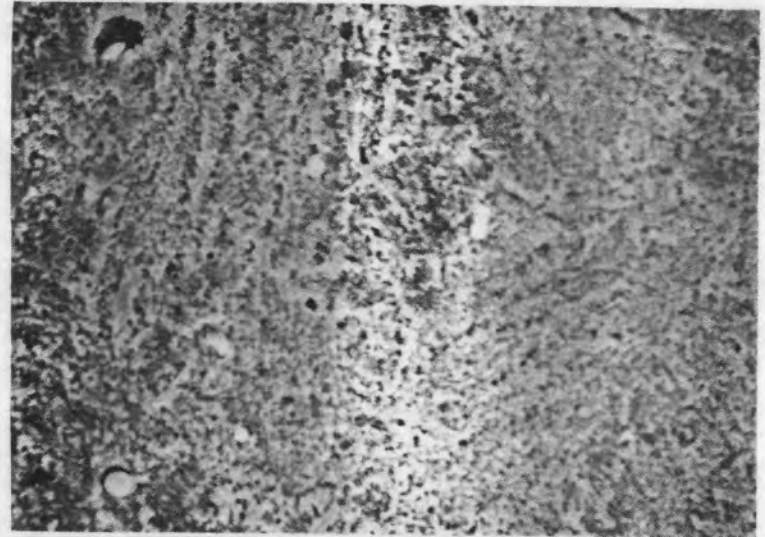
2 μm

INEL 4 0980

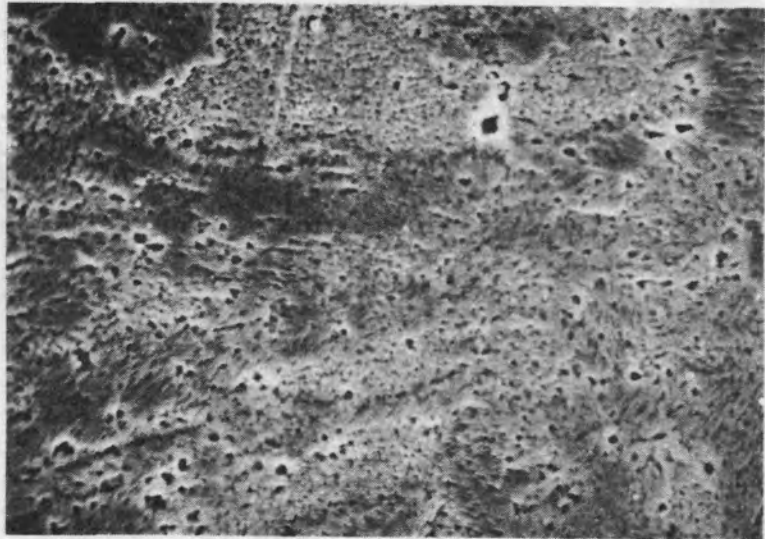
Figure A-12. SEM micrographs of 17-4 PH SS Standards A<sub>31</sub>, A<sub>35</sub>, A<sub>36</sub> and A<sub>37</sub>.



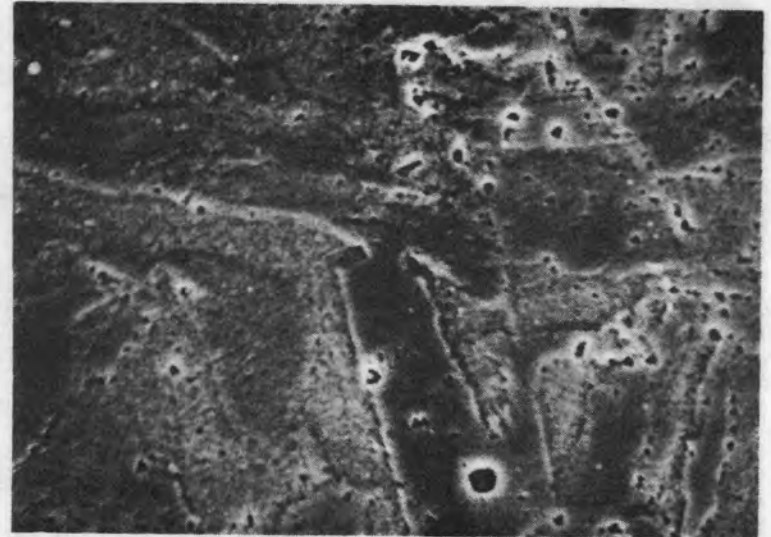
A<sub>41</sub>, 240 min., 977 K (1300°F) 2 μm



A<sub>45</sub>, 240 min., 1144 K (1600°F) 2 μm



A<sub>46</sub>, 240 min., 1200 K (1700°F) 2 μm

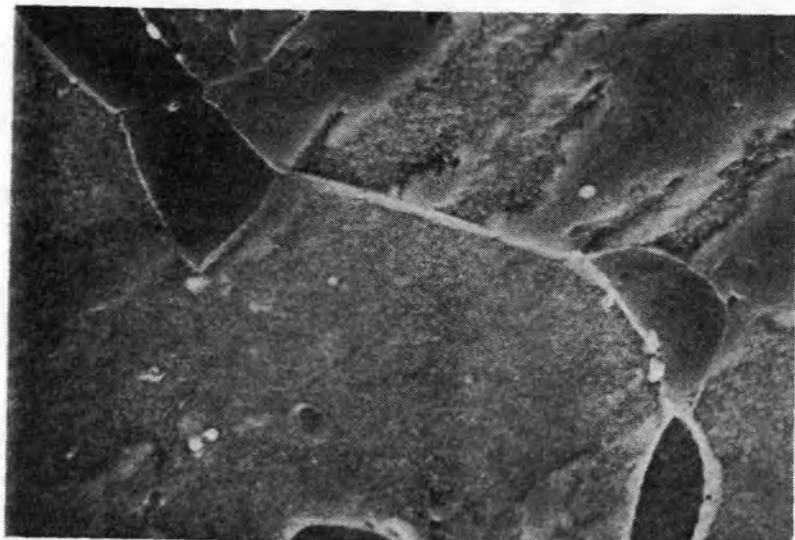


A<sub>47</sub>, 240 min., 1255 K (1800°F) 2 μm

INEL 4 0981

Figure A-13. SEM micrographs of 17-4 PH SS Standards A<sub>41</sub>, A<sub>45</sub>, A<sub>46</sub> and A<sub>47</sub>.

A-19



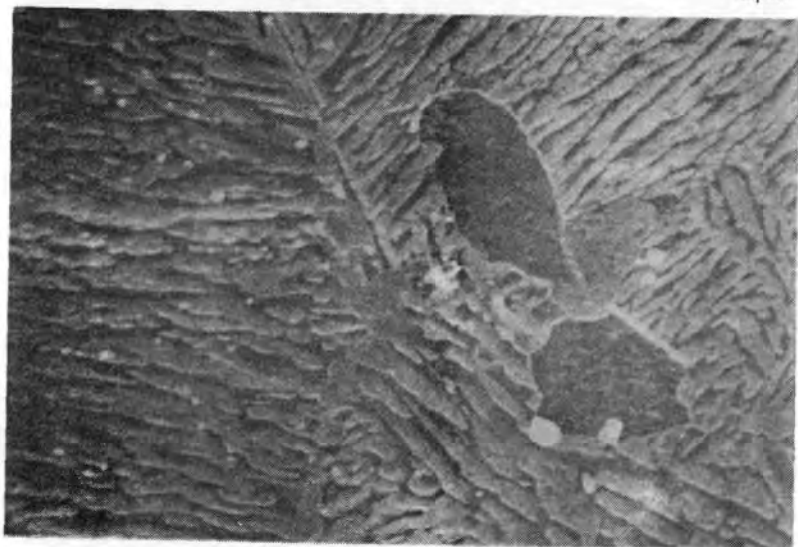
H8 sample 2, Rc = 34.0

2  $\mu$ m



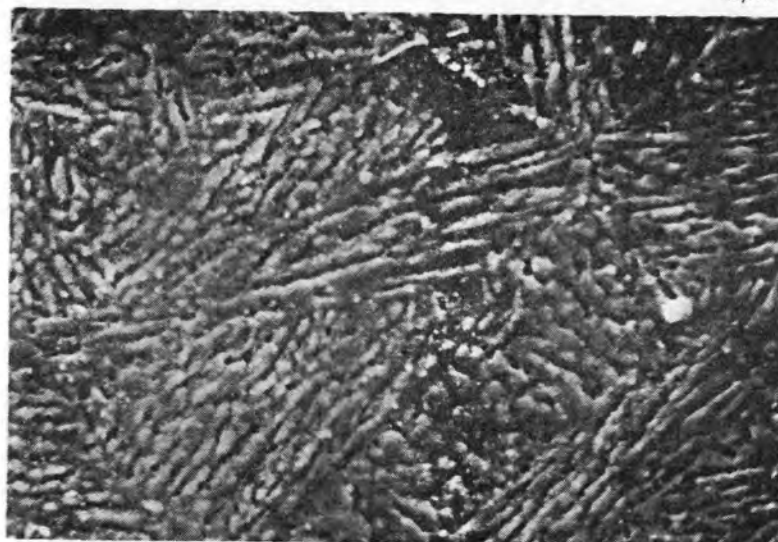
A<sub>27</sub>, 60 min., 1255 K (1800°F), Rc = 35.0

2  $\mu$ m



B8 sample 2, Rc = 35.0

2  $\mu$ m



A<sub>24</sub>, 60 min., 1116 K (1550°F), Rc = 35.4

2  $\mu$ m

INEL 4 0982

Figure A-14. A comparison of H8 Sample 2 and B8 Sample 2 with annealed Standards A<sub>27</sub> and A<sub>24</sub>.

lower end of this temperature range. The lamellar spacing of B8 Sample 2 (0.24  $\mu\text{m}$ ) is comparable with the spacing (0.20  $\mu\text{m}$ ) of the annealed Standard A<sub>24</sub>, suggesting it experienced a temperature of approximately 1116 K (1550°F). The uncertainty in temperature was about  $\pm 28$  K (50°F).

In order to estimate the temperatures of H8 Samples 11 and 15, and B8 Sample 7 near the top of the plenum assembly, commercial 17-4 pH standards at the H1100 condition were heat-treated at 700, 755, 783, and 866 K (800, 900, 950, and 1100°F) for 13 hours and then air-quenched. The hardness values of H8 and B8 samples were compared with the hardness numbers of the annealed standards (see Figure 14 of the text). The comparison suggests that the H8 Samples 11 and 15, and B8 Sample 7 have experienced temperatures of 700, 762, and 755 K (800, 913, and 900°F), respectively. The uncertainty in temperature was about  $\pm 28$  K (50°F).

Several standards taken from the 304L SS portion of Section H8-2 near the top of the reactor head (Subsection H8-23, Figure 2 in the text) were heat-treated for one hour at temperatures 700 K through 1477 K (800 and 2200°F) and water-quenched. The 304 SS microstructures were examined by both optical microscopy and SEM. Also, the Rockwell-B hardness was measured. Sample 5 (304 SS) from B8 leadscrew at the A-hot leg axial location was also examined. Table A-2 presents the data from the 304 annealed standards, the B8 Sample 5 near the A-hot leg, and the 304 SS Sample 7a from the H8 leadscrew. The hardness-versus-temperature values are plotted in Figure A-15. From Figure A-15, the temperatures of the B8 Sample 5 and the H8 Sample 7a were determined to be about 911 and 1189 K (1180 and 1670°F), respectively. The optical and SEM microstructures of the 304 SS B8 Sample 5 at A-hot leg shown in Figures A-16 and A-18, respectively, compare well with the annealed Sample B<sub>13</sub> [heated at 922 K (1200°F) for one hour and water-quenched]. The optical and SEM micrographs of the annealed 304L SS Standards (B<sub>11</sub> through B<sub>17</sub>) are shown in Figures A-16 through A-19.

TABLE A-2. ROCKWELL-B HARDNESS MEASUREMENTS FROM ANNEALED 304L SS STANDARDS AND SAMPLES

Subsection/ Sample	304L SS Standards	Annealing History		Rockwell-B Hardness (RC)
		Time (min)	Temperature K (°F)	
H8-21	B <sub>11</sub>	60	700 (800)	91.73 ± 0.12
H8-23	B <sub>12</sub>	60	811 (1000)	91.13 ± 0.11
H8-23	B <sub>13</sub>	60	922 (1200)	87.40 ± 0.35
H8-23	B <sub>14</sub>	60	1144 (1600)	86.10 ± 0.61
H8-23	B <sub>15</sub>	60	1255 (1800)	70.57 ± 0.59
H8-23	B <sub>16</sub>	60	1366 (2000)	71.93 ± 0.95
H8-23	B <sub>17</sub>	60	1477 (2200)	70.27 ± 1.10
H8 Sample 2	7a	--	--	80.00 ± 0.20
B8 Sample 3	5(A-hot leg)	--	--	87.67 ± 0.32

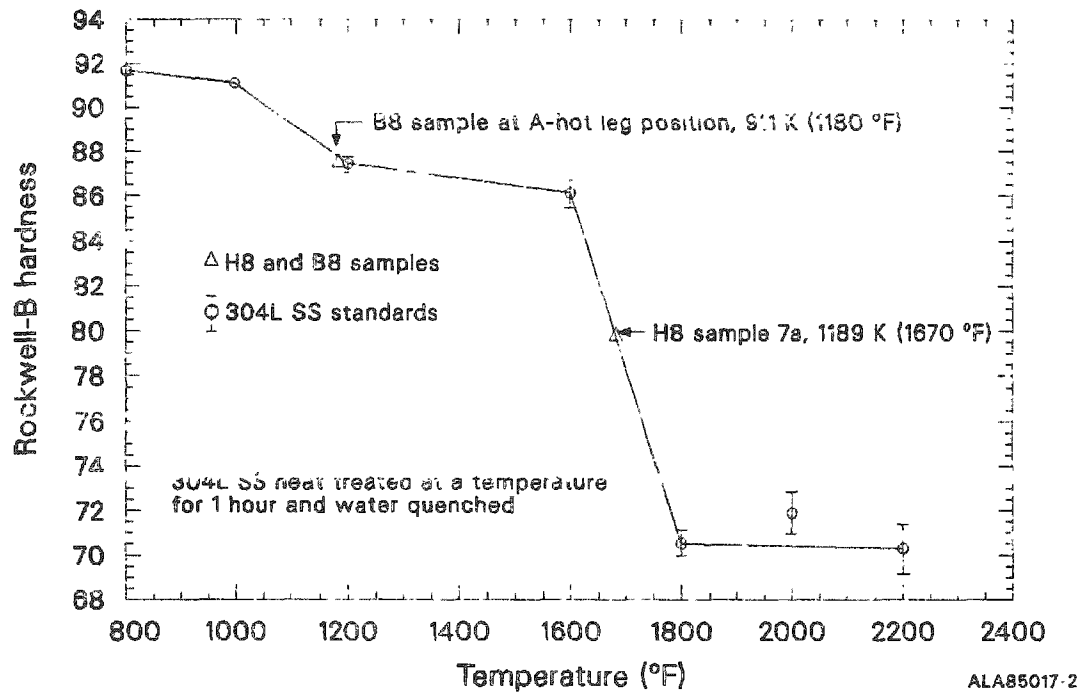
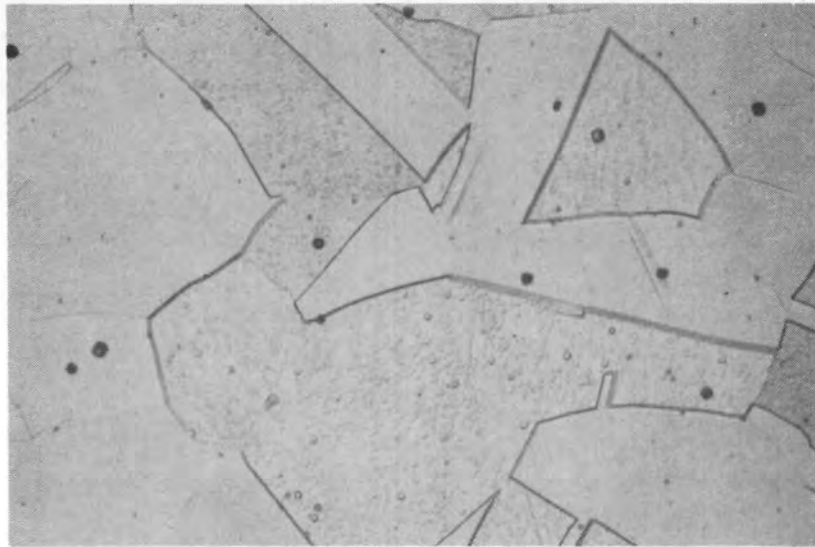
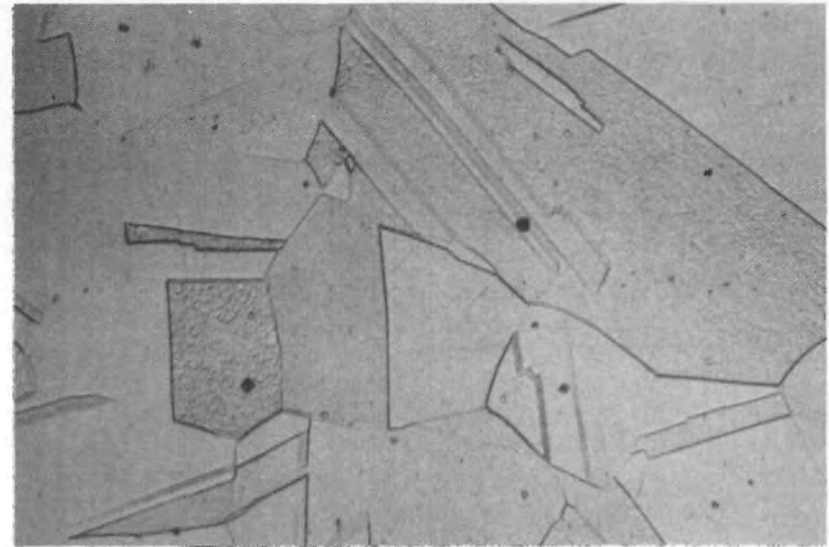


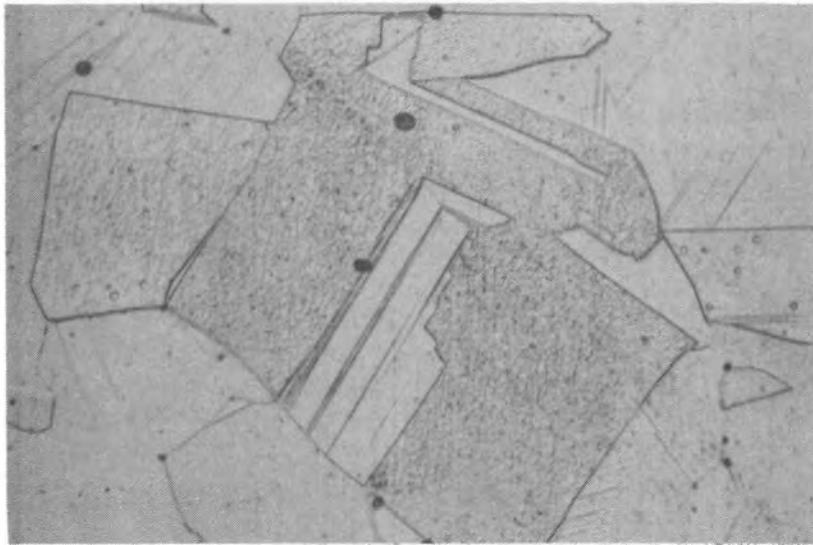
Figure A-15. Rockwell-B hardness versus temperature of 304L SS standards.

(a) B<sub>11</sub>, 60 min., 700 K (800°F)

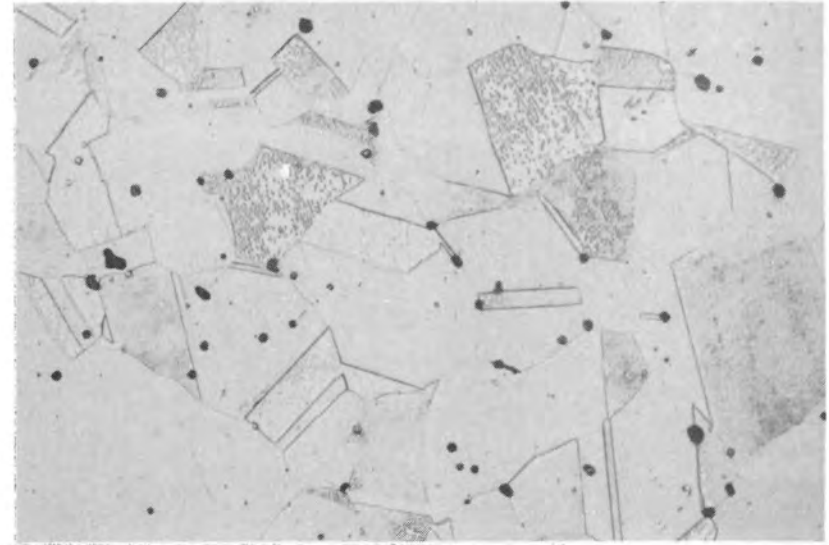
20 μm

(b) B<sub>12</sub>, 60 min., 811 K (1000°F)

20 μm

(c) B<sub>13</sub>, 60 min., 922 K (1200°F)

20 μm



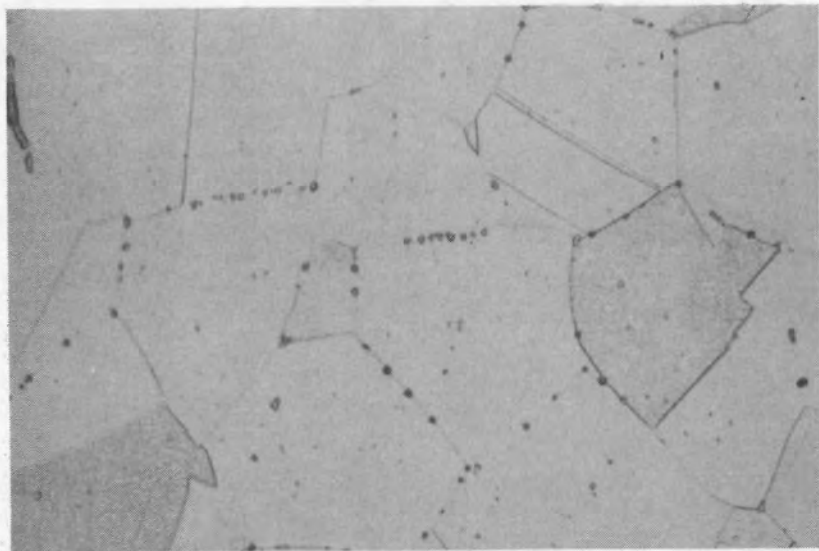
(d) B8 sample 5 at A hot leg

20 μm

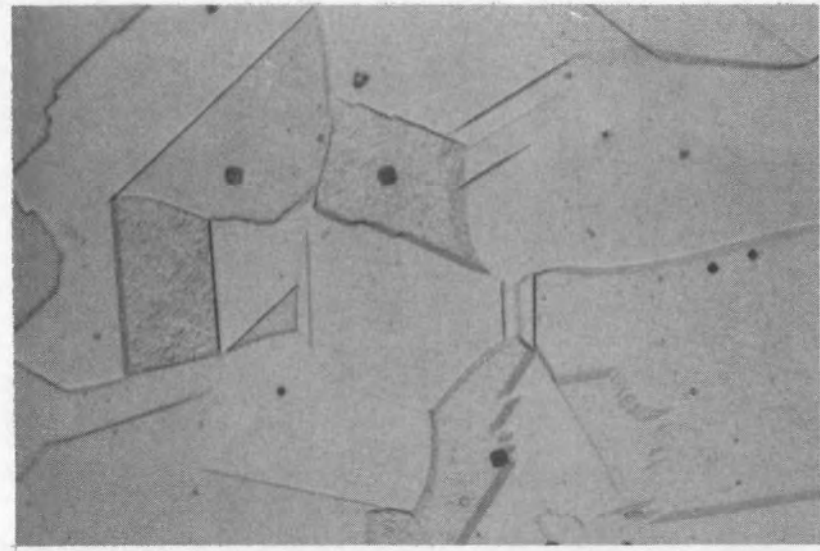
INEL 4 0983

Figure A-16. Optical micrographs of annealed 304L SS standards B<sub>11</sub>, B<sub>12</sub> and B<sub>13</sub>, and B8-A Hot Leg Sample 5.

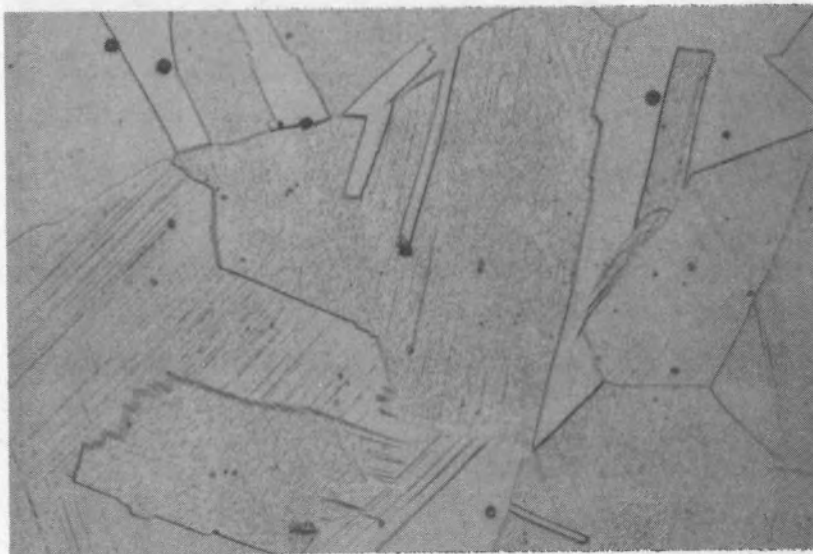
A-24



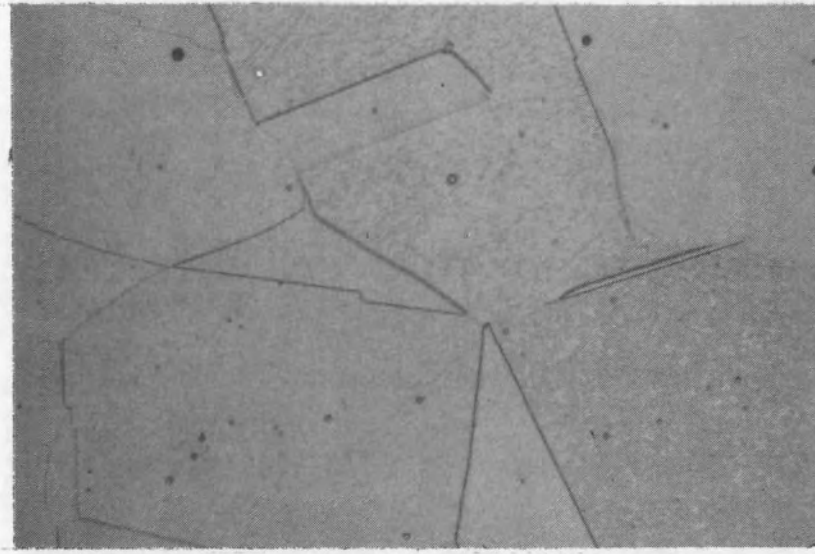
(a) B<sub>14</sub>, 60 min., 1144 K (1600°F) 20 μm



(b) B<sub>15</sub>, 60 min., 1255 K (1800°F) 20 μm



(c) B<sub>16</sub>, 60 min., 1366 K (2000°F) 20 μm

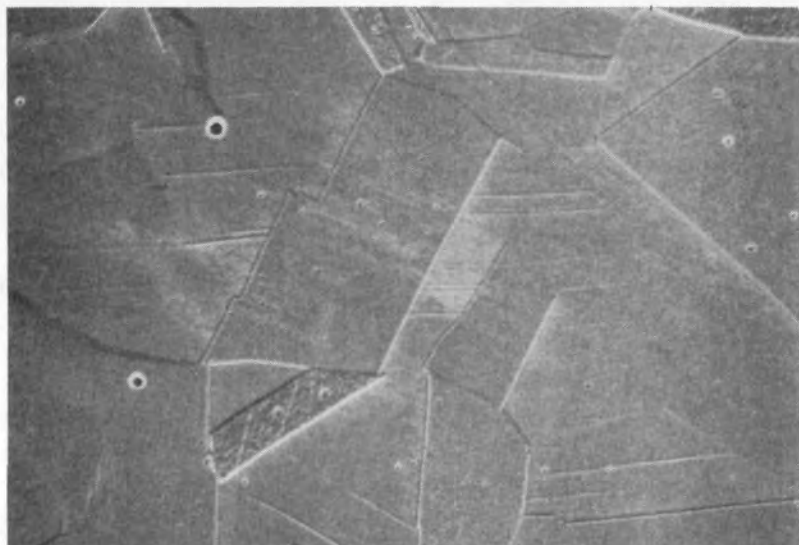


(d) B<sub>17</sub>, 60 min., 1477 K (2200°F) 20 μm

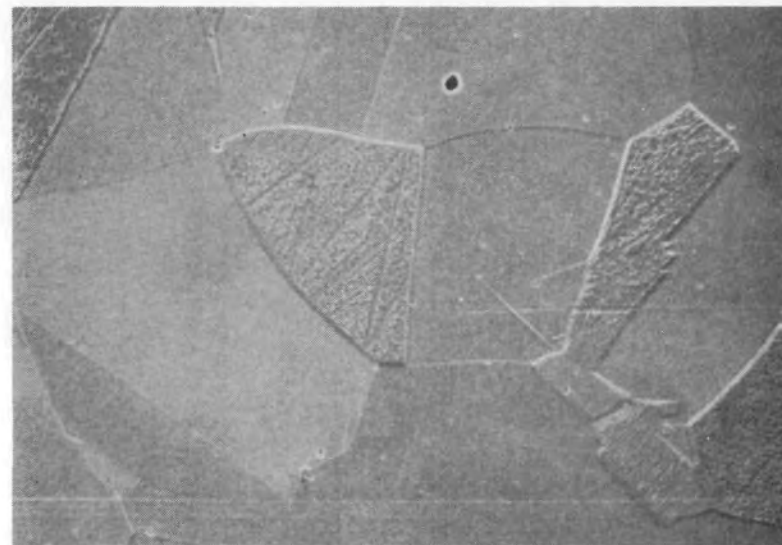
INEL 4 0984

Figure A-17. Optical micrographs of annealed Standards B<sub>14</sub>, B<sub>15</sub>, B<sub>16</sub> and B<sub>17</sub>.

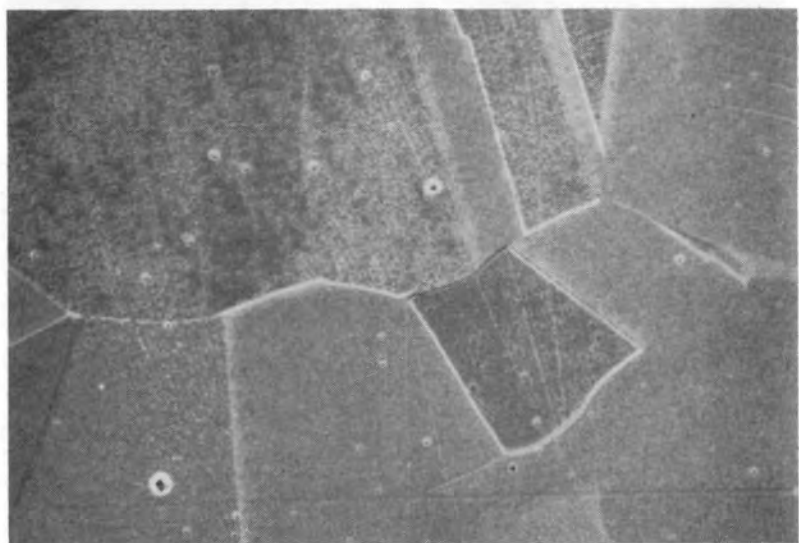


B<sub>11</sub>, 60 min., 700 K (800°F)

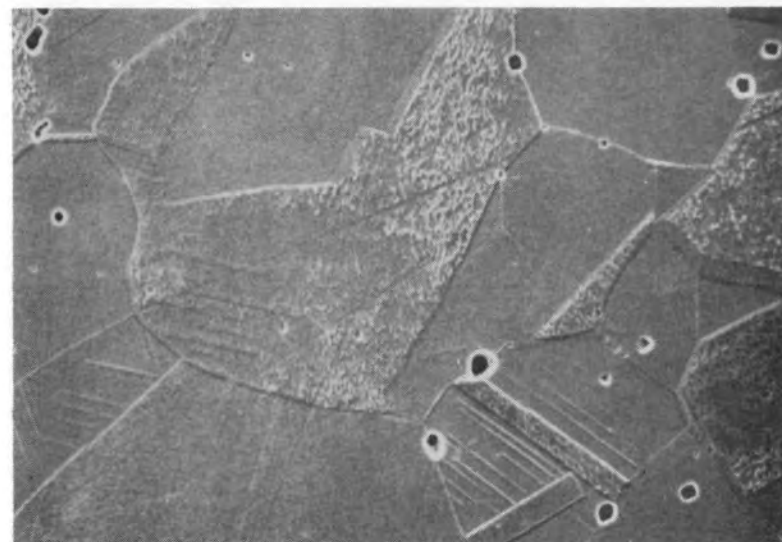
10 μm

B<sub>12</sub>, 60 min., 811 K (1000°F)

10 μm

B<sub>13</sub>, 60 min., 922 K (1200°F)

10 μm

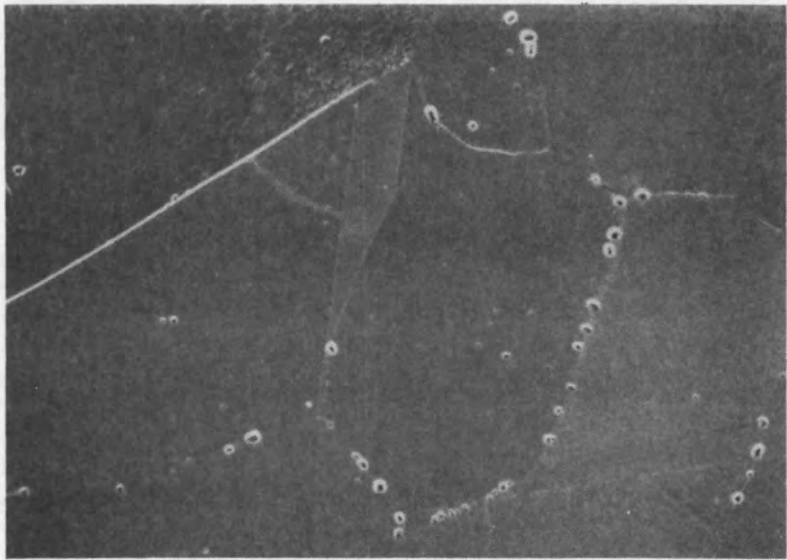


B8 sample 5 at A hot leg

10 μm

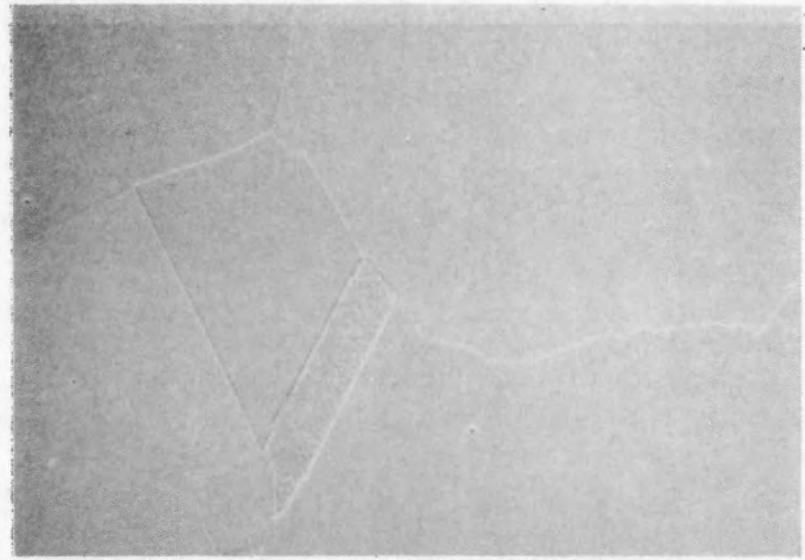
INEL 4 1008

Figure A-18. SEM micrographs of annealed 304L SS Standards B<sub>11</sub>, B<sub>12</sub>, and B<sub>13</sub>, and B8-A Hot Leg Sample 5.



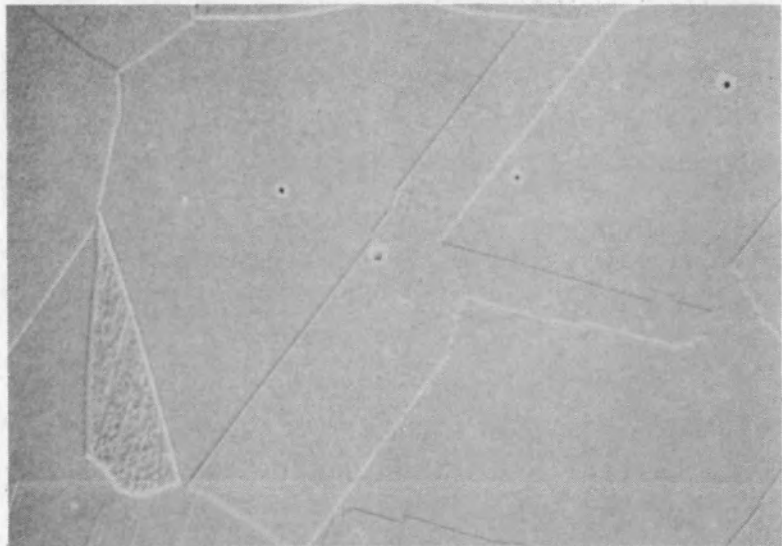
B<sub>14</sub>, 60 min., 1144 K (1600°F)

10 μm



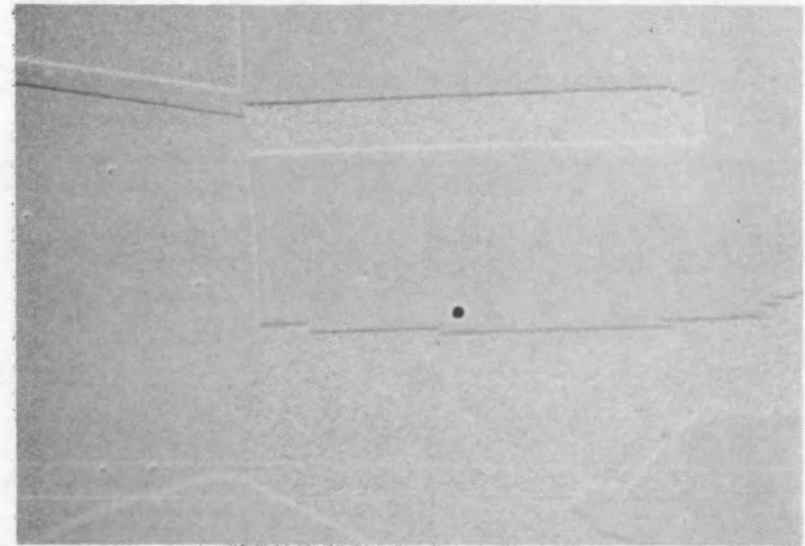
B<sub>15</sub>, 60 min., 1255 K (1800°F)

10 μm



B<sub>16</sub>, 60 min., 1366 K (2000°F)

10 μm



B<sub>17</sub>, 60 min., 1477 K (2200°F)

10 μm

INEL 4 1009

Figure A-19. SEM micrographs of annealed 304L SS Standards B<sub>14</sub>, B<sub>15</sub>, B<sub>16</sub>, and B<sub>17</sub>.



2





.

.

